



Biomass Conversion in Ionic Liquids - in-situ Investigations

Kunov-Kruse, Andreas Jonas

Publication date:
2013

Document Version
Publisher's PDF, also known as Version of record

[Link back to DTU Orbit](#)

Citation (APA):
Kunov-Kruse, A. J. (2013). *Biomass Conversion in Ionic Liquids - in-situ Investigations*. Technical University of Denmark.

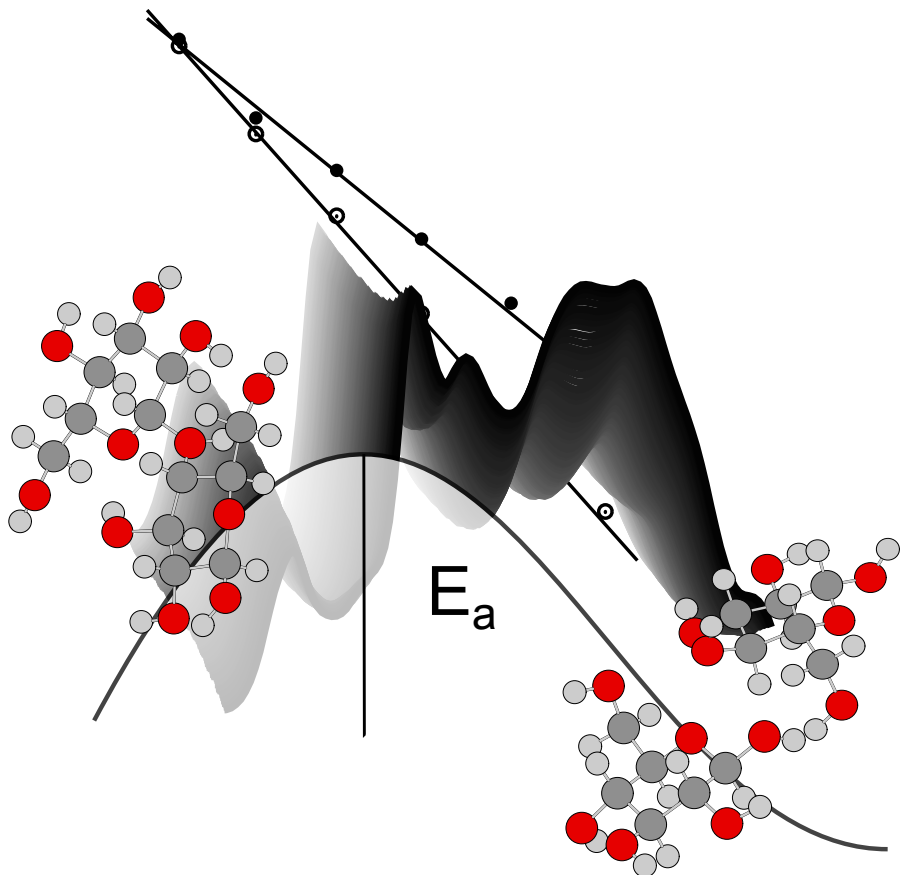
General rights

Copyright and moral rights for the publications made accessible in the public portal are retained by the authors and/or other copyright owners and it is a condition of accessing publications that users recognise and abide by the legal requirements associated with these rights.

- Users may download and print one copy of any publication from the public portal for the purpose of private study or research.
- You may not further distribute the material or use it for any profit-making activity or commercial gain
- You may freely distribute the URL identifying the publication in the public portal

If you believe that this document breaches copyright please contact us providing details, and we will remove access to the work immediately and investigate your claim.

Biomass Conversion in Ionic Liquids - *in-situ* Investigations



Andreas Jonas Kunov-Kruse
Ph.D. Thesis 2013

DTU Chemistry
Department of Chemistry

Andreas Jonas Kunov-Kruse

Biomass Conversion in Ionic Liquids- in-situ Investigations

Technical University of Denmark

Ph.D. Thesis

Author's e-mail addresses:

ajoku@kemi.dtu.dk or andreasjk@gmail.com

Andreas Jonas Kunov-Kruse, May 31, 2013

Printed on DTU

Cover illustrations: Reaction coordinate diagram showing hydrolysis of cellobiose in the front of time resolved in-situ FTIR spectra recorded during cellulose hydrolysis in an ionic liquid. In the background a part of an essential Arrhenius plot is shown.

Preface

This Ph.D. thesis is a part of the requirements to obtain the Doctor of philosophy degree from the Technical University of Denmark. The Ph.D. study has been financed by the Danish Ministry for Science, Innovation and Higher Education's initiative "Catalysis for Sustainable Energy" (CASE) as a part of the "Direct biomass conversion to fuels" project. I am sure that my time as a Ph.D. student will forever remain as a very interesting chapter of my scientific carrier, where I have been given a unique opportunity to combine my interests for fundamental chemistry with multidisciplinary engineering work. I've had the chance to involve myself in many projects with my colleagues. Though the main focus has been on the direct biomass conversion to fuels, which will be the focus in this thesis, I have been involved in several other interesting projects, especially concerning in-situ monitoring in other related forms of ionic liquid chemistry.

I would like to thank my two supervisors Professor Rasmus Fehrmann and Associate Professor Anders Riisager, not only for their supervision, guidance and inputs to this thesis, but also for their great trust in my capacities and their immense moral and economic support every time I presented them with new and uncertain ideas. Thank to my officemate Steffen Buus Kristensen for many interesting discussions, good collaboration and help in several projects and finally for his inputs to my thesis.

There are several of my senior DTU colleagues, besides my supervisors, that offered me guidance during my Ph.D study and for this I am truly grateful. A few of them deserves a special recognition for the time they have invested in me: Associate Professor Irene Shim for always taking time to guide me through the struggles I had concerning quantum mechanical calculations, Associate Professor Rolf W. Berg for his valuable guidance concerning vibrational spectroscopy and to Senior Researcher Saravanamurugan Shunmugavel for great collaboration and all the guidance he has offered me through his huge knowledge of sugar and ionic liquid chemistry. I would also thank former postdoc Olivier Nguyen van Buu for his great help and advices regarding ionic liquid synthesis in the early stages of my project, where the ionic liquid field was new to me.

I would thank Ph.D. Students Jonas Andersen and Phillip Malcho for a fruitful cooperation in the project concerning glucose conversion to HMF catalyzed by chromium salts. Jonas and

I had a great and intensive collaboration especially in the first stages of the related infrared experiments and to Phillip especially for many good discussions and valuable inputs based on his profound knowledge of coordination chemistry. Very importantly I would like to emphasize that all credit from the XANES/EXAFS studies discussed later in the thesis should solely be attributed to Jonas. In the NO_x oxidation and capture project I very much enjoyed the close cooperation and many good discussions with Associate Professor Susanne Mossin and Peter Thomassen. Thank to Assistant Professor Søren Kegnæs for inputs to the thesis and for an interesting collaboration in the project concerning in-situ monitoring of amine oxidations together with Ph.D. Student Jerrik Mielby and Morten Larsen.

In the project concerning the broader commercialization of the invented add-on devices for ATR-FTIR spectroscopy, I would like to thank Special Adviser Majken Kramer Overgaard for investing a lot of time and energy in the project management and supporting me and the project in a lot of related matters. A special thank to my supervisor Anders Riisager who from the beginning was very supportive and encouraged me to follow this path. I would also like to thank Associate Professor Søren Birk Rasmussen for his help and involvement in the recent part of the commercialization project and for his inputs to the thesis. Finally, I would also like to thank and recognize Jens Piltoft and Christian Petersen from the DTU mechanical department for their enthusiasm, hard work and many multidisciplinary and engineering talents, which has been an invaluable asset for the project, and to whom I hope for a long and fruitful cooperation in the future.

I would also like to thank my skilled colleagues at the Chemistry Department's workshop, for a great cooperation during several projects - especially Jimmie Thomsen, Ishaq Khaliqdad, Troels Varming-Petersen and Andreas Graff for making the, sometime quite challenging, devices for the ATR-FTIR instrument for several constructive and crucial inputs in the design process.

Most of all I would like to thank my beloved wife for her great support and her patience during the writing of this thesis, while ensuring a calm and cozy everyday life for the whole family including our two kids Emma and Jonas.



Andreas Jonas Kunov-Kruse
Copenhagen, May 31, 2013

Abstract

Due to rising oil prices and global warming caused by CO₂ emissions, there is an increased demand for new types of fuels and chemicals derived from biomass. This thesis investigates catalytic conversion of cellulose into sugars in ionic liquids and the important platform chemical 5-hydroxymethylfurfural (HMF). The thesis focuses on kinetic and mechanistic investigations using new in-situ FTIR spectroscopic methods based on the ATR-principle.

At first the kinetics of cellulose hydrolysis and the simultaneously HMF formation was investigated in the ionic liquid 1-butyl-2,3-dimethylimidazolium chloride using sulfuric acid, solid acids and Lewis acidic chromium(III)chloride as catalysts. Initially the important glycosidic group vibration was located at 1155 cm⁻¹. The new in-situ spectroscopic method successfully determined activation energies for hydrolysis to be 92-96 kJ/mol regardless of the catalyst used. The often used cellulose model cellobiose was found to hydrolyze substantially easier with an activation energy of only 69 kJ/mol. The activation energies of HMF formation could simultaneously be determined to be 84 and 102 kJ/mol for Brønsted and Lewis acidic catalysis respectively. The low activation energies suggest that the ionic liquid acts co-catalytic by stabilizing the oxocarbenium transition state.

The chromium catalyzed conversion of glucose to HMF in ionic liquid 1-butyl-3-methylimidazolium chloride with CrCl₃·6H₂O and CrCl₂ as catalysts was investigated. The CrCl₃·6H₂O catalyst exhibited high initial conversion rates but suffered from pronounced product inhibition. The rates were 2-3 higher if water was removed simultaneously during reaction. Independent of whether water was presence or not activation energies were found to be 100-102 kJ/mol. For CrCl₂ the initial rates were around 8 times lower but the activation energy was identical the the ones found for CrCl₃·6H₂O. Thus the activity was attributed to around 12 % of chromium(III) that was found to present in the sample. The CrCl₂ showed no sign of product inhibition and followed first order kinetics, which resulted in high conversion at longer reaction times compared to CrCl₃·6H₂O. In a proposed mechanism this was suggested to be due to a Cr^{II}/Cr^{III} synergy. A kinetic model based on active monomeric [CrCl₆]³⁻ species was proposed showing that the product inhibition resulted in second order like kinetic behavior. The fructose dehydration was investigated in both the presence and absence of CrCl₃·6H₂O. The partly dehydrated fructose intermediates were accumulated in the absence of chromium and water, leading to formation of humins. In the presence of CrCl₃·6H₂O the reaction was selective and the rates were 6-30 times higher with an activation energy of 74 kJ/mol. The the-

sis identifies the product inhibition as a major challenge for technical utilization of chromium catalysts in biomass conversion.

Dansk Resumé

Stigende oliepriser og global opvarmning har ført til et øget behov for at udvikle nye flydende brændsler samt kemikalier, der kan udvindes af celluloseholdig biomasse. Denne afhandling undersøger den katalytiske omdannelse af cellulose i ioniske væsker til sukkerstoffer samt det vigtige platform kemikalie 5-hydroxymethylfurfural (HMF). Afhandlingen fokuserer især på kinetikken og mekanismerne bag disse processer gennem in-situ undersøgelser med nye in-frarøde spektroskopiske metoder baseret på ATR-princippet.

I afhandlingens første del blev kinetikken bag hydrolysen af cellulose og den sideløbende omdannelse af sukkerstoffer til HMF i 1-butyl-2,3-dimethylimidazolium chlorid undersøgt, under brug af katalysatorer som svovlsyre, faste syrer samt Lewis surt chrom(III)chlorid. En ny in-situ spektroskopisk metode var i stand til at bestemme aktiveringsenergiene for cellulose hydrolysen til 92-96 kJ/mol, uafhængigt af katalysatortype. Cellobiose, som ofte anvendes som en model for cellulose, kunne hydrolyseres betydeligt nemmere end cellulose, med en aktiveringsenergi på 69 kJ/mol. Aktiveringsenergien for dannelsen af HMF blev bestemt til hhv. 84 og 102 kJ/mol ved brug af svovlsyre og chrom(III)chlorid hhv. Sammenlignet med tilsvarende reaktioner i vand var aktiveringsenergiene meget lave, hvilket antydede at den ioniske væske fungerede som co-katalysator under reaktionen.

I afhandlingens anden del undersøges omdannelsen af glukose til HMF i den ioniske væske 1-butyl-3-methylimidazolium chlorid undersøgt med chrom(II) og chrom(III) salte. $\text{CrCl}_3 \cdot 6\text{H}_2\text{O}$ var indledningvist meget katalytisk aktiv, men led under udtalt produkt inhibering. Reaktionshastighederne kunne øges 2-3 gange hvis vandet blev fjernet løbende under reaktionen. Uafhængigt af tilstedeværelsen af vand kunne aktiveringsenergiene for omdannelsen af glukose til HMF bestemmes til 100-102 kJ/mol. For CrCl_2 var reaktionshastighederne indledning vist omkring 8 gange lavere end med chrom(III)chlorid, mens aktiveringsenergien var identisk. Da det samtidigt kunne vises at 12 % af chrom(II) var blevet oxideret til chrom(III) blev den katalytiske aktivitet tilskrevet disse chrom(III) species. chrom(II)/chrom(III) systemet viste ingen tegn på produkt inhibering og fulgte første ordens kinetik, hvilket resulterede i betydelig højere omdannelse ved længere reaktionstider sammenlignet med den rene chrom(III)chlorid. Dette blev forklaret via en mekanisme, der byggede på en synergi mellem chrom(II) og chrom(III). Monomere $[\text{CrCl}_6]^{3-}$ komplekser blev forslået som de aktive species. En kinetisk model blev opstillet, der kunne vise at produkt inhiberingen resulterede en anden ordens lignede kinetik. Fruktose dehydreringen blev undersøgt både med og uden chrom(III) chlorid. Delvist dehydrerede intermediater af fructose blev akkumuleret under reaktionen,

hvilket førte til dannelsen af huminer. Den $\text{CrCl}_3 \cdot 6\text{H}_2\text{O}$ katalyserede reaktion var selektiv og 6-30 gange hurtigere med en aktiveringsenergi på 74 kJ/mol. Afhandlingens resultater peger på den udtalte produktinhibering som en af de største udfordringer der skal løses for, at kunne anvende chrom katalysatorer i omdannelsen af celluloseholdig biomasse i ioniske væsker i teknisk skala.

Abbreviations and Notations

ATR - Attenuated Total Reflectance
[BDMIM] - 1-butyl-2,3-dimethylimidazolium
[BMIM] - 1-butyl-3-methylimidazolium
CASE - Catalysis for Sustainable Energy
DFT - Density Functional Theory
DMSO - Dimethyl sulfoxide
DOE - Department of Energy
 E_a - Activation energy
[EMIM] - 1-ethyl-3-methylimidazolium
ESR - Electron Spin Resonance
EU - European Union
EXAFS - Extended X-Ray Absorption Fine Structure
FAME - Fatty Acid Methyl Ester
FDA - 2,5-furandicarboxylic acid
FTIR - Fourier Transform Infrared
HF - Hartree-Fock
HMF - 5-hydroxymethyl-furfural
[HMIM] - 1-methylimidazolium
HPLC - High Performance Liquid Chromatography
IR - Infrared
IRC - Intrinsic Reaction Coordinate
kJ - kilo Joule
LCA - Linear Combination Analysis
LN - natural logarithm
 NO_x - nitrogen oxides
PET - Polyethylene terephthalate
PJ - Peta Joule
ppm - Parts per million
TPD - Temperature Programmed Desorption
UN - United Nations
US - United States

δ detontes bending vibration

ν detontes stretching vibration

List of Publications

International Journals

Project related:

1. "Revisiting the Brønsted acid catalysed hydrolysis kinetics of polymeric carbohydrates in ionic liquids by in-situ ATR-FTIR spectroscopy" A. Kunov-Kruse, A. Riisager, S. Saravanamurugan, Rolf W. Berg, Steffen B. Kristensen and R. Fehrmann, *Green Chemistry*, *submitted 2013*
2. "In situ Spectroscopic Studies of the Chromium Catalyzed Glucose Conversion to HMF" A. Kunov-Kruse, J. Andersen, P. Malcho, K. Ståhl and A. Riisager, *in preparation*

Other Publications:

1. "High performance vanadia-anatase nanoparticle catalysts for selective Catalytic reduction of NO by ammonia", S.B. Kristensen, A. J. Kunov-Kruse, A. Riisager, S.B Rasmussen, R. Fehrmann, *Journal of catalysis* 284 (2011) 60-67
2. "Experimental and ab initio DFT calculated Raman Spectrum of Sudan I, a Red Dye" A.J. Kunov-Kruse, S.B. Kristensen, C. Liu, R.W Berg, *Journal of Raman Spectroscopy* 2011, 42, 1470-1478
3. "Dependency of the hydrogen bonding capacity of the solvent anion on the thermal stability of feruloyl esterases in ionic liquid systems" B. Zeuner, T. Ståhlberg, O.N. van Buu, A.J. Kunov-Kruse, A. Riisager, A.S. Meyer, *Green Chemistry*, 13 (2011) 1550-1557
4. "Separation of Fluegas components by SILP (Supported Ionic Liquid-Phase) Absorbers" P Thomassen, A. Kunov-Kruse, S. Mossin, H. Kolding, S. Kegnaes, A. Riisager and R. Fehrmann, *ECS transactions*, 50 (2012) 433-442
5. "High capacity CO₂ absorption by amine containing ionic liquids: Reversibility and mechanistic studies" S. Saravanamurugan, A. Kunov-Kruse, A. Riisager, R. Fehrmann, *ChemSusChem* *submitted 2013*

Patents and patent Applications

1. "NO sorption by ionic liquids" A. Riisager, A. Kunov-Kruse, S. Mossin and R. Fehrmann, patent application no. EP11191127.7, 2011
2. "An Add-on system for an ATR-IR cell" A. Kunov-Kruse, patent application no. EP12174782.8/US61667837, 2012

3. "An Add-on cap for ATR-FTIR spectroscopy studies" A. Kunov-Kruse, J. Thomsen, patent application no. EP12174778.6/US61667923 2012
4. "An add-on system for photochemical ATR-IR spectroscopy studies" A. Kunov-Kruse, J. Thomsen, patent application no. EP12174780.2/ US61667786, 2012
5. "An improved method of preparation of nanoparticulate metal oxide catalysts" S.B. Kristensen, A. J. Kunov-Kruse, A. Riisager and R. Fehrmann, patent application no. EP13164087.2 2013

Conference Contributions, Oral

1. "Novel deNO_x catalysts for biomass fired units", S.S.R. Putluru, S.B. Kristensen, A. J. Kunov-Kruse, J. Due-Hansen, A. Riisager and R. Fehrmann, Europacat X, (Glasgow Scotland, 28th of August to 2nd of September 2011).
2. "Alternative deNO_x katalysatorer", S.B. Kristensen, A. J. Kunov-Kruse, A. Riisager and R. Fehrmann, DK2, (oral, Lyngby Denmark, 16-17th of June 2010).
3. "New Ionic Liquid Catalyst Systems for valorization of biomass Resources" A.Riisager, T. Ståhlberg, S. Saravanamurugan, O.N. Van Buu, A.J. Kunov-Kruse, P. Fristrup, (Keynote, 4th International Congress on Ionic Liquids (COIL-4), Arlington, USA, June 15-18 2011.)
4. "Selective Gas Absorption by Ionic Liquids and by Supported Ionic Liquid-Phase (SILP) Absorbers" R. Fehrmann, A. J. Kunov-Kruse, S. L. Mossin, S. B. Rasmussen, S. Shunmugavel, H. Kolding, S. Kegnæs, A. Riisager (oral presentation, Symposium BBB: "Functional Materials and Ionic Liquids" San Francisco 9-13/4 2012)
5. "Alternative potassium resistant deNO_x catalysts" S.B. Kristensen, A.J. Kunov-Kruse, A. Riisager, S.S.R. Putluru, R. Fehrmann, (Oral, 15th Nordic Symposium on Catalysis, Mariehamn, Åland, Finland, June 10-12, 2012)
6. "Separation of flue gas components by ionic liquids - fundamental chemistry and industrial application" R. Fehrmann, A. J. Kunov-Kruse, S. L. Mossin, S. Kegnæs, H. Kolding and A. Riisager (Keynote, ECS Fall Meetings 2012, Honolulu, Hawaii, October 7-12)
7. "Flue Gas Cleaning by Ionic Liquids - Fundamental Chemistry and Industrial Application" P. Thomassen, A.J. Kunov-Kruse, S.L. Mossin, H. Kolding, S. Kegnæs, A. Riisager, Rolf W. Berg and R. Fehrmann (Molten salts discussion group, X-Mas Meeting, Burlington House, London , December 17 2012)
8. "Selective Gas Absorption by Ionic Liquids and by Supported Ionic Liquid-Phase (SILP) Absorbers" R. Fehrmann, A.J. Kunov-Kruse, S.L. Mossin, S.B. Rasmussen, S. Saravanamurugan, H. Kolding, S. Kegnæs, A. Riisager. (invited talk, MRS springmeeting, San Francisco, California, april 10-12 2013)

Conference Contributions, Poster

1. "Designing multifunctional ionic liquids for biomass processing" A. J. Kunov-Kruse, A. Riisager and R. Fehrmann (Poster presentation Green Solvents for Synthesis, October 10 - 13, 2010, Berchtesgaden/Germany)

2. "Applying the Cosmo Model for the Design of New Ionic Liquids for Carbohydrate dissolution" A. J. Kunov-Kruse, A. Riisager and R. Fehrmann (poster presentation, 4th Congress on ionic liquids, June 15-18 2011, Arlington, Virginia)
3. "Nano-sized SCR deNOx catalysts" , S. B. Kristensen, A. J. Kunov-Kruse, A. Riisager and R. Fehrmann, Europacat X, (poster presentation, Glasgow Scotland, 28th of August to 2nd of September 2011).
4. "In-situ Spectroscopic Determination of Catalytic Cellulose Depolymerization" A. J. Kunov-Kruse, A. Riisager and R. Fehrmann 15th International Congress on Catalysis, (poster presentation of July 1-6 2012, Munich)
5. "Fast and accurate determination of the reaction kinetics of cellulose hydrolysis in ionic liquids using in-situ ATR-FTIR" A.J. Kunov-Kruse, A. Riisager, S. Shunmugavel, R.W. Berg, S.B. Kristensen, R. Fehrmann (Poster presentation, Green solvents, Boppard, Germany 8-10 october 2012)

Contents

Preface	iii
Abstract	v
Dansk Resumé	vii
Abbreviations and Notations	ix
List of Publications	xi
1. Introduction - Fuels From Biomass	3
1.1. Biofuels from food - Ethical challenges	4
1.2. Biofuels from Lignocellulosic biomass - Technological challenges	6
1.3. Ionic Liquids for lignocellulose dissolution	8
1.4. The furanic platform	8
1.5. Outline of the thesis	10
2. In-situ Investigation of Cellulose Hydrolysis in Ionic Liquids	11
2.1. Introduction to cellulose hydrolysis	12
2.1.1. Enzymatic hydrolysis of cellulose	14
2.1.2. Can simple catalysts mimic enzymatic hydrolysis?	15
2.1.3. Experimental Challenges of the Cellulose hydrolysis	17
2.1.4. Cellulose Hydrolysis in Ionic Liquids	18
2.2. Developing a new Method for <i>In-situ</i> Monitoring Cellulose Hydrolysis	20
2.2.1. Identifying the True Group Vibrations of the Glucoside Bond	21
2.2.2. The Glycoside Band in the Literature	26
2.2.3. Overlap with the Glucoside band	27
2.2.4. Development of the experimental setup	28
2.3. Results and discussion	30
2.3.1. Brønsted catalyzed hydrolysis of the glucoside bond	30
2.3.2. Glucose Conversion during Hydrolysis	39
2.3.3. Heterogeneous Catalysts for Cellulose Hydrolysis	44
2.3.4. Lewis Acidic Catalysts: Hydrolysis in Presence of Cr ³⁺	45
2.4. Concise Conclusions	54
3. Chromium catalyzed glucose conversion	57
3.1. In-situ Investigations of the Chromium Catalyzed Glucose Conversion	58
3.1.1. The apparent kinetics of glucose conversion in presence of CrCl ₃ ·6H ₂ O	59
3.1.2. The kinetics of glucose conversion during anhydrous conditions	64
3.1.3. Dependency on chromium concentration	69
3.1.4. Glucose conversion catalyzed by Cr ^{II} species	70
3.1.5. Reactions orders of glucose - Derivation of a unifying model	74
3.2. Fructose dehydration	79
3.2.1. Anhydrous Chloride Catalyzed Fructose dehydration	79
3.2.2. Chloride Catalyzed Fructose dehydration in the presence of water	84
3.2.3. Cr ^{III} Catalyzed Fructose dehydration	86
3.3. Concise Conclusions	90
4. Experimental and Calculations	93
4.1. Preparing ionic liquid solutions	93
4.1.1. Preparation of reaction mixtures	94
4.2. in-situ ATR-FTIR spectroscopy	94
4.2.1. Recording of in-situ ATR-FTIR spectra	95
4.2.2. Transmission FTIR	97

4.2.3. Correction of the ATR-spectra	97
5. Concluding remarks and outlook.	103
Bibliography	105
Appendix	109
A. Supporting figures introduction	109
B. Supporting spectral data cellulose hydrolysis	113
B.4. Calculated spectra of Cellulose related structures	114
B.5. Experimental spectra of Cellulose related compounds	115
B.6. Elucidation of δ_{C2-H} modes in [BMIM]Cl	116
B.7. Comparison of Experimental and Calculated spectra: Glucose and Cel- lobiose	118
B.8. Detailed descriptions of selected vibrational modes	120
B.9. Spectra of HMF and Levulinic acid	126
B.10. Rates of H ₂ SO ₄ catalyzed cellulose hydrolysis	129
B.11. Rates of H ₂ SO ₄ catalyzed cellobiose hydrolysis	132
B.12. Rates of HMF formation during H ₂ SO ₄ catalyzed cellulose hydrolysis . . .	136
B.13. Rates of HMF formation during H ₂ SO ₄ catalyzed cellobiose hydrolysis . .	138
B.14. Theoretical structures during cellobiose hydrolysis	140
B.15. Post reaction HPLC Analysis	141
B.16. Rates of SO ₄ ²⁻ /TiO ₂ catalyzed cellulose hydrolysis	142
B.17. Correction of difference spectra from SO ₃ H-SBA15 catalyzed hydrolysis .	143
B.18. Rates of Cr ³⁺ catalyzed cellulose hydrolysis	144
B.19. Rates of HMF formation during Cr ³⁺ catalyzed cellulose hydrolysis	146
C. Supporting data for chromium catalyzed conversions	149
C.20. HMF standard curve	149
C.21. Glucose Conversion in Microreactor in Presence of CrCl ₃ ·6H ₂ O	152
C.22. Glucose Conversion in Anhydrous Thin Films in Presence of CrCl ₃ ·6H ₂ O .	156
C.23. Glucose Conversion in Anhydrous Thin Films in Presence of CrCl ₂	160
C.24. Second order Plots	164
C.25. Chloride Catalyzed Fructose Dehydration Thin Films	167
C.26. Chromium Catalyzed Fructose Dehydration Thin Films	172
D. Automatic deconvolution package for gnuplot - Short documentation	175
E. Article - Project related	181

Introduction - Fuels From Biomass

This chapter will identify and introduce important technical and ethical challenges related to biomass derived fuels and chemicals. The introduction will aim to put the scientific results of the following chapters into a broader context.

During the recent years the enormous environmental impact our use of fossil is causing has become gradually more evident. The main problem is caused by emissions of CO₂, formed in every combustion of carbon based fuels including coal, oil, gas and biomass, which are a non-toxic gas but due to being a greenhouse gas it contributes to the global warming. In Europe alone, the UN reports a temperature increase of 1 °C over the last 35 years^[2], while recent studies suggests that the worse is yet to come. During the writing of this thesis the average CO₂ concentration in atmosphere for the first time in the human history reached 400 ppm^a. The

^aThe acknowledged Scripps Institution of Oceanography has in May 2013, for the first time ever, reported daily average values above 400 ppm^[1]. Figures showing the CO₂ content in the atmosphere is found in figure 1.1 and appendix: figure A.1 on page 110.

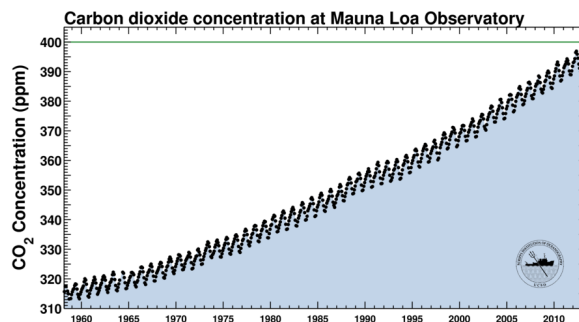


Figure 1.1.: Showing the development of CO₂ from 1958 to may 2013^[1].

last time similar levels were reached was 3-5 million years ago in the Pliocene epoch, where the CO₂ content in the atmosphere was 365-415 ppm^[3,4]. As this, in a geological sense, is very close to the present, the Pliocene epoch serves as a very good model for studying forthcoming climates changes we will experience in around century when the full effect of the present CO₂ levels are reached^[5-7]. This suggests a rather gloomy picture of the future, where the global temperatures will be around 3-4 °C higher than today at low latitudes and around 10 °C higher close to the poles^[4-6]. This clearly emphasizes the importance of working towards much lower CO₂ emissions.

1.1. Biofuels from food - Ethical challenges

A broad range of different technological initiatives and breakthroughs are required to lower the future CO₂ emissions. Especially, the transportation area is difficult because the present combustion-engine driven technologies and their infra-structure depends almost entirely on liquid fuels. The majority of these fuels are produced from crude oil, which in addition to the unwanted environmental effects, is beginning to be a very expensive solution as oil-prices have raised significantly the last years and are expected to rise further^[8]. There has started to emerge more competitive electronic driven cars, which in principle can be powered by CO₂ neutral electricity from sources such as e.g. wind- and waterpower or nuclear or biomass fired power plants. The future impact of electrification on the transport sector is very hard predict and no reliable prognosis are available. However, there is no doubt that these technologies will require many years to develop before they are able to outmatch gasoline and diesel driven transportation and even the most optimistic scenarios estimate at least 40 years before the electrification of the transportation sector will be complete^[9]. However, substitutes for both diesel and gasoline can relatively easy be derived from several types of crops. Ethanol can be mixed with gasoline in rather high ratios using present combustion technologies, and with minor modifications up to around 85 %^[10]. Fuel ethanol can be obtained from fermenting

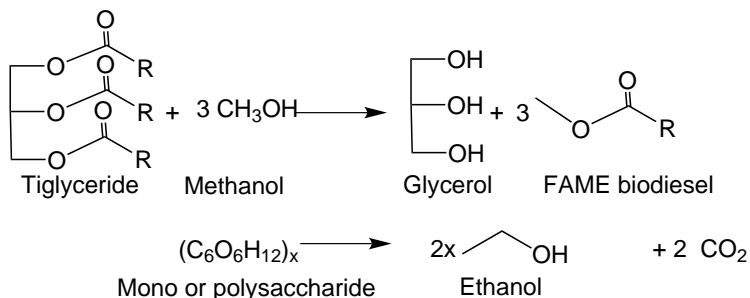


Figure 1.2.: Showing principle in production of FAME biodiesel and ethanol.



Figure 1.3.: Oil palm and maize are two of the most important crops for first generation biofuels^[13].

the sugars found in several types of crops while high quality diesel substitutes such as Fatty Acid Methyl Esters (FAME), can be produced from transesterification of fatty triglycerides extracted from oil containing crops^[11,12], see figure 1.2 on the preceding page. Especially the United States (US), Brazil and the European Union (EU) have based a large part of their goals to reduce CO₂ emissions on the these type of biofuels, which are often referred to as first generation biofuels because the use eatable crops as feedstock^[14,15]. However, there has been raised several problematic issues related to first generation biofuels. The steep rise of the oil prices in 2005-2006 increased the demand for fuel ethanol that caused tripling of the global ethanol prices^b. This resulted in an increasing ethanol production thus causing in a rapid increase in demand for feedstock. The tragic outcome of this bioethanol adventure was a proportional price increase in essential crops like e.g. corn, which lead to the food crisis in 2007-2008, where poor citizens of third world counties suddenly became unable to afford food^[14,16-18]. The food crisis pointed towards very serious ethical drawbacks of basing fuel consumption and economy on eatable crops.

Recently attention has been brought to another serious, but rather ironic, environmental problem arising from the production of first generation biofuels. Several studies questions if first generation biofuels on the whole contribute to reduce CO₂ emissions^[19-23]. The increasing demand for crops to bioethanol and FAME biodiesel production has led to a rapid deforestation in fertile tropical regions like e.g. Indonesia, Malaysia, Borneo and Brazil^[19,20]. Several studies has shown that the CO₂ emissions from tropical deforestations are much more considerable than assumed earlier. Deforestation do not alone release carbon equivalent to the living trees and plants, but much worse also releases significant amounts of the carbon bound in enormous

^bThe development of ethanol and corn prices during 2005-2009 reported by Hertel and Beckman^[16] are included in appendix: see figure A.2 on page 111.

peat layers hidden below the forests, which can be up to 20 meters deep. These subterranean peat layers comprises one of the world's largest carbon reservoirs^[19–23]. In a recent study the carbon footprint of the deforestation related to Brazil's cultivation of sugar canes, soy bean and palm oil in the Amazonas up until year 2020 are considered. The study estimates that it will take around 250 years of cultivation of crops, assuming all would be used to produce biofuels, to make up for the CO₂ emissions caused by the same deforestation^[20]. This clearly emphasizes that even though a fraction of the overproduction of food, in especially the US and EU, can be converted into biofuels thereby reducing CO₂ emissions, the overall contribution from first generation biofuels could very well end up causing more CO₂ emissions than it saves.

1.2. Biofuels from Lignocellulosic biomass - Technological challenges

Lignocellulosic biomass is a common term for a broad range of biomass comprising wood, grasses and non-eatable parts of food crops like straw and corn stover. Biofuels made from lignocellulosic sources are often referred to as second generation biofuels. In lignocellulosic biomass the plant cell walls are surrounded by a matrix of cellulose, lignin and hemicellulose that provides structure and mechanical strength. While the lignin is a rather complex and heterogeneous polymeric material consisting of polyphenols and related compounds, cellulose has a uniform polymeric structure comprising glucose linked together with β -(1 \rightarrow 4)-glucosidic bonds. Lignocellulosic biomass is a readily available resource with a total annual production by photosynthesis of $170\text{--}200 \cdot 10^9$ tons^[25,26].

After a comparison with amylase found in starch, which comprises a analog structure where the glucose units are linked together with α -(1 \rightarrow 4)-glucoside bonds, one should expect cellu-

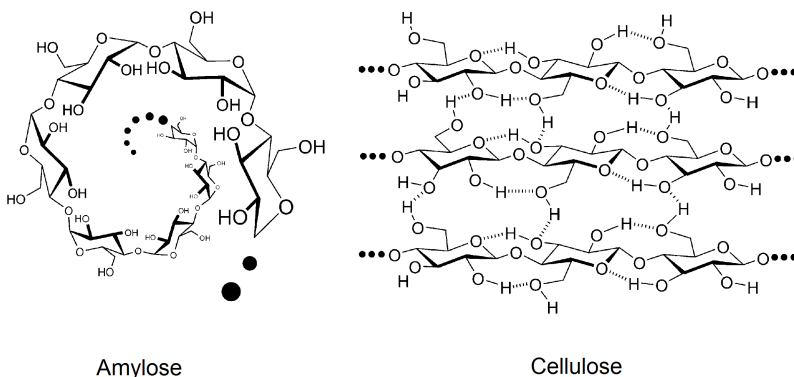


Figure 1.4.: Schematic structures of amylose and cellulose^[24].

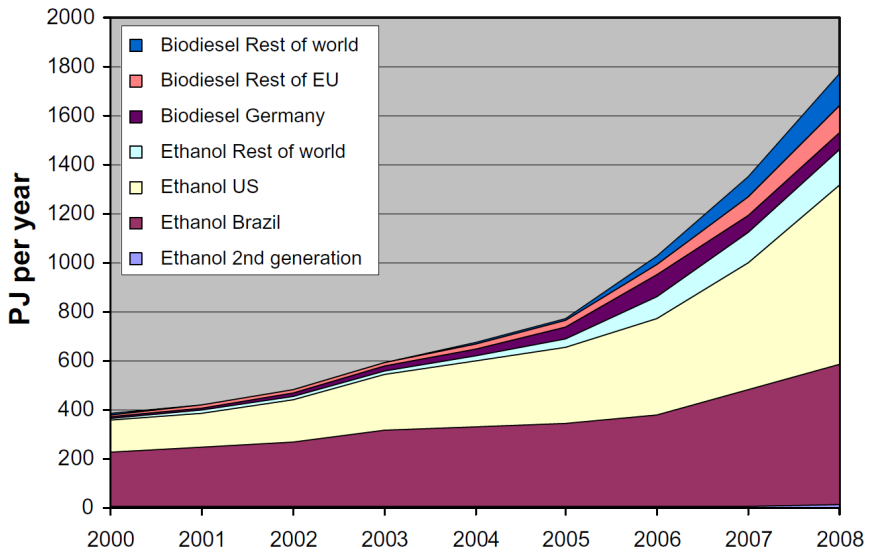


Figure 1.5.: Shows the global production of biofuels^[27]

lose and starch to have very similar properties, see figure 1.4 on the preceding page. However, while the α -(1 \rightarrow 4)-glucosidic bonds make structure starch amorphous and easy soluble in water and thus easy hydrolyzable by both enzymes and acid, the β -(1 \rightarrow 4)-glucosidic results in a very stable well-organized crystalline structure. Thus cellulose appears in indigestible crystalline fibers that are very resistant towards both acidic and enzymatic hydrolysis. This makes the utilization of the of lignocellulosic biomass very challenging from a technical point of view and a lot of technological improvements is required in order to make second generation biofuels profitable. Today the contribution from second generation bioethanol is negligible from an economic point of view, see figure figure 1.5. Further it should be noticed that second generation biofuels produced with the present technologies, are neither very sustainable nor green as they even with the newest generations of enzymes still requires an aggressive acidic pretreatment of the biomass^[28,29]. In a review by Rinaldi et al. it is shown that production of 1 kg ethanol from wood produces around 40 kg of waste. And as Rinaldi et al. point out, that even though the majority of this waste is contaminated water, it will require significant amounts of resources to remove the contaminants bringing it back to a drinkable quality^[26]. This points towards a general problem for the development of second generation biofuels: As the ethical challenges decreases significantly they seem almost inverse proportional to the technical challenges, and significant breakthroughs are required to make the second generation biofuels sustainable in both an environmental and commercial sense.

1.3. Ionic Liquids for lignocellulose dissolution

Ionic liquid is a group of salts that melts at lower temperatures^c, typically comprising a bulky organic cation and a smaller inorganic anion. They appear as very tunable solvents and a very wide range of properties can be achieved by combining different types of cat- and anions. Further they exhibit the quite unique properties that they have no or negligible vapor pressure. In 2002 Rogers and co-workers published a paper with an interesting discovery: Some ionic liquids could dissolve cellulose in rather high amounts^[30]. This property has been assigned to the very strong hydrogen bond accepting properties that especially halides, carboxylates and formates possess in the anhydrous environments of the ionic liquids^[31,32]. Thus the dissolution happens as the anions are able to break up the crystalline structure of the cellulose crystals. When cellulose is dissolved the glucoside bonds of the become very exposed and can easily be hydrolyzed in by acidic catalysts. The cellulose can also be precipitated from the ionic liquid by addition of small amounts of water, yielding amorphous cellulose, which is significantly easier to hydrolyze enzymatically even in aqueous slurry. This pretreatment could offer a competitive alternative to the present used acidic pretreatments used in second generation ethanol plants. Recent techno-economic studies have suggested that this procedure might become a commercially attractive alternative in the future^[33,34].

1.4. The furanic platform

Even though ethanol is the bioderived chemical that of today are of the greatest economic importance, it is only one out of many important chemicals that can be derived from biomass. The general use of ethanol as a substitute for oil is limited as it can mainly be used as a gasoline substitute. In 2004 the US Department of Energy (DOE) listed a top ten comprising the most important chemicals derived from biomass. Especially the chemical 5-hydroxymethylfurfural (HMF) was identified as one of the most important future biomass derived chemicals^[8,35-38]. HMF are produced by triple dehydration of C-6 sugars, and thus it can also be produced from cellulose. HMF are the precursor for a broad range of important chemicals which are much more valuable than ethanol, see figure 1.6 on the next page. Of greatest present value is the the 2,5-furandicarboxylic acid (FDA) that can replace terephthalic acid in the production of important polyesters like polyethylene terephthalate (PET) used in synthetic fibers and containers for beverage and food. But HMF are also likely to play an important role in as precursor for high quality fuels, as it can be hydrogenated into 2,5-dimethylfuran (DMF)^[39,40]:

^cTypically the limit is set at 100 °C

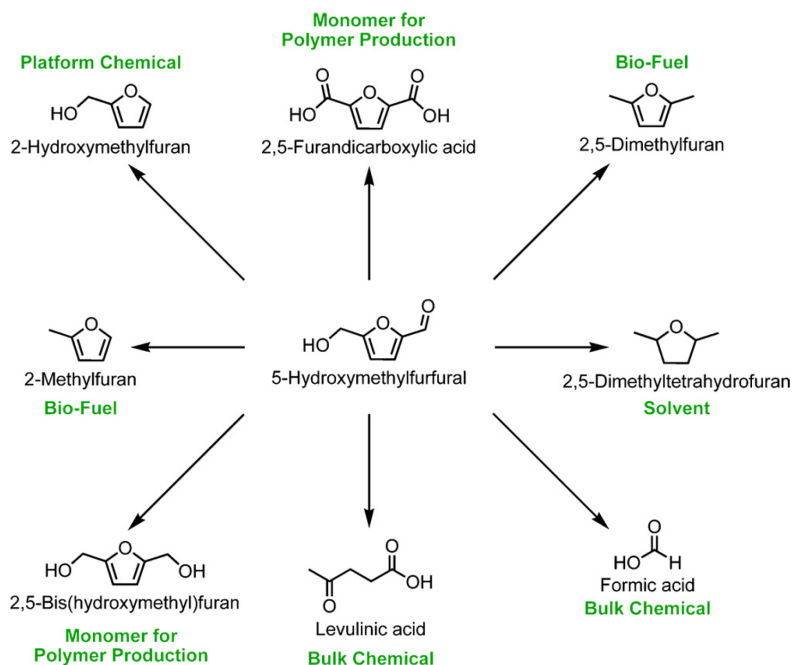
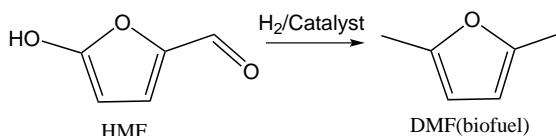


Figure 1.6.: The furanic platform: A broad range of valuable chemicals, fuels and solvents are easily obtained from platform chemical 5-hydroxymethylfurfural (HMF) [35].



DMF is considered a high quality biofuel. Due to a very low oxygen content the energy density is close to gasoline. Further it has a higher octane number, is non-hydroscopic and delivers a cleaner exhaust compared to ethanol/gasoline blends with a lower content of unburned hydrocarbons and NO_x [41–43].

Technologies are already commercially available to produce HMF from fructose, especially for making PET substitutes mainly for beverage bottles [44–47]. These present pioneering technologies are indeed very important as they serve as a springboard for later technologies. However, the present methods for HMF production can hardly be considered as sustainable in the longer term, due to the problems described in section 1.1 on page 4, as both fructose and glucose are far from unlimited resources. Therefore the goal must be to replace these initial technologies with methods that allow the production of HMF from cheap non-eatable lignocellulosic

biomass. However, as explained earlier it is very challenging to utilize the sugars contained in cellulose, and this field are far from a commercial level.

1.5. Outline of the thesis

The thesis will be focusing on combining ionic liquids abilities to dissolve lignocellulosic biomass with efficient catalysts that can convert the cellulose into sugars and HMF. A lot of catalysts has been screened and investigated in ionic liquids the past years, however there seem to be a lack of focus on the understanding of the catalytic processes themselves, which seem rather different compared similar to processes in water and other traditional solvents.

The thesis will approach this challenge through in-situ investigations using especially Fourier Transform Infrared (FTIR) spectroscopy. In chapter 2 the hydrolysis of the glucoside bond in ionic liquids, using Sulfuric acid, solid Brønsted acids and chromium(III)chloride catalysts, will be investigated. This chapter will also include the studies of the simultaneously HMF formation.

Chapter 3 will focus on the chromium chloride catalysts that are among the most promising catalyst for selective production of HMF in ionic liquids^[48]. The recent years there has been quite a intense controversy in the literature concerning these chromium catalysts^[48-55]. Some of this controversy seem to originate from insufficient understanding of these catalytic systems. Chapter 3 will focus on the kinetics of the last steps where glucose is isomerized to fructose and then dehydrated to yield HMF.

In-situ Investigation of Cellulose Hydrolysis in Ionic Liquids

This chapter will focus on the mechanistic and kinetic understanding of the acid catalyzed hydrolysis of cellulose in ionic liquids. Aspects and opinions from the literature will be presented and discussed in relation to experimental results from a kinetic study using an unconventional approach based on a new ATR-FTIR methodology. This chapter will also serve as documentation of this new in-situ ATR-FTIR methodology

Processes involving saccharification of lignocellulosic biomass through hydrolysis of cellulose, is a field that has been studied intensively during the last century^[56-58]. There are several types of catalysts that can catalyze the hydrolysis of poly- and disaccharides including cellulose. This results in several possible variations of the mechanism for cellulose hydrolysis depending on the type of catalyst. Typical catalyst types include Brønsted acids^[59-63], Lewis acids^[64-68] and enzymes^[69,70]. Further the forms of cellulose investigated are very different and includes: Raw lignocellulosic biomass as wood and straw^[60,67], micro crystalline cellulose^[71], pretreated/amorphous cellulose and cellulose models such as cellobiose^[72] and various D-glucospyranosides^[61-63]. As it will be shown later in this chapter the solvent also seems to have a significant impact on the results from these studies. The literature of cellulose hydrolysis is quite immense and very heterogeneous, and care should be taken when comparing results across this very wide field of research.

The mechanism of hydrolysis of cellulose and other poly- and disaccharides in water has been studied extensively and especially the older literature, is very rich in detailed and fundamental kinetic and mechanistic studies^[61-63,73,74]. Ionic liquids are as mentioned very interesting, as some of them are able to dissolve cellulose and thereby make the glucoside bonds, that are normally protected within the crystalline structure, available to hydrolysis. However, there are starting to emerge a few but meticulous studies of the kinetics of cellulose hydrolysis in ionic

liquids. With the results from these studies it seems likely that the ionic liquid does more than just to ease the access to the glucoside bond by dissolution of the cellulose^[26,60,75]. However, very little is yet known about the kinetics and the actual mechanistic details for the cellulose hydrolysis in ionic liquids. During my Ph.D. studies I have investigated the reaction kinetics during hydrolysis of the glucoside bond in ionic liquids, using a new methodology based on *in-situ* ATR-FTIR spectroscopy.

In the following introductory section the aim will not be to give an extensive review comprising the complete field of cellulose hydrolysis. Instead focus will be brought to the mechanistic and kinetic aspects relevant to understand the cellulose hydrolysis in ionic liquids and thus aid the understanding of the later experimental results presented in this chapter.

2.1. Introduction to cellulose hydrolysis

At figure 2.1 on the next page a schematic drawing shows the mechanism of Brønsted acid catalyzed cellulose hydrolysis. In the first step an equilibrium is reached resulting in a small fraction of protonated glucoside bonds. The glucoside bond is a poor base and in general only strong acids will protonate it. The next step, is widely considered to be the rate determining step, here the protonated glucoside bond is cleaved and releases the non-reducing end, and leaves the reducing end as a positive charged carbenium ion. The carbenium ion is stabilized by donating some of the positive charge to the adjacent oxygen atom thereby creating a oxocarbenium species forced into an halfchair conformation^[62,63,73,74,76]. In the final steps the oxocarbenium species is hydrated, to create the final product and release the proton. This step is considered fast and makes the rate independent on the water concentration^[60,75]. Thus the rate only depends on the concentration of glucan and acid. The factors affecting the formation and stabilization of the oxocarbenium species are therefore the keys to understand the mechanisms of the glucoside bond hydrolysis.

The acid catalyzed hydrolysis of the glucoside bond in water is a relatively slow process with an activation energy around 130 kJ/mol. Several authors have investigated the hydrolysis of glycoside bonds in water through models such as D-glucopyranosides and disaccharides^[62,63,74]. In these studies it is observed that the activation energies of the hydrolysis over a variety of glycosidic bonds are quite similar, and are typically all found in the range of 130 to 140 kJ/mol for various C-6 disaccharides. Often it is implied that the apparent high stability of cellulose compared to e.g. starch, comes from a higher chemical resistance towards hydrolysis - however this is not exactly true. In general the α configuration is actually slightly harder to hydrolyze than β configuration, thus the activation energy for hydrolysis of maltose is around 5 kJ/mol higher than for cellobiose^[63,77]. However, this relatively small difference suggests

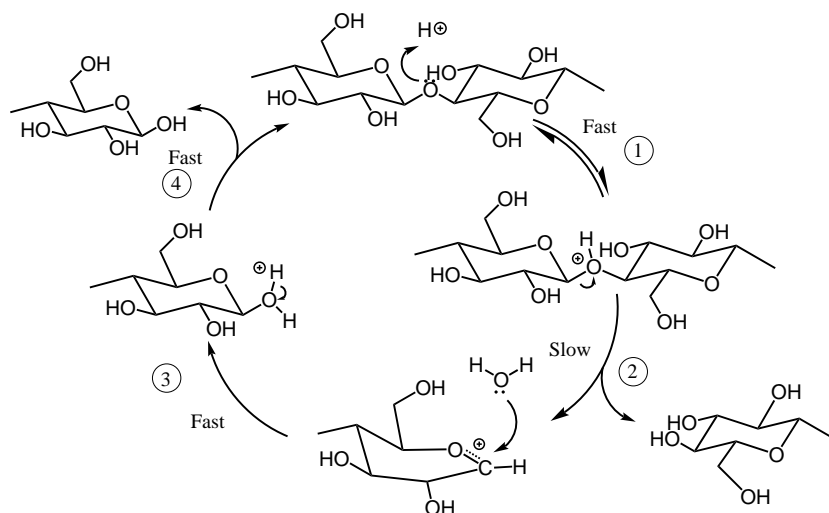


Figure 2.1.: Schematic illustration of mechanism for Brønsted acid catalyzed cellulose hydrolysis.

that the transition states to hydrolysis of the different glucospyranosides are very similar, and emphasizes that the apparent high stability of cellulose does not originate from a higher stability of the glycoside bond itself, but from its insoluble nature.

The only common disaccharide which is significantly easier to hydrolyze is sucrose (around 110 kJ/mol in water^[77,78]). This has been suggested to be due to the furanic oxocarbenium ions of fructose having significantly lower energies than the pyranose analogs.

A very important point made by Vernon^[73] is that in the high energy of the reaction barrier cannot alone be understood, merely as a consequence of the unfavorable positive charge on the oxocarbenium species. The pyranose ring has to make a quite drastic conformational change in order to form the oxocarbenium ion where the preferred planar configuration around the positive $C=O^+$ group is prevented due to the pyranose ring structure. Thus a lot of strain is introduced into the pyranose structure. This conformational addition to the reaction barrier is exemplified very well by comparing the activation energies of cellobiose hydrolysis of around 130 kJ/mol with the corresponding activation energy of simple acetals that are typically only around 50-60 kJ/mol^[79]. This clearly points out how huge a part of the reaction barrier energy that comes from conformational consequences due to the pyranose ring.

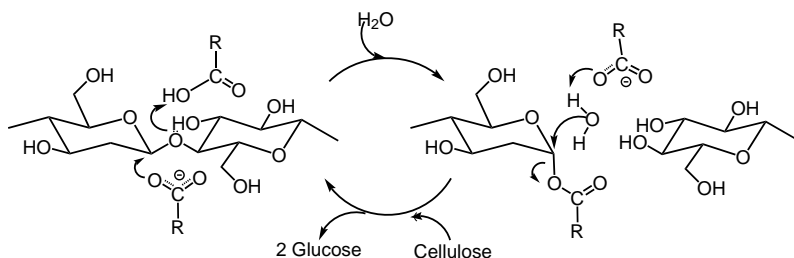


Figure 2.2.: Schematic illustration of mechanism for enzyme catalyzed cellulose hydrolysis. It is shown how the acid and base pair of the cellulase site work together during the attack on the glucoside bond.

2.1.1. Enzymatic hydrolysis of cellulose

Enzymatic hydrolysis is a very sophisticated process. The active center of a cellulase enzyme contains of a carboxylic acid and a base, typically an deprotonated amino acid group^[69,70,80–82]. In figure 2.2 a typical enzyme catalyzed hydrolysis mechanism is shown. The carboxylic acid attacks the glucoside bond with its proton and simultaneously the base approaches the C1 position on cellulose^[69,70,81]. Despite the much lower acidity of the proton in cellulases, the simultaneous base attack on C-1 makes the cleavage of the glucoside bond possible as the high-energy transition state, involving the half-chair oxocarbenium ion, is stabilized and in some cases perhaps completely avoided. There is very large difference between the various cellulases. Some of the cellulases still are still associated with fairly high activation energies at around 70 kJ/mol or even more^[80,83], while some of the enzymes obtained from arctic cold water bacteria have activation energies as low as 13-20 kJ/mol^[84] while a typical range is around 20-45 kJ/mol^[85,86].

Another advantage of the enzymes is that they are very selective towards glucose. Strong acids will degrade the formed glucose, as they also catalyzes a series of isomerization, dehydration, and condensation reactions yielding a lot of unwanted degradation products. Even though there are examples suggesting successful combination of ionic liquids with weaker coordinating anions and enzymes^[87,88], the strong basic anions that enables the dissolution cellulose, like eg. chloride or acetate^[30,32], tend to denature the enzymes and thus the activity will be lost or strongly reduced^[89,90]. In other words the combination of high amounts of dissolved cellulose in ionic liquids hydrolyzed by efficient cellulases are simply not likely, because it is the same hydrogen bond forming properties of the anion wanted for the cellulose dissolution, that makes the ionic liquids very aggressive towards the complex macro structures of the enzymes. However, as it will be discussed later there is a lot of inspiration found in the cellulases when understanding the hydrolysis of cellulose ion ionic liquids.

2.1.2. Can simple catalysts mimic enzymatic hydrolysis?

It is hard to believe that activation energies of 13kJ/mol of the arctic cellulases compared to the activation energy of 130 kJ/mol of the Brønsted acids describes the same reaction, just in presence of two different catalysts, that are even working under related mechanisms. This large gap tells that there is an obvious room for improvement in the design or engineering of new catalysts, that works smarter than the simple mineral acids.

Using stronger acids will have a positive influence on the rate as the concentration of protonated glucoside bonds will increase^[26,60]. However, the protonation is not the rate limiting step and will have no influence on the reaction barrier itself. Often water will be present in rather high concentration compared to the acid catalyst, in practice limiting the strongest acid species to the H_3O^+ ions anyway. Further an increase of the actual acid strength could cause increased formation unwanted byproducts^[75].

There has been very little focus on improving the catalyst by engineering the way the catalyst works. To realize this approach a much better and more detailed understanding of the mechanism will be needed. But there actually are a few very interesting examples in the literature, of simple catalysts that demonstrates that it is possible to find catalytic pathways, with lower reaction barriers.

Weaker acids like acetic acid will normally not show any activity towards cellulose hydrolysis, as they can simply not protonate the glucoside bond^[75]. However, Moiser et al. showed that the dicarboxylic acids maleric and succinic acids actually exhibited surprisingly good activity for both cellobiose and cellulose hydrolysis in water^[91,92]. Actually the group showed that maleric acid was slightly more active at 175 °C than sulfuric acid^a. Succinic acid also showed high activity but was slightly less active than the two others. This was very remarkably as the maleic and succinic acids only have pK_a values of the first proton of respectively 1.9 and 4.2 (In comparison the H_3O^+ ion has a pK_a value of -1.74). The dicarboxylic acids further showed significantly higher glucose yields due lower glucose degradation. They tried to determine the activation energies, but they were unfortunate not so reliable and thus could be compared with literature values (standard deviations up to 39 kJ/mol). vom Stein et al. found similar results in a recent study with oxalic acid as catalyst in aqueous high salt content solutions^[93]. The low pK_a values of the acids used in those studies, should result in so low concentrations of the protonated glucoside bond that the cellulose hydrolysis would practically not occur. It suggests that the dicarboxylic acids did not only act as proton donors, but suggested that the carboxylate groups could act in a cellulase like manner and stabilize the oxocarbenium ions^[93].

^aBoth maleric acid and sulfuric acid were used in concentrations of 50 mM/L under identical conditions.

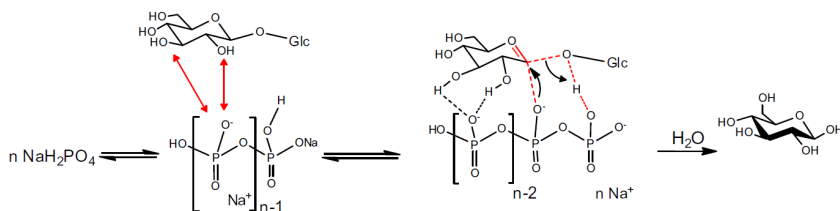


Figure 2.3.: Reaction mechanism proposed by Charmot and Katz^[94] that shows the cellulase like role of hydrogenphosphate existing in aqueous NaH_2PO_4 buffer solution.

An even more surprising result was reported by Charmot and Katz^[94]. By coincidence they found that a NaH_2PO_4 buffer solution had unexpected high activity towards cellobiose hydrolysis at 90 °C. This was highly unexpected as the buffer solution was only slightly acidic with a pH at 4. Their control experiments further emphasized the importance of their results: H_3PO_4 did not show any hydrolysis activity at all and HCl only showed very little hydrolysis activity compared to the NaH_2PO_4 buffer system. They determined accurate activation energies as low as 59 and 74 kJ/mol for cellobiose and maltose respectively. These values are only around the half of the values for activation energies reported in numerous other studies^[62,63,73,74,77], and is to my knowledgeable by far the lowest trustworthy non-enzymatic activation energies reported in the literature.

They proposed a mechanism for the hydrolysis process, which is reproduced in figure 2.3. The mechanism is based on catalytically active hydrogen phosphate oligomeric species formed in the buffer solution, that act very much like the cellulases, for comparison see also figure 2.2 on page 14. This gives a reasonable explanation for the unexpected low reaction barrier, and tells that there really is a great potential for designing new catalysts for cellulose hydrolysis. However, there does not need to be formed oligomers before a cellulase like attack can occur, and thus it is likely that the catalytic activity may have been caused simply by H_2PO_4^- and HPO_4^{2-} species. A comparison between the study of Charmot et al. and the three before mentioned studies with the dicarboxylic acids, also suggests an important point: A basic site should be available to stabilize the oxocarbenium ion during reaction as shown in figure 2.3. In studies of Moiser et al. and vom Stein. et al. no basic group was present in higher concentrations and thus much lower activities were observed^[91-93]. It is very likely that the limiting factor in the system was not the acidity, but the low amount of carboxylate groups. This can also explain why maleric acid was so much more active than the others: Not only did the lower pK_a of maleric acid result in a higher H_3O^+ concentration, but equally important also in a higher carboxylate concentration. This also explained why the pure dicarboxylic acids in ionic liquids exhibit poor catalytic properties, as they will exclusively exist in the acidic form^[26,60,75]. However, the catalytic activity in ionic liquids of the analogous monobasic salts, would indeed be very interesting to study. I have synthesized a series of these catalyst where one of the

protons has been exchanged with a [BMIM] cation. Unfortunately time has not allowed for the catalytic testing of those systems, but will hopefully be the objective for future research.

2.1.3. Experimental Challenges of the Cellulose hydrolysis

A lot of insight in the mechanism of hydrolysis of cellulose is gained from working with model systems such as cellobiose or simple glucopyranosides. Various factors have been investigated by measuring numerous of activation energies and performing isotope exchange experiments on these systems^[62,63,73,76,77]. However, the catalytic investigations on real lignocellulosic biomass or more realistic model systems, such as micro-crystalline cellulose or pretreated cellulose, are from an experimental point of view much more complicated. One quite simple method is to just measure the amounts of soluble sugars and oligomers produced by hydrolysis e.g. by High Performance Liquid Chromatography (HPLC). This method works fairly well in water on untreated crystalline cellulose as the reaction is very heterogeneous and mostly occurs on the surface of the cellulose fibers. However if amorphous cellulose is used, or especially if the cellulose is dissolved in ionic liquids, the reaction will happen all along the cellulose chains and the amount of water soluble products will only account for a fraction of the total amount of hydrolysis products^[26,95]. Thus the neglect of the partly hydrolyzed cellulose and insoluble oligomers can result in a significant underestimation of the actual reaction rate.

A more accurate measure for the rate of hydrolysis is obtainable if knowledge about the degree of polymerization is included in the calculation of the rate. The most common and straight forward method to determine the degree of depolymerization, which can be done by measuring the total amount of reducing sugars: All the cellulose oligomers, independent of length, will comprise one glucose unit that can convert into the open aldehyde form, see figure 2.4 on the following page (a). This aldehyde can be oxidized selectively using Cu(II), where after reduced copper in form of the Cu(I)-2,2-bicinchoninate complex can be detected quantitatively by UV-Vis spectroscopy^[96-98]. Another way to measure the reducing sugars is by using dinitrosalicylic acid that can also be detected by UV-Vis spectroscopy^[99].

The degree of polymerization can also be determined by gel-permeation chromatography that measures the distribution of molecular weights^[26,100-103]. The partly hydrolyzed cellulose is prior to analysis made soluble in DMSO by derivatization. An often used derivative is to make the tricarbonyl of cellulose by reaction with phenyl isocyanate, see figure 2.4 on the next page. This treatment does not affect the degree of polymerization and the method is considered to be very accurate, but requires a lot of analysis work and specialized and expensive equipment.

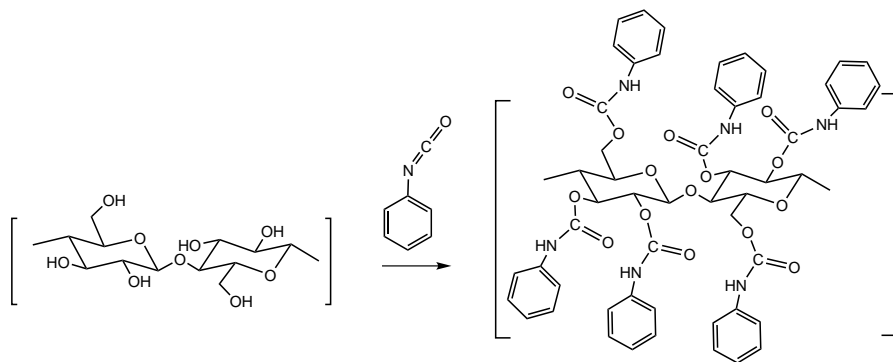
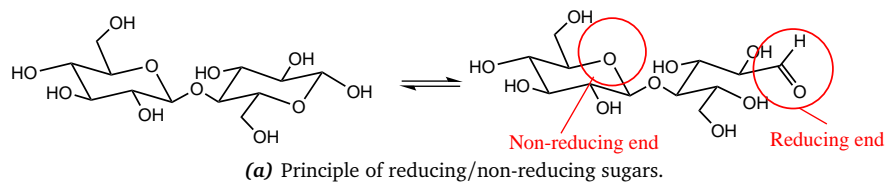


Figure 2.4.: (a) Example showing reducing and non-reducing ends of cellobiose. (b) Formation of DMSO soluble cellulose tricarbanilate.

In ionic liquids the cellulose depolymerization has also been followed by monitoring the drop in viscosity during reaction^[60,104]. However, this method is not general applicable as the viscosity is a function of other factors than just the degree of polymerization of the dissolved cellulose, namely the temperature which makes it useless in determining activation energies of the reaction.

2.1.4. Cellulose Hydrolysis in Ionic Liquids

Since the cellulose was first reported soluble in ionic liquids by Swatloski^[30], the research on the cellulose hydrolysis in ionic liquids has been very intensive. In the recent years several review papers have summed up the work and progress in this field^[25,105,106]. However, most of the studies have so far focused on the product distribution after a given time of cellulose hydrolysis and kinetic investigations are rarely performed. As very different types of reaction conditions are often used it is hard to compare the results of these studies. This lack of articles concerned with a more systematically kinetic approach to cellulose hydrolysis, is likely due to the mentioned high experimental workload and difficulties associated with the determination of the hydrolysis rates. To my knowledge only three groups have determined activation energies of the hydrolysis in ionic liquids^[26,60,75,107]. These groups all use different methods for analysis and calculation of reaction rates which results in some dispersion of the

found activation energies, however all three articles show that the activation energies found are remarkably lower than the ones earlier reported in water.

In the most recent studies by Dee and Bell, they include contributions from cellulose oligomers, glucose, cellobiose and degradation products such as HMF when calculating the reaction rates. Their studies result in activation energies for the hydrolysis of both Avicel cellulose and pre-treated *Miscanthis* cellulose at around 95 kJ/mol^[75,107]. The indirect contribution to the rate of hydrolysis, lost due to the side reactions leading to humin formation is not incorporated into their hydrolysis rates. They found that the initial rate of hydrolysis itself showed a first order dependency on acid concentration and on the concentration of glucans, but was independent of the water concentration. Judging from their supplementary material the rates used for calculation of the activation energies were the initial pseudo-zero order rates, which are often used in practice to estimate reaction rates^[95,108,109].

Vanoye et al. also discussed different ways of analyzing samples and chose only to use the soluble sugars measurable by HPLC, which in their opinion was the most reliable method. However, most of the oligomers are not soluble in water and would have been filtered off before analysis, thereby their contribution to the reaction rate is neglected. Rates were estimated as first order rates, which in principle are the most correct way to do it but it's clear from their supplementary material that significant glucose degradation occurs within the time of reaction used to calculate the rate. Thus the use of first order rates under the assumption that the formed glucose is stable was most likely contributing to an underestimation of the hydrolysis rates. They found the activation energies for cellulose and cellobiose to be 111±12 kJ/mol and 102±kJ/mol respectively.

Dee and Bell also argues that Vanoye et. al, among others underestimate the reaction rates and thus are reporting activation energies that are slightly to high. On the basis of the data supplied by Vanoye et. Al, Dee and Bell recalculates the activation energies to 92 and 84 kJ/mol for cellulose and cellobiose respectively^[60,75].

Rinaldi et al. reports an activation energy of 108±5 kJ/mol for hydrolysis of α -cellulose in the ionic liquid [BMIM]Cl. They do not supply an Arrhenius plot in the article, but only graphically shows the rate based on the number of scissions calculated from the average molecular weight. After an initiation period the apparent rates seem to follow pseudo zero order kinetics, as they use a very low amount of catalyst. The numbers of scission are calculated solely from the weight-averaged degree of polymerization found by gel-permeation chromatography of the cellulose. This method has shown to be very accurate to determine the degree of polymerization in cellulose. But by merely taking the degree of polymerization of cellulose into account

and neglecting the other product such as e.g. HMF, they most probable underestimates the rates.

Although the ways of measuring and calculating the activation energies deviate in these studies, it is noticeable that all activation energies are significant lower in ionic liquids compared to the ones reported in water. Lowering the activation energy by around 20-40 kJ/mol will have enormous impact on the apparent kinetics. This phenomenon is not discussed much in the literature even though this aspect of the ionic liquids, seems to be just as exciting as their ability to dissolve the cellulose. Not any of the authors who reported these lower activation energies comes with any detailed mechanistic suggestions to why the kinetics differs so much from the ones found in water.

In a very recent study by Phan et al.^[110] the effect of the anions during hydrolysis of methyl α - and β -D-glucopyranosides in water with five different strong acids was investigated. They showed that even though the proton activity was identical, over a range of strong acids in water, they observed a strong rate dependency of the different acid types. They could correlate this difference to the anions of acids. Further they observed an increasing positive anion effect on the hydrolysis rate when they mixed in 1,4-dioxane thereby lowering the solvation of the anions in the water. They suggested that the chloride and bromine anions directly participate in the hydrolysis via. stabilization of the charged transition state.

Vanoye et al. reported a bisection of the rate of cellobiose hydrolysis in [EMIM]Cl when increasing the water concentration from around 3 mol/L to 6 mol/L^[60]. In water-poor ionic liquids the properties of anions such as halides and carboxylates are very different compared to the ions are surrounded by a coordination sphere of water^[32]. Therefore it seems very likely that such anions could stabilize the oxocarbenium species during the hydrolysis thereby lowering the activation energy significantly.

2.2. Developing a new Method for *In-situ* Monitoring Cellulose Hydrolysis

As described in the previous section the ionic liquids them selves could have some co-catalyzing effect on the hydrolysis of cellulose, by stabilizing transition states and high energy intermediates. It seems that the reason why this area is so poorly investigated is because none of the present methods for analyzing the cellulose hydrolysis are very optimal. Either they are very time consuming or requires very expensive laboratory equipment, and the lack of better methods seem to be a main bottleneck for more research in the field. Further would more efficient methods to measure rates, also allow for more efficient catalyst screening.

In the following a new method will be presented for measuring rates during cellulose hydrolysis in ionic liquids. The idea behind this method is that the glucoside bond should have a couple of characteristic group vibrations that are exclusively associated with the glucoside bond. These can then be monitored in-situ during the reaction. As infrared spectroscopy obey Lambert-Beers equation, the band of such group vibrations would be proportional to the concentration of glucoside bonds. This means that by knowing where the group vibrations of the glucoside bond are, and by separating them from other bands in the spectra it should be possible to monitor the hydrolysis of cellulose in-situ. A method directly measuring the concentration of the glucoside bond would not be dependent on the solubility of the products in water, on glucose degradation, humin formation but would solely give information of the hydrolysis rate of the glucoside bond.

2.2.1. Identifying the True Group Vibrations of the Glucoside Bond

The group vibrations of smaller molecules such as water or CO₂ are often used as textbook examples of the typical vibration type in vibrational spectroscopy^[111-113]. However, moving away from the simple textbook examples towards bigger complex molecules like cellulose one should be careful to interpret all the bands merely as simple group vibrations. A lot of the vibrational modes in larger molecules comprises very mixed types of deformations that occurs simultaneously at places all over the molecule. Several of these mixed modes do not at all resemble the simple and ideal isolated bending or stretching modes from the ideal textbook examples.

Comparing the drawn structures of glucose and cellulose it would at first seem reasonable that the only difference in the infrared spectra, would be the few vibrations related to the two extra OH groups of glucose instead of a few vibrations related the glucoside bond. If this was true the spectra of cellulose and glucose would be very easy to distinguish. Unfortunately this is not the case and the difference in the vibrational spectra is far more complicated. Thus great care must be taken in the interpretation of the spectra of the real reaction mixtures during hydrolysis, as they would consist of very complex, heterogeneous mixtures of cellulose, oligomers, glucose and various by- and degradation products.

When "polymerizing" glucose to cellulose acetal groups are formed and bond lengths at and around the acetal group changes, see figure 2.5 on the following page. The result is, that even though similar modes are found in the spectra of both the monomer and polymers, some bands slightly shift position due to new bond lengths and several modes either increase or decrease in intensity. Both the shifting and change of IR activity of the vibrational modes of the acetal group and its neighbor bonds, results in two quite different spectra. With several changes in

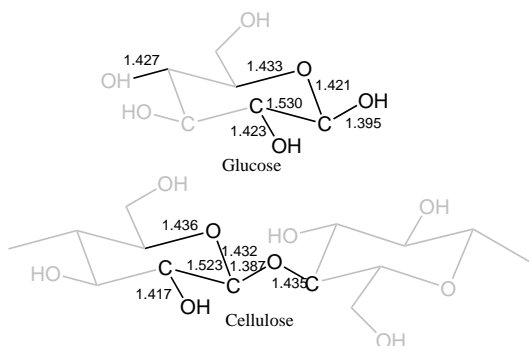


Figure 2.5.: Calculated bond lengths in glucose and cellulose (inner glucoside bond of cellotepentose).

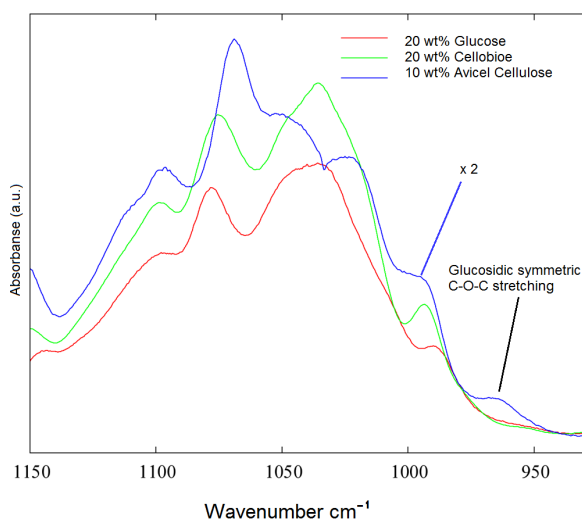


Figure 2.6.: Transmission difference spectra of 20 wt% glucose, 20 wt% cellobiose and 10 wt% cellulose dissolved in [BMIM]Cl with spectra of [BMIM]Cl subtracted. Intensity of difference spectra of cellulose is normalized by multiplying with 2. Spectra was measured on neat liquid 10 μm films using a sandwich cell with AgCl windows on a Perkin-Elmer paragon 1000 instrument.

the spectrum after polymerization, it makes it very challenging to actually identify the group vibrations of the glucoside band.

To increase the understanding of the experimental FTIR spectra, the theoretical infrared spectra were calculated using density functional theory (DFT)^b. Then analysis of the vibrational modes was performed and the spectra compared with the experimental transmission FTIR

^bCellobiose and cellotriose structure initially was optimized then a vibrational spectrum was calculated using gaussian09^[114] B3LYP/6-311+G(d,p). Spectra were scaled with an factor of 0.983

spectra of cellulose, cellobiose and glucose and their solutions in [BMIM]Cl. The initial experimental spectra showed that there was a band present at 970 cm^{-1} in cellulose solutions, that was not found in the solutions of glucose or cellobiose, see figure 2.6 on the preceding page. From the analysis of the calculated spectra it was predicted that the glucoside bond of cellobiose had a symmetric stretching vibration (in the following denoted $\nu_{sym,C-O-C}$) at 965 cm^{-1} , however it had a very low infrared activity, probably as a consequence of the symmetric structure of cellobiose. Apart from the stretching of the glucoside bond the OH groups in the O1 and O4 positions respectively, were contributing to this mode by bending; thereby it seemed that the overall change in dipole moment during the vibration was canceled out yielding in a low infrared activity (IR).

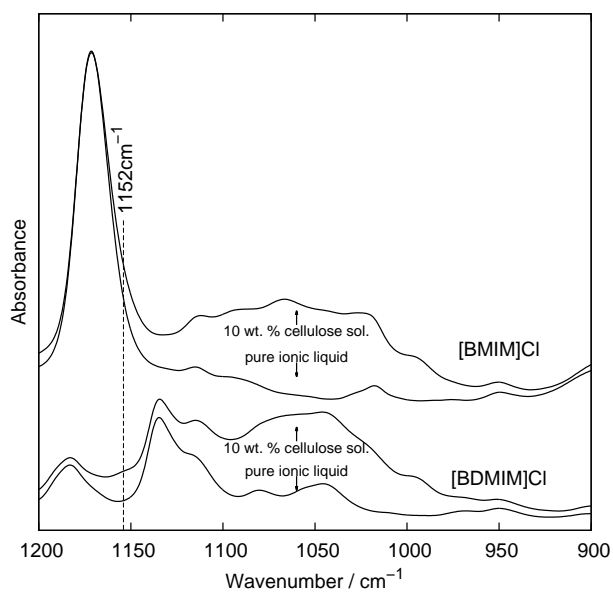
When calculating the spectrum for cellotriose, the relative IR activity of the $\nu_{sym,C-O-C}$ mode however increased significantly. This offered an explanation why the band was clearly visible in the spectrum of cellulose but not in cellobiose. Even though the $\nu_{sym,C-O-C}$ band was detectable in a 10 wt.% [BMIM]Cl solution of cellulose, the intensity was still low. After the first attempts to quantify this band during in-situ monitoring of the hydrolysis, it unfortunately became clear that the intensity of the $\nu_{sym,C-O-C}$ band at 970 cm^{-1} was too low and unsuitable for quantitative use.

More theoretical investigations of the infrared spectra of cellulose oligomers were performed through calculations of the spectra of cellotetraose and cellopentaose. A relatively large difference was observed in the calculated spectra of glucose, cellobiose, and cellotriose. But beyond cellotriose it seemed like the number of glucose units "converged" towards a more general representation of cellulose where the addition of extra glucose units did not impact the calculated spectra significantly. This was also found to be the case for the experimental spectra. All the calculated spectra along with experimental spectra of glucose, cellobiose and cellulose and some of its oligomers can be found in appendix: see figure B.1 on page 114 and figure B.2 on page 115.

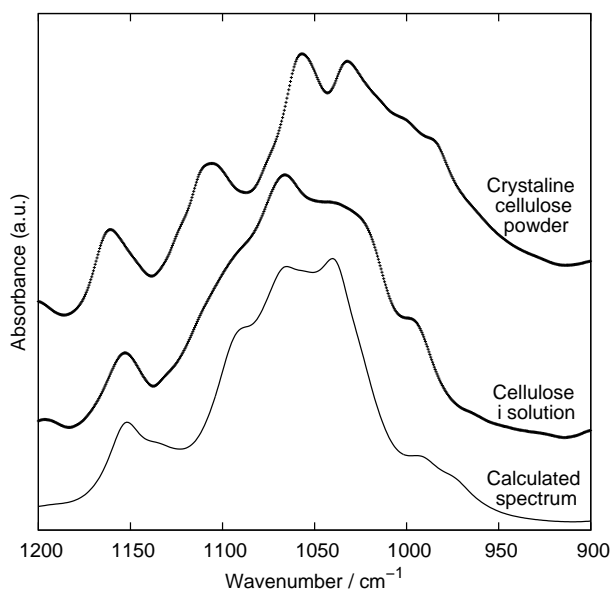
The glucosidic antisymmetric C-O-C stretching band at around 1155 cm^{-1} (denoted $\nu_{asym,C-O-C}$) was predicted to be quite intense in all the calculated spectra and seemed to be a better choice for quantitative analysis of the glucoside bond^c. The calculated spectrum showed some resemblance with the recorded spectrum of micro-crystalline Avicel cellulose powder, but the crystallinity seemed to introduce some difference, see figure 2.7(b) on the following page. Therefore a spectrum of 10 wt.% cellulose in [BMIM]Cl was recorded. However, the $\nu_{asym,C-O-C}$ 1155 cm^{-1} band of cellulose could not be resolved in solution of [BMIM]Cl, due to overlap with a very intense bending mode of the C2-H proton in [BMIM]Cl^d, see figure 2.7(a) on the following page. As this band shifted and broadened slightly during dissolution of cellu-

^cThe approximate $\nu_{asym,C-O-C}$ mode is shown among other selected modes at figure 2.8 on page 26. A representation of the detailed $\nu_{asym,C-O-C}$ mode can be found in appendix, see figure B.7 on page 121.

^dThe vibration related to of the band 1172 cm^{-1} band of [BMIM]Cl was elucidated by DFT calculations and deuterium exchange experiments. See appendix figure B.3 on page 116 and experimental section for more information.



(a)



(b)

Figure 2.7.: **Top:** Showing corrected ATR-FTIR spectra of 10 wt.% cellulose solutions in [BMIM]Cl and [BDMIM]Cl and the pure ionic liquids at 120°C . **Bottom:** Experimental spectra compared to calculated spectra of cellotetraose. The top is solid microcrystalline Avicel cellulose powder. In the middle a difference spectrum showing 10 wt.% avicel cellulose in [BDMIM]Cl at 120°C , where a spectrum of the pure ionic liquid was subtracted.

lose, the difference spectrum would in most cases only show an intense s-curve shape around 1170cm^{-1} . This band was present in all common 1,3-alkylimidazolium ionic liquids and in the spectrum of the popular ionic liquid 1-ethyl-3-methyl-imidazolium chloride ([EMIM]Cl) this band was even more intense.

Instead solutions of cellulose in 1-butyl-2,3-dimethyl-imidazolium chloride was made (in the following denoted [BDMIM]Cl), see figure 2.7 on the preceding page. [BDMIM]Cl has very similar properties as [BMIM]Cl, the C2 proton is just substituted with a methyl group. As expected [BDMIM]Cl showed no strong absorptions around 1152cm^{-1} , and a high quality difference spectrum showing cellulose in solution could be obtained, see bottom of figure 2.7 on the facing page. When comparing to the calculated spectra of cellotetraose and cellopentaose they matched the spectrum of the dissolved cellulose very well, suggesting that the DFT simulation was actually able to describe the experimental spectrum very well.

The spectrum of glucose was investigated in a similar way. In water the β -pyranose form of glucose is known to be dominant, however it was not possible to find literature investigating this equilibrium in ionic liquids. Therefore several conformers of both the β and α isomers were optimized. The spectra of the most stable can be found in appendix, see figure B.5 on page 118. The simulated spectra showed some resemblance with the experimental, however the calculations systematically seemed to overestimate the position of the bands. The same tendency though less pronounced, was observed for cellobiose (Appendix: figure B.6 on page 119). It is hard to find literature that discuss the theoretical infrared spectra of glucose in any other forms than crystalline or aqueous^[115-117]. However, it seems likely that the lack of a solvent model induces this effect. In the longer cellulose oligomers this effect is probably less apparent as internal hydrogen bonds are allowed to be formed between the glucose units.

As earlier mentioned, the spectral difference of cellulose and glucose is more than just the exchange of two OH groups for a glucoside bond. The DFT calculation seemed very successfully to simulate the spectrum of cellulose, but less accurate for glucose. However, looking at some of the strong characteristic modes in the $950\text{-}1200\text{ cm}^{-1}$, shown at figure 2.8 on the next page, it is clear that the modes are very alike. It seems very complicated to give a detailed explanation why some of these modes seem to shift position, to gain or to lose intensity, but it seems quite obvious that it is the case. An important point to make out of this is, that even though some of these bands are much more intense than the glucoside $\nu_{\text{asym,C-O-C}}$ bands, they should not be used in the quantitative analysis during hydrolysis as the bands within the region of $1140\text{-}1000\text{ cm}^{-1}$ as both cellulose and glucose have intense bands dispersed all over this region. In such case the quantitative analysis would not give the isolated kinetics of the hydrolysis, but an unknown mixture of kinetics of the hydrolysis and the glucose conversion. Therefore the apparent bands in this region will very likely express an unknown mixture of

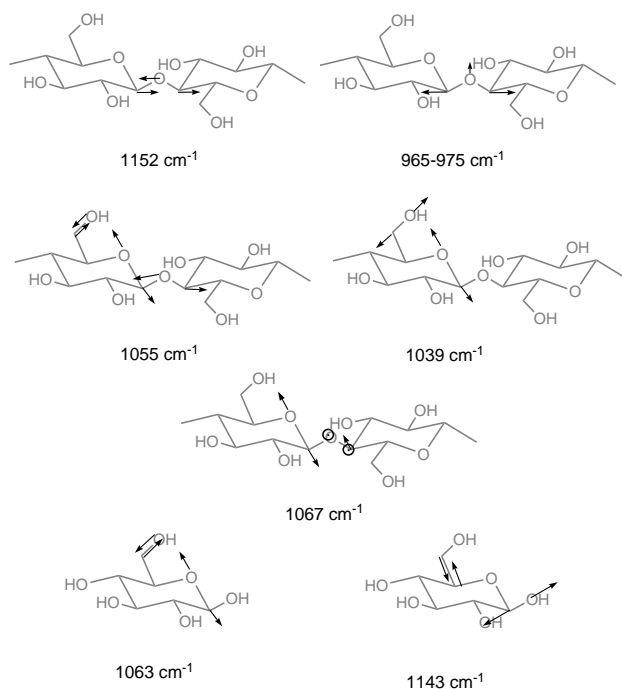


Figure 2.8.: Approximate representations of selected modes in cellulose and glucose. For reasons of clarity contributions from C-H and O-H bending are not shown, precise modes can be seen in appendix: see figures B.7-B.11 on pages 121-125

modes from both glucose and cellulose, and are therefore unsuited to discriminate between glucose and cellulose

2.2.2. The Glycoside Band in the Literature

Earlier spectroscopic identification of the glycoside bond has been the subject of a lot of studies^[118-130]. As early as in the 1960's Marchessault and Liang investigated infrared spectra of polysaccharides including cellulose, chitin and Xylan^[121-124]. They concluded that the vibrations of the glycoside bond was located at 1161 cm^{-1} in cellulose and at 1151 and 1165 cm^{-1} for chitin and xylan respectively. But this was questioned by Blackwell et al. in the 1970's as they argued that several of the mono-saccharides had bands very close to the band claimed to be the glycoside C-O stretching band by Marchessault and Liang^[125,126]. In this study I too observed that the C1-O1 stretching band of glucose indeed is close to the glycoside band of cellulose, with a position around 1135 - 1140 cm^{-1} in the deconvoluted spectra. The opinion of Blackwell, that the glycoside stretching band therefore not could be located around 1155 cm^{-1} , due to similarities with spectra of the mono saccharides, was dominant in the liter-

ature until the 1990's^[118,120]. However, Sekkal et al. recognized a band at around 1160 cm^{-1} to be characteristic of polysaccharides, a band they also reported present in the Raman spectra as a shoulder band, although they assigned a band at around 1090 cm^{-1} to be the glucoside stretching band in cellulose^[120].

In the late 1990's the group of Nikonenko developed a computer based deconvolution method that could sharpen the wide bands in the spectra of both mono- and polysaccharides that allowed for much better resolution of the rather broad bands in the $1600\text{-}800\text{ cm}^{-1}$ region^[127,128]. In later articles they developed the method further and delivered significant proof, based on analysis of numerous mono- and polysaccharides, that bands around $1150\text{-}1175\text{ cm}^{-1}$ indeed were characteristic for polysaccharides, and showed that they could easily be distinguished from the neighbor bands after a deconvolution of the spectra. It has not been possible to find later papers questioning these findings of Nikonenko et al.^[129,130].

In a study Kiefer et al. showed that glucose and cellobiose in 1-Ethyl-3-Methylimidazolium Acetate can be distinguished using ATR-FTIR spectroscopy. As it will be discussed later, they do however do not analyze the characteristic glucoside bands, which most possible leads to spurious results^[131]. They demonstrate an approach that can be used in combination with a Linear Combination Analysis (LCA) approach - a computer based data processing technique using linear algebra methods, that are able to separate components in a mixture. LCA requires that high quality spectra of the pure components can be obtained.

Looking into the theoretical literature, there have not been a lot of studies of the vibrational spectra of cellulose similar to the one presented here. I'm only aware of two very recent papers by Barsberg et al. that follows a similar approach^[132,133]. They investigated the vibrational spectra of cellotetraose and cellotetraose with a similar approach. They also found the antisymmetric stretching band to be located at around 1160 cm^{-1} and confirm this location in experiments using ATR-FTIR spectroscopy^[133].

2.2.3. Overlap with the Glucoside band

Previous in this section it was shown that the $1155\text{-}1165\text{ cm}^{-1}$ band indeed is characteristic for the glucosidic $\nu_{\text{asym,C-O-C}}$ mode. However, for the analytical use of the band during in-situ studies of cellulose hydrolysis, it is very important that overlap with other bands is taken into account. During the in-situ studies, that will be presented in the following, it was found by post reaction analysis with HPLC that the two main products from the hydrolysis of cellulose were glucose and HMF. As discussed the 1140 cm^{-1} band of glucose can be distinguished from the $1155\text{-}1165\text{ cm}^{-1}$ band of cellulose. A spectrum of HMF can be found in the appendix, see figure B.12 on page 127. Here it is clear that the $\nu_{\text{asym,C-O-C}}$ of HMF fortunately is located

slightly higher at around 1189 cm^{-1} and has no overlap with the $1155\text{-}1165\text{ cm}^{-1}$ band. As it will be shown later, the $\nu_{\text{asym,C-O-C}}$ band of HMF is responsible for an isosbestic point at around 1177 cm^{-1} . It can thus be concluded that HMF should not interfere during the glucoside band monitoring.

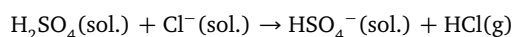
Small amounts of HMF can however be rehydrated to carboxylic acids such as levulinic acid and formic acid. A spectrum of levulinic acid can be found in appendix at figure B.12 on page 127. Here it is shown that levulinic acid does in fact have a band of medium strong intensity at 1165 cm^{-1} which could interfere if levulinic acid is present in high concentrations. However, the amount of formed levulinic acids was very small during the hydrolysis experiments, and should not influence the initial rates to any significant extent. However, at high conversion where the concentrations of glucoside bonds are low and the concentrations of levulinic acid are increasing, this overlap should be taken into account. On figure B.13 on page 128 found in the appendix, the spectra in the the $\nu_{\text{C=O}}$ region of solutions of HMF and levulinic acid in [BMIM]Cl are shown. The spectra were not used for a thorough calibration taking the different refractive indices of HMF and levulinic acid into account, but still shows it is reasonable to say that the extinction coefficients of the $\nu_{\text{C=O}}$ bands at 1669 and 1705 cm^{-1} of HMF and levulinic acid are similar.

2.2.4. Development of the experimental setup

The development of experimental equipment and methods that could be used for reliable in-situ monitoring of cellulose hydrolysis in practice has been very challenging. After the elucidation of the $\nu_{\text{C-O-C}}$ modes of the glucoside bond, numerous of different experimental setup strategies were applied, before the final steady and reproducible methodology was developed. However, this phase resulted in the fruitful development of various add-on modifications to the experimental setup with much wider applications than just the monitoring of cellulose hydrolysis, and in July 2012 three European patent applications were submitted, which are currently all proceeding into the PCT phase^[134-136]. Before the actual results of the in-situ investigations of the cellulose hydrolysis will be presented, I will start with a short exposition of the progress resulting in the final experimental designs.

Initially the ionic liquid solutions were investigated in a sandwich cell with AgCl windows and with thin plastic spacers on a Perkin-Elmer Paragon 1000 FTIR instrument. A heatable sandwich cell was commercially available, but was very expensive with AgCl windows and it did not seem like the optimal choice. Instead a new setup was purchased comprising a Nicolet iS5 spectrometer and an ATR-cell with a diamond top plate that could be heated up to 300°C (a short introduction to ATR-FTIR spectroscopy is included in the experimental section see:

section 4.2 on page 94). A reaction mixture containing cellulose, ionic liquid and a sulfuric acid catalyst was premixed in ionic liquid and freeze quenched and stored cold until use (see experimental section). At first the reaction was sought to be monitored in a thin liquid film, where a small steel cap on top of the sample was isolating it from the ambient laboratory atmosphere. Through gas in and outlets on the cap, the sample was subjected with a flow of slightly humidified nitrogen, to supply the water needed for the hydrolysis. The idea was that the reaction temperature was so far below the boiling point of the sulfuric acid so it would maintain in solution. An Arrhenius study based on a band around 960 cm^{-1} was made and an activation energy at around 80 kJ/mol was found. But further investigations made it clear that this was not the activation energy of the cellulose hydrolysis as the catalyst did not remain in the film for very long. It was speculated that the protons could leave the very chloride ion rich solution in the form of hydrochloric acid, which is far more volatile:



It is likely that the measured activation energy at this time was actually related to the evaporation process and the changes in spectra were related to the difference between sulfuric acid and hydrogen sulfate. Another problem with the thin film technique was that when applying a heterogeneous catalyst it would quickly precipitate into the bottom of the film layer and resulted in a steady growing spectral contribution from the solid material. Finally it was concluded that the thin film technique was not suited for monitoring the hydrolysis of cellulose. However, in the next chapter it will be shown how the thin film technique was very useful in other processes.

Instead a small microreactor concept was developed, that allowed magnetic stirring of the sample during in-situ monitoring using a custom build stirring device (see further details in Experimental Section). The glass microreactor had a volume approximately around $25\ \mu\text{L}$, and could contain around 15-20 mg reaction mixture and a small 2x5 mm Teflon coated magnet rod at the same time. The reactor was sealed during reaction using a little Teflon o-ring. The reactor was hollow in the bottom and directly fixed on the preheated diamond top plate, thereby allowing the evanescent IR wave to penetrate the bottom of sample^[134], photographs and a schematic drawing can be found at figure 4.2 on page 96 in the experimental section. Rapid heating of the sample to the set-point temperature was insured by the combination of the small volume and the stirring.

2.3. Results and discussion

2.3.1. Brønsted catalyzed hydrolysis of the glucoside bond

The hydrolysis of Avicel Cellulose and cellobiose was investigated in [BDMIM]Cl using 1.7 wt.% sulfuric acid as catalyst. Sulfuric acid was chosen as the kinetics are well characterized by more conventional methods^[26,60,75,107]. Reactions were carried out from 90 to 140 °C in steps of 10 °C in the stirred micro reactor while ATR-FTIR spectra were constantly recorded during reaction. Looking at figure 2.9 on the next page *in-situ* infrared spectra recorded during hydrolysis catalyzed by sulfuric acid at 120 °C are shown as difference spectra^e. Difference spectra recorded at other temperatures can be found in appendix: see figure B.16 on page 131.

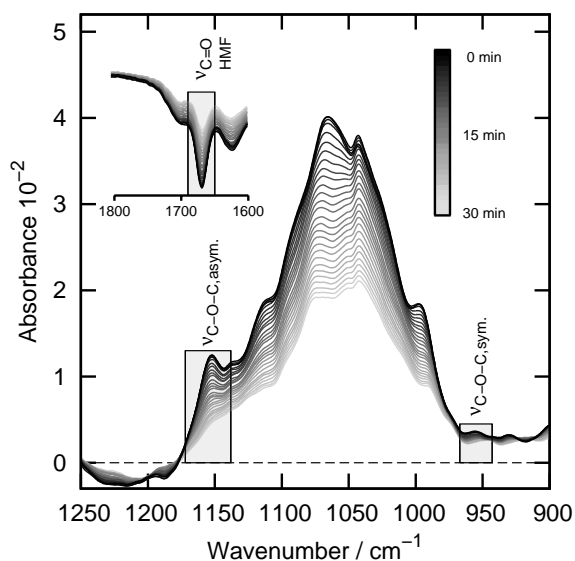
The intensity of the 1157 cm⁻¹ band was only of medium to weak intensity in the spectrum of pure cellulose, and further cellulose comprised only around 7.4 v/v % of the reaction mixtures^f. This induced some problems and uncertainties in the determination the absolute areas of the 1157 cm⁻¹ band in the ATR-spectra, even when advanced deconvolution procedures were applied. These problems were however overcome by the use of the difference spectra, which canceled out the spectral contribution of the ionic liquid. From the deconvolutions of the difference spectra very accurate measures of the changes of intensity of the 1157 cm⁻¹ band could be obtained during hydrolysis.

The difference spectra were produced by choosing a pseudo steady state spectrum when the change in the spectra over time in the 1160-1000 cm⁻¹ regions was negligible (See appendix: Figures B.15, B.19 from page 130 and forward). Then this spectrum was subtracted from all the previous spectra recorded at a given time (See appendix: Figures B.16 and B.20 from page 131). The spectra were deconvoluted by using voigt functions, see figure 2.10 on page 32. Equivalent function parameters were supplied as initial guess during the deconvolutions of all spectra. This method allowed very accurate determination of the initial rates expressed as absorbance·s⁻¹ which were later used for the determination of activation energies.

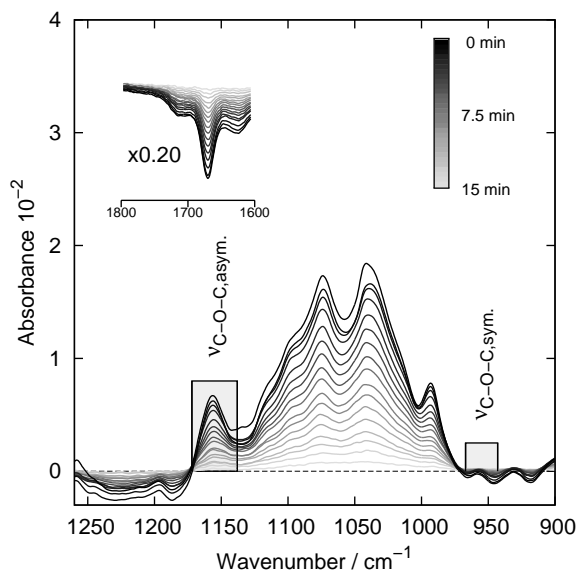
On the in-situ ATR-FTIR difference spectra a rapid decrease of the intensity of the strong bands at 1070-1060 cm⁻¹ was evident during cellulose hydrolysis. These bands, were as earlier discussed, assigned to C-O-C stretching from in the pyranose ring of cellulose. These bands did initially indeed show pronounced linear decrease at initial times and were tempting to use in the monitoring of the reaction, as suggested by others^[131]. However, as mentioned does glucose also have significant absorption bands at in this region, thus the decrease of those

^eThe difference spectra were produced by subtracting one selected pseudo steady state from each of the preceding spectra. The procedure will be elaborated in the following.

^fcellulose has a density around 1.46 g/cm³ and [BDMIM]Cl a density around 1.05 g/cm³.



(a) Cellulose hydrolysis at 120°C



(b) Cellobiose hydrolysis at 120°C

Figure 2.9.: Corrected ATR-FTIR difference spectra recorded during the hydrolysis of Avicel cellulose and cellobiose in catalyzed with 1.7 wt.% sulfuric acid [BDMIM]Cl at 120°C. The difference spectra express the change in spectra over 120 and 15 minutes of reaction for cellulose and cellobiose respectively. The symmetric and antisymmetric glucoside C-O-C stretching bands are highlighted with boxes. The insert shows the 1800-1600 cm^{-1} range. Notice the scale difference on y-axis.

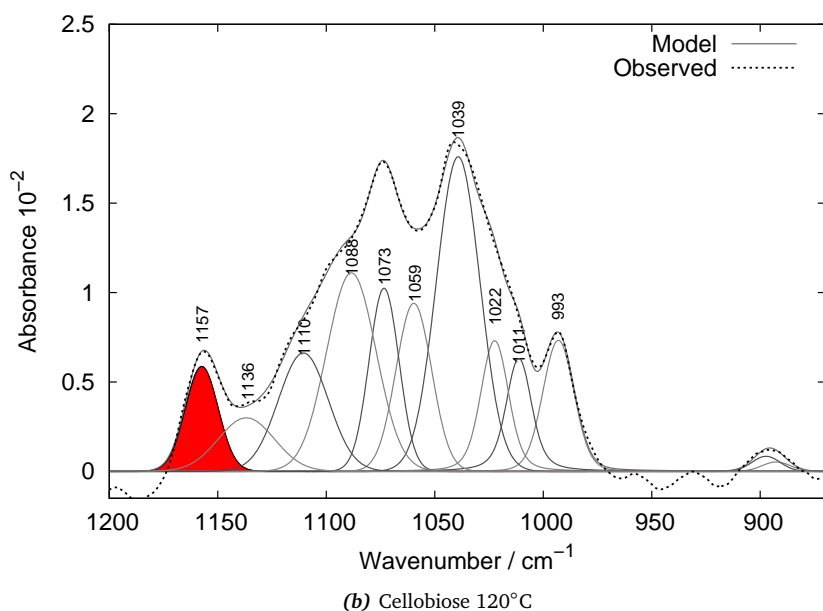
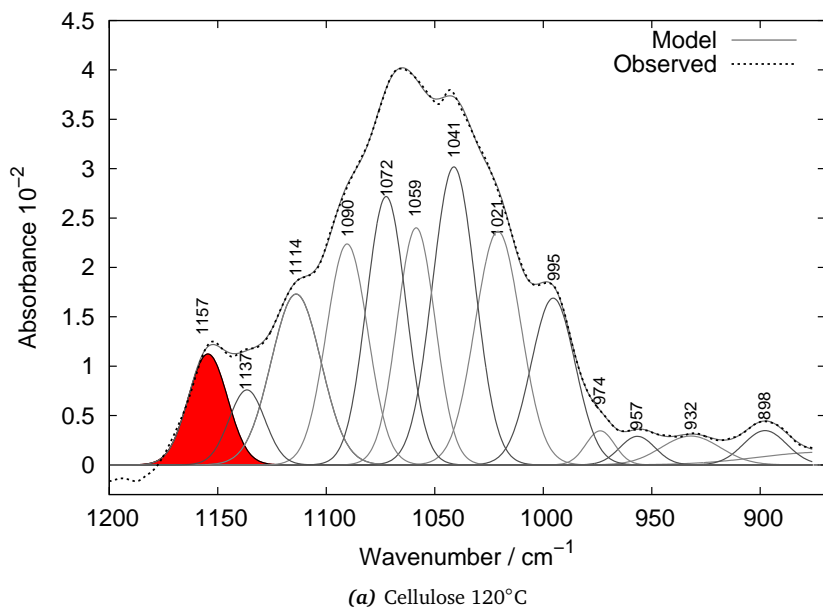


Figure 2.10.: Corrected ATR-FTIR difference spectra of cellulose, cellobiose and glucose corresponding to initial times in the reaction at 120 °C with samples containing 1.7 wt.% sulfuric acid. The spectra were deconvoluted with voigt functions. Difference spectra were generated by subtracting pseudo steady state spectra from the initial times spectra, thus the difference spectra corresponds to change in spectra during 120 and 15. minutes reaction. The glucosidic $\nu_{\text{asym,C-O-C}}$ band is marked with red. Corresponding plot of control experiment with glucose can be found in appendix: See figure B.17 on page 132.

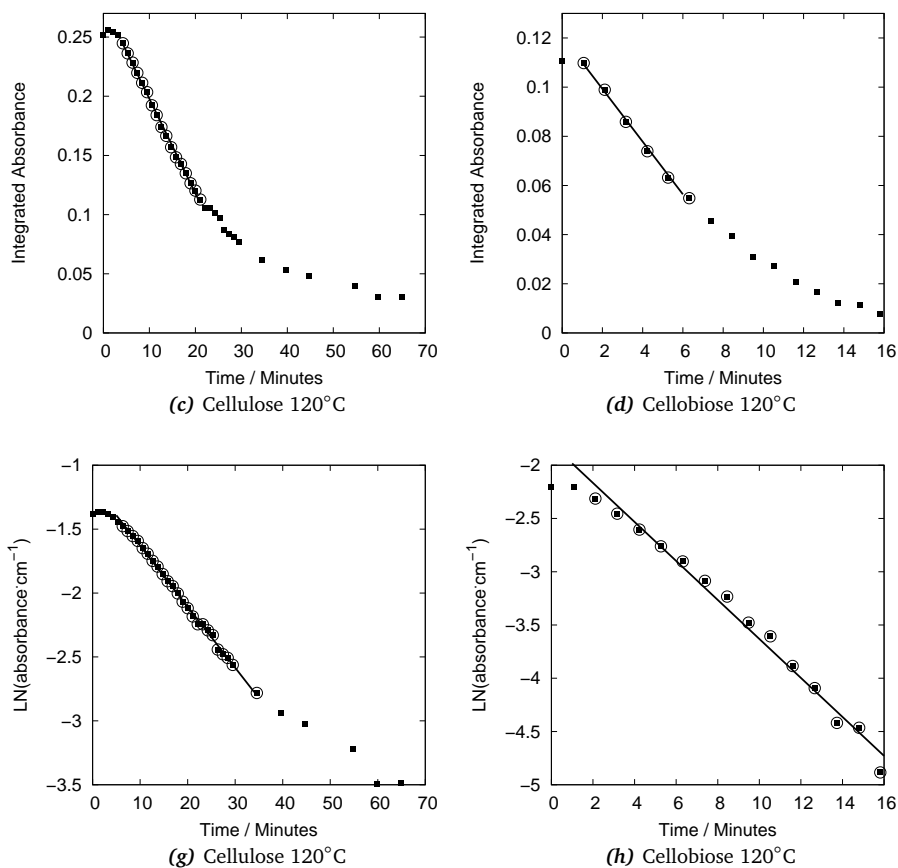


Figure 2.11.: *Top:* Showing decrease in the integrated band intensity of the $\nu_{asym,C-O-C}$ band at during acid catalyzed hydrolysis of **cellulose**(left) and **cellobiose**(right) at 120°C in $[\text{BDMIM}]\text{Cl}$. The points surrounded by circles marks the points used for determination of the initial pseudo zero-order rate. Similar plots for all the investigated temperatures found in appendix on figures B.14 and B.18. *Bottom:* It is shown that the decrease fits 1^{st} order kinetics until late in the experiments. This apparent deviation is probable due to overlap with levulinic acid band at 1165 cm^{-1} formed from HMF rehydration.

bands will simultaneously express an unknown mixture of cellulose hydrolysis and glucose degradation.

On the top of figure 2.11 the decrease of the 1157 cm^{-1} band during hydrolysis of cellulose and cellobiose is shown. For cellulose a slight increase of the 1157 cm^{-1} band was initially observed, probably due to incomplete dissolution of the cellulose, as the reaction mixtures were stored at low temperatures in a glassy state, prior to the experiments. However, within a short time period a steady linear decrease was observed allowing initial rates to be determined. As time proceeded the apparent rate of hydrolysis slowly decreased. Dee and Bell shows

that the initial rate of hydrolysis is first order dependent with respect to the concentration of dissolved glucoside bonds^[75]. The logarithm to the integrated absorbance is over time is shown on to bottom of figure 2.11 on the previous page. These plots show that the rates of both cellulose and cellobiose hydrolysis was first order dependent of the concentration of glucoside bonds. However, after around 35 minutes the apparent reaction rate started to deviate from the first order reaction kinetics. However, there does not seem to be any obvious reason to argue that this should be due to product poisoning of the acid catalyst.

It seems much more likely that the growing concentration of levulinic acids interferes with the monitoring of the glucosidic $\nu_{asym,C-O-C}$ band through its relatively strong absorption band at 1165 cm^{-1} . This interpretation is justified by looking at the increase of the intensity of the shoulder band at around 1705 cm^{-1} assigned to carboxylic acid $\nu_{C=O}$ mode, showing that some amount of levulinic acid was formed, see the insert on figure 2.10 on page 32. This shows that the method was very accurate to describe the reaction rates at moderate conversion but fails to describe the kinetics it at very high conversions due to the formation levulinic acid. The focus of this study has been on the initial rates for the determination of activation energies, but it would have been straight forward to develop a simple correction procedure, that could account for contribution of the 1165 cm^{-1} band of levulinic acid.

For all the investigated temperatures the initial rates could be determined very accurately, and can be found in appendix (see figure B.14 on page 129 and table B.1 on page 130). The activation energy for the hydrolysis of cellulose with sulfuric acid was determined to $96.4 \pm 4.1\text{ kJ/mol}$, see figure 2.12 on the next page. This value is in excellent agreement with a recent values of 92-96 kJ/mol reported by Dee and Bell for analogous cellulose hydrolysis in [EMIM]Cl^[60,75,107].

Cellobiose is often used as a model for to study cellulose hydrolysis. This is an attractive choice due to the high solubility of cellobiose in many solvents, which ease the analysis procedure. Accordingly, the in-situ behavior of the initial hydrolysis rates were investigated (see appendix: figure B.18 and table B.2). The reaction mixture was prepared with a cellobiose concentration on 10.5 wt.% thereby keeping the formal concentration of anhydroglucose the same as the cellulose solution. In retro-perspective it became clear that this results in a glucoside bond concentration that is only the half of the glucoside bond concentration in the investigated cellulose mixture. Even though this should expect to give an lower initial rate due to the first order rate dependency of glucoside bond concentration, the apparent cellobiose hydrolysis rates were quite surprisingly noticeable higher compared to cellulose. This was also reflected directly in the Arrhenius plot where the apparent activation energy for cellobiose hydrolysis was found to as low as $69.6 \pm 3.0\text{ kJ/mol}$, which is significantly lower than for cellulose - see figure 2.12.

Dee and Bell too observed that the hydrolysis rate of cellobiose was around two times faster

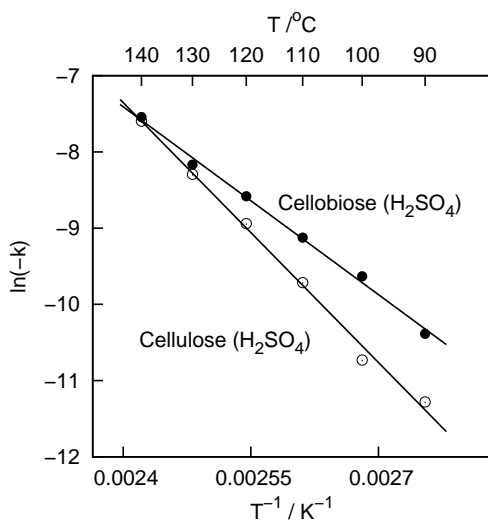


Figure 2.12.: Arrhenius plot for the hydrolysis of cellulose and cellobiose in using 1.7 wt.% sulfuric acid as catalyst.

than for cellulose even though the glucoside concentration was only the half. They did not report an activation energy for cellobiose hydrolysis, but faster rate indicates a lower activation energy^[75]. Extrapolation to the same glucoside bond concentration would result in cellobiose rates around three to four times higher compared to cellulose which indeed supports these unexpected results.

Although this surprising difference in activation energies between cellobiose and cellulose is supported by earlier reported results^[60,75], a control experiment were performed to exclude the possibility that fast loss in the intensity of the IR 1155 cm⁻¹ band from cellobiose, was due to simultaneous conversion of the formed glucose into HMF. Such type of errors would increase the apparent rate and lead to a possible underestimation of the activation energy. Hence the conversion of 10 wt% glucose in [BDMIm]Cl with 1.7 wt% sulfuric acid was followed in-situ to make sure that the loss of intensity of the band around 1142 cm⁻¹ of glucose actually could be distinguished from the glycoside $\nu_{asym,C-O-C}$ band around 1157cm⁻¹. During the experiment it was clear that glucose was converted into HMF and carboxylic acids (raise of $\nu_{C=O}$ bands at 1669 1705 cm⁻¹ respectively). The different spectra were derived as before, and clearly showed that there were no absorption bands at 1157 cm⁻¹ as it was also seen in the case of the difference spectra of cellulose and cellobiose (see appendix:figure B.17 on page 132). As reported earlier by Nikonenko et al. the 1157cm⁻¹ band is indeed characteristic for polymeric species, and can easily be distinguished from the 1142 cm⁻¹ band of glucose by deconvolution^[129,130].

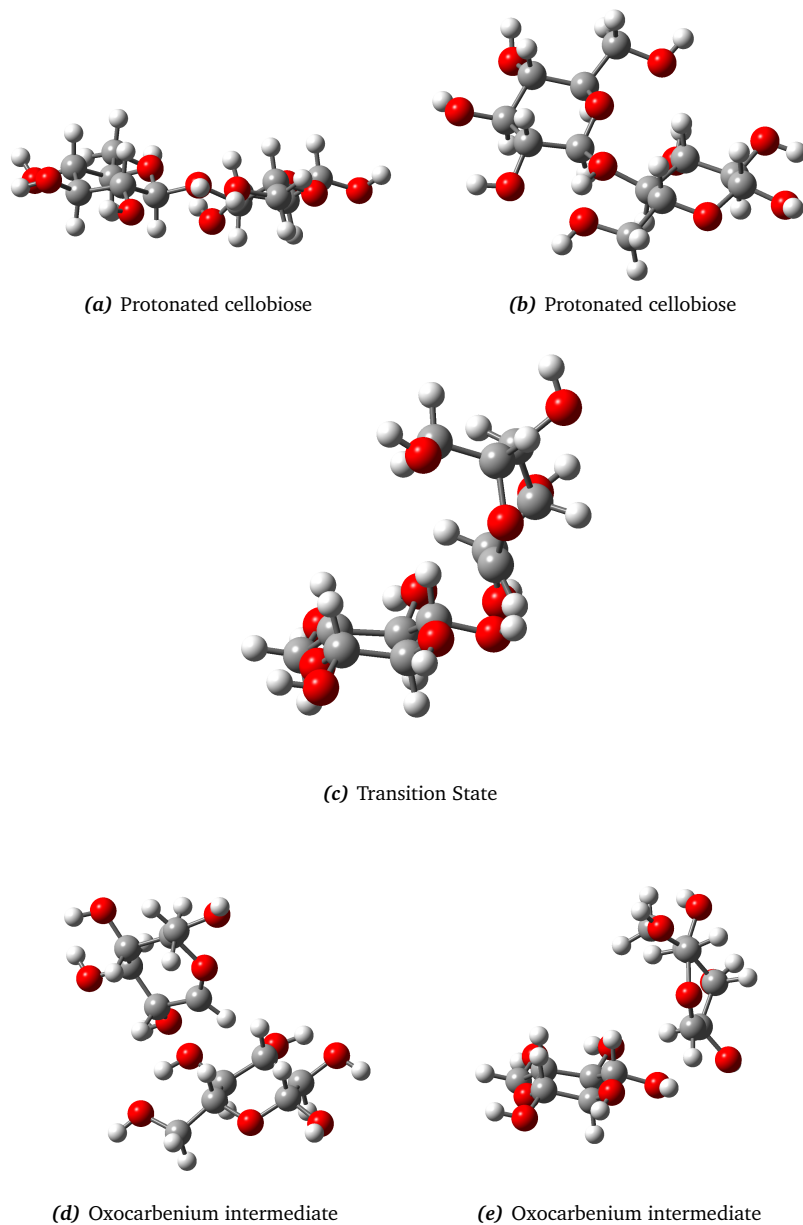


Figure 2.13.: Showing structures along reaction coordinate for cellobiose hydrolysis: (a) and (b) shows different views of protonated cellobiose, and (c) the transition states that connect it to the oxocarbenium intermediate (d) and (e). Notice the pronounced rotation of the pyranose rings with respect to each other during cleavage of the glucoside bond.

The huge difference of around 25 kJ/mol difference in the activation energies of the cellobiose and cellulose is surprising, as the properties of the glucoside bond itself should be expected to almost identical. As earlier discussed, Vernon already noticed in 1967 that stabilization of positive charge in transition states and intermediates was not alone making the reaction barrier^[73]. Conformational stress due to rearrangement of the pyranose rings during reaction also share the reason for the relatively high reaction barrier during hydrolysis.

I tried to model critical step in the reaction with *ab initio* molecular calculations^g. A transition state connecting the protonated cellobiose and the intermediate where the glucoside bond is broken and the oxocarbenium species was formed was located. The structures can be found at figure 2.13 on the preceding page. The oxocarbenium had the well-known half chair conformation, induced by the double bond character of the O5-C1 bond^[137]. The transition state was best described as a slightly distorted boat conformation far from the preferred planar configuration around the double bound oxygen. The transition state had one imaginary frequency at $i166\text{ cm}^{-1}$, oscillating in the direction of the reaction coordinate (see appendix: figure B.23 on page 140). The energy of the transition state was around 80 kJ/mol with respect to the reactants, but should not be taken to literally as the Hartree-Fock method normally to underestimate the energy required during breakage of covalent bonds significantly^[112,138].

But what is very important to note is the change in angle between the two pyranose rings: In the initial protonated state, cellobiose is most stable in the planar configuration shown at the top of figure 2.13, but during the reaction the pyranose rings rotates with respect to each other, and in order to minimize the energy and the angle between the pyranose rings is close to 90° before the glucose and the oxocarbenium intermediate is obtained. In a very recent study Liang et al. models the reaction pathway of cellobiose in water with a very sophisticated level of theory, also simulating the water solvent very accurately^[72]. Interestingly, they too observe that the pyranose rings make the same significant twist before they passes by the critical transition state that results in the oxocarbenium species^h.

This gives a very reasonable explanation for the big difference in activation energy of cellobiose and cellulose hydrolysis: The cellobiose dimer has flexibility around the glucoside bond, allowing the structure to rearrange so the reaction barrier can lowered. However, the long polymeric cellulose chain will in practice not have any flexibility around the glucoside bond, as a rotation would require an unrealistic translation of the rest of the cellulose chain. Thus it is very likely that the activation energy will rise very significantly if the opportunity for this rearrangement is not present during breakage of the bond.

^gAt this time I had no acces to a High Performance Computing system, and all calculations was performed on a laptop computer. Gaussian09 with Hartree-Fock/6-31G(d) was used because of the limited computing resources at the time.

^hThis twist can be seen very clear in the screen shot in the supporting material^[72]. This screen-shot is included in the appendix: see intermediate("R4") on figure B.24 on page 140.

Another surprising aspect of the results, also briefly discussed in the introduction to the chapter, is that both activation energies are much lower than the one found in water. As cellulose is not soluble in water this deviation is more understandable, but the huge deviation from the very well documented activation energy for cellobiose hydrolysis in water at around 130 kJ/mol cannot be explained by poor dissolution. The kinetics of the hydrolysis of glycosidic bonds in ionic liquids are still poorly investigated and in the few studies refereed to earlier, the authors tend to compare their results with the results obtained from water^[26,60,75,107]. Choosing to compare with hydrolysis in water must be explained more as consequence of the huge availability to experimental kinetic data obtained in water, than water being an especially suited choice for comparison with ionic liquids. Water and the halide containing ionic liquids have very different properties, which can be exemplified by the loss of the ability to dissolve cellulose if the ionic liquid contains just a few percentage of water: just with a slight coordination to water, the properties of the halide ions are changed. The extreme high concentration of halide ions in these ionic liquid melts creates an environment that is very far from the ones found in water.

As mentioned Phan et al. showed that the hydrolysis rate of glycosidic bonds are enhanced by the presence of halide ions even in mixtures with very high water concentrations. And when shielding these anions from water by addition of 1,4-dioxane, the rates were significantly increased^[110]. The ionic liquid is the case where all water is removed, and the reaction proceed in an environment, where the halide ions is extremely strongly coordinating. This effect was also reported by Vanoye et al. that showed that the rate of cellobiose hydrolysis in [EMIM]Cl dropped significantly if water was present in high concentrations.

Stabilization of the oxocarbenium species is indeed possible, shown by the much lower activation energies of the cellulase enzymes and the phosphate buffer system described in the introduction^[80,83–86,94]. Therefore it seems very likely that the ionic liquids acts actively like a co-catalysts that helps to stabilize the charge on the oxocarbenium species during the hydrolysis.

The reason why the same big difference is not found in the activation energy of cellulose and cellobiose hydrolysis in water, could be that the poor stabilization of the positive charge is what determines the size of the reaction barrier, yielding a similar and much higher activation energy for both reactions. In ionic liquids it seems, in the perspective of these results, that halide ions can indeed stabilize the positive charge on the oxocarbenium species very effectively, lowering this contribution to the reaction barrier. In ionic liquids it therefore seems like it is conformational limitations during the bond breakage, that determines the size of the reaction barrier.

2.3.2. Glucose Conversion during Hydrolysis

The products from glucose conversion produced simultaneously with the hydrolysis of cellulose is a very heterogeneous mixture of many different derivatives formed during these reactions. The kinetics of the conversion of glucose to yield HMF is a complicated process with several routes and potential critical steps.

Glucose itself is not very reactive and requires isomerization into fructose which is much more reactive. This step is relatively slow. When fructose is formed it exists simultaneously as several different isomers including furanoses, pyranoses and the open form. This equilibrium is complex and simultaneously dependent on both solvent and temperature^[139,140]. In the literature various combinations of solvents and catalysts has been used, yielding very different results. In water the activation energy catalyzed by mineral acids is determined to be quite high at around 137-151 kJ/mol^[141,142].

A very interesting study by Marcotullio shows that the efficiency and selectivity of the conversion of d-xylose to furfural in water by mineral acids is significantly enhanced by the presence of chloride ions^[143]. In the presence of high NaCl in concentrations the reaction rates were increased by a factor of 4. Binder and Raines investigated the promoting effect of lithium halides during conversion of cellulose, glucose and fructose to HMF with various types of catalysts in N,N-dimethylacetamide^[144]. They observed a strong promoting effect of halide ions. They could even see that the halide ions were catalytically active themselves, and showed a direct first order dependency on the rate of fructose dehydration. Qi et al. investigated the dehydration of fructose in 30/70 % mixtures of acetone/water and acetone/DMSO with an Brønsted acidic ion-exchange resin^[145,146]. They found the activation energy to be highly dependent on solvent as it was determined to around 60 and 100 kJ/mol for the acetone/DMSO and acetone/water systems, respectively. They found the pre-exponential factor to be much lower for the acetone/DMSO system though. This is however not very surprising as protons cannot “dissolve” in acetone/DMSO as in water, thus the system becomes a truly heterogeneous catalytic system and thus exhibit a much lower turnover frequency. Very interestingly the group later investigated the reaction in [BMIM]Cl with the same ion-exchange resin and determined the rates to be high and the activation energy to be around 62 kJ/mol^[145]. This again points to unique characteristics of the ionic liquids that in this case seem to be able to decrease the activation energy almost to half with respect to the one found in water.

During the hydrolysis of cellulose an intense sharp band at 1669 cm^{-1} appeared independently along with two broad bands at 1705 and 1623 cm^{-1} . The band at 1669 cm^{-1} can be assigned to the $\nu_{\text{C=O}}$ of the carbonyl group on HMF, while a related increase of the band at around 1623 cm^{-1} corresponds to the $\delta_{\text{H-O-H}}$ bending mode of the water, which is being formed during dehydration of fructose. The weak shoulder at around 1705 cm^{-1} was as mentioned assigned to

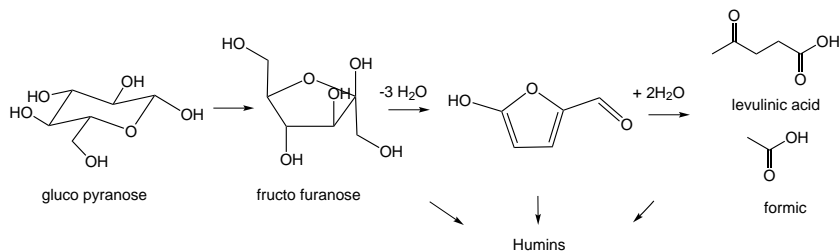


Figure 2.14.: Simplified scheme showing the overall steps in the conversion of glucose. Glucose is very stable until it is isomerized into fructose that can be dehydrated to HMF. HMF can be rehydrated to form levulinic acid and formic acids. Both fructose, HMF and the carboxylic acids can polymerize to form insoluble dark polymers called humins.

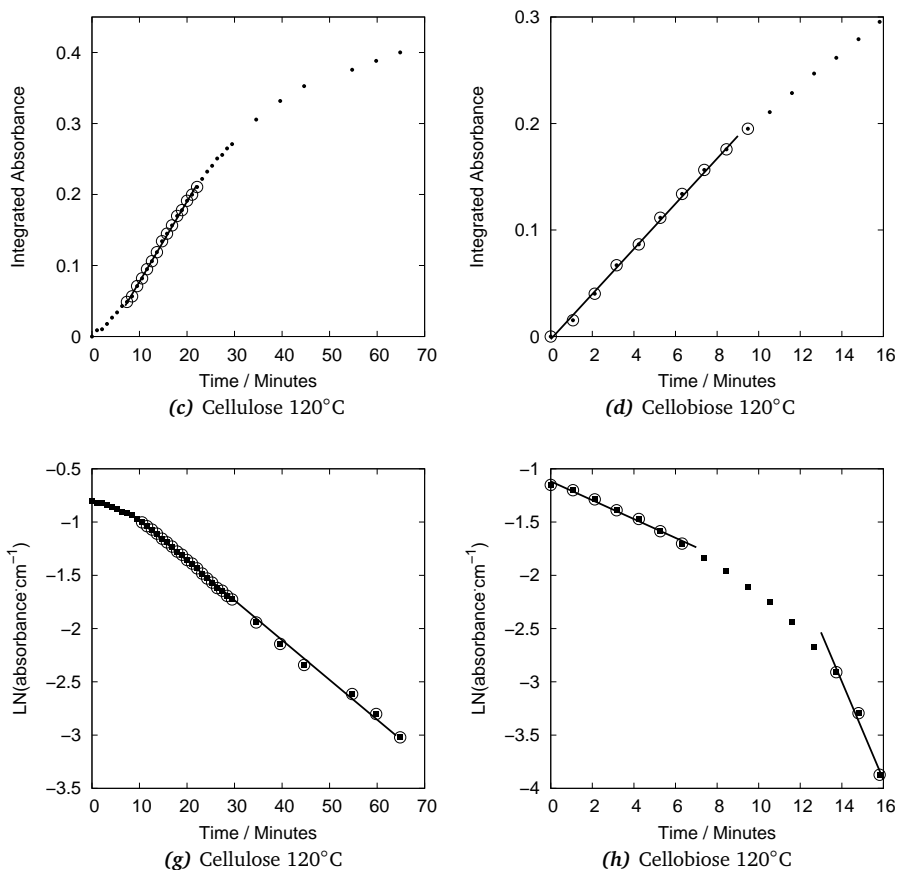


Figure 2.15.: Top: showing formation of HMF expressed as growth of the $\nu_{C=O}$ 1669 cm^{-1} band during acid catalyzed hydrolysis of **cellulose**(left) and **cellobiose**(right) at 120 °C in $[\text{BDMIM}]\text{Cl}$. The points surrounded by circles show the points used for determination of the initial pseudo zero-order rate. Similar plots for all six temperatures investigated can be found at in appendix at figures B.21 and B.22. Bottom: Shows natural logarithm to the change in the 1669 $\nu_{C=O}$ during hydrolysis of cellulose and cellobiose. See text for further explanations.

$\nu_{C=O}$ modes associated with formic and levulinic acid formed by the re-hydration of HMF. Post-reaction analysis by HPLC confirmed glucose and HMF to be the main products with smaller amounts of cellobiose and carboxylic acids present (see appendix figure B.25 on page 141). No significant amounts of fructose were observed during the hydrolysis of cellulose. The $\nu_{C=O}$ band of HMF at 1669 cm^{-1} is very intense, and thus analytically very useful to describe the initial rates of HMF formation. From the HPLC results and the initial size of the 1705 cm^{-1} shoulder, it seemed reasonable to assume that the formation of levulinic acid was negligible in the beginning of the experiment. Therefore the growth for the 1669 cm^{-1} band could be used as a good measure of the initial HMF formation rate. Thus the band areas of 1669 cm^{-1} were determined in all difference spectra using Gaussian deconvolution.

The corresponding development of the 1669 cm^{-1} band is shown as a function of time at figure 2.15 on the preceding page (Similar plots for all temperatures can be found in appendix). The same difference spectra were used as for the monitoring of the glucosidic $\nu_{asym,C-O-C}$ band. However, as these difference spectra were produced to show the disappearance of the glucoside bond as positive bands, the 1669 cm^{-1} band of HMF would appear as a large negative band at initial times of the experiments. Therefore they were multiplied with a factor -1 before deconvolution. For reasons of clarity the development is converted, to show a growth in the HMF concentration as a function of time¹. From these plots initial pseudo zero-order rates could be determined. In a short period of time the rates of HMF formation was quite slow. As argued earlier this is partly explained by that cellulose initially has to be completely re-dissolved after the reaction mixture is being heated up from the frozen state.

But this effect seems more pronounced in the cases of HMF formation than for the hydrolysis itself, and the initial slow rate of HMF formation are probable caused as the hydrolysis of long cellulose chains at very initial times, predominantly will produce oligomers, and an induction period is needed before a steadier production rate of glucose was reached. The "initial rates" was determined of the plots after this induction period, see figure 2.15 (a). This was not the case for cellobiose where fast initial rates were reached instantly, as the hydrolysis of each glucoside bond released 2 glucose molecules.

The initial rates as a function of temperature expressed an pronounced Arrhenius dependency, see figure 2.16 on the following page. Starting with the activation energy for HMF formation during cellulose hydrolysis, it was determined to $94.7\pm 3.7\text{ kJ/mol}$, which is remarkably close to the activation energy at 96.4 ± 4.1 determined for the cellulose hydrolysis. Looking at figure 2.15, the formation of HMF shows an ideal first order dependency of glucose. I interpreted this as the reaction rates are limited by the low glucose concentration due to low the rates of cellulose hydrolysis. Thus the activation energy found here is probably not the real activa-

¹If I_0 expresses the absolute value of the 1669 cm^{-1} band area in the initial difference spectrum and $I(t)$ the band area at each spectra at a given time, then the growth of HMF was expressed as $I_{HMF}(t) = |I(t) - I_0|$. For the first order dependency plots $I(t)$ was used.

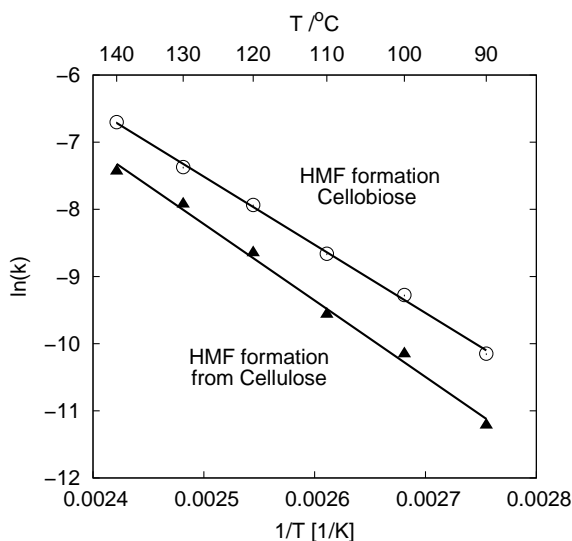
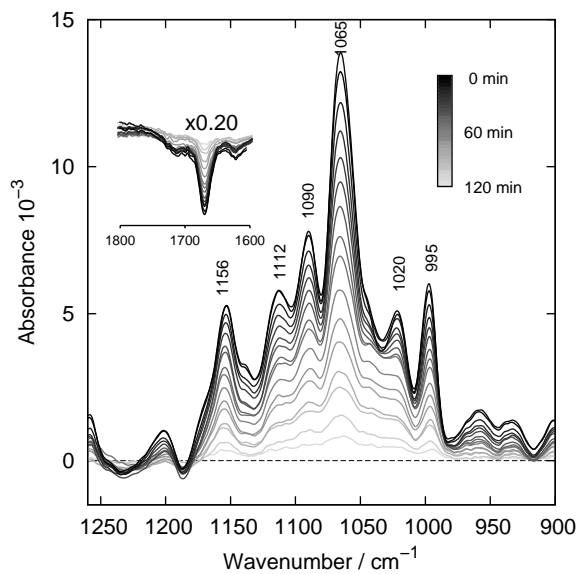


Figure 2.16.: Arrhenius plot for HMF formation during the hydrolysis of cellulose and cellobiose in using 1.7 wt.% sulfuric acid as catalyst.

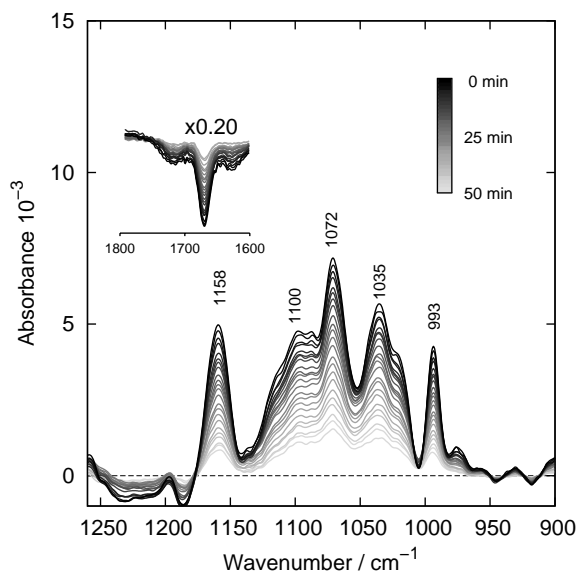
tion energy for glucose conversion, but an indirect reproduction of the activation energy for cellulose hydrolysis found in the previous section.

The activation energy for HMF formation during cellobiose hydrolysis was found to 85.0 ± 1.8 kJ/mol. With the significant lower cellobiose activation energy at 69.6 ± 3.0 kJ/mol, the found activation energy could be believed to be the actual activation energy for HMF formation. This is in perfect agreement with a value reported by Vanoye et al. that finds the acid catalyzed activation energy of glucose degradation in [EMIM]Cl to be 84.7 kJ/mol^[60]. Qi et al. determined the activation energy for dehydration of fructose in [BMIM]Cl to be 62.2 kJ/mol with a strong Brønsted acid as catalyst^[145]. Hence the activation energy for HMF formation at 85.0 kJ/mol can be assigned to the Brønsted catalyzed isomerization of glucose to fructose. At figure 2.16 (d) a first order plot is made for HMF formation during cellobiose analogues to the one for cellulose. Here it is obvious that the apparent reaction rate cannot be fitted with any simple dependency, as the concentration of glucose is controlled both by the fast production by hydrolysis of cellobiose and the slightly slower consumption by the subsequent isomerization.

This is also evident when looking qualitatively at the difference spectra for cellulose and cellobiose hydrolysis. The difference spectra recorded during hydrolysis at 90 °C can be found on figure figure 2.17 on the next page. The spectra shows a period of 120 and 50 minutes respectively, that is chosen as the conversions of glucoside bonds in this period are approximately equal. The faster rate of cellobiose hydrolysis was covered in the previous section. What is also



(a) Cellulose hydrolysis at 90°C



(b) Cellobiose hydrolysis at 90°C

Figure 2.17.: Corrected ATR-FTIR difference spectra recorded during the hydrolysis of Avicel cellulose and cellobiose in catalyzed with 1.7 wt.% sulfuric acid [BDMIM]Cl at 90°C. The difference spectra express the change in spectra over 120 and 50 minutes of reaction for cellulose and cellobiose respectively. The insert shows the 1800-1600 cm^{-1} range. Notice the scale on y-axis.

noticeable are the relative difference of changes in the 1140-1000 cm^{-1} regions, that describes various modes of pyranose ring of both glucose and the cellulose. The change in this region is significantly larger in the shown period of time for cellulose. This shows quantitatively that the glucoside bond at this temperature is hydrolyzed significantly faster than the produced glucose is converted. At 120 °C this is still evident (see figure 2.9 on page 31), whereas it is hard to realize at 140 °C (All used difference spectra can be found in appendix: see figures B.20 and B.16).

2.3.3. Heterogeneous Catalysts for Cellulose Hydrolysis

For the technical applications of cellulose hydrolysis it is most likely that a heterogeneous catalyst will be preferred, and analytical methods that can handle solid catalyst screening are needed. Therefore the method was applied on two different heterogeneous catalysts.

At first a sulfonic acid functionalized SBA-15 type mesoporous silica catalyst, synthesized by my colleague Saravanamurugan, was applied as catalyst^[147]. These types of catalysts have been used for various reactions in liquid phase and are known to be quite resistant to leaching even in water^[148]. The powderous catalyst was left with pure [BDMIM]Cl to equilibrate in an oven at 120 °C overnight. The [BMIM]Cl impregnated catalyst was then mixed with a 10 wt.% cellulose mixture to yield in a mixture containing 6 wt.% cellulose and 13 wt.% catalyst. The strong IR bands of Si-O vibrations allowed the homogeneity of the sample to be monitored, and the catalyst dispersion in the slurry was found to be steady during the hydrolysis experiments^l. The reaction was indeed much slower than expected. After around 4 hours the reaction was stopped. The background signal during the experiment was not completely stable as observed in the previous described experiments, but by exploiting the isosbestic point at 1177 cm^{-1} the difference spectra could be corrected (see e.g. figure 2.9 on page 31 for comparison). The effect of the correction procedure is shown in appendix: see figure B.27 on page 143.

After the isosbestic correction the rate of hydrolysis could be determined by deconvolution of the 1155 cm^{-1} band. The rate of hydrolysis was found to be $5.08 \cdot 10^{-6} \pm 1.1\%$ absorbance $\cdot\text{s}^{-1}$. Compared to the isothermal rate for sulfuric acid catalyzed hydrolysis the apparent rate was around 26 times lower. If the molar concentration of acidic sites is taken into account, it results in a turn over frequency is 19 times higher for the sulfuric acid compared to the SBA-15 catalyst^k. Thus the catalyst indeed acts like a heterogeneous catalyst without leaching protons out in the ionic liquid. Furthermore, this suggests that the cellulose do not reach the active sites deep down the long channels of the catalyst. The catalyst had a surface area of around 565 m^2/g with a channel diameter of around 9 nm^[147]. Lai et al. synthesized a similar SO_3H -

^lIf stirring was not applied, a steady growing signal 1050 cm^{-1} was observed, due to catalyst precipitation on the ATR diamond.

^kcalculated with respect to ealier published acidity values for the same catalyst^[147].

SBA-15-catalyst with incorporated magnetic particles in the structure, comprising an almost identical content of SO₃H sites^[149]. They used it in the hydrolysis of both cellobiose and cellulose. At 120 °C for 1 hour reaction they experienced a complete conversion of cellobiose whereas they for cellulose experienced a conversion of only 26 % after three hours of reaction at 150 °C. This suggests that the catalyst is not active by leaching protons into the reaction media, but also suggests that this type of catalysts may not be a good choice for cellulose hydrolysis: Because even though the sulfonic acids are very active in the hydrolysis of the glucoside bonds, the long cellulose chains will discover severe problems to diffuse into the long narrow pores. The result is that only the acid sites, which are available, are the ones in the mouths of the pores.

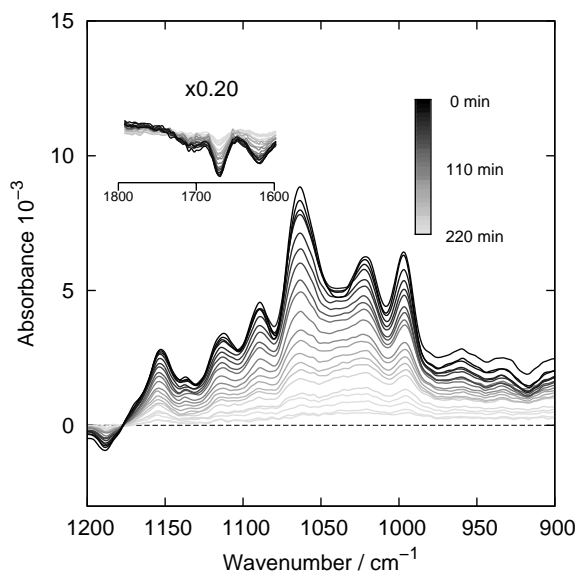
Hydrolysis in Presence of Sulfated Anatase

In our group we have developed a very active type of catalyst based on very small and stable sulfated anatase nanoparticles with a very high surface acidity. These catalysts have previously been used in gas-phase reactions^[150-152]. The catalyst was tested for activity towards cellulose hydrolysis in a temperature range from 130-160 °C with steps of 10 °C in a slurry containing 20 wt.% of the solid catalyst in a 10 wt.% cellulose [BDMIM]Cl solution. Opposite SO₃H-SBA-15 catalyst the anatase catalyst mixed very easily within seconds with the ionic liquid phase just by gentle stirring with a spatula. The anatase catalyst was found to be much more active for cellulose hydrolysis and glucose conversion than the SO₃H-SBA-15. The apparent activation energy for cellulose hydrolysis was here determined to be 94.3 ± 3.6 kJ/mol which is almost identical to the value obtained for H₂SO₄, suggesting that hydrolysis proceeds via very similar reaction mechanisms (see figure 2.19 on page 47). A comparison of rates at 130 °C with the experiment using sulfuric acid as catalyst yields in an almost identical turnover frequency for the two systems¹. This could on the one hand mean that the catalyst is almost leaching protons fast out into the ionic liquid as reported by Rinaldi et al. as when using ion-exchange resin catalysts^[26]. But it could also be due to the fact that the catalyst exists as an almost colloidal like suspension of nano-particles making the acidic sites very accessible for the glucoside bonds.

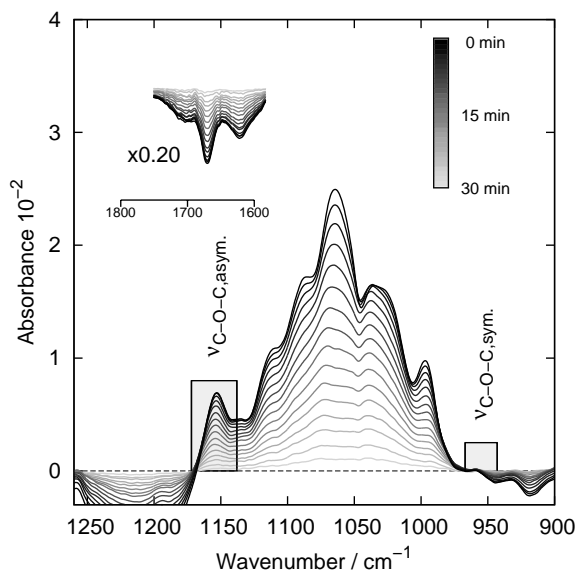
2.3.4. Lewis Acidic Catalysts: Hydrolysis in Presence of Cr³⁺

Several Lewis acidic transition metal ions are known to be active catalysts for cellulose hydrolysis and further a lot of them are also very active catalysts for the isomerization of glucose to

¹Acid concentration has been calculated using values found by temperature programmed desorption of NH₃, which were reported previously^[151]



(a)



(b)

Figure 2.18.: (a) Difference spectra recorded during hydrolysis in a slurry of 6 wt.% cellulose using 13wt.% $\text{SO}_3\text{H-SBA-15}$ catalyst in $[\text{BDMIM}]\text{Cl}$ at 120°C . These spectra were corrected assuming an isosbestic at 1177 cm^{-1} , comparison with original spectra can be found in appending - see figure figure B.27 on page 143. (b) Cellulose hydrolysis in a slurry containing 8wt.% cellulose and 20% sulfated anatase catalyst in $[\text{BDMIM}]\text{Cl}$. Notice the difference y-axis scales

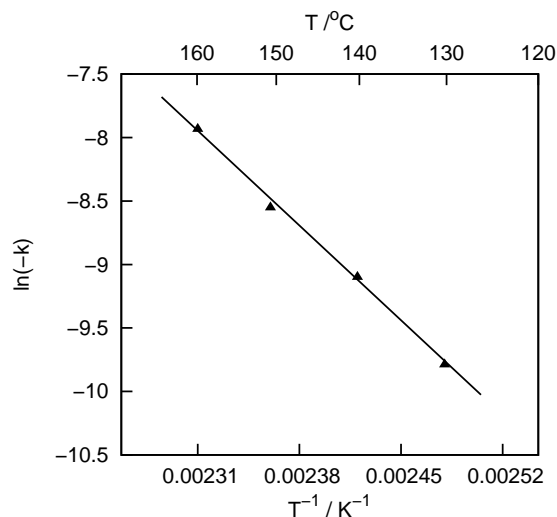
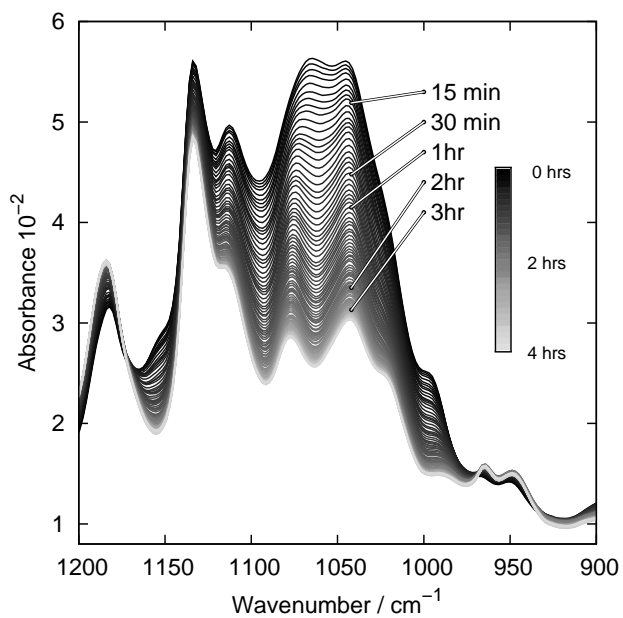


Figure 2.19.: Arrhenius plot for the hydrolysis of cellulose in using 20 wt.% sulfated anatase as catalyst.

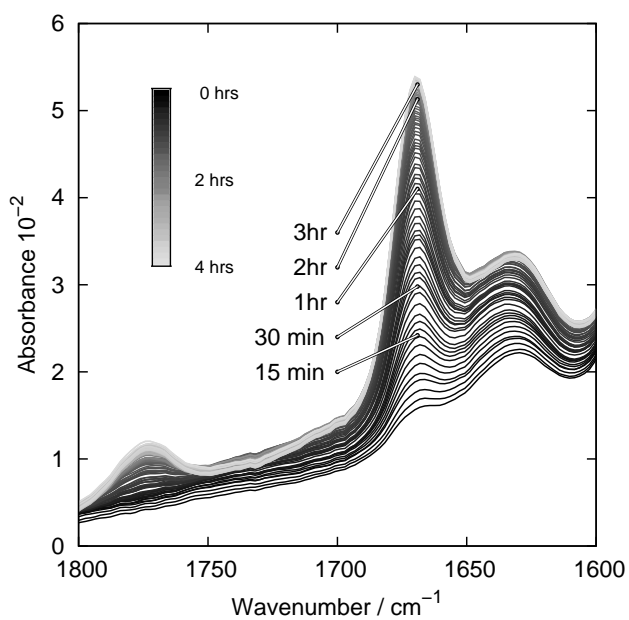
fructose and in the subsequent dehydration to HMF^[64–68,153]. This ability, combined with high selectivity, makes several of these systems very attractive and important in the future vision of a competitive bio-refinery. Especially Cr²⁺/Cr³⁺ salts has received a lot of attention in the later years, as they are known to be both very active and selective catalysts in all the steps for selective conversion of cellulose to HMF. However, very little is known about how these catalysts actually works.

It is especially the latter conversion of glucose into HMF that has received the main attention. This subject will be treated thoroughly in the next chapter. To my knowledge much less attention has been paid to the cellulose hydrolysis itself, and I have not been able to find kinetic data for the hydrolysis step in the literature. This is as explained earlier much likely due to the challenge of investigating this step experimentally. In the following a study of the chromium catalyzed cellulose depolymerization will presented, which was performed using a slightly modified version of the in-situ ATR-FTIR methodology used in previous sections.

For the in-situ investigations of chromium catalyzed hydrolysis of cellulose a concentrated [BDMIM]Cl solution containing CrCl₃·6H₂O was mixed with a cellulose solution yielding in a mixture containing 1.48 wt.% CrCl₃·6H₂O and 10 wt% cellulose, corresponding to roughly 10 mol % catalyst. Selected regions of the spectra recorded during 4 hours hydrolysis at 130 °C are shown at figure 2.20 on the following page.



(a)



(b)

Figure 2.20.: Showing corrected in-situ ATR-FTIR spectra during hydrolysis of 10 wt.% cellulose in $[\text{BDMIM}]\text{Cl}$ using 1.48 wt.% $\text{CrCl}_3 \cdot 6\text{H}_2\text{O}$ at 130°C

At first a pseudo steady state spectrum was chosen as in previous sections, where the changes in the recorded spectra over time were negligible. The manual subtraction of this spectrum from each of the preceding spectra was however a quite trivial and time consuming task. For the experiments described above, more than a full month of work hours was put into quite trivial work with the deconvolution of each spectrum, thus pointing at a severe drawback of the usability of the presented method.

In the time after the previous described experiments a lot of work was put into the development of a more efficient method for data processing of the spectra. I developed a complete software package based on script programming for the freely available gnuplot, which could ease the heavy workload associated with the deconvolutions. The package had at this time been successfully tested in various other applications where quantitative information was drawn out of huge amounts of spectral data^[154,155].

Instead of subtracting the pseudo steady state spectrum from each of the preceding spectra, the pseudo steady state spectrum was initially fitted using a sum of an appropriate amount of Gaussian functions using commercial software:

$$BG(x) = \sum_{i=1}^n bga_i \cdot e^{\frac{(x-bgcen_i)^2}{(2-bgwid_i)^2}} \quad (2.1)$$

where bga_i , $bgcen_i$ and $bgwid_i$ denote parameters for the amplitude, center and width of the individual functions used to fit the background. This function, here denoted $BG(x)$, comprised a very good analytical approximation of the background, that from a programming point of view, was much easier to handle compared to a file with hundreds of data points (see gray dotted lines at figure 2.21 on the next page).

The initial difference spectrum was deconvoluted using a sum of Gaussian functions, here denoted $F(x)$, with similar parameters as the Voigt functions used during data processing in the previous sections:

$$F(x) = \sum_{i=1}^n a_i \cdot e^{\frac{(x-cen_i)^2}{(2-wid_i)^2}} \quad (2.2)$$

Where a_i , cen_i and wid_i denote parameters for the amplitude, center and width of the individual functions used to fit the difference spectrum. Then all the parameters comprising amplitude, center and width for $F(x)$ and $BG(x)$ was loaded into gnuplot using script programming. Subsequent all the spectra was automatically deconvoluted using the sum of $F(x)+BG(x)$ where appropriate values for all a_i , cen_i and wid_i parameters were found using non-linear least squares regression. In this way the deconvolutions were in practice performed on the difference spectra in a similar manner as the as the manual deconvolutions described earlier.

Each time a spectrum was fitted; these parameters were used as the initial guess for the next spectrum and so on. However, the commercial deconvolution software Peakfit, used in the previos sections, probably used more advanced algorithms. Thus it was needed to alter the

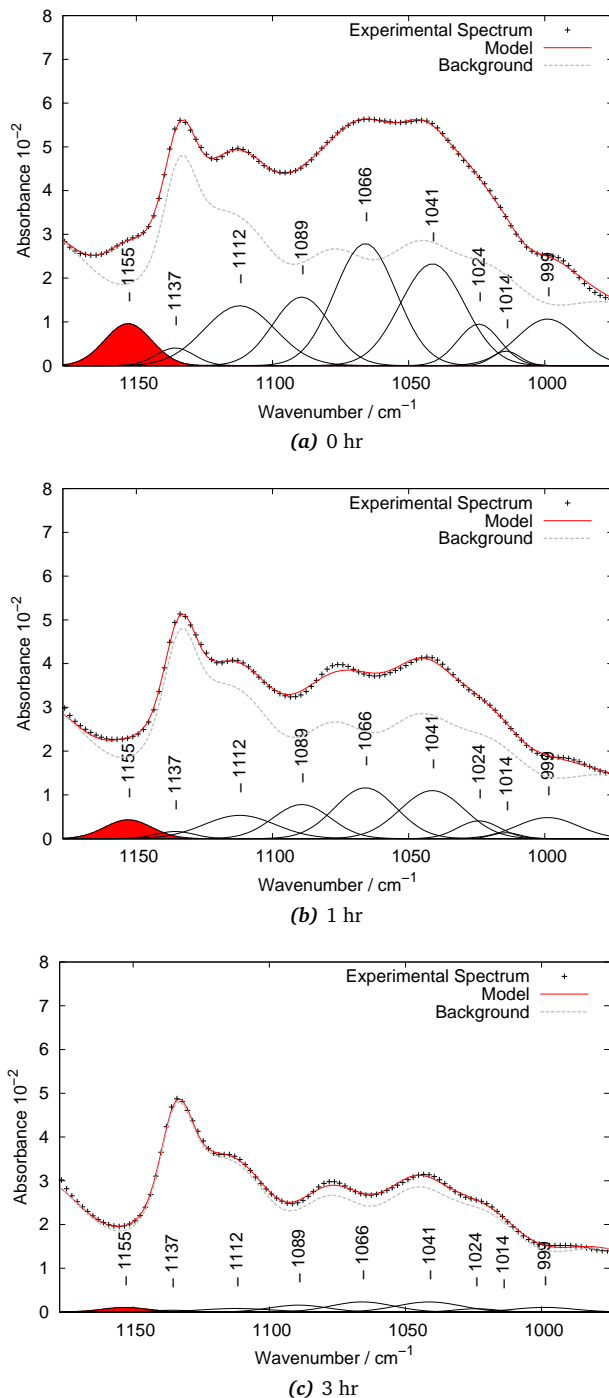
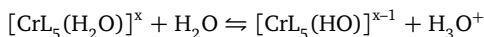


Figure 2.21.: Gaussian deconvolutions of selected spectra during hydrolysis of cellulose by $\text{CrCl}_3 \cdot 6\text{H}_2\text{O}$.

combinations of constraints used in the deconvolutions slightly. The best fitting procedure was obtained by constraining the center parameters while optimizing the amplitude and width. If all parameters were optimized it could in some arbitrary cases occur, that a band would start to "wander off" thus randomly introducing errors. A graphical output, similar to examples shown at figure 2.21 on the facing page, was generated and saved from the deconvolution of each spectra, to document the quality of the deconvolution^m.

The development of the 1155 and 1669 cm⁻¹ during hydrolysis of cellulose can be found at figure 2.22 on the next page. The signal to noise ratio for cellulose became quite significant at high conversions, still it was quite clear that both the rates of the cellulose hydrolysis and the HMF formation showed very pronounced first order kinetics, at least for several hours. It could be argued that the rate of the HMF formation started to decrease faster than what could be explained just by an exponential first order decay. This subject will be discussed in details in the next section, where evidence that the chromium catalyst to some degree is inhibited by the products, will be presented.

The temperature dependency of the rates showed a very good Arrhenius trend, see figure 2.23 on the following page. Activation energies were found to be 92.3±1.2 and 102.2±5.0 kJ/mol for cellulose hydrolysis and HMF formation respectively. The higher activation energy for the conversion of glucose compared to the hydrolysis is also implicated from the deconvolutions at figure 2.21, where a deviation from the model can be seen at around 1175 cm⁻¹ due to a slight accumulation of glucose during the reaction. The activation energy was found to be 102 kJ/mol for the formation of HMF. This reaction will be discussed in much more detail in the next chapter. To my knowledge the activation energy of cellulose hydrolysis using CrCl₃·6H₂O or similar catalysts has not been determined before. Quite surprisingly, the activation energy for chromium catalyzed hydrolysis of the glucoside bond was determined to 92.3±1.2 kJ/mol which is practically identical to the activation energy at 96.4 kJ/mol when using H₂SO₄. As Lewis acids exhibit Brønsted acidity in presence of water, then the explanation at first seemed straight forward, as the similar activation energy of the CrCl₃·6H₂O catalyst, could be related to the formation of catalytically active H₃O⁺ species:



However the Brønsted acidic strength of such Cr^{III} complexes rather low with pK_a values of around 4.2^[156], which are comparable to acetic acid that are known to be almost catalytically inactive towards the hydrolysis of cellulose^[26,60,75]. As the CrCl₃·6H₂O catalyst contrary was observed to be very catalytically active, exhibiting turnover frequencies similar to sulfuric acid, it would seem unlikely that activity should be related to its Brønsted acidity, despite the similar

^mThere have been deconvoluted thousands of spectra using the described method, thus I have chosen to show only representative examples and not to include them all in the appendix.

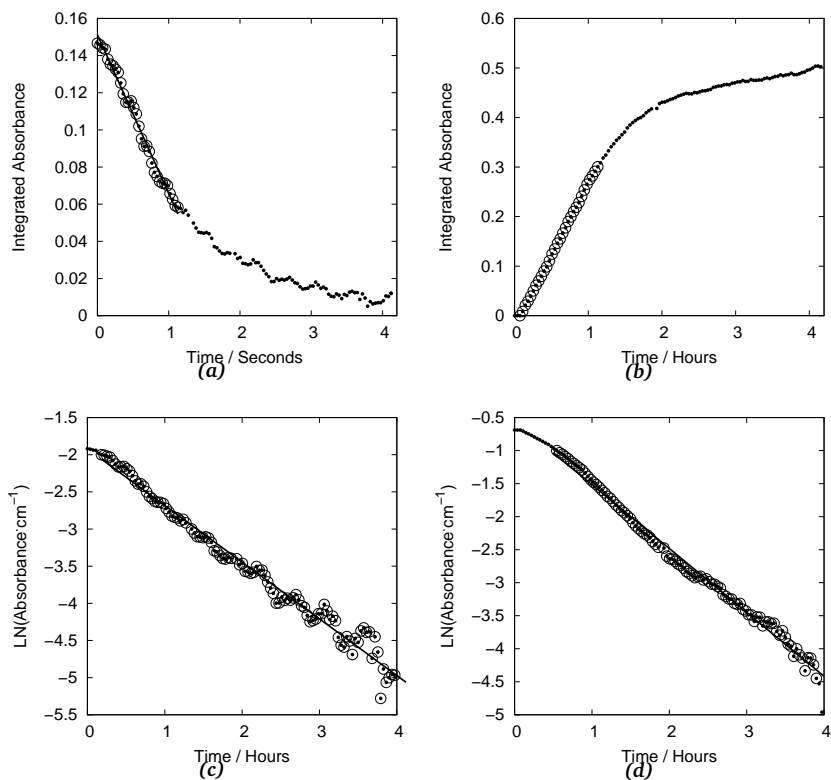


Figure 2.22.: (a) and (b): Change of intensity of band at 1155cm^{-1} and 1669cm^{-1} during cellulose hydrolysis using CrCl_3 . The bands are characteristic for the glucoside bond $\nu_{\text{asym,C-O-C}}$ and $\nu_{\text{C=O}}$ of cellulose and HMF respectively. (c) and (d) shows the corresponding first order plots.

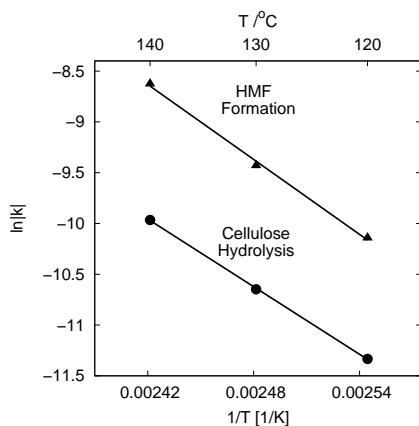


Figure 2.23.: Arrhenius plot showing natural logarithm of hydrolysis rates rates of glucose as a function of $1/T$. The rates are expressed as integrated absorbance per second

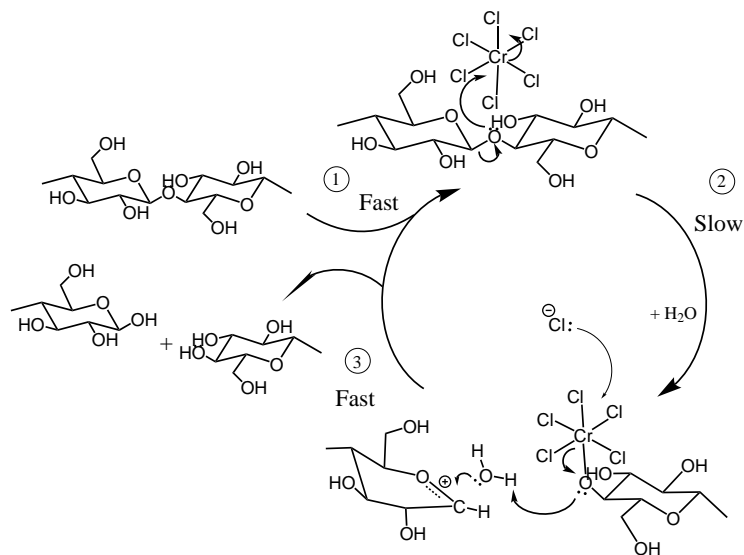


Figure 2.24.: Proposed mechanism for cellulose hydrolysis catalyzed by $[\text{CrCl}_6]^{3-}$ species. The $[\text{CrCl}_6]^{3-}$ species are discussed later. For clarity the $[\text{BMIM}]^+$ cations balancing the overall charge of the active species are not included.

activation energies. This suggested that the reaction passed through an almost identical transition state independent whether the active species was Brønsted or Lewis acidic. On figure figure 2.24 a mechanism for the hydrolysis of cellulose using Cr^{III} as catalyst is proposed. The active species is suggested to be $[\text{CrCl}_6]^{3-}$, which exhibits quite unique properties compared to the analogous $[\text{Cr}(\text{H}_2\text{O})_6]^{3+}$ that are typical found aqueous in solutions of $\text{CrCl}_3 \cdot 6\text{H}_2\text{O}$ ^[159]. In the first step the oxygen in the glycosidic bond is attacked by the Lewis acidic chromium chloride species. After the chromium species coordinate to the glycosidic bond it dissociates into an oxocarbenium ion and an alkoxy species during the rate determining step. By comparison with mechanism catalyzed by protons, see figure 2.1 on page 13, it suddenly becomes clear why the Brønsted and Lewis catalyzed reactions results in identical activations energies, as are they both forced over the same transition state to form the oxocarbenium intermediate independent on catalyst. In the third fast step water hydrates both the alkoxy group and the oxocarbenium, leaving the hydrolyzed glucoside bond and the released chromium site.

A strange phenomena observed during this part of the study, which I have not seen described in the literature, was the rise of a sharp and well defined band at around 1773 cm^{-1} during

ⁿConvincing evidence for chromium(III) to predominantly exists as reactive $[\text{CrCl}_6]^{3-}$ species in alkylimidazolium chloride based ionic liquids has recently been confirmed by in-situ Extended X-Ray Absorption Fine Structure (EXAFS) experiments by simultaneous studies by Andersen et. al and Zhang et al.^[53,157,158]. An elaborated discussion of the $[\text{CrCl}_6]^{3-}$ species in $[\text{BMIM}]\text{Cl}$ are found in the following chapter.

the reactions (see figure figure 2.20 on page 48 (b)). The rate was significantly slower than for both the hydrolysis and the HMF formation, and the activation energy was estimated to be roughly around 138 kJ/mol. The band can most probably be assigned to a $\nu_{C=O}$ mode, but the position is unusually high, and cannot be assigned to carboxylic acids, aldehydes or ketones. Esters usually have quite high $\nu_{C=O}$ bands, up to around 1750 cm^{-1} for aliphatic and slightly lower for aromatic compounds.

Even though the spectrum suggest that this unknown species should be present in quite significant amounts, HPLC analysis showed only showed sign of HMF and small amounts of 5-(hydroxymethyl)-2-furalic acid and at early times fructose^[158]. There are two obvious reasons why the species was not found by HPLC: If the $\nu_{C=O}$ band was associated with ester groups of polymeric humin compounds it would not be soluble in the aqueous eluent and therefore not be detected. However, the band is very sharp and well defined and the high position suggests that it is one well defined species and not a variation of several slightly different ester groups. Further would an ester in a humin like polymer most likely have neighbors like oxygen and aromatic groups which will redshift the band position, thus a position of such $\nu_{C=O}$ this high is not likely.

Another possibility is that the species is not stable in the eluent and can therefore only be observed in-situ. A carbonyl group with a $\nu_{C=O}$ band in this region could be consistent with either acid chlorides or acid anhydrides. However, the anhydrides will have two bands in the area due to both symmetric and antisymmetric stretching modes. However, the acid chlorides fits perfect with the shape and position of the band. The acid chloride will quickly be hydrolyzed if exposed to water. Along the formation of the carbonyl band at 1773 cm^{-1} a weaker band was observed at around 810 cm^{-1} that was not found when hydrolysis was performed with sulfuric acid. This band could be consistent with ν_{C-Cl} modes. However, it has not been possible to find reports, which show that acid chlorides have been formed under similar conditions. More in-situ studies as well as post reaction analysis should be performed to identify the actual nature of this species.

2.4. Concise Conclusions

A thorough comparative analysis of the infrared spectra of cellulose, its oligomers and glucose in the $1200\text{-}950\text{ cm}^{-1}$ region was presented. Through a combination of experimental spectra and theoretical spectra calculated by DFT a band of medium intensity at around 1155 cm^{-1} and a weak band at around 970 cm^{-1} were respectively assigned to the antisymmetric and symmetric C-O-C stretching modes of the glucoside bond in cellulose.

A new methodology based on in-situ ATR-FTIR was shown to be an accurate way to monitor the hydrolysis of the glucoside bond of cellulose and cellobiose in [BDMIM]Cl as well as the

simultaneous formation of HMF. The activation energy for hydrolysis of the glucoside bond was found to be 96.4 ± 4.1 and 69.6 ± 3.0 kJ/mol for cellulose and cellobiose respectively. The value for cellulose was in good correspondence with recent values determined in ionic liquids, whereas the value for cellobiose hydrolysis was surprisingly low as the bonds was expected to be very equal in chemical nature. Molecular modeling showed that this difference could be related to conformational rearrangements around the glucoside bond prior to formation of the critical oxocarbenium ion. These rearrangements seemed only possible for cellobiose and perhaps short chain oligomers. This emphasize that despite the chemical similarities care should be taken when using cellobiose as a model for cellulose.

The kinetics of HMF formation during hydrolysis were elucidated by quantification of the $1669 \text{ cm}^{-1} \nu_{C=O}$ band of HMF. The HMF formation during cellulose hydrolysis seemed to be limited by the slow hydrolysis rate, and the activation energy was found to be 94.7 ± 3.7 kJ/mol - practically identical to the one found for hydrolysis of cellulose. The activation energy for HMF formation during cellobiose hydrolysis was found to be 85.0 ± 1.8 kJ/mol and was assumed to be the actual activation energy for the sulfuric acid catalyzed glucose isomerization, in perfect agreement with literature values.

The method was also applied to two heterogeneous catalysts. First a sulfonic acid functionalized mesoporous SBA-15 catalyst was tested and showed very low activity towards cellulose hydrolysis. This could probably be explained by the difficulties of the long cellulose chains to reach the major part of active sites within the narrow pores inside SBA-15 structure, thus the reaction was speculated only to take place in the pore mouths. The other catalyst was a nanoparticulate sulfated anatase catalyst, which showed remarkably high activity. This could either be due to leaching of protons into the ionic liquid media, or due to heterogeneous catalysis in a very good and almost colloid-like suspension of the small nano-particles in the ionic liquid. The activation energy was determined to 94.3 ± 3.6 kJ/mol.

Finally the Lewis acid catalyzed hydrolysis of cellulose was investigated using the Lewis acidic catalyst $\text{CrCl}_3 \cdot 6\text{H}_2\text{O}$. A surprising outcome of this study was that the activation energy was found to be 92.3 ± 1.2 practically identical to the one found for sulfuric acid. This was explained in a proposed mechanism showing that the Lewis acid catalyzed mechanism would form the same type of oxocarbenium species independent of the catalyst.

The HMF formation in presence of chromium seemed to proceed via another mechanism than when using sulfuric acid, as the activation energy of 102 kJ/mol was significantly higher compared to sulfuric acid. The slow formation of a strange carbonyl species was observed at around 1773 cm^{-1} . The activation energy for formation of this species seemed to be signifi-

cantly higher than the other reactions. The spectral features could be consistent with acid chlorides, but more investigation needs to be performed to elucidate the nature of this species.

Chromium catalyzed glucose conversion

In the previous chapter it was shown that both Brønsted acids and Lewis acids are able to catalyze the hydrolysis of glucoside bonds and the subsequent transformation of the produced glucose into HMF and even further into carboxylic acids and humins. Even though sulfuric acid is a very active catalyst for the entire process it is not very selective and significant amounts of the products are lost due to the formation of humins. The last few years several transition metal chlorides and even alkaline earth metal chlorides have been investigated as catalysts for this process^[48,64-68,153]. In the famous work by Zhao et al.^[48] the group showed that especially chromium chloride in oxidation state +2 and +3 were very efficient in both the isomerization of glucose and the subsequent dehydration of fructose to HMF with almost 100 % selectivity. They concluded that CrCl_2 were the most active oxidation state of chromium, as both the conversions and HMF yields were significant higher than when using $\text{CrCl}_3 \cdot 6\text{H}_2\text{O}$. For some time it was almost neglected that CrCl_3 also was active in the reaction. The group of Pidko and Hensen has published a quite extensive amount of article concerned with the structure of the active chromium complex and its catalytic role in the conversion of glucose^[50-53]. By DFT calculations they show that the highest transition state is 63 kJ/mol for the glucose isomerization catalyzed by CrCl_2 in alkyl-imidazolium chlorides^[50-52]. In another study they however conclude that CrCl_3 is much more active than CrCl_2 , and calculate the activation energies to respectively 66 and 93 kJ/mol^[53]. In none of their numerous papers within this field they actually attempt to determine an activation energy experimentally.

Several studies on the other hand reports that Cr^{III} is in fact more active than Cr^{II} , at least at shorter reaction times^[49,144]. There are several good reasons why the catalytic activity of Cr^{III} has been questioned. Cr^{III} species are known to form the some of the most kinetic stable complexes among all of the transition metals, and is often used as the textbook example of "inert" coordination compounds. Measuring the half-time for ligand exchange in water of

the $[\text{Cr}(\text{H}_2\text{O})_6]^{3+}$ complex it is around 40 hours^[160]. The activation energy of the ligand exchange process in water has been determined in several studies to be as high as 100-110 kJ/mol^[161-165]. For comparison the activation energy for ligand exchange in aqueous Cr^{II} complexes is as low as 14 kJ/mol^[160]. With this in mind it is clear that the concept of a catalytic active Cr^{III} species has been handled with some skepticism. There are however several indications in literature showing that the concept of active Cr^{III} species, should not be eliminated simply as a knee-jerk reaction solely based on common knowledge. First of all, as it was also implicated in the previous chapter, the activation energy for catalyzed isomerization itself seem to be in the same order of magnitude as the referred ligand exchange processes in water. Furthermore the majority of classical coordination chemistry is performed solely with water as a solvent or in mixtures where water is present in very high concentrations, thus it can not necessarily be compared directly to ionic liquid chemistry.

Looking in the older literature there are examples of labile Cr^{III} systems with significantly faster ligand exchange kinetics, and even in water there are several of examples of Cr^{III} species that cannot be considered kinetically inert. Banerjee et al. showed that the rate for ligand exchange of water with the amino acid glycine, in $[\text{Cr}(\text{H}_2\text{O})_6]^{3+}$ under slightly acidic aqueous conditions, was surprisingly high. The authors could determine the activation energy to be as low as around 52 kJ/mol^[166]. The group speculated that the reason for the fast kinetics was the formation of an ion pair of $[\text{Cr}(\text{H}_2\text{O})_6]^{3+}$ and glycine prior to exchange.

Narusawa et al. studied the aquation and chloride anation of various Cr^{III} complexes in strong hydrochloric acidic solutions (9-12M)^[167] and found activation energies as low as 32 kJ/mol for the exchange processes. It seemed to be a consequence of the strong ionic environment. Similar results were reported by later studies^[168-170]. This suggests that the ligand exchange process of Cr^{III} complexes in some cases can exhibit much higher rates than the one known from aqueous systems in general. The results presented in previous chapter shows that one should keep an open mind when comparing reactions in water and ionic liquids. The ionic liquids seem to be able to alter some of the catalytic pathways.

3.1. In-situ Investigations of the Chromium Catalyzed Glucose Conversion

The most papers concerned with chromium catalyzed glucose conversion are often performed using quite different reaction parameters, such as catalyst loading, temperature and reaction time. This makes these studies very hard to compare, and it is quite rare to see actual kinetic data reported. In the following the results of an extensive kinetic study of the chromium catalyzed glucose conversion into HMF will be presented. The investigations have been performed using the in-situ ATR-FTIR method presented in the earlier chapter. Kinetic experiments were performed using a similar procedure as for the investigations of the cellulose

hydrolysis. In the simultaneous discussion of the kinetics some structural indications of the active species obtained from in-situ EXAFS experiments are included. The credit for these in-situ EXAFS experiments including the data analysis and interpretation solely belongs to Ph.d. student Jonas Andersen as a part of his master thesis project in 2012^[157,158].

3.1.1. The apparent kinetics of glucose conversion in presence of $\text{CrCl}_3 \cdot 6\text{H}_2\text{O}$

The green $\text{CrCl}_3 \cdot 6\text{H}_2\text{O}$ salt is a cheap Cr^{III} source that dissolves fast in [BMIM]Cl yielding in a pink solution probably due to the loss of water ligands. If a solution of $\text{CrCl}_3 \cdot 6\text{H}_2\text{O}$ in [BMIM]Cl is left out in the ambient atmosphere it will turn green due to the absorption of water. The solutions was made by preparing [BMIM]Cl solutions of chromium and glucose separately by applying gentle heating and mixing them afterwards to ensure both complete dissolution of both cellulose and chromium chloride, and to avoid glucose conversion before the experiments started. Initially the reactions was investigated in the microreactor described previously at temperatures from 80-130 °C in steps of 10 °C. On figure 3.1 on the following page the conversion of glucose at 80, 110 and 130 °C is shown.

For the quantification of HMF the $\nu_{\text{C}=\text{O}}$ at around 1670 cm^{-1} was used and for glucose the intense $\nu_{\text{C}6-\text{O}6}$ band at 1042 cm^{-1} was chosen, as it did not seem to have any significant overlaps with HMF in this region except from a weaker shoulder band. The development over time showed an unexpected behavior at high conversion by approaching an asymptotic flat shape when significant changes was still observed for the 1670 cm^{-1} $\nu_{\text{C}=\text{O}}$ band of HMF. At first this was explained by the glucose isomerization only being the first step to obtain HMF, thus the final formation of HMF could be delayed as fructose and other intermediates that might not absorb as strongly at 1042 cm^{-1} . However, at later times in the experiment no significant amounts of fructose or other intermediates could be detected by HPLC.

Instead it turned out that when HMF was dissolved in [BMIM]Cl the weak shoulder at around 1040 cm^{-1} suddenly became very intense (see appendix - figure C.1 on page 149). At this point intensive work hours were already put into the data processing of a comprehensive amount of spectra. Instead of reprocessing all spectra using another band a correction procedure was developed to clean out the contribution of HMF to the intensity of 1042 cm^{-1} band of glucose: The relation between the 1670 and 1040 cm^{-1} bands of HMF in [BMIM]Cl was investigated at different concentrations (see appendix: Figures C.2 and C.3 on pp. 150-151). It was as expected found that these two IR bands of HMF were indeed proportional, and hence the contribution from HMF to the area of the 1042 cm^{-1} band of glucose, could be subtracted from the deconvoluted band area using this simple relationship.

The development of HMF and glucose concentrations, expressed as integrated absorbance, for selected temperatures is shown in figure 3.2 on page 61. At these figures the concentration of glucose is shown using the described correction procedure. Data for all six temperatures

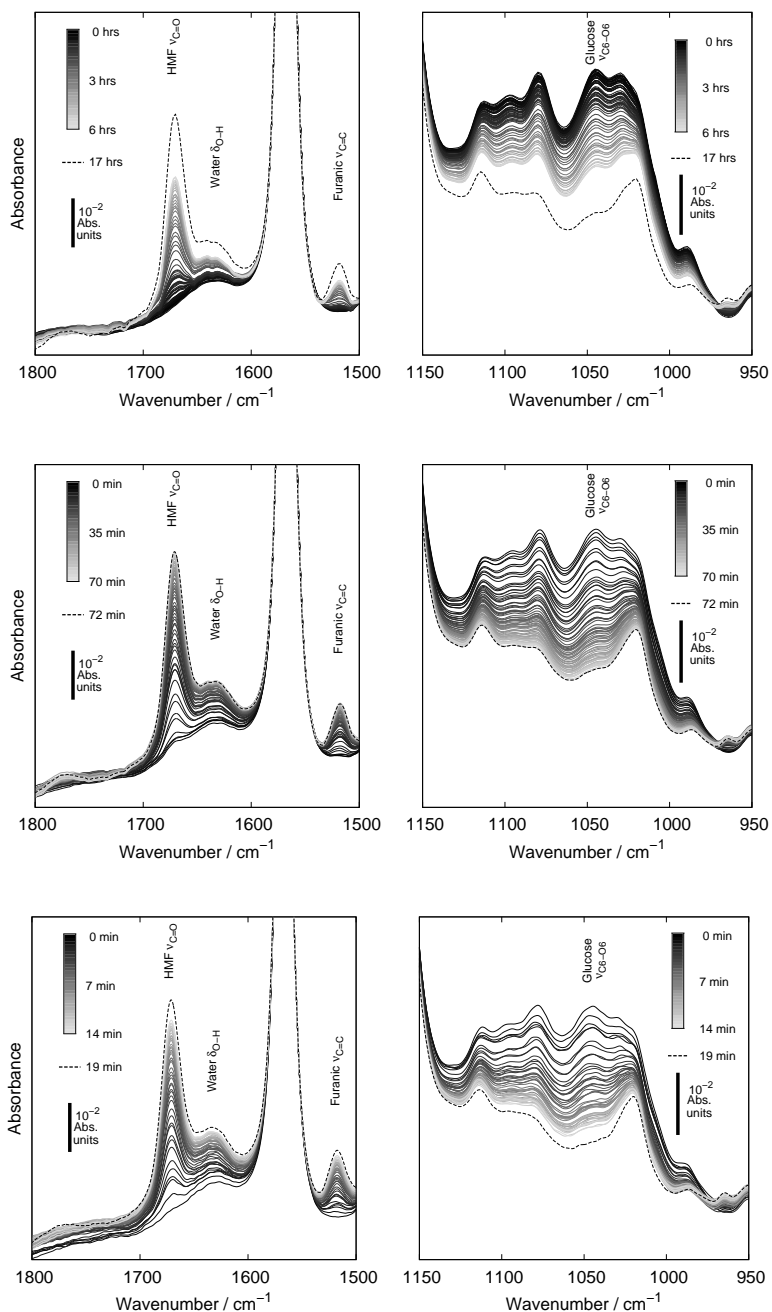


Figure 3.1.: *In-situ* AFT-FTIR spectra of glucose conversion at 80, 110 and 130 °C, from top to bottom respectively, all in the presence of $\text{CrCl}_3 \cdot 6\text{H}_2\text{O}$ in the sealed microreactor. Selected full region spectra can be found in appendix: see figure C.6 on page 154

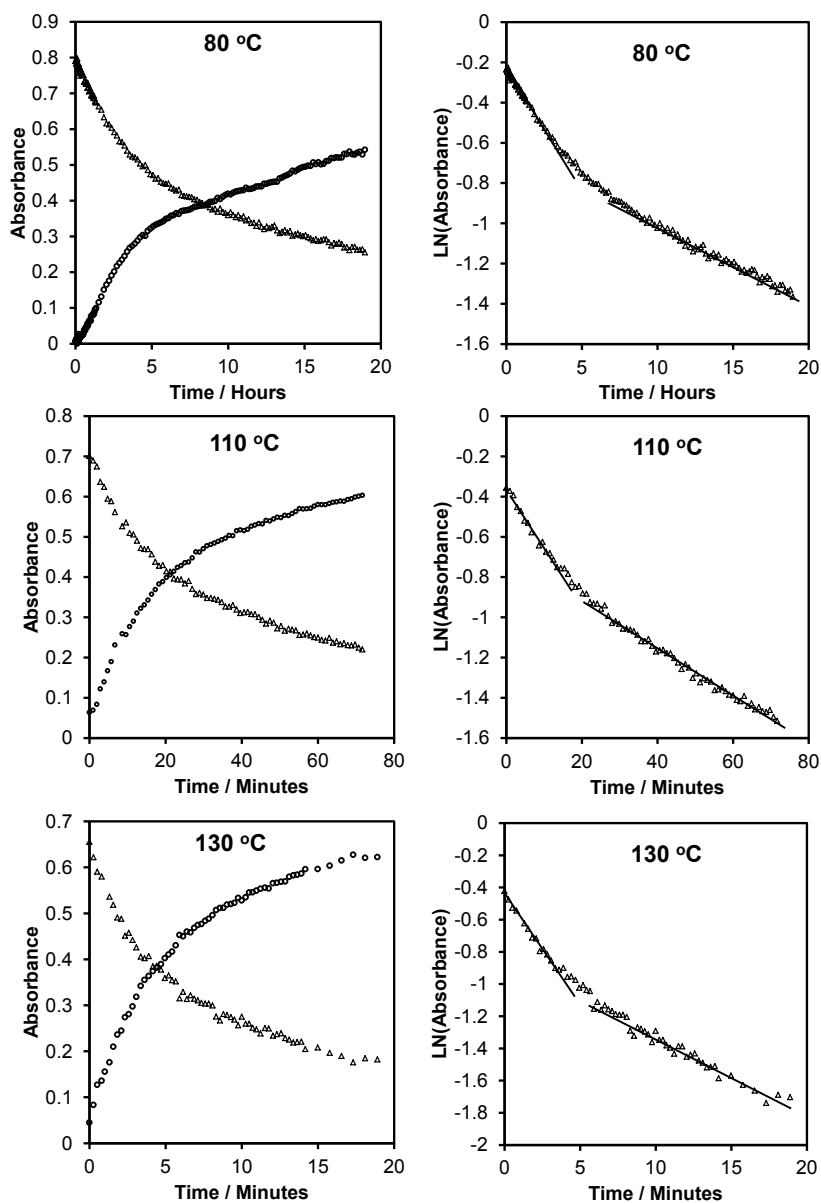


Figure 3.2.: *Left:* Development of 1670 and 1042 cm^{-1} bands during glucose conversion at 80, 110 and 130 °C in the presence of $\text{CrCl}_3 \cdot 6\text{H}_2\text{O}$ in the sealed microreactor. The area of the 1042 cm^{-1} is corrected from the contribution from HMF according to figure C.2 on page 150. *Right:* Natural logarithm to glucose concentration expressed as absorbance. Δ shows the corrected area of the 1042 cm^{-1} band due to glucose, while \circ shows the 1670 cm^{-1} band due to HMF. Indicative lines are shown to illustrate first order domains.

Table 3.1.: Final conversions and yields estimated from absorbances of 1670 and 1042 cm^{-1} bands

Temperature	HMF yield	Conversion	Selectivity	reaction time
130°C	65%	72%	90%	19 min
110°C	63%	68%	93%	72 min
80°C	59%	68%	87%	19 hrs

comparing the raw with the uncorrected data is found in appendix on figure C.4 on page 152, together with representative full region spectra on figure C.6.

The reaction was assumed to be first order with respect to glucose, and this assumption was tested by plotting the natural logarithm of the glucose band area, as a function of time (see figure 3.2 on the preceding page right hand side). At lower conversions the reaction does exhibit first order kinetics, however after some time the rate decreases more than what can be related to first order dependency of glucose. As explained in the introduction to this chapter Cr^{III} complexes are strongly coordinating species, and are known to make very kinetic stable complexes especially with water. For each reaction turn-over three water molecules are formed along with one HMF molecule. This increasing competition of the free chromium sites could very well explain why we see this unexpected high decrease in reactivity of the chromium species as the reaction proceeds. This hypothesis will be explored further in the following sections of this chapter. The reaction did at all six temperatures that were investigated, exhibit a fast first order rate initially, and then at higher conversions, a much slower rate which also seemed to be first order.

As a very exact calibration study has not been made in this chapter, it was in general chosen to present the development of HMF and glucose as absorbances instead of converting them to concentrations. However, from the HMF standard curve and from theoretical conversion of the wt.% concentration to v/v % basis by using table values for densities, it was possible to make some reasonable estimates of the total conversions and yields. These values are presented in table 3.1. Here it gives reasonable selectivities around 90 % for all temperatures, which is in good correspondence with literature values^[48,153]. Especially taking into consideration that the formation of the unknown carbonyl species with a $\nu_{\text{C=O}}$ absorption band at around 1773 cm^{-1} , covered in previous chapter, also appeared in these experiments.

The values for conversion corresponds very well to literature values that all reports a maximum conversion around 70-75% for Cr^{III} catalyzed conversion of glucose in ionic liquids, when starting from similar glucose concentration^[48,55]. At lower glucose concentrations or higher chromium concentrations it is however possible to reach a more or less complete conversion of glucose^[171]. This supports the assumption water and HMF were able to inhibit the catalyst. Due to the high time resolution of the experiments, the initial rates could be determined accu-

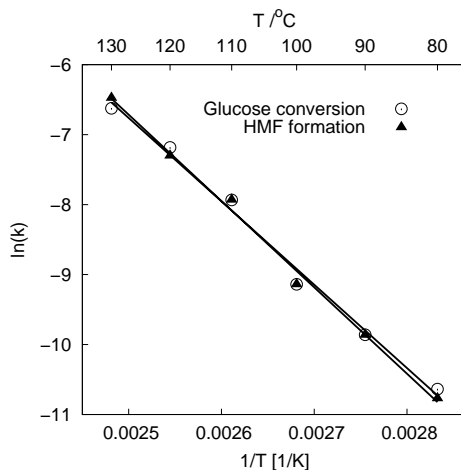


Figure 3.3.: Arrhenius relation between natural logarithm to initial and reciprocal temperature. Rates are in integrated absorbance per second.

rately from the spectroscopic data. These calculated rates are presented in the Arrhenius plot in figure 3.3. Surprisingly the extinction coefficients of the 1670 and 1040 cm^{-1} bands were by coincidence very similar. The activation energies were found to be 99.0 ± 4.5 kJ/mol and 102.6 ± 3.6 kJ/mol for glucose conversion and HMF formation respectively, which is identical within the experimental uncertainty suggested by the standard deviations. Not unexpected this indicates that the rate limiting step, is the glucose isomerization. It is a very good reproduction of the 102.2 kJ/mol found for glucose isomerization during cellulose hydrolysis. This is significantly higher than the theoretical activation energy calculated by DFT to around 63 kJ/mol by Pidko et al., suggesting that the calculated transition state may not describe the actual transition state very well^[50–53].

Qi et al. reported a similar activation energy at 114 kJ/mol using micro wave radiation, which is in reasonable agreement with the one reported here^[171]. The in-situ FTIR determination of the reaction rates allows for a time-resolution as good as a few seconds. This allowed for the determination of the initial pseudo zero order rates, on the basis of several data points, even at higher temperature. Qi et al. uses post reaction analysis by HPLC, which has got a much lower time-resolution, that even at the high rates are as low as around 1 minute and hence they use the overall first order rates. The use of first order rates with as low as three data points and at very different conversions intervals, introduces uncertainties in the individual rate determination. Especially at higher temperatures this should expect to cause significant problems. Even though their rates results in very straight Arrhenius plot which is a bit surprising, see figure C.7 on page 155.

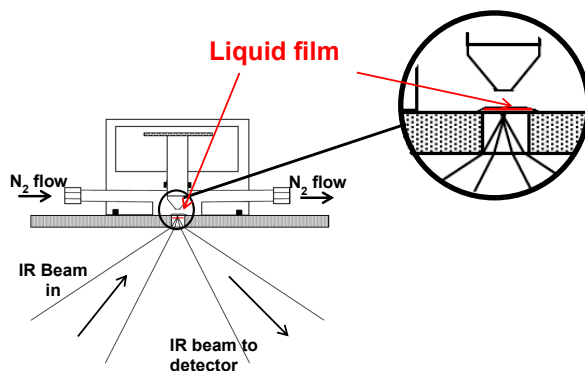


Figure 3.4.: ATR-FTIR setup used to investigate the reactions in thin ionic liquid film.

3.1.2. The kinetics of glucose conversion during anhydrous conditions

In the previous section it was shown that there was a strong deviation from the initial first order kinetics beyond 30-35 % conversion, suggesting that the chromium catalyst was possibly inhibited by the products from the dehydration. In the light of the massive attention on the chromium catalyzed conversion of glucose in ionic liquids, it is remarkably so that focus on factors concerning the kinetics has been so very little. However, more groups have seen that the chromium catalysts seem to be sensitive to inhibition. Zhao et al. also observed that the reaction could be strongly inhibited by coordinating ligands: By adding the inert glucose like hemiacetal dimer of glyceraldehyde during reaction they could suppress the yield from 70 to 20 %. By adding the strongly coordinating ligand 2,2'-bipyridine they could almost block the reaction completely, yielding in only 2 % HMF^[48]. Hu et al. investigated the influence of reaction time and temperature using 9.5 wt.% glucose in tetraethyl ammonium chloride with $\text{CrCl}_3 \cdot 6\text{H}_2\text{O}$ as catalyst. Much like in this study observed that the conversion could not be raised much above 70 % even at high temperatures and long reaction times. This indicates that the catalyst could be almost completely deactivated by the formed products^[55].

The penetration of the evanescent beam into the ionic liquid is below $2 \mu\text{m}$ when using a diamond ATR plate. This low penetration together with the extremely low vapor pressure of ionic liquids, has allowed us to study the reaction in-situ in a very thin ionic liquid film, while applying a flow of dry nitrogen on over the film. In this way the dependency of water was explored using the same reaction mixtures made from $[\text{BMIM}]\text{Cl}$, glucose and $\text{CrCl}_3 \cdot 6\text{H}_2\text{O}$. Water was removed in-situ by the flow of dry nitrogen over the sample.

Initially it was assumed that it was possible to remove both water and HMF simultaneously, and then solely measure the glucose disappearance rate. The HMF concentration in the thin film was however not at all affected by the flow of nitrogen. Even if we applied strongly reduced

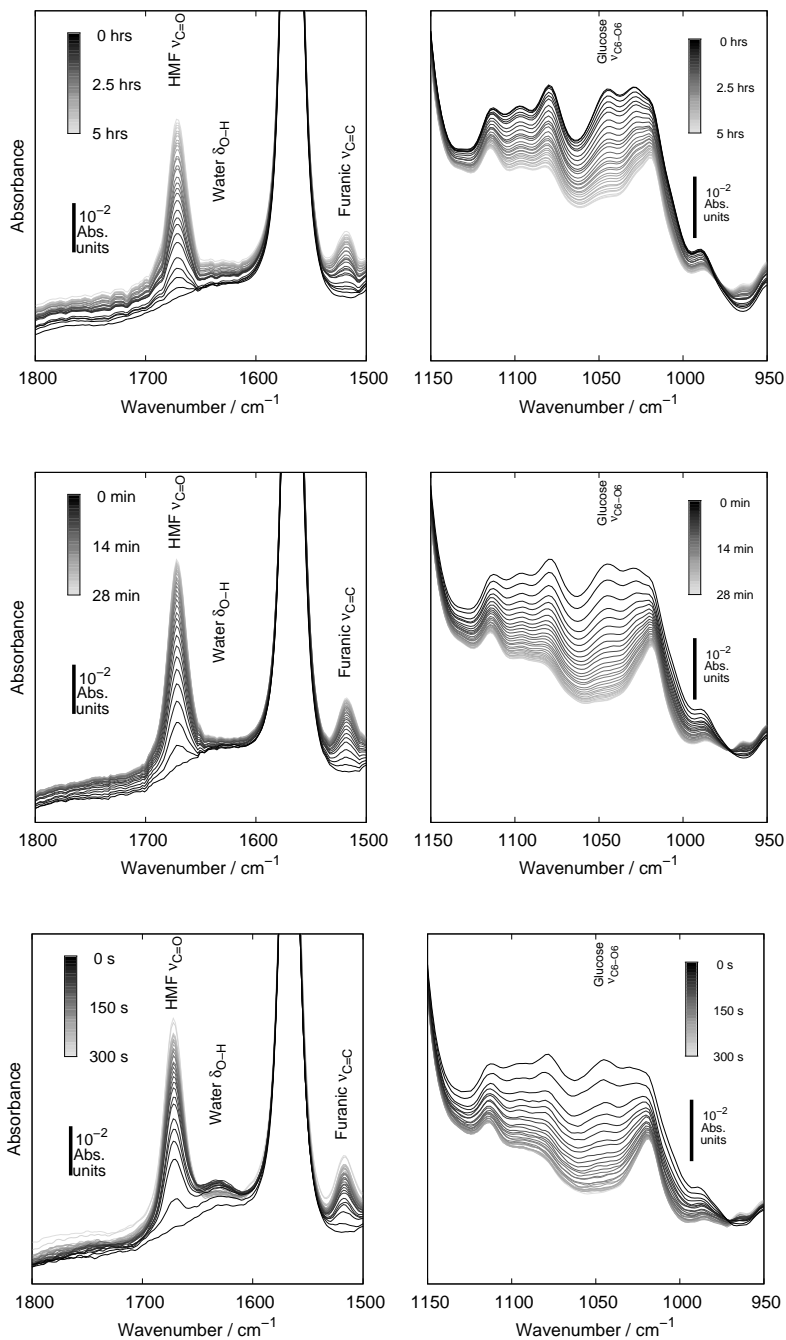


Figure 3.5.: In-situ AFT-FTIR spectra recorded during glucose conversion at 80, 110 and 130 °C, from top to bottom respectively, in the presence of CrCl_3 in thin film dried by nitrogen flow during reaction

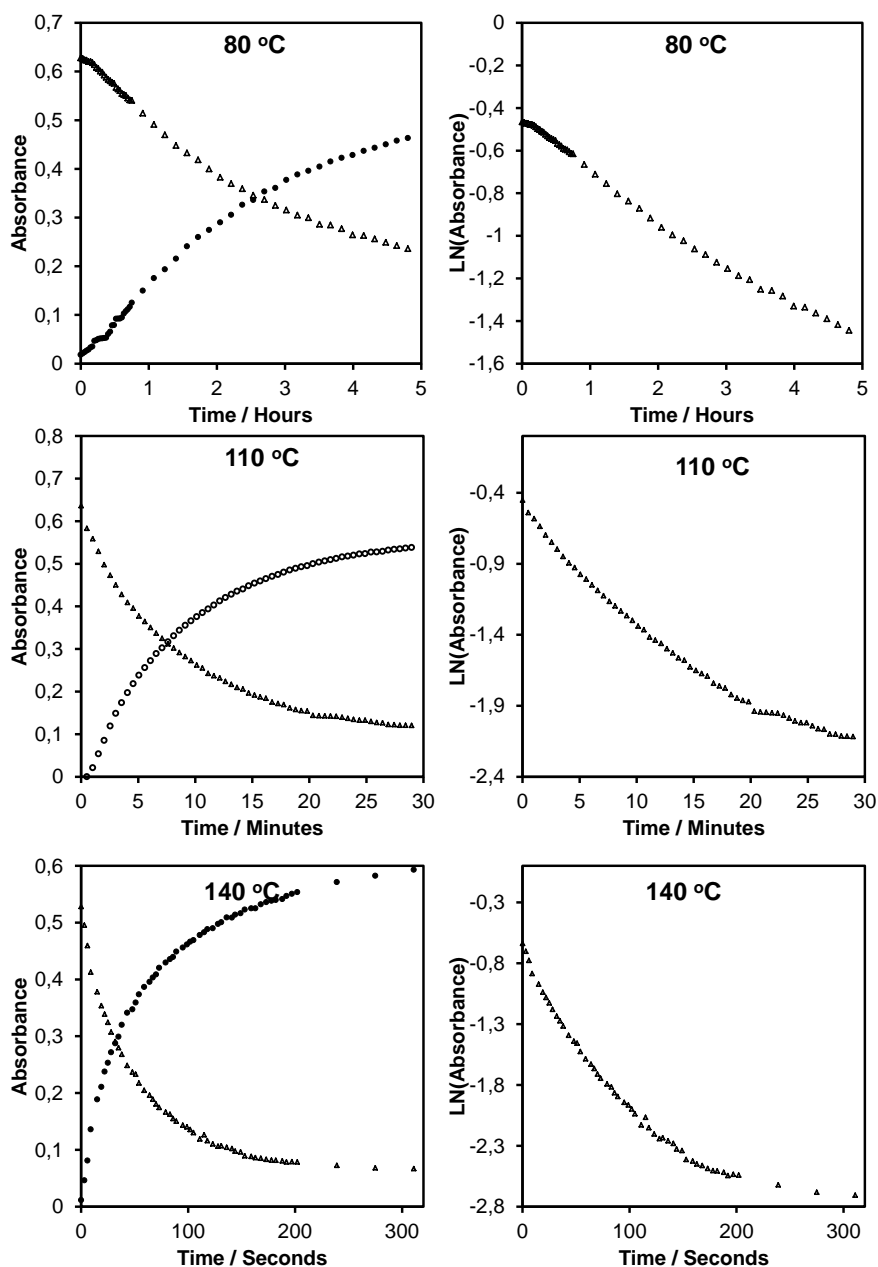


Figure 3.6.: Left: Development of 1670 and 1042 cm^{-1} bands during glucose conversion at 80, 110 and 130 °C presence of CrCl_3 in thin film dried by a nitrogen flow during reaction. The area of the 1042 cm^{-1} is corrected from the contribution from HME according to figure C.2 on page 150. Right: Natural logarithm to glucose concentration expressed as absorbance. Δ shows the corrected area of the 1042 cm^{-1} band of glucose while \circ shows the 1670 cm^{-1} band of to HME.

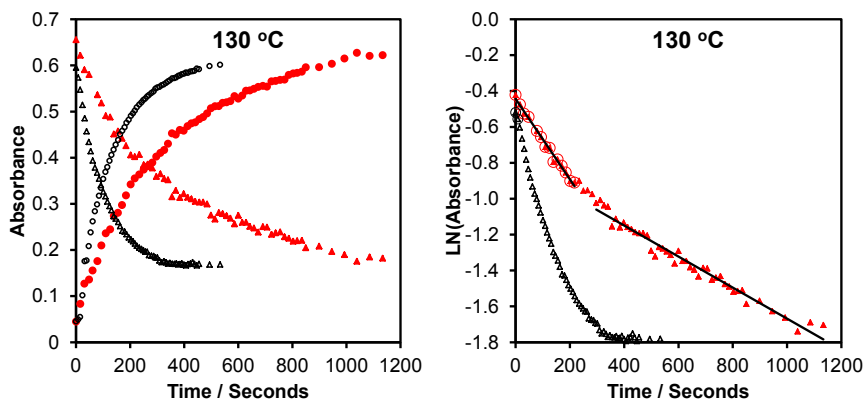


Figure 3.7.: Conversion of glucose into HMF in $[BMIM]Cl$ using $CrCl_3 \cdot 6H_2O$ as catalyst at 130 $^{\circ}C$. Filled red series shows the reaction in the sealed microreactor whereas the hollow black points shows the reaction in the anhydrous thin film. Triangle shows the relative formation of HMF (1670 cm^{-1} band) and circles shows the relative consumption of glucose (corrected 1042 cm^{-1} band).

pressure the result was the same, HMF was very strongly bound by the ionic liquid film^a. It was possible however to remove practically all water from the sample simultaneously with the dehydration of sugar in the solution. The low water content was insured by monitoring by the absence of OH stretching and bending modes at around 3400 and 1600 cm^{-1} . At very high reaction rates at $130\text{ }^{\circ}C$ the film was not completely water-free though.

Spectra recorded during selected temperatures can be found in figure 3.5 on page 65. As shown the water from the $CrCl_3 \cdot 6H_2O$ initially was removed very fast by the nitrogen flow, and the water concentration was kept at a constant very low level throughout the reaction. The removal of water had a significant influence on the reaction rates. On figure 3.7 the reaction in the sealed microreactor is compared to the reaction in the anhydrous thin film. The initial rates were found to be around 2-3 times higher than with water present, showing that water indeed was inhibiting the chromium catalyst. In the microreactor the reaction followed first order kinetics after until approximately 35 % conversion whereafter the rate decreases and a new and lower steady 1st order rate was obtained. For the anhydrous thin films the first order domains seems less apparent and at conversions after around 60 % the rate decreased and gradually approached zero.

There are two hypotheses that would explain the slower rate in the presence of water: The first could be higher activation energy due to the blocking of a more favorable mechanism. This could be the case if the ligand exchange process suddenly became the rate determining step.

^aA thin film of a HMF solution in $[BMIM]Cl/CrCl_3$ was exposed to reduced pressure at 20 mbar in-situ on the ATR plate. At $100\text{ }^{\circ}C$ HMF concentration in $[BMIM]Cl$ over a period a negligible change (less than 10%) was observed over 20 minutes. In the flow of dry nitrogen absolutely no change in HMF concentration could be observed in this period of time.

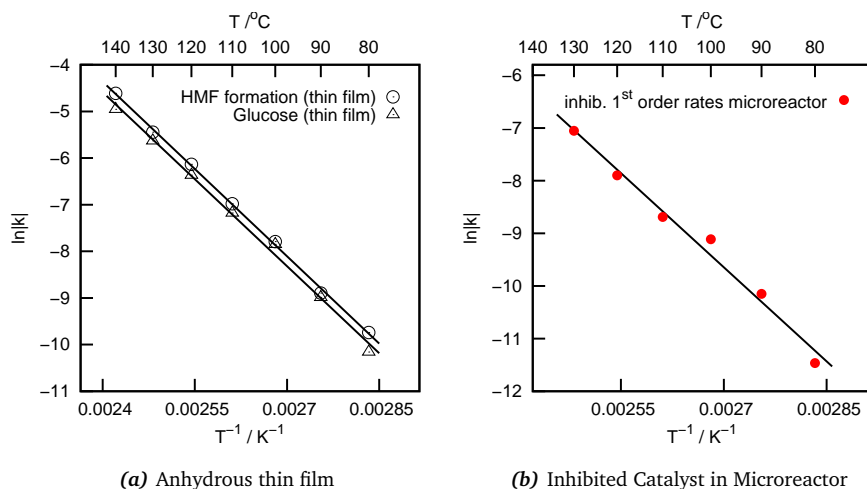


Figure 3.8.: (a) Arrhenius plot of initial zero order rates obtained from reactions in anhydrous thin films. (b) Arrhenius plot of the slow first order rates obtained from reactions in the microreactor, after inhibition by products. Rates are corresponding to the slow rate shown in figure 3.7 (right hand side)

The other explanation could be that the activation energy was the same but water was blocking some of the active chromium sites. The activation energies for the glucose isomerization in the anhydrous film was determined to be 103.8 ± 1.6 and 103.5 ± 3.2 kJ/mol for HMF formation and glucose consumption respectively, see figure 3.8 (a). Because the rates are significantly higher in the anhydrous film but activation energy, determined from the initial rates, is identical this clearly indicates that the inhibition happens by blocking of the active chromium sites but leaves the reaction mechanism the same.

As it is seen on the comparison on figure 3.8 (b), the first order rate approaches a constant value after the catalyst is inhibited with the products. These inhibited first order rates was determined using the spectroscopic data from the reactions in the microreactor, and the activation energy was determined to 99.12 ± 6.2 kJ/mol. This emphasizes that at high water and HMF concentrations the inhibition mechanism is still blocking of the chromium active sites.

After some time the reaction almost completely stops whether water is present or not, at and the conversion curve approaches an asymptotic value. As told earlier the coordination of HMF to the $[BMIM]Cl-CrCl_3$ is indeed very strong. Pure HMF has a boiling point just around $115^\circ C$ very similar to water, but is much harder to remove from the thin films. This suggests that that also HMF is most likely a very strong inhibitor of the active chromium species, and explains why HMF yields higher than around 75 % therefore is not reported under similar reactant and product conditions.

In a recent study by Bali et al, they explored the catalytic activity of several Cr^{III} and Cr^{II} com-

plexes for glucose conversion in [EMIM]Cl. They showed that the $\text{CrCl}_3(\text{THF})_3$ salt requires an activation, where the catalyst is heated in the ionic liquid, prior reaction to exhibit high activity. But after activation shows to be the most active chromium salt for the HMF conversion^[49]. They also showed that Cr^{III} complexes with very strong coordinating ligands such triacetylacetonate chromium(III) are practically inactive. The triacetylacetonate chromium(III) complex is known to be as kinetically stable as the hexaaquachromium complex^[172]. It is very likely that HMF can form the same kind of very stable complexes with Cr^{III} .

3.1.3. Dependency on chromium concentration

It had been argued that the catalytic activity of Cr^{II} and Cr^{III} towards glucose isomerization could rely on the formation transient chromium dimers, and evidence has been presented that such dimers are likely to exist in mixtures of chromium chloride, glucose and ionic liquids^[50,52,53]. If the active species are transient chromium dimers, these species must be formed from two chromium monomers prior to the coordination to glucose and subsequent reaction. A direct consequence of the hypothesis is that it would make catalytic activity second order dependent on the chromium concentration. Even if the catalytic activity is due to a mixture between active chromium monomers and dimers the reaction dependency must at least be higher than 1.

A classic reaction order experiment was performed where the glucose concentration was kept constant and the concentrations of $\text{CrCl}_3 \cdot 6\text{H}_2\text{O}$ were varied from the concentration of around 10 mole % with respect to glucose down to around 1 mole %. The rates were determined using the anhydrous thin film method described earlier, to ensure that the water added along with the chromium catalyst would not influence the experiment. The rate plotted against concentration is plotted in a double logarithmic plot at figure 3.9 on the following page. The rate and concentration showed a very ideal first order relationship with a coefficient of 0.97 ± 0.047 . This very clearly suggests that the active species are not related to transient dimeric chromium species, but solely comprises monomeric chromium species.

However this does not mean that the dimeric species could not exist and could play an important role. Recent results from our laboratories using Electron Spin Resonance spectroscopy (ESR) by Malcho and Mossin, suggest that dimeric Cr^{III} species are formed, along with a broad heterogeneous series Cr^{III} complexes, during the conversion of glucose with $\text{CrCl}_3 \cdot 6\text{H}_2\text{O}$ in [BMIM]Cl^[173]. However, the kinetic investigations presented earlier in this chapter suggest that these species actually could be partly responsible for the deactivation of the proposed catalytically active $[\text{CrCl}_6]^{3-}$ species.

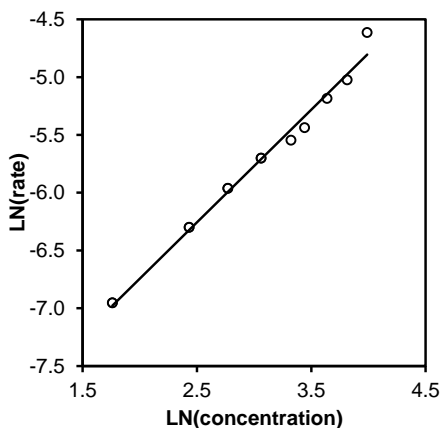


Figure 3.9.: Rate dependency of $\text{CrCl}_3 \cdot 6\text{H}_2\text{O}$ content at $140\text{ }^\circ\text{C}$ under anhydrous conditions. Rates converted to mol/s using the standard curve and concentrations are in mmole Cr^{III} /g solution. The slope was determined to be 0.97 which shows that the glucose conversion is first order dependent on the chromium concentration.

3.1.4. Glucose conversion catalyzed by Cr^{II} species

The first systematic screening of metal chloride catalysts for glucose conversion in ionic liquids by Zhao concluded that CrCl_2 results in higher HMF yields than any of the tested catalysts. Around 95 % conversion could be achieved with CrCl_2 whereas $\text{CrCl}_3 \cdot 6\text{H}_2\text{O}$ only resulted around 70 % conversion^[48]. Normally the Cr^{II} species are considered very unstable due to very easy oxidation by oxygen or even by water to Cr^{III} . However, the oxygen solubility in ionic liquids is extremely low compared to other solvents^[174], and this makes Cr^{II} species quite stable in dry ionic liquids. Therefore the catalytic activity of CrCl_2 was tested on glucose in $[\text{BMIM}]\text{Cl}$. $[\text{BMIM}]\text{Cl}$ was out gassed carefully before the CrCl_2 solution was made, to avoid oxidation to Cr^{III} . Further the reaction mixture were prepared in glove box.

The reaction was carried out in a thin film, the same way as described in the previous section, at temperatures from 110 to $140\text{ }^\circ\text{C}$ in steps of $10\text{ }^\circ\text{C}$. Selected spectra and developments of the characteristic band areas can be found at figure 3.10 on the next page and figure 3.11 on page 72 and in appendix on figures C.10-C.12 on pages 158-160. The rate was observed to be remarkably slower than when using the CrCl_3 as catalyst. Initially another weaker $\nu_{\text{C=O}}$ shoulder band was rising at around 1690 cm^{-1} together with the more intense 1670 cm^{-1} $\nu_{\text{C=O}}$ band of HMF. At first this was assumed to be byproducts formed due to the presence of Cr^{II} , however later it was found that this was not exactly the case. The possible origin of this band will be discussed later, during the section concerned with fructose dehydration starting at page 79. On basis of the HMF formation the activation energy was determined to be $104.1 \pm 8.1\text{ kJ/mol}$, see figure 3.12 on page 73. The identical activation energy suggests that it could be

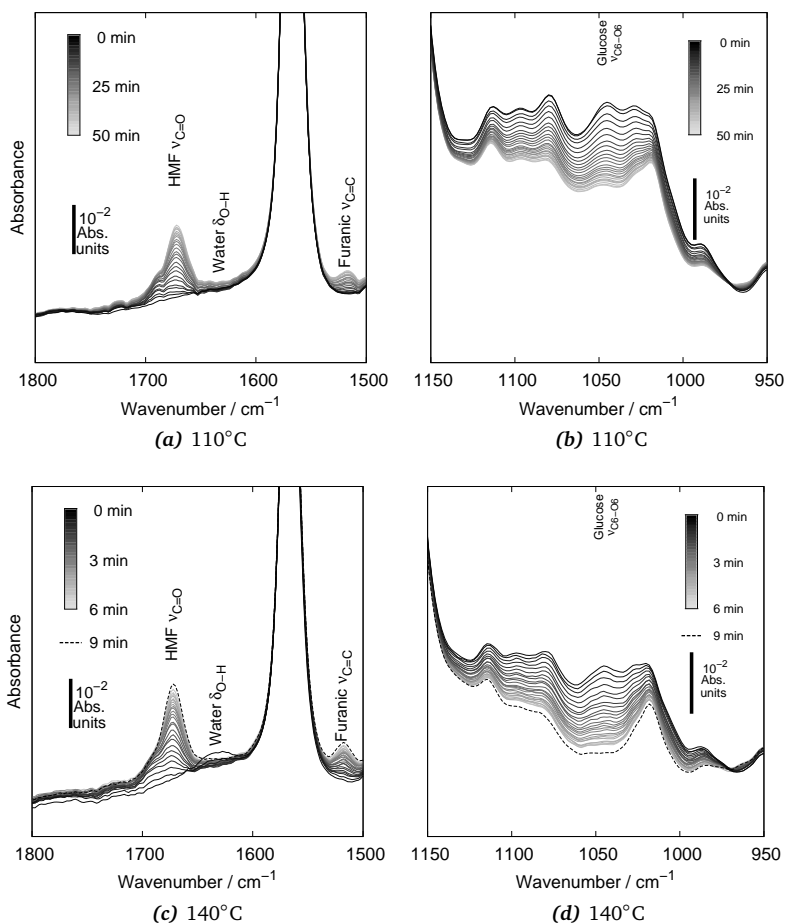


Figure 3.10.: In-situ AFT-FTIR spectra recorded during glucose conversion at 110 and 140 °C in the presence of CrCl_2 in thin film of anhydrous bmimcl dried by nitrogen flow during reaction.

the same species responsible for the glucose isomerization whether CrCl_2 or $\text{CrCl}_3 \cdot 6\text{H}_2\text{O}$ was used as catalyst. It cannot be excluded that both Cr^{II} and Cr^{III} species are active in the reaction mechanism thus yielding in the same activation energy. The formal turnover frequency was however around 8 times lower for CrCl_2 than CrCl_3 . As mentioned earlier, as part of this project the chromium/glucose/[BMIM]Cl systems and was investigated by in-situ EXAFS at 80 °C by Ph.D. student Jonas Andersen^[157,158]. It was found that the Cr^{III} species of the CrCl_3 solutions were existing in the form of $[\text{CrCl}_6]^{3-}$ complexes, and when glucose was added the formation of $[\text{CrCl}_4\text{glucose}]^{1-}$ complexes was observed, showing that the $[\text{CrCl}_6]^{3-}$ is a likely candidate for the catalytically active species. In this complex, glucose made a bidentate coordination to the chromium center through its oxygen atoms, see appendix: figure C.15 on

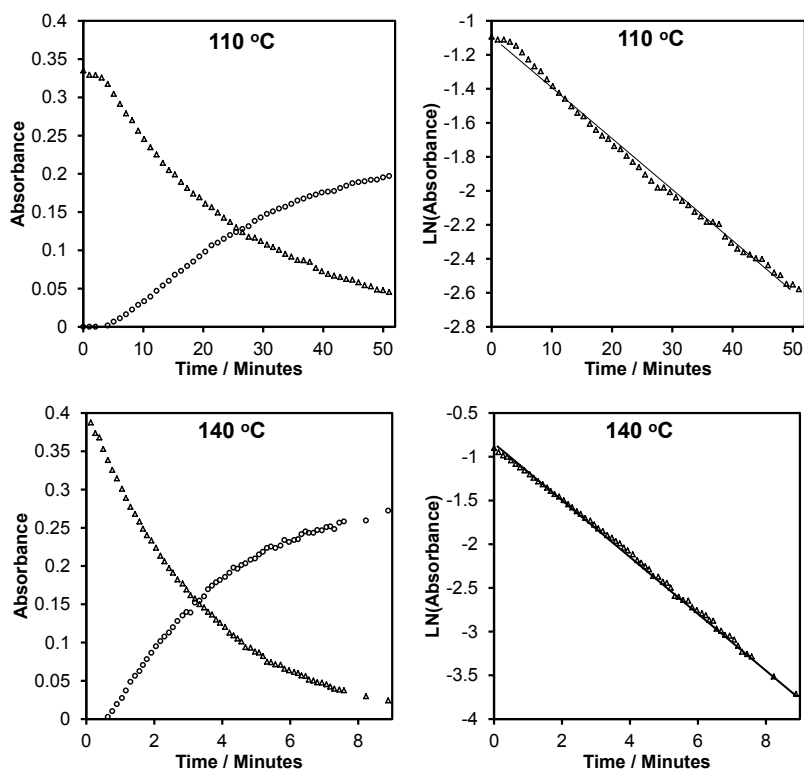


Figure 3.11.: *Left:* Development of 1670 and 1042 cm^{-1} bands during glucose conversion at 110 and 140 °C presence of CrCl_2 in thin film dried by nitrogen flow during reaction. The area of the 1042 cm^{-1} is corrected from the contribution from HMF, according to figure C.2 on page 150. *Right:* Natural logarithm to glucose concentration expressed as absorbance. Δ shows the corrected 1042 cm^{-1} band area of glucose, while \circ shows the 1670 cm^{-1} band due to HMF.

page 163. The formation of similar $[\text{CrL}_4\text{glucose}]$ complexes during isomerization reactions of glucose is known from literature^[175,176].

An even more surprising result of the EXAFS experiments was that around 12 % of the chromium in $[\text{BMIM}]\text{Cl}$ solutions containing CrCl_2 and glucose were determined to exist as Cr^{III} species. If the CrCl_2 solution contains 12 % $[\text{CrCl}_6]^{3-}$ this could provide a good explanation for the apparent catalytic activity of CrCl_2 , that catalyzes the reaction at the same activation energy as when using CrCl_3 , but at a 8 times lower turnover frequency. Cr^{II} is, as mentioned, known to be oxidized very easily to Cr^{III} , which means that the earlier reported activity of CrCl_2 , could very well be due to partly oxidation to CrCl_3 .

If the active species so far seem to be related to Cr^{III} , a very good question is: Why are there several trustworthy reporting of higher yields obtained with CrCl_2 than $\text{CrCl}_3 \cdot 6\text{H}_2\text{O}$ or similar Cr^{III} salts? It could very well be that it is in fact the $[\text{CrCl}_6]^{3-}$ that is among the most active

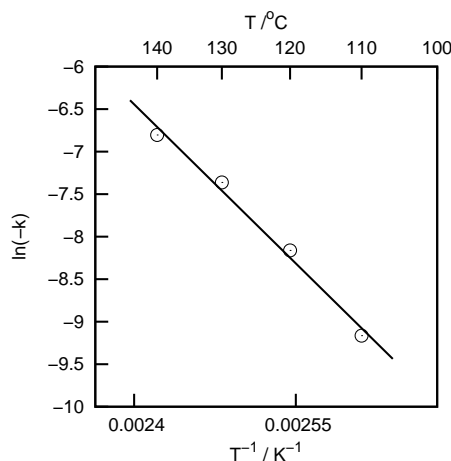


Figure 3.12.: Arrhenius plot showing the HMF formation rates temperature dependence, during glucose conversion in anhydrous $[BMIM]Cl$ with $CrCl_2$ present.

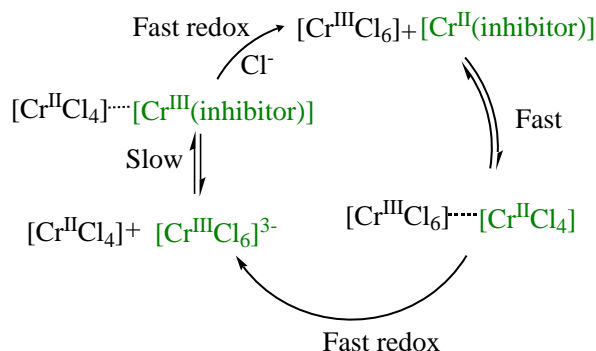


Figure 3.13.: Proposed mechanism for fast regeneration of $[CrCl_6]^{3-}$ species in the presence of Cr^{II} species

common transition metal species for the glucose isomerization, with very high initial rates. In the previous section it was however shown how sensitive the $[CrCl_6]^{3-}$ catalyst is to inhibition by the products from the fructose dehydration. At higher concentrations of water and HMF it seems like complexes of the type $[Cr(Cl)_x(HMF)_y]$ and $[Cr(Cl)_x(H_2O)_y]$ are formed that cannot be regenerated fast to activate the $[CrCl_6]^{3-}$ species. A simple way to overcome the inert nature of Cr^{III} complexes in general is to mix it with a small amount of Cr^{II} . Cr^{II} and Cr^{III} can very easily exchange electrons via ligand bridges and thus swap oxidation states^[160]. As mentioned in the introduction, the ligands of Cr^{II} complexes can be exchanged very fast, and when the inhibiting ligands are exchanged with chloride, the Cr^{II} complex is reoxidized by Cr^{III} . This mechanism is proposed schematically in figure 3.13 where it is shown how the presence of Cr^{II} prevents the inhibition of the active $[CrCl_6]^{3-}$.

A strong support for this mechanism is shown on the right-hand side of figure 3.11 on page 72, where the first order dependency of glucose is shown. Opposite to the reactions carried out solely with CrCl_3 species as catalyst, an almost ideal first order dependency was observed in the $\text{CrCl}_2/[\text{BMIM}]\text{Cl}$ system, showing no signs of product inhibition. This explained why higher conversions can be obtained when using CrCl_2 , the reaction just has to proceed long enough as the $\text{Cr}^{\text{II}}/\text{Cr}^{\text{III}}$ synergy will ensure that the active species can be regenerated. However, will a catalytic system comprising only Cr^{III} species, at moderate reaction times result in significant higher yields, due to the much higher initial rates. This offers a reasonable explanation why there has been so much confusion around the active oxidation state of the chromium catalyst used for glucose conversions in ionic liquids.

This knowledge could be very useful from a technical point of view, where the product inhibition of chromium will cause problems in a large scale production of HMF from biomass. Here it seems quite likely that the product inhibition can be completely avoided by reducing a small fraction of the $\text{CrCl}_3 \cdot 6\text{H}_2\text{O}$ catalyst. This could be obtained by adding a cheap reducing agent such as metallic zinc.

3.1.5. Reactions orders of glucose - Derivation of a unifying model

The observed reaction orders of catalytic reactions are often discussed in detail as they provide important mechanistic insight. The earlier mentioned study of Qi et al. argued that the reaction kinetics of the Cr^{III} catalyzed glucose conversion was first order in glucose^[171]. Although from a mechanistic point of view this might be true, the apparent kinetics do not exhibit an ideal first order dependency of glucose due to the product inhibition. However, as it was shown in the previous sections the kinetics can be understood through modified first order kinetics.

Rasrendra et al. quite surprisingly showed that the conversion of glucose in DMSO catalyzed by aluminum triflate exhibited pronounced second order kinetics. They explained this by a possible rate determining step where two glucose molecules coordinated simultaneously to the metal center^[177]. That a dimerization-like step should be rate determining for the isomerization, seems from a mechanistic point of view highly unlikely. For the $\text{CrCl}_3/[\text{BMIM}]\text{Cl}$ systems this would also directly contradict the experimental structures suggested by EXAFS, showing a preferred bidentate coordination of *one* glucose molecule to each chromium center.

For the conversions in the sealed microreactor, see figure 3.6 on page 66, the analysis using the product inhibited first order kinetics gave a very reasonable explanation of the kinetics, which were further strongly supported by the almost ideal first order kinetics of the $\text{Cr}^{\text{II}}/\text{Cr}^{\text{III}}$ system. However, when water was removed, leaving only HMF to inhibit the catalyst, the reaction course was however no longer well described with the product inhibited first order reaction kinetics.

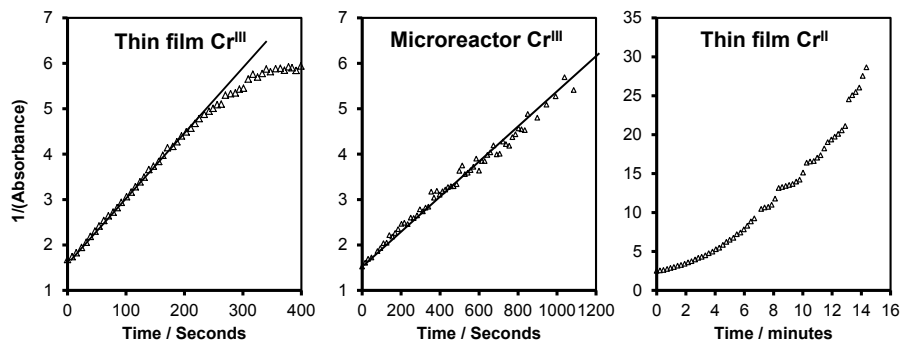


Figure 3.14.: Reciprocal absorbance as function of time during catalytic conversions of glucose at 130 °C in [BMIM]Cl under different circumstances. A straight line indicates apparent second order reaction kinetics. Similar plots for all temperatures are found in appendix: See figures C.16-C.18 on pages 164-166.

Quite surprisingly figure 3.14 shows that the reaction course can also partly be described by apparent second order kinetics in the cases where product inhibition is pronounced. This apparent second order behavior, is however less pronounced at lower temperatures (see appendix: Figures C.16-C.18 on pages 164-166). At higher conversions a strong deviation from the apparent second order kinetics becomes pronounced. The use of in-situ reaction monitoring has provided much more detailed reaction course profiles than earlier reported^[171,177]. Even though the reactions initially indeed exhibit some first order kinetics, the detailed reaction course profiles has showed that the chromium catalyzed reactions, with exception of the Cr^{II}/Cr^{III} system, do neither follow simple first nor second order kinetics due to product inhibition. It is in fact quite well known for range other catalytic systems that the reaction order can change over the course of the reaction^[178].

In the following an unifying kinetic model will be presented. The derivation of the model is inspired by an approach presented by Blackmond known as *reaction progress kinetic analysis*^[178] and the considerations often used for deriving kinetic expressions in bio catalysis^[179-181].

Basically the reaction kinetics can be understood through the three important *equilibriums 1-3* shown in figure 3.15(a) on the next page. *Equilibrium 1* is the important pre-equilibrium in the catalytic cycle while equilibriums 2 and 3 are responsible for the off-cycle inhibition. EXAFS showed that Cr^{III} existed predominantly as $[\text{CrCl}_6]^{3-}$ in solutions comprising only [BMIM]Cl and $\text{CrCl}_3 \cdot 6\text{H}_2\text{O}$, while a steady state comprising predominantly $[\text{CrCl}_4\text{glucose}]^-$ was reached after adding a surplus of glucose to the mixture, see *equilibrium 1*. The activation energy required to form the $[\text{CrCl}_4\text{glucose}]^-$ complexes from $[\text{CrCl}_6]^{3-}$ and glucose is unknown, but are assumed to be lower than the activation energy of the isomerization (This assumption is shown experimentally to be true later in the next section). The rate is directly dependent on

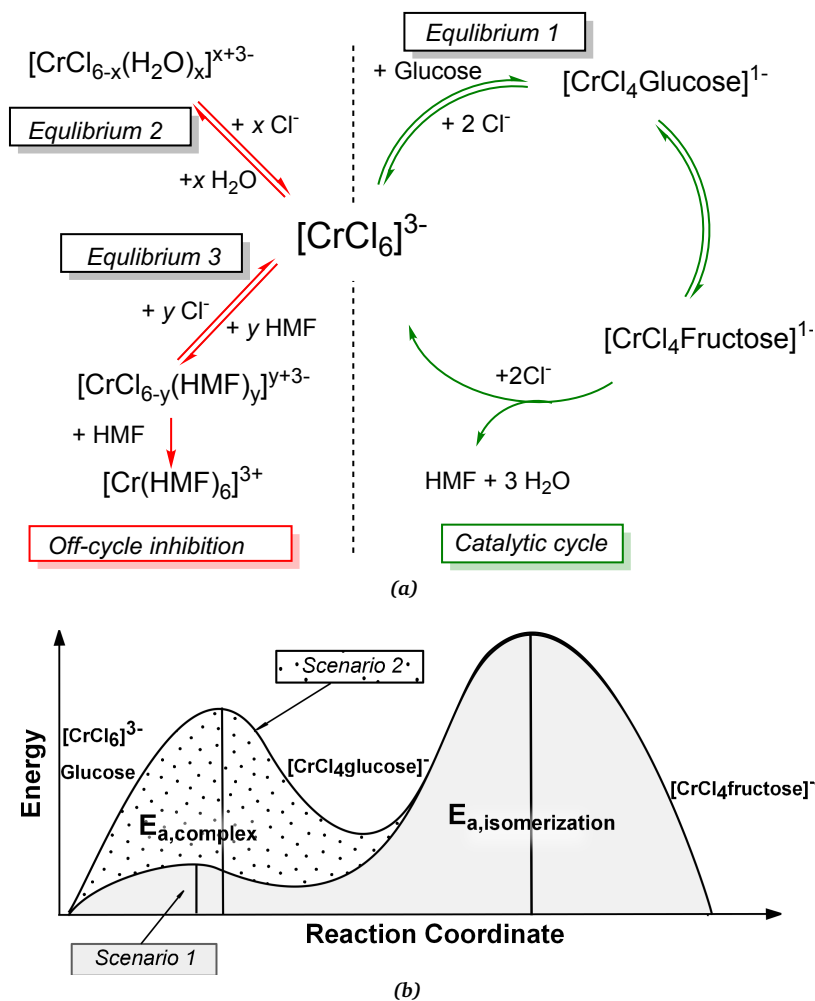


Figure 3.15.: (a) Proposed kinetic model based on the major three equilibria with the $[\text{CrCl}_6]^{3-}$ species that result in the complicated kinetics of the reaction. Green arrows denotes reactions within the catalytic cycle, while red arrows denotes reactions related to the off-cycle inhibition. (b) Two different types of scenarios both consistent with the same apparent activation energy, but with different sizes of barriers for complex formation with the catalyst. **Notice:** The first reaction barrier associated with complex formation, $E_{a,\text{complex}}$, is assumed to be associated with the kinetics of all three equilibria 1-3.

the concentration of $[\text{CrCl}_4\text{glucose}]^-$ complexes, and can at all times be described with the unimolecular expression in equation (3.1):

$$r = k_{\text{isomerization}} \cdot [\text{CrCl}_4\text{glucose}]^- \quad (3.1)$$

At least at early times of reaction it is reasonable to apply the steady state approximation. The steady state approximation states that the kinetics related to intermediate formation can be neglected and hence does not influence the overall kinetics^[179-181]. In this case the intermediate is the chromium glucose complex. Thus the kinetics is understood solely through a pseudo first order dependency of glucose, and the rate can be expressed as:

$$r_{\text{initial}} = k'_{\text{isomerization}} \cdot [\text{glucose}] \quad (3.2)$$

However equation 3.2 is only the true at initial times where the glucose concentration is significantly larger than concentrations of water and HMF hence the *equilibriums 2* and *3* will have very little or no impact on the apparent kinetics. As the reaction precedes the concentrations of HMF and water are no longer insignificant and start to compete with glucose for the available chromium sites, in the following denoted $[\text{Cr}_{\text{free}}]$. Thus the importance of *equilibriums 2* and *3* can no longer be neglected, and the general kinetic case becomes more complicated:

$$r = k''_{\text{isomerization}} \cdot [\text{glucose}][\text{Cr}_{\text{free}}] \quad (3.3)$$

As accumulation of HMF and water occurs the *equilibriums 2* and *3* start to have significant impact the concentration of $[\text{CrCl}_4\text{glucose}]^-$, which decreases due to the limited amount of available free chromium sites.

It is however not necessarily a consequence that a catalyst will be strongly inhibited just because it is engaging in off-cycle equilibriums. To analyze this problem the two different scenarios in figure 3.15(b) on the facing page are set up, both of which are consistent with the same experimental apparent activation energy. In the first scenario the activation barriers for the complex formations with the catalyst are significantly smaller than the apparent activation energy, e.g. $E_{a,\text{complex}} \ll E_{a,\text{isomerization}}$, and the different co-existing complex types can interchange rapidly. This scenario is known from e.g. Brønsted acid catalyzed reactions, where the barrier for proton exchange is as low as 10.0 kJ/mol^[182]. This scenario also seem to fit well with the apparent fast catalytic pre-equilibriums of the $\text{Cr}^{\text{II}}/\text{Cr}^{\text{III}}$ mixture, as it was previous explained by the proposed mechanism on figure 3.13 on page 73. This is analogous again

basically an effect due very low barriers for complex formation with the Cr^{II} species that as mentioned earlier are as low as 14 kJ/mol ^[160].

However scenario 1 on the other hand seems unlikely for the Cr^{III} complexes, where the complex formations are assumed to be associated with a significant activation energy, even though this activation energy seems lower compared to the ones in aqueous systems. For the Cr^{III} systems scenario 2 on figure 3.15(b) on page 76 seems more likely, in which the activation energy for the complex formations is of a considerable size. In this case the kinetics of the competing equilibriums become relevant to the overall kinetics, as fast interchanges between the complexes are not possible, like they were in the first scenario. Thus the steady state approximation which neglects the influence of complex formation step, yielding the first order expression in equation 3.2, is not valid for this Cr^{III} catalyst. Hence as the reaction proceeds and the kinetics will deviate substantially from the initial pseudo first order kinetics, which would normally be expected from similar catalytic cases, where the steady state approximation in most cases are found to be valid.

Applying this model it is suddenly obvious why the kinetics shows an apparent second order dependency on glucose: The absolute values of the equilibrium constants, associated with *equilibriums 1-3* in figure 3.15(a), are unknown. However, each time the concentration of glucose decreases due to catalytic conversion, a proportional amount of HMF and water is produced resulting in an unknown - but proportional - reduction of the available chromium sites. Thus the available amount of active chromium sites decreases proportional to the glucose concentration: hence $[\text{Cr}_{\text{free}}] \propto [\text{glucose}]$ become true in equation (3.3). Thus the apparent rate will resemble apparent second order dependency of glucose, see equation (3.4):

$$r = k''''_{\text{isomerization}} \cdot [\text{glucose}]^2 \quad (3.4)$$

However this is not because the mechanism is bimolecular with respect to glucose, and it should be emphasized that the $k''''_{\text{isomerization}}$ is neither a regular nor a trivial second order rate constant, as it will depend on several other factors including the unknown equilibrium constants in *equilibriums 1-3*. This means that an experiment keeping the amount of $\text{CrCl}_3 \cdot 6\text{H}_2\text{O}$ catalyst constant, while varying the glucose concentration, would most likely show the initial rates to be first order dependent on the glucose concentration. This is also strongly suggested from the reactions in the presence of $\text{Cr}^{\text{II}}/\text{Cr}^{\text{III}}$ that directly reveal the true first order nature of the chromium catalyst in the absence of the inhibition.

At high conversions the reaction rates in the thin [BMIM]Cl films starts to deactivate faster than what can explained by the pseudo-second order kinetics (see figure 3.14 and appendix: figure C.17 on page 165). After some time the deactivation seems so pronounced as it

seems like the catalyst seem to suffers from irreversible deactivation. At these conversions the chromium and HMF ratio approaches 1:6, thus it seems possible that the formation of $[\text{Cr}(\text{HMF})_6]^{3+}$ complexes could be responsible for the irreversible inhibition (see figure 3.15(a)). The the lability of the possible $[\text{Cr}(\text{HMF})_6]^{3+}$ complexes could resemble the ones of the typical aqueous complexes which are far more inert than complexes in the ionic liquid.

The presented model shows how complex the kinetics of the Cr^{III} catalyst are and that the reaction under normal conditions can be understood both trough modified first order kinetics and through the apparent resemblance to second order kinetics. The product inhibition, which results in apparent second order like kinetics, may pose one of the largest challenges in the technical utilization of biomass conversion in ionic liquids by chromium chloride, that today seems like one the most promising systems to selectively transform cellulose into HMF.

3.2. Fructose dehydration

Fructose is much more reactive than glucose. After the isomerization of glucose the formed fructose is rapidly dehydrated in the ionic liquids. The dehydration still needs a catalyst, but several papers reports that the halide ions themselves are catalytic active in the dehydration of fructose, hence the dehydration of fructose happens spontaneously in halide containing ionic liquids at significant rates^[143,144,183]. But whether it is the halide ions, the chromium species or a mixture that acts as the primary dehydration catalysts during chromium catalyzed glucose conversion, seem somewhat ambiguous in the literature. The high selectivity towards HMF could suggest that chromium plays a dominant role in both the isomerization and dehydration step^[48], while other reports halide ions themselves to be very active and selective in the conversion of fructose to HMF^[183]. In this section the fructose dehydration in $[\text{BMIM}]\text{Cl}$ has been investigated under several different conditions using in-situ ATR-FTIR monitoring in order to elucidate the specific catalytic role of chromium during this last fast step.

3.2.1. Anhydrous Chloride Catalyzed Fructose dehydration

Because the chloride ions themselves are able to catalyze fructose dehydration, the reaction was initially investigated in the absence of chromium. The reaction was carried out in a thin film of $[\text{BMIM}]\text{Cl}$ under anhydrous conditions at 130 °C. The spectra recorded during the reaction is shown in figure 3.17 on page 81. Quite surprisingly the initial dehydration of fructose, under anhydrous conditions, resulted in a significant formation of a carbonyl species with the $\nu_{\text{C=O}}$ band located around 20 cm^{-1} higher than HMF. With exception from a shoulder band in the reactions using CrCl_2 , no significant absorption band at 1690 cm^{-1} was observed during

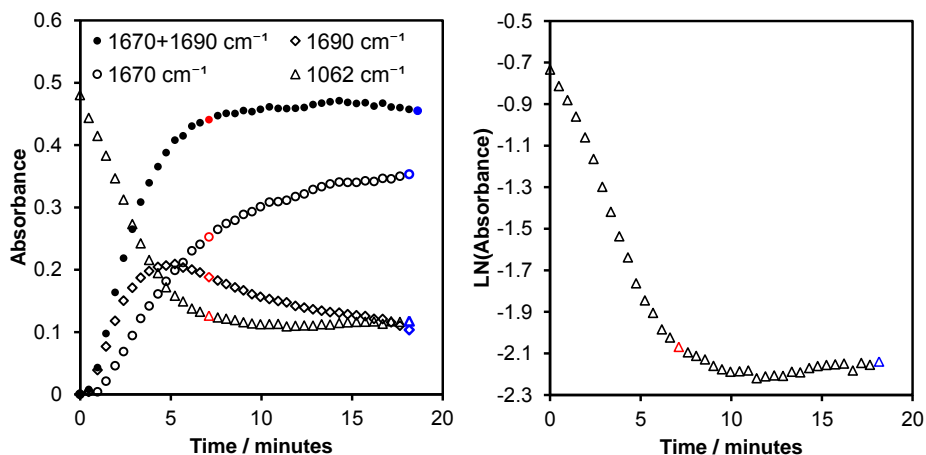


Figure 3.16.: Showing the development of carbonyl bands during fructose dehydration at 130 °C in a thin film of pure [BMIM]Cl dried by nitrogen flow during reaction. The 1062 cm^{-1} area is corrected from the C-O stretching contribution from HMF.

any of the other experiments. HMF has a very characteristic $\nu_{\text{C}=\text{O}}$ band at around 1670 cm^{-1} . This position of the $\nu_{\text{C}=\text{O}}$ band is low compared to aldehydes in general because of the aromaticity of the furanic ring. The intensity increase of both carbonyl stretching bands were slightly delayed with respect to the fructose conversion, see figure 3.17 (a). The delay of the intensity increase of the 1670 cm^{-1} band was significantly more pronounced than the 1690 cm^{-1} band and the initial rate of the increase was significantly slower.

The new carbonyl species at 1690 cm^{-1} lacked from the characteristic furanic C=C stretching band found in the spectra of HMF at around 1517 cm^{-1} . Instead the new 1690 cm^{-1} band rose together with another new band at around 1620-1615 cm^{-1} that most likely could be interpreted as another kind of C=C stretching band. The conversion of sugar into HMF was fast and completed after approximately 7 minutes, but at this time steady-state in carbonyl stretching region was far from reached, see red line on figures 3.16 and 3.17. At this stage a similar intensity of the two $\nu_{\text{C}=\text{O}}$ bands at 1670 and 1690 cm^{-1} was observed. Beyond this time a slow conversion of the species at 1690 cm^{-1} into the band at 1670 cm^{-1} continued, suggesting that the unknown carbonyl species could partly be converted to HMF. This observation was further supported as the intensity of the characteristic C=C stretching band of the furanic ring at 1517 cm^{-1} also increased along with a decrease of the intensity of the 1620 cm^{-1} band of the unknown species. It should again be emphasized that there was almost no conversion of fructose in this time interval. Later the conversion approached a pseudo steady state comprising a mixture of carbonyl stretching bands. At this time the 1670 cm^{-1} was dominant but a significant amount of the 1690 cm^{-1} band was still present, see blue line on figure 3.17.

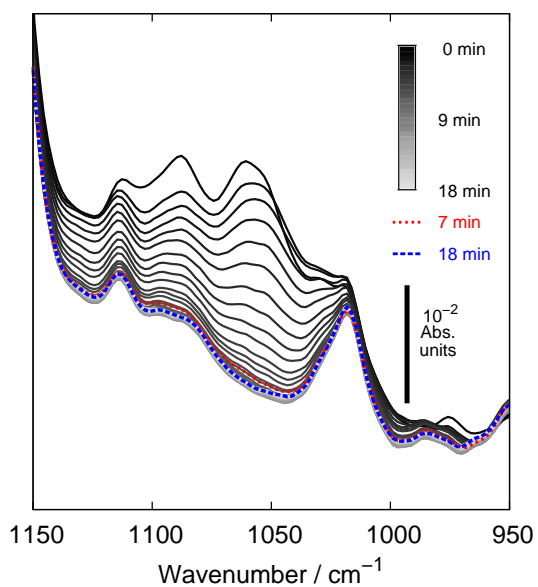
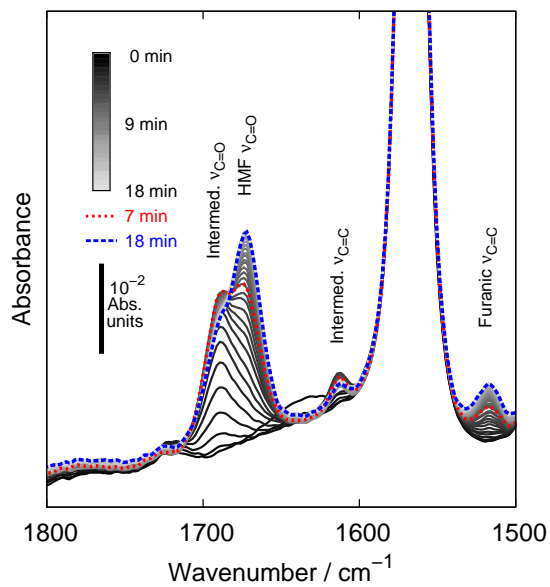


Figure 3.17.: In-situ AFT-FTIR spectra of fructose dehydration at 130 °C in thin film of pure [BMIM]Cl dried by nitrogen flow during reaction. Note that the red line shows when all fructose is converted while the blue line shows the pseudo steady state.

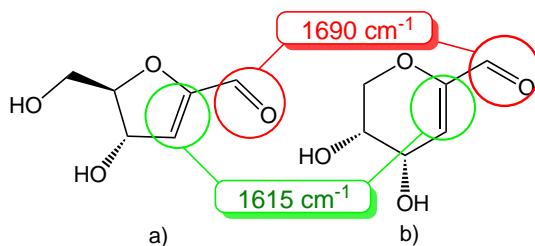


Figure 3.18.: Metastable intermediates formed from the doubly dehydration of fructofuranose and fructopyranose. (a) (4*S*,5*R*)-4-hydroxy-5-hydroxymethyl-4,5-dihydrofuran-2-carbaldehyde and (b) (3*R*,4*S*)-3,4-dihydroxy-3,4-dihydro-2*H*-pyran-6-carbaldehyde^[140]. The experimental stretching vibration frequencies marked with red and green were in good correspondence with calculated vibrations.

There are several of possible intermediate species during the dehydration of fructose. The intermediates appearing during acid catalyzed dehydration of fructose have been investigated in detail in a few recent studies using in-situ NMR spectroscopy^[140,184]. Especially the two metastable intermediates (4*S*,5*R*)-4-hydroxy-5-hydroxymethyl-4,5-dihydrofuran-2-carbaldehyde and (3*R*,4*S*)-3,4-dihydroxy-3,4-dihydro-2*H*-pyran-6-carbaldehyde equivalent to the doubly dehydrated fructofuranose and fructopyranose intermediates respectively, were found in significant concentrations during the dehydration^[140], see figure 3.18. They are contrary to HMF not stabilized though an aromatic structure and are hence considered to be very reactive. Especially the pyranic compound is in general thought to be responsible for a great part of the the unwanted humin formations, as further dehydration will not result in a stable aromatic compound^[140]. But the reactive furanose intermediate could as well be responsible for the formation of unwanted products if it is not selectively dehydrated to yield in HMF.

Especially these two intermediates are found in significant amount during fructose dehydration, suggesting that this last dehydration step, is likely to be rate determining. This point has also been suggested by DFT calculations on the bromide ion catalyzed dehydration, that found the last dehydration step to be the rate determining^[183].

By own DFT calculations the $\nu_{C=C}$ and $\nu_{C=O}$ modes of HMF and the intermediates calculated. Both of these intermediate gave a very reasonable spectral match compared to the species formed under the experiments, see figure 3.18 (Detailed vibrational modes are found in appendix: figure C.20 on page 169). The carbonyl stretch is calculated to be around 30 cm^{-1} higher for these species than for HMF, and the stretching of the sole double-bonds are around 120 cm^{-1} higher than the intense furanic symmetric C=C stretching mode, which also resembles the observed absorptions quite well.

A proposed reaction scheme that is consistent with the spectroscopic observations is shown in figure 3.19 on the facing page, where it should be emphasized that the equilibrium is most likely pushed significantly towards the furanose form **1a**. It seems like the anhydrous conditions allows a very fast reaction pathway for the two first dehydration steps (**1**→**2**). But the

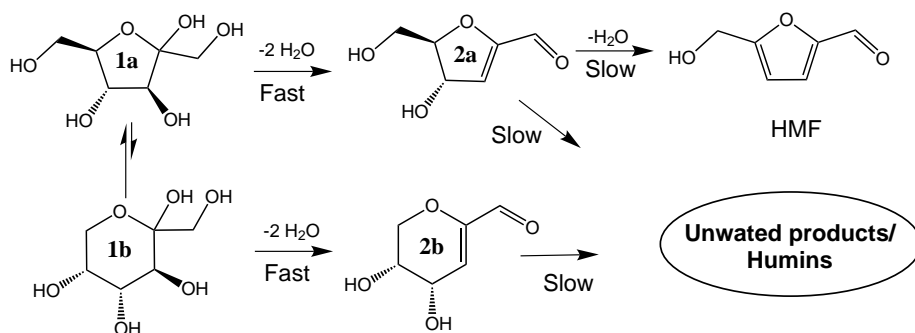


Figure 3.19.: Proposed reaction pathways during anhydrous chloride catalyzed fructose dehydration. Notice that the equilibrium is pushed towards the furanose form **1a**.

selective dehydration for the last step seems to be significantly slower. Thus it accumulates the reactive doubly dehydrated intermediates, **2a** and **2b**, for some time, which leads to other irreversible side reactions than just HMF formation. The overall conversion of fructose seems to be fast, which is quantified from the corrected area of the 1062 cm^{-1} band of fructose. It seems like the initial dehydration steps proceeds after pseudo-zero order kinetics, which can be explained by the surplus concentration of chloride ions. The shown development of the 1062 cm^{-1} band is also corrected by subtraction of the contribution from C-O stretching modes of HMF similar to the procedure used for correction of the 1042 cm^{-1} band of glucose described and used earlier. However, it seems like this correction is rather poor, especially at later times of the experiment, as the 1062 cm^{-1} band does not approach zero and actually increases slightly towards the end. This could be due to the incomplete dehydrations leaving more OH groups in the system than a complete triple dehydration to HMF would, hence the absorbance in the C-O stretching region is more pronounced compared to an equivalent amount of HMF.

Others have suggested that humins are the product of condensation of HMF and sugars via aldol condensation type of reactions^[75]. Therefore control experiments were performed: Solutions of glucose and a mixture of glucose and HMF in [BMIM]Cl was treated under same anhydrous conditions at $130\text{ }^{\circ}\text{C}$ as described above. However, these solutions were very stable even at $130\text{ }^{\circ}\text{C}$, at least during the 30 minutes of the control experiment. This showed that as soon HMF was formed it was stable under these conditions.

Consequently it seems like the proposed scheme are able to describes the main steps in the reactions, where the main point is that the anhydrous chloride anions allows a fast reaction path for the doubly dehydration into non-aromatic carbonylic compounds absorbing at 1690 cm^{-1} , **1**→**2**. The last dehydration however is significantly slower which is evident due to the slow conversion into aromatic carbonylic compounds absorbing at 1670 cm^{-1} . The slow

conversion of the unstable doubly dehydrated intermediate will probably result in several side reactions and could be one out of several humin formation mechanisms. Humins comprising condensation products of the described intermediates should be expected to comprise both carbonyl and C=C groups, with similar spectroscopic appearance as the intermediates **2a** and **2b** themselves. Thus similar 1690 and 1620 cm^{-1} bands will to some degree still appear after the humin formation.

3.2.2. Chloride Catalyzed Fructose dehydration in the presence of water

To investigate if the accumulation of dehydration intermediates and subsequent side reactions, was caused by the anhydrous conditions in the thin film, an analogous experiment was performed where water vapor was present in the nitrogen gas. By humidifying the nitrogen at room temperature the gas phase contained approximately 2.8 v/v % water.

In-situ spectra recorded during the hydrous dehydration of fructose, shown at figure 3.20 on the next page, where water was clearly present indicated by the significant $\delta_{\text{O-H}}$ band from water. The conversion of fructose was significantly slower in the presence of water, however the rise of the 1690 cm^{-1} carbonyl band was almost completely suppressed and fructose seemed to be converted selectively into HMF in the presence of water. The conversion of fructose seemed to follow first order reaction kinetics very well.

The overall total initial carbonyl formation rate from dehydration of fructose, in the previous described anhydrous film experiment, were about $20.0 \cdot 10^{-4} \text{s}^{-1}$, and out of this the 1670 cm^{-1} band of HMF contributed with around $7.9 \cdot 10^{-4} \text{s}^{-1}$. In the wet film the initial HMF formation rate was $4.3 \cdot 10^{-4} \text{s}^{-1}$ but after around two minutes where some of the water had been removed, it increased slightly to around $7.6 \cdot 10^{-4} \text{s}^{-1}$. This suggested that water in high concentrations also affects the initial dehydration steps of fructose to some degree.

The much higher selectivity when small amounts of water was present, can be explained by the blocking of the fast reaction pathway of the two first steps resulting in an accumulation of the doubly dehydrated intermediates. It is known that just a small percent of water changes the properties of [BMIM]Cl significantly.

A shoulder band at 1690 cm^{-1} was also formed during the CrCl_2 catalyzed glucose conversion. In the light of the previous observations it is very likely that this band was caused by the same unselective dehydration of the fructose formed from the isomerization. However, it should be emphasized that the extremely anhydrous conditions are created by the special and somewhat artificial conditions of the thin film experiments and are not likely under more pragmatic conditions in bulk reactors.

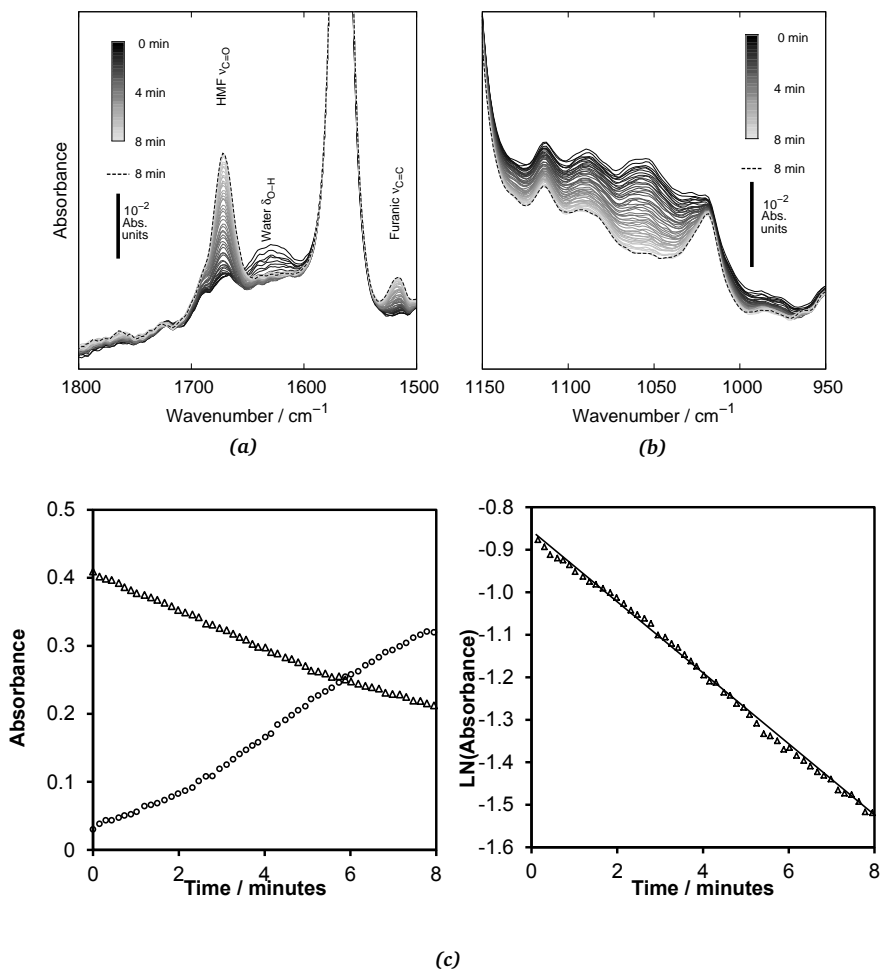


Figure 3.20.: (Top) In-situ ATR-FTIR spectra of fructose dehydration at 130 °C in a thin [BMIM]Cl film in the presence water due to exposure to a flow of humid nitrogen. (Bottom) The development in the band areas of 1670 cm^{-1} (HMF) and the corrected 1062 cm^{-1} band (fructose). The straight line indicates that the reaction follow first order kinetics.

3.2.3. Cr^{III} Catalyzed Fructose dehydration

Chromium is known to be active as catalyst in both the isomerization of glucose and the dehydration of fructose in ionic liquids. However, as shown above the chloride ions themselves are very active catalysts in the dehydration of fructose. Thus it is hard to say whether chromium is mostly responsible for the isomerization part of the total glucose conversion or if chromium species also play a key role in the dehydration of fructose? Even though the activation energy for ligand exchange of the $[\text{CrCl}_6]^{3-}$ species seems to be significantly lower than the 110 kJ/mol for the Cr^{III} complexes found in water, the activation energy of the glucose isomerization is still quite high at 102 kJ/mol thus of a comparable order of magnitude. As fructose dehydration, even in the absence of a metal catalyst, is known to be quite fast in halide based ionic liquids it could be more doubtful how the $[\text{CrCl}_6]^{3-}$ species actually participate in the dehydration step. Therefore the kinetics of fructose dehydration were investigated in the presence of $\text{CrCl}_3 \cdot 6\text{H}_2\text{O}$ in thin films of $[\text{BMIM}]\text{Cl}$ from 80 to 140 °C in steps of 10 °C.

On figure 3.21 on the facing page spectra of selected temperatures of fructose dehydration in the presence of $\text{CrCl}_3 \cdot 6\text{H}_2\text{O}$ in $[\text{BMIM}]\text{Cl}$ is shown. Rates at all temperatures as well as examples of full region spectra can be found in appendix: see figures C.23-C.25 on pages 172-174. It was not possible to keep the films anhydrous as the initial production rate of HMF and water was faster than the evaporation of water into the nitrogen flow. The rates were very fast and the selectivity towards HMF seemed to be significantly higher than the chloride catalyzed dehydration. At 130 °C the majority of the fructose was converted within a minute. The fast rate itself indicated strongly that chromium indeed was much more active as a catalyst than the chloride ions. Contrary to parts of the glucose conversion reactions courses, the rates fitted poorly with pseudo second order kinetics (appendix: figure C.24 on page 173). Looking at the first order reaction plot shown at the right-hand side of figure 3.22 a strong first order dependency is shown at lower conversions, although the inhibition becomes significant at higher conversions.

From the initial rates the activation energy could be determined to 74.1 ± 3.1 kJ/mol, see Arrhenius plot in figure 3.23 on page 89. Like the low activation energy reported for acid catalyzed fructose dehydration^[145], this reaction barrier is likewise much lower than for the isomerization of glucose. This also explains why the absence of fructose in samples after reaction is often reported, as the isomerization is much slower than the subsequent dehydration^[48,75]. Another quite important point to make of these experiments is that the activation energy for ligand exchange of the $[\text{CrCl}_6]^{3-}$ species initially is lower or at least equal to this activation energy of 74.1 kJ/mol, which is substantially lower than for typical Cr^{III} complexes in water.

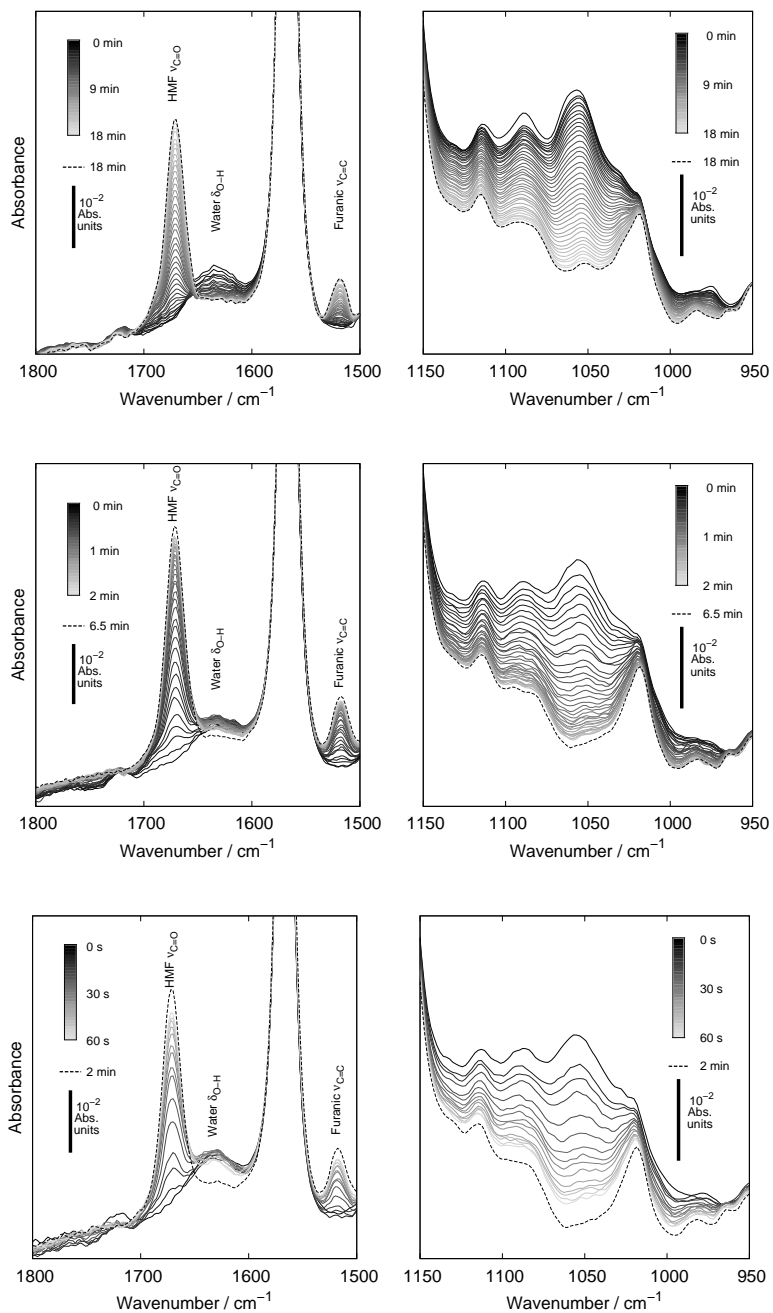


Figure 3.21. In-situ AFT-FTIR spectra of fructose dehydration at 80, 110 and 130 °C, from top to bottom respectively, in the presence of $\text{CrCl}_3 \cdot 6\text{H}_2\text{O}$ in thin film dried by nitrogen flow during reaction.

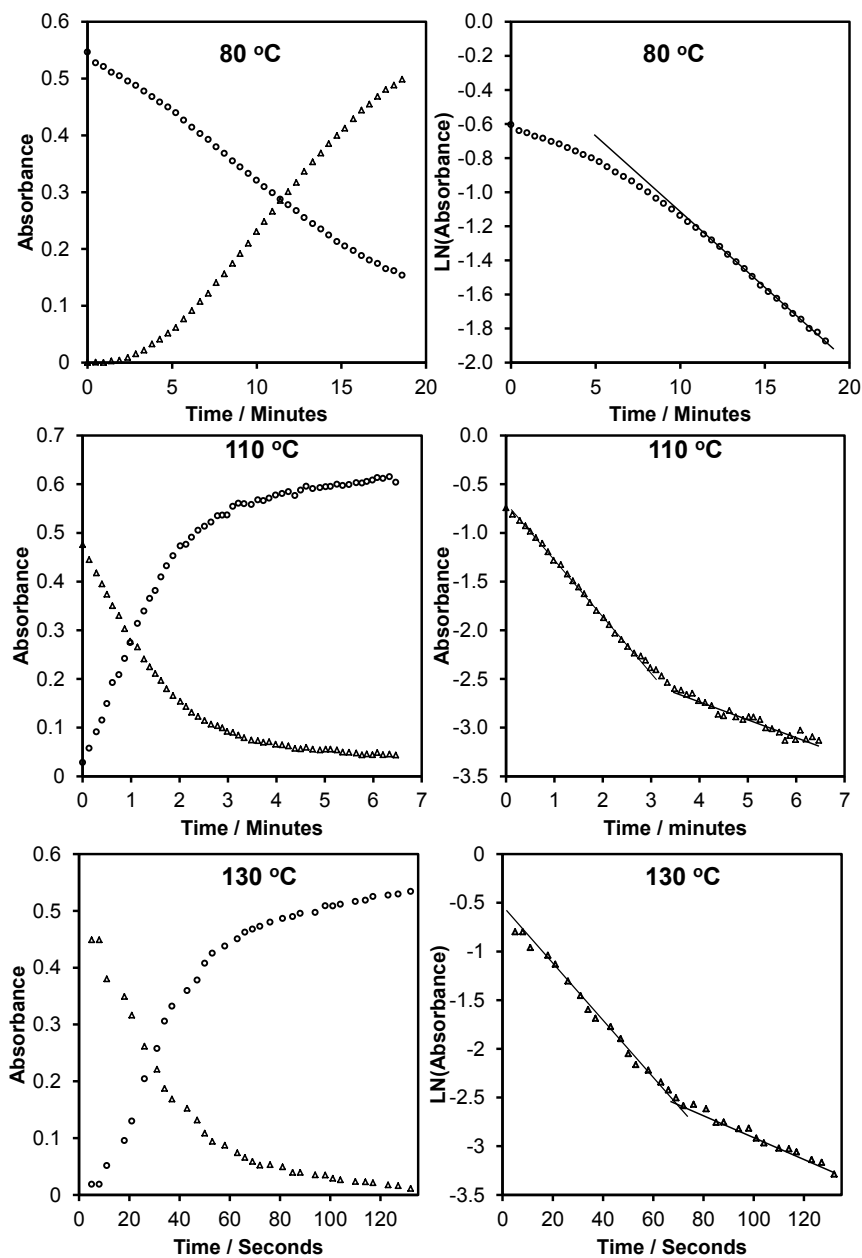


Figure 3.22.: *Left:* Development of 1670 and 1062 cm^{-1} bands during fructose dehydration at 80, 110 and 130 $^{\circ}\text{C}$ presence of $\text{CrCl}_3 \cdot 6\text{H}_2\text{O}$ in thin films exposed to a flow of dry nitrogen. The area of the 1062 cm^{-1} is corrected from the contribution from HMF *Right:* Natural logarithm to glucose concentration expressed as absorbance. Δ shows the corrected 1062 cm^{-1} band of fructose while \circ shows the 1670 cm^{-1} band due to HMF. Straight lines indicate first order reaction kinetics.

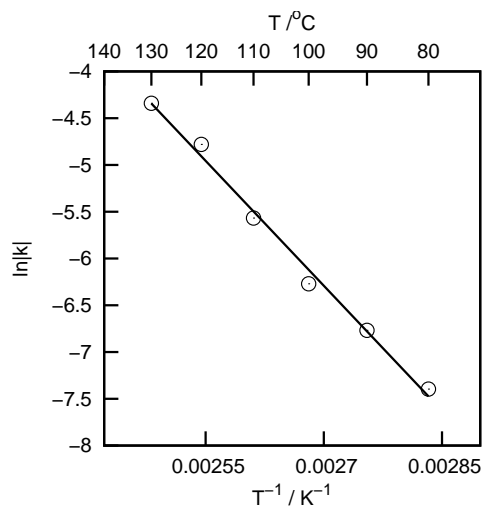


Figure 3.23.: Arrhenius plot based on HMF formation rates in absorbance s^{-1} during fructose dehydration in thin films of $[\text{BMIM}]\text{Cl}$ in the presence of $\text{CrCl}_3 \cdot 6\text{H}_2\text{O}$.

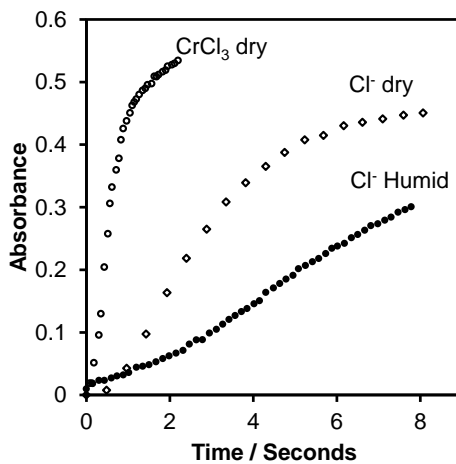


Figure 3.24.: Comparison between the growth dehydration of fructose at 130°C in thin films of $[\text{BMIM}]\text{Cl}$. For the humid chloride catalyzed series and the chromium catalyzed series only the development of the 1670 cm^{-1} band is included, whereas the sum of the 1670 and 1690 cm^{-1} bands are showed for the dry chloride catalyzed series.

The rate of the dehydration under the three different conditions investigated in the previous sections are compared in figure 3.24 on the previous page. The apparent rate in the presence of $\text{CrCl}_3 \cdot 6\text{H}_2\text{O}$ is 17-30 times faster than under humid conditions, and 6 faster than the dry chloride ion catalyzed dehydrations. Further the chloride concentration is close to around 100 times higher than the concentration of chromium resulting turnover frequencies around 600 and 1700-3000 times higher for chromium than for chloride. In the light of the previous results it could be speculated that the high selectivity of chromium partly should be understood through the ability to lower the reaction barrier for especially the last dehydration step, as this will prevent the doubly dehydrated species to exist long enough to react spontaneous in side reactions leading to humin formation.

3.3. Concise Conclusions

In this chapter the chromium catalyzed conversion of glucose or fructose in $[\text{BMIM}]\text{Cl}$ in the presence of 10 mol% $\text{CrCl}_3 \cdot 6\text{H}_2\text{O}$ or CrCl_2 has been investigated using in-situ ATR-FTIR spectroscopy. For $\text{CrCl}_3 \cdot 6\text{H}_2\text{O}$ the reactions were studied in two different reaction setups. The first was a small sealed micro reactor that allowed a study of the the reaction while the products were accumulating. In the other experiments the same reaction were studied in a thin ionic liquid film, which was simultaneously dehydrated by a flow of dry nitrogen. Conversions were estimated to around 70 % with an estimated selectivity towards HMF of around 90 %. Initially the reaction seemed first order with respect to glucose; however the rate deviated substantially from the initial first order kinetics after around 30-35% conversion. Hereafter a significant lower rate was obtained. The reaction courses were to complicated to be explained by ideal integer order kinetics.

The initial rates of reactions the anhydrous thin film were significantly higher (2-3 times) compared sealed micro reactor. HMF too seemed to act like a strong inhibitor which quite surprisingly resulted in apparent second order kinetics, which at first was unexpected taking the general perception of the reaction mechanism into account.

Table 3.2.: Summation of activation energies in kJ/mol determined using the initial formation rates of HMF during conversion of glucose. ^a Determined from apparent first order rates of glucose consumption at high conversions.

Reaction conditions	Formal catalyst	E_a
Microreactor(glucose)	$\text{CrCl}_3 \cdot 6\text{H}_2\text{O}$	102.6±3.6
Microreactor (glucose - inhibit.)	$\text{CrCl}_3 \cdot 6\text{H}_2\text{O}$	99.1±6.2 ^a
Microreactor(cellulose)	$\text{CrCl}_3 \cdot 6\text{H}_2\text{O}$	102.2±5.0
Anhydrous thin film	CrCl_3	103.8±1.6
Anhydrous thin film	CrCl_2	104.1±8.1

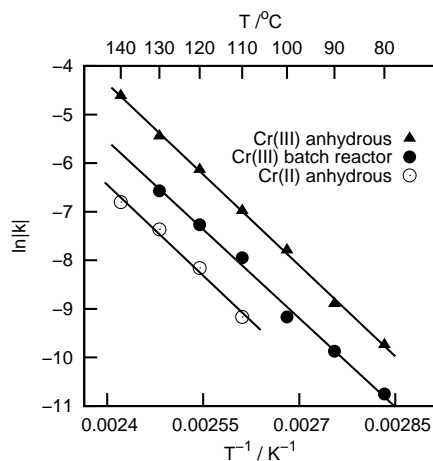


Figure 3.25.: Comparison of Arrhenius plots based on initial HMF formation rates as absorbance s^{-1} in $[BMIM]Cl$ under various conditions.

The initial reaction rate dependency of the $CrCl_3$ concentration was determined to be first order. This shows in a very simple way that the active species do not comprise the earlier proposed transient dimeric species, but shows that the active species is better understood through monomeric chromium species.

The reaction in the presence of $CrCl_2$ was investigated in thin anhydrous $[BMIM]Cl$ films. The apparent rates were found to be around 8 times lower compared to conversions in presence of $CrCl_3 \cdot 6H_2O$. Opposed to the experiments using $CrCl_3 \cdot 6H_2O$ the $CrCl_2$ catalyst did not show behavior to be product inhibited and was found to be first order dependent on the glucose concentration even at high conversions.

The initial rates were used to determine activation energies, see summary at figure 3.25 and table 3.2. Even though the rates in the different experiments deviated substantially, the activation energies were all found to be equal within the experimental uncertainties. This emphasized that the reaction was likely to be product inhibited and suggested that it was the same type active site both in the presence and absence of water and in the sample containing $CrCl_2$. The difference was the available amount active sites. By determination of an identical activation energy using first order rates in the presence of high amounts of water and HMF formed at high conversions in the microreactor, this assumption was further fortified as this led to the same activation energy. In-situ EXAFS results suggested the active species to be related to a complex of the type $[CrCl_6]^{3-}$. This species was observed to coordinate to glucose.

What was surprising was that the activation energy also was identical even when $CrCl_2$ was used as catalyst, despite much lower reaction rates. Complementary in-situ EXAFS results showed that around 12 % of the $CrCl_2$ was oxidized to $[CrCl_6]^{3-}$ species. Therefore it was

proposed that the catalytic activity of the [BMIM]Cl/CrCl₂ system was directly related to the formation of these [CrCl₆]³⁻ species. However, the presence of Cr^{II} species seemed to play an important kinetic role as they seemed to be responsible for the continuous regeneration of the active sites. This was explained to be explained through a mechanism where the Cr^{II} and Cr^{III} complexes were able to swap oxidation states by electron transfer through a temporary ligand bridge. Hence the inhibited chromium complexes could be fast regenerated into the active [CrCl₆]³⁻ species. This synergy could be very important from a technical point of view, if CrCl₃·6H₂O in ionic liquids are to be used on a larger scale. It suggests that it is possible to achieve fast first order kinetics without product inhibition through an intended reduction of a smaller fraction of the CrCl₃·6H₂O catalyst to Cr^{II}.

A model was derived showing that the apparent second order kinetics could be related to inhibition of the chromium catalyst. At high conversions the rate decreased even more rapidly indicating that HMF deactivated the catalyst irreversibly.

Fructose dehydration was investigated through reactions in thin ionic liquid films in the presence and absence of chromium. The dehydration catalyzed by chloride was investigated both under anhydrous and humid conditions. The chloride catalyzed dehydration during anhydrous conditions was very fast but incomplete, resulting in an accumulation of doubly dehydrated intermediates. A significant amount of these intermediates were converted into HMF in a reaction with a much lower rate. However, the pronounced accumulation of the reactive intermediates did also seem to result in a significant amount of irreversible side reactions leading to humin formation. A reaction pathway during anhydrous conditions was proposed, that suggested that the two first dehydration steps were fast, whereas the third dehydration step was much slower and thus responsible for the accumulation of doubly dehydrated intermediates. If water was present during the dehydration of fructose, the overall fructose conversion rate was much slower. It was proposed that water through coordination to the chloride ions especially decreased the rate of the two first dehydration step, as no or very little accumulation of the doubly dehydrated intermediate was observed. Instead a steady and relative selective reaction towards HMF was observed.

In the presence of 10 mol % CrCl₃·6H₂O the reaction was 6-30 times faster, and very selective. This indicated that the proposed [CrCl₆]³⁻ species also was very active in all three steps of the selective dehydration of fructose into HMF. The activation energy of this reaction was determined to 74.1±3.1 kJ/mol. This also shows that activation energy ligand exchange of the [CrCl₆]³⁻ species is lower or at least equal to this activation energy, which is substantially lower than typical values for Cr^{III} complexes in water. Again this emphasizes that care should be taken when comparing chemistry in aqueous medium and ionic liquids.

Experimental and Calculations

4.1. Preparing ionic liquid solutions

For the dissolution of cellulose (Avicel, Sigma-Aldrich) and 1,4- β -cellobiose (99%, Sigma-Aldrich) the powders were added to a round bottled flask containing ionic liquid 1-butyl-2,3-dimethylimidazolium chloride (95% Sigma-Aldrich) or 1-butyl-3-methyl-imidazolium chloride (95% Sigma-Aldrich), at 120 °C. The solutions were maintained at 120 °C under reduced pressure (10-15 mbar) and magnetic stirring for 2 hours in an oil bath. Because the [BDMIM]Cl became very viscous during the dissolution of cellulose, it was necessary to change the dissolution procedure: instead the Avicel cellulose and the powderous [BDMIM]Cl were carefully mixed in a beaker before heating. This solid powder-mixture was then transferred to a round bottled flask and heated in a oven at 140 °C for 15 minutes, to produce a homogenous solution. Then the solution was out gassed at 120 °C under reduced pressure for 2 hours, to remove water.

Solutions of [BMIM]Cl were observed to be stable as supercooled liquids (at least several years) but [BDMIM]Cl solutions crystallized within days at room temperature, however a homogenous mixture could be restored by gentle heating in an oven at 90 °C for 15 minutes. To prepare solutions of glucose and fructose were ground to a fine powder and added to ionic liquid powder in a beaker. The mixtures was heated in an oven at 110 °C for approximately 5-15 minutes. By this procedure clear glucose solutions were produced without sign of coloration.

For the chromium catalyzed conversion a concentrated [BMIM]Cl or [BDMIM]Cl solution was prepared containing 14.8 wt.% $\text{CrCl}_3 \cdot 6\text{H}_2\text{O}$.

4.1.1. Preparation of reaction mixtures

To prepare the reaction mixtures one equivalent of water was added to a solution of either cellulose, cellobiose. Then the solution was equilibrated for 2 hours at 90 °C. Approximately 2 g of the ionic liquid containing water and cellulose or cellobiose was added the catalyst at 60 °C in a small glass beaker, which was rapidly mixed by hand using a spatula for 1 minute and then freeze quenched in a acetone/dry ice mixture. The reaction mixtures were sealed with a lid using parafilm and stored on dry-ice until use. The resulting concentrations of cellulose and cellobiose were 10 and 10.6 wt. % respectively keeping the concentration of anhydroglucose constant. Catalyst concentration was 1.7 wt% when sulfuric acid was used, 1.48 wt.% for $\text{CrCl}_3 \cdot 6\text{H}_2\text{O}$ and 20 wt.% when the sulfated anatase catalyst was used. The reaction mixtures were stored in a sealed glass container and cooled with dry ice until use. The same batch of reaction mixture was used for all temperatures in an Arrhenius series. When using SBA-15- SO_3H catalyst it was necessary to impregnate it with [BMIM]Cl over night (in an oven oven at 120 °C) before the actual reaction mixture could be prepared. This procedure resulted in a reaction mixture of 6 wt.% cellulose and 13 wt.% catalyst.

4.2. in-situ ATR-FTIR spectroscopy

All the in-situ IR experiments were carried out using ATR-FTIR spectroscopy. The optical design of one of the ATR cells used in this thesis is shown in figure 4.1 on the facing page. The ATR cell is inserted into the FTIR-spectrometers sampling chamber thus the most ATR cells can be fitted into nearly every commercial FTIR spectrometer. In the ATR cell, the beam from the IR source is passed through mirrors and focused into the diamond at the sampling area. The sample is in direct contact with the upper side of this diamond. Due to the Attenuated Total Reflectance principle an evanescent wave passes a few micrometers through the sample before it is reflected back into the diamond and further through the optics of the ATR cell, which guides it towards the detector of the instrument. Although the optical design and principles are very different from the well known traditional transmission FTIR, where the beam passes directly through the sample, the spectra are, after a mathematical correction, almost identical. Thus the corrected ATR spectrum is in principle equivalent to the transmission spectrum recorded on a micrometer thin film of the same sample. The correction procedure are discussed later in this section.

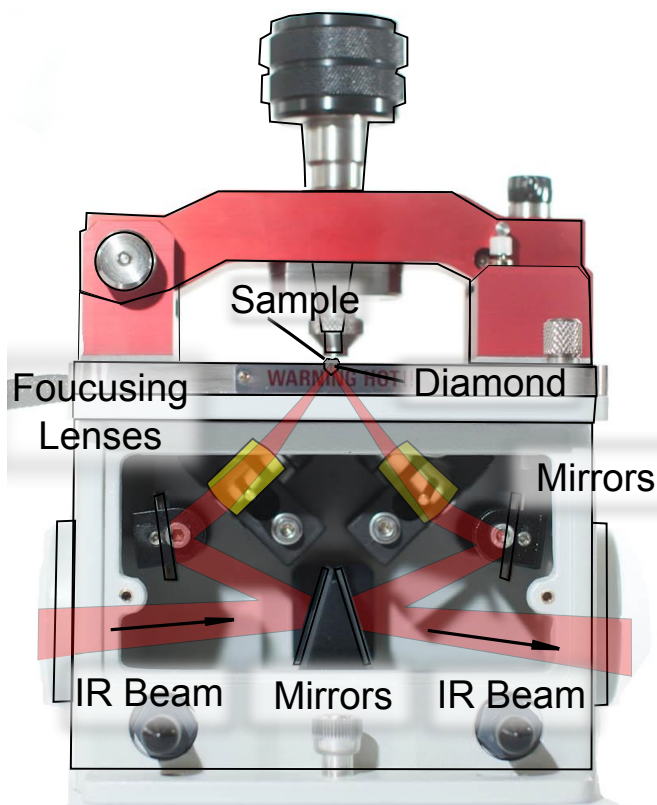


Figure 4.1.: Principle of the heatable Specac Golden Gate ATR cell for the experiments involving chromium catalysts. The principles of the Pike ATR cell used for the other experiments was almost identical.

4.2.1. Recording of in-situ ATR-FTIR spectra

The spectra were recorded using a Nicolet iS5 Spectrometer equipped with a 45° GladiATR diamond ATR cell from Pike Technologies heatable up to 300 °C. The gladiATR cell contained a built-in heating coil and a thermocouple so the temperature could accurately be controlled by an external control box. The temperature was kept constant in each experiment. To monitor the reactions in-situ a home build microreactor system was developed^[134]. The micro reactor itself was a small 25 micro liter custom made glass cap that could be loaded with reaction mixture before installing on the ATR top plate, see figure 4.2 on the next page. Approximately 15 mg of the quite viscous reaction mixture was quickly loaded into the glass reactor at room temperature, together with a small Teflon coated magnet rod (5x2 mm). The reactor was applied on top of the preheated diamond ATR-plate and magnetically stirred by a home built device was placed around the reactor to supply horizontal magnetic stirring. Between 4-

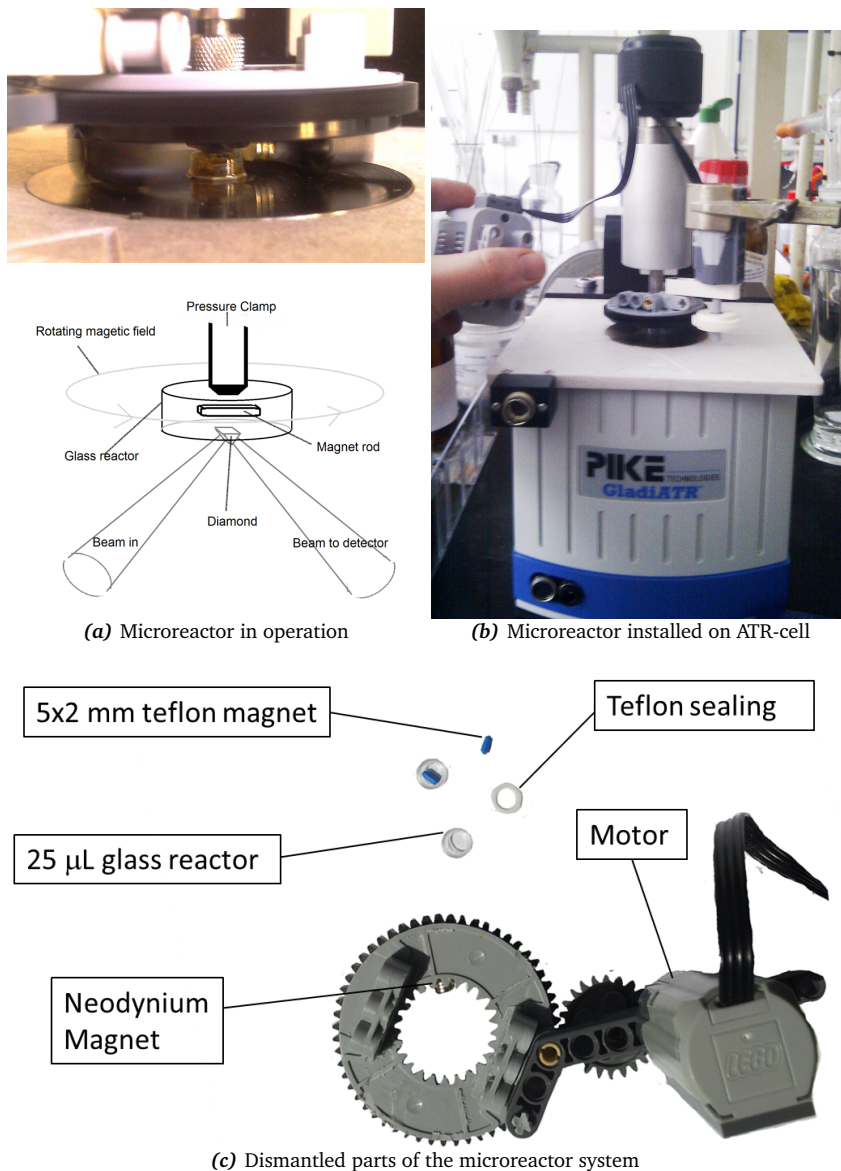


Figure 4.2.: **a)** Top shows photograph of the microreactor setup during cellulose hydrolysis in $[BD-MIM]Cl$, while the bottom shows a scheme of the microreactor in operation. **b)** Shows the microreactor system installed on top of the heatable Pike GladiATR ATR-cell (**NB:** on the picture the cell is not installed in the spectrometer). **c)** Shows the part of the microreactor system.

80 scans were recorded depending on the reaction rates (approximately 5 seconds to 2 minutes of recording) with 4 cm^{-1} resolution. The ATR-cell was itself was purged with dry nitrogen during experiments, to avoid gas spectrum contributions from water and CO_2 . Reference spectra of cellulose oligomers were made from powder samples with cellotriose, cellotetraose and cellopentaose, which were all purchased from Megazymes.

For the thin film experiments a thin ionic liquid film was dispersed on the diamond and the metal cap was then quickly put on top of the sample to seal it from the ambient atmosphere. Then a dry nitrogen flow (AGA, approximately 35 mL/min) was applied, see figure 3.4 on page 64. Due to the faster kinetics only 2 scans was used at higher temperatures yielding a recording time below 3 seconds. For all experiments where chromium was used as catalyst a High-temperature Golden Gate diamond ATR-cell from Specac was used instead of the Pike ATR-Cell. The Specac and Pike cells where equivalent in design and functionality. The only difference of the two cells was that the pike cell used rounded focusing mirrors in stead of flat mirrors and focusing lenses. There was no difference in the spectra obtained from the two different cells.

4.2.2. Transmission FTIR

The transmission FTIR spectroscopy was performed using a Perkin-Elmer Paragon 1000 instrument and a sandwich cell with AgCl windows at room temperature. The samples of cellulose and glucose was prepared as described above. Spacers was made from a $10\ \mu\text{m}$ polyethylene film, ensuring a constant path length. The empty sandwich cell with AgCl windows and spacer was used as a background. The chamber was purges with nitrogen during recording of spectra where 64 scans was applied.

4.2.3. Correction of the ATR-spectra

ATR-FTIR is a very well suited technique for obtaining spectra of liquids. The low penetration depths are in most cases a big advantage as this ensures transmission in all the measured regions. However, an ATR-FTIR spectrum is not equivalent to an transmission spectra as the evanescent waves penetration depth is a changing as a function of wavelength. Further the penetration depth is also dependent on the IR-beam's incident angle into the ATR crystal, the ATR crystals refractive index and the sample refractive index. The penetration depth can be calculated as:

$$d_p = \frac{\lambda}{2\pi n_1 \sqrt{\sin^2 \phi - (n_2/n_1)^2}} \quad (4.1)$$

where d_p , λ , ϕ , n_1 , and n_2 are the penetration depth, wavelength, incident angle, ATR crystal refractive index and sample refractive index respectively. This makes the recorded spectra distorted compared to a corresponding transmission spectra. However, a quite simple mathematical correction will transform the ATR spectra into an approximation of the corresponding transmission spectra. However, the refractive index changes during a strong infrared absorption^[112], which makes the simple correction a rather poor approximation of the equivalent transmission spectra, where the bands tend to shift as a function of their intensity. However, all ATR spectra in this thesis are corrected with the built-in "Advanced ATR Correction Algorithm" of the Thermo Fisher OMNIC 8.2 software. This algorithm takes these local variations of the refractive index into account, resulting in a very good approximation of the corresponding transmission spectra^[185]. Another problem with ATR-FTIR spectroscopy, that is quite often neglected, is the importance of knowing the refractive index of the sample. This can cause some practical problems when working with more exotic or novel substances such as ionic liquids and their mixtures. However, a fairly good approximation for the refractive index of a mixture is to simply take the volume weighted average of the refractive indices^[186]:

$$n_{ab} = \varphi_a n_a + \varphi_b n_b \quad (4.2)$$

where n_{ab} is the refractive index of the mixture, φ_i and n_i the volume fractions and the refractive indices of the individual components respectively. Finding a trustworthy density for cellulose was challenging as a lot of the literature values often include the pores of a typical cellulose structure, which results in a too low density. However, Sun et al. developed a method where they could determine the actual density of a related type of cellulose to be 1.46 g/cm^3 ^[187]. The refractive index of cellulose is very dependent on the type of cellulose and the different directions in the cellulose fibers^[188], however Barsberg et al. determined a suitable refractive index they used for ATR correction of microcrystalline cellulose to 1.46^[133]. It was not possible to find data for [BDMIM]Cl, so instead the data for [BMIM]Cl was used. [BMIM]Cl has a density of 1.05 g/cm^3 . The refractive index of 1,3-dialkylimidazolium based ionic liquids varies from around 1.4 in the case of very weakly interacting anions to around 1.50-1.57 for the very strongly interacting anions such as halides, acetates or formates^[189,190]. Refractive index of chloride based imidazolium ionic liquids were around 1.50-1.53 depending on temperature and chain lengths^[190]. Kuzmina et al. reported a refractive index of 1.503 for [BMIM]Cl at 85°C that was used in the calculation, as the other refractive indices were reported at room temperatures. These values are inserted in equation 4.2 for a 10 wt.% solution of cellulose in [BMIM]Cl:

$$n_{[\text{BMIM}]\text{Cl}, \text{cellulose}} = \varphi_{\text{cellulose}} n_{\text{cellulose}} + \varphi_{[\text{BMIM}]\text{Cl}} n_{[\text{BMIM}]\text{Cl}} = \frac{0.1}{1.46} \cdot 1.46 + \frac{0.9}{1.05} \cdot 1.503 = \underline{1.500}$$

By comparison of the difference spectra of 10 wt.% cellulose solutions in [BMIM]Cl and [BD-MIM]Cl they were found to be identical in the 1100-900 cm^{-1} region, thus the refractive index 1.50 of was assumed applicable to the [BDMIM]Cl solutions as well. The same refractive index was used for the cellobiose and glucose solutions and the refractive index was assumed to be constant during reaction. Before the ATR corrections the spectra were corrected for the slightly unstable background signal by subtracting a constant by assuming zero absorbance at 4000 cm^{-1} if necessary.

Deconvolution of Spectra

Difference spectra were produced by subtracting a spectrum corresponding to the pseudo steady-state from each spectrum before analysis. The difference spectra were deconvoluted with PeakFit using the built-in Voigt area approximation algorithm. After fitting of the first spectrum the parameters were saved and used in the fitting of the rest of the spectra series to ensure comparability between the deconvolutions. For each series the spectra with the most intense signals were deconvoluted at first using the original set of parameters, thereafter the value of the integrated peak was found by integration and the new parameters were saved in a file. Then these parameters were used as the initial guess for the next spectrum. This approach was continued until a substantial amounts of spectra were deconvoluted and the initial pseudo-zero order rate could be estimated. During deconvolution the band widths were constrained.

The reaction rates of the hydrolysis reactions were determined on the basis of the area of the band around 1157 cm^{-1} in the deconvoluted spectra. The difference spectra was used because it in principle eliminates the spectrum of the ionic liquid, making the deconvolution simpler hence more accurate. The spectrum that was subtracted from all the other spectra during reaction was chosen as the pseudo steady state, as no absolute steady state occurred within reasonable time. This procedure indeed showed to produce very high quality values of the reaction rates. This means that the absolute value of the absorbance of the 1157 cm^{-1} derived from the difference spectra varies a little from experiment to experiment. However, the absorbances on initial raw spectra are identical, and the initial rates do not change no matter which pseudo steady state spectrum was chosen.

The experiments with $\text{CrCl}_3 \cdot 6\text{H}_2\text{O}$ as catalyst were processed using an automated Gaussian deconvolution procedure in gnuplot, which saved a lot of time for data processing. This method is described in detail in chapter 2. The same automated deconvolution procedure was used to determine the development of the $\nu_{\text{C=O}}$ band at 1669 cm^{-1} used for the determination of the HMF formation rates during hydrolysis.

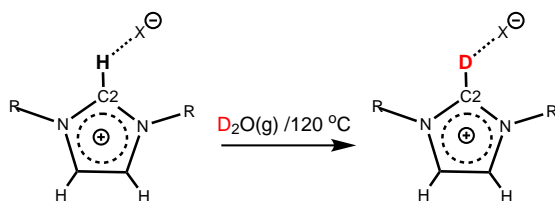


Figure 4.3.: Selective in-situ exchange of proton in C2 position in imidazolium based ionic liquid

in-situ deuterium exchange experiments

In 1,3-alkylimidazolium ionic liquids the proton in the C2 position is slightly acidic. Hence it can selectively be exchanged by deuterium during dissolution in D_2O , if anions of the ionic liquids are just slightly acidic^[32,191]. This was initially done before we purchased the heatable ATR cell by making 1 wt.% solutions of the ionic liquid in D_2O (Sigma-Aldrich 99.0%). After some days the ionic liquid was isolated by evaporation of the D_2O at 120 °C. However, a faster and more efficient method was developed to do the deuterium exchange in-situ in a thin ionic liquid film using the home build metal cap. Nitrogen was bubbled through a small flask containing D_2O at a rate of 15mL/min. The ionic liquid film was then exposed to the D_2O saturated nitrogen at 120 °C. In practice higher D/H exchange ratios could be obtained with this method compared to the method described by Jeon et al.^[191] while still selectively exchanging the proton in the C2 position, see figure 4.3. The results are shown in appendix: see figures B.3 and B.4 on page 116 and 117. These experiments were very useful to elucidate the spectral features of [BMIM]Cl as there exists no unambiguous interpretation of the infrared spectrum in the literature^[191]

HPLC analysis

After the hydrolysis of the cellulose with sulfuric acid, spot checks (100 and 120 °C) were taken from some of the experiments to confirm the presence of glucose and HMF. The samples were diluted with 0.7 mL d_6 -DMSO as H^1 -NMR was attempted but unsuccessful as analytic method before HPLC. The reaction mixtures were analyzed by HPLC with RI detection (Agilent 1200 series, 30 cm Aminex[®] HPX-87H column, with 0.005M H_2SO_4 in MilliQ water as eluent at a flow rate of 0.6 mL/min). The retention time of the formed product peaks (glucose, HMF, levulinic acid and formic acid) were identified by comparison with their individual references.

In the chromium catalyzed experiments the same procedure was applied, however water was used instead of d_6 -DMSO.

Calculation of theoretical spectra

Density functional theory and Hartree-Fock calculations were performed with Gaussian09^[114]. Starting structures of cellulose oligomers were adopted from the experimental crystal structure obtained by Nishiyama et al.^[192]. Initially, the structure was optimized with Hartree-Fock using the 6-31G(d) basis set and then refined with DFT using the B3LYP functional and the 6-311+G(d,p) basis set. For glucose 4 different conformers of the β form was optimized and 3 different conformers of the α form was optimized. The reported spectra correspond to the conformers with the lowest energy. All spectra were scaled with a factor of 0.983 according to Sundaraganesan et al.^[193].

For the calculations on the transition state connecting protonated cellobiose and the oxocarbenium + glucose intermediate HF/6-31(d) was used. Initially the structures of the planar protonated cellobiose and oxocarbenium + glucose were optimized. Then the search for the transition state connecting these structures was performed using the built-in *Synchronous Transit-Guided Quasi-Newton* (STQN) method. The found transition state had only one imaginary frequency. The validity of this transition state was further investigated using a *intrinsic reaction coordinate* (IRC) calculation yielding the expected oxocarbenium + glucose structure to the right hand side of the transition state. However, on the other side the twisted version of protonated cellobiose structure, described in chapter 2, was obtained instead of the planar structure given as input to the STQN calculation.

Concluding remarks and outlook.

New kinetic and mechanistic aspects of cellulose conversion into HMF in chloride based ionic liquids has been investigated thoroughly with in-situ FTIR spectroscopy using Brønsted acids and Lewis acidic chromium catalysts.

Initially the two characteristic infrared stretching bands of the glucoside bond were identified at 1155 cm^{-1} and 970 cm^{-1} . The sulfuric acid catalyzed hydrolysis of cellulose and cellobiose in the ionic liquid [BDMIM]Cl was monitored in-situ by ATR-FTIR spectroscopy using the band at 1155 cm^{-1} in a custom made microreactor. The disappearance of the glucoside bond could be quantified by deconvolution of the spectra. From the initial rates the activations energies of cellulose and cellobiose hydrolysis could be determined to 94 and 69 kJ/mol respectively. The lower activation energy of cellobiose hydrolysis was explained by a more favorable transition state that became possible due to increased rotational freedom around the glucoside bond. This suggest that when cellobiose is used as a model for cellulose the results should be used with some caution.

The method could also be successfully be applied to two heterogeneous catalysts. The investigation of cellulose hydrolysis catalyzed by the Lewis acidic salt $\text{CrCl}_3 \cdot 6\text{H}_2\text{O}$ yielded an almost identical activation energy at 92 kJ/mol that was explained by a mechanism suggesting similar transitions states for the Brønsted and Lewis acid catalyzed hydrolysis. The found activation energies where in general much lower compared to the ones reported in water, which suggests that the ionic environment could have an active co-catalyzing role by stabilizing the positive charged oxocarbenium transition states and intermediates during hydrolysis.

HMF formation could be investigated simultaneously with the hydrolysis. The activation energy was found to 85 and 102 kJ/mol respectively for sulfuric acid and $\text{CrCl}_3 \cdot 6\text{H}_2\text{O}$. In the case of $\text{CrCl}_3 \cdot 6\text{H}_2\text{O}$ another carbonyl species was formed with a C=O stretching band at around 1773 cm^{-1} .

In chapter 3 the kinetics of chromium catalyzed glucose conversion was investigated by in-situ ATR-FTIR monitoring in the microreactor as well as in thin anhydrous ionic liquid films. The $\text{CrCl}_3 \cdot 6\text{H}_2\text{O}$ catalyst was found to suffer from pronounced product inhibition, and the rates were 2-3 times higher when water was removed during the reactions. The activation energies were however found to be identical at around 100-102 kJ/mol. The inhibition led to a pronounced deviation from the expected pseudo first order kinetics, especially at higher conversions, which surprisingly in some cases resulted in apparent second order behavior. The active species was proposed to be monomeric $[\text{CrCl}_6]^{3-}$ forming bidentate $[\text{CrCl}_4\text{glucose}]^-$ complexes with glucose. The conversion of glucose in the presence of CrCl_2 was also investigated in the thin anhydrous ionic liquid films. While the activation energy was found to be identical to the reactions catalyzed by $\text{CrCl}_3 \cdot 6\text{H}_2\text{O}$ the rates were around 8 times lower, which suggested that $[\text{CrCl}_6]^{3-}$ was the actual active species, which was also supported by EXAFS. Despite the lower initial rates the $\text{Cr}^{\text{II}}/\text{Cr}^{\text{III}}$ system showed no signs of product inhibition but followed first order kinetics, which at longer reaction times resulted in a higher total glucose conversion compared to $\text{CrCl}_3 \cdot 6\text{H}_2\text{O}$. This was explained by a proposed mechanism combining the high lability of the Cr^{II} species and fast swaps of oxidation states between the Cr^{II} and Cr^{III} species, regenerating the inhibited Cr^{III} species.

A general and unifying kinetic model was proposed, showing how a combination of first order dependency of glucose and product inhibition could explain the apparent second order kinetics for the Cr^{III} catalyzed reactions.

Fructose dehydration was investigated in both the presence and absence of $\text{CrCl}_3 \cdot 6\text{H}_2\text{O}$. The chloride ions catalyzed the two first dehydration steps of fructose very fast under anhydrous conditions. This resulted in an accumulation of intermediates as the last dehydration step seemed to be slower. These intermediates seemed both to yield humins and HMF. If water was present the first two dehydration steps were much slower and the accumulation of intermediates was avoided which led to increased HMF selectivity. In the presence of chromium the dehydration was 6-30 times faster, which clearly emphasized that chromium plays a catalytic key role in both the isomerization and dehydration. The activation energy was determined to 74 kJ/mol.

Both the results from chapter 2 and 3 further emphasize that care should be taken when comparing chemical processes carried out in water and ionic liquids, as the ionic environment are very different from the ones found in aqueous solutions. Finally the chapter identifies that one of the major challenges for large scale utilization of chromium catalysts in HMF production, are to overcome the product inhibition. This could possibly be solved by reducing a smaller fraction of the Cr^{III} catalyst by a cheap reducing agent such as zinc which could prevent the product inhibition.

Bibliography

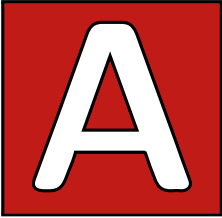
- [1] <http://keelingcurve.ucsd.edu/> - 21th of May 2013.
- [2] Bernstein, L.; et al. *Climate Change 2007: Synthesis Report Summary for Policymakers Intergovernmental Panel on Climate Change (IPCC) 2010*.
- [3] Schneider, B.; Schneider, R. *Nat. Geosci.* **2009**, *3*, 6–7.
- [4] Pagani, M.; Liu, Z.; LaRiviere, J.; Ravelo, A. C. *Nat. Geosci.* **2009**, *3*, 27–30.
- [5] Dowsett, H. J.; Chandler, M. A.; Robinson, M. M. *Phil. Trans. R. Soc. A* **2009**, *367*, 69–84.
- [6] Dekens, P. S.; Ravelo, A. C.; McCarthy, M. D. *Paleoceanography* **2007**, *22*, 1–12.
- [7] Lunt, D. J.; Haywood, A. M.; Schmidt, G. A.; Salzmann, U.; Valdes, P. J.; Dowsett, H. J. *Nat. Geosci.* **2009**, *3*, 60–64.
- [8] Wery, T. A.; Holladay, J. E.; White, J. F. Top value added chemicals from biomass: I. results of screening for potential candidates from sugars and synthesis gas Technical report, Pacific Northwest National Laboratory (PNNL), Richland, WA (US), **2004**.
- [9] Hacker, F.; Harthan, R.; Matthes, F.; Zimmer, W. *ETC/ACC technical paper* **2009**, *4*, 56–90.
- [10] Wang, M. J. *Power Sources* **2002**, *112*, 307–321.
- [11] Gerpen, J. *Fuel Process Technol.* **2005**, *86*, 1097.
- [12] Hahn-Hägerdal, B.; Galbe, M.; Gorwa-Grauslund, M.; Liden, G.; Zacchi, G. *Trends Biotechnol.* **2006**, *24*, 549–556.
- [13] *Royalty free photos obtained from: <http://www.colorbox.dk> - 15th of May 2013.*
- [14] Babcock, B. A. *China. Econ. Rev.* **2012**, *4*, 407–426.
- [15] Buyx, A.; Tait, J. *Science* **2011**, *332*, 540–541.
- [16] Hertel, T. W.; Beckman, J. Commodity price volatility in the biofuel era: An examination of the linkage between energy and agricultural markets Working paper, February , **2011**.
- [17] Tangermann, S. *ICTSD, Issue Paper* **2011**.
- [18] Headey, D.; Fan, S. *Agricultural Economics* **2008**, *39*, 375–391.
- [19] Carlson, K. M.; Curran, L. M.; Asner, G. P.; Pittman, A. M.; Trigg, S. N.; Adeny, J. M. *Nature Clim. Change* **2012**, *3*, 283–287.
- [20] Lapola, D. M.; Schaldach, R.; Alcamo, J.; Bondeau, A.; Koch, J.; Koelking, C.; Priess, J. A. *PNAS* **2010**, *107*, 3388–3393.
- [21] Page, S. E.; Siegert, F.; Rieley, J. O.; Boehm, H.-D. V.; Jaya, A.; Limin, S. *Nature* **2002**, *420*, 61–65.
- [22] Fearnside, P. M.; Laurance, W. F. *Ecol. Appl.* **2004**, *14*, 982–986.
- [23] van der Werf, G. R.; Morton, D. C.; DeFries, R. S.; Olivier, J. G.; Kasibhatla, P. S.; Jackson, R. B.; Collatz, G. J.; Rander-son, J. *Nat. Geosci.* **2009**, *2*, 737–738.
- [24] Rinaldi, R.; Schüth, F. *Energy Environ. Sci.* **2009**, *2*, 610–626.
- [25] Stark, A. *Energy Environ. Sci.* **2011**, *4*, 19–32.
- [26] Rinaldi, R.; Meine, N.; vom Stein, J.; Palkovits, R.; Schüth, F. *ChemSusChem* **2010**, *3*, 266–76.
- [27] Sims, R. E.; Mabee, W.; Saddler, J. N.; Taylor, M. *Bioresour. Technol.* **2010**, *101*, 1570.
- [28] Ishola, M. M.; Jahandideh, A.; Haidarian, B.; Brandberg, T.; Taherzadeh, M. J. *Bioresour. Technol.* **2013**.
- [29] Novozymes A/S. *Cellulosic ethanol- Novozymes Cellic Ctec3, Application note* ; 2012.
- [30] Swatloski, R. P.; Spear, S. K.; Holbrey, J. D.; Rogers, R. D. *J. Am. Chem. Soc.* **2002**, *124*, 4974–4975.
- [31] Kahlen, J.; Masuch, K.; Leonhard, K. *Green Chemistry* **2010**, *12*(12), 2172–2181.
- [32] Guo, Z.; Lue, B.; Thomassen, K.; Meyer, A.; Xu, X. *Green Chem.* **2007**, *9*, 1362–1373.
- [33] Klein-Marcuschamer, D.; Simmons, B. A.; Blanch, H. W. *Biofuels, Bioprod. Biorefin.* **2011**, *5*, 562–569.
- [34] Sen, S. M.; Binder, J. B.; Raines, R. T.; Maravelias, C. T. *Biofuels, Bioprod. Biorefin.* **2012**, *6*, 444–452.
- [35] Boisen, A.; Christensen, T.; Fu, W.; Gorbanev, Y.; Hansen, T.; Jensen, J.; Klitgaard, S.; Pedersen, S.; Riisager, A.; Ståhlberg, T. *Chem. Eng. Res. Des.* **2009**, *87*, 1318–1327.
- [36] Tong, X.; Ma, Y.; Li, Y. *Appl. Catal., A* **2010**, *385*, 1–13.
- [37] Rosatella, A. A.; Simeonov, S. P.; Frade, R. F.; Afonso, C. A. *Green Chem.* **2011**, *13*, 754–793.
- [38] Bozell, J. J.; Petersen, G. R. *Green Chem.* **2010**, *12*, 539–554.
- [39] Chidambaram, M.; Bell, A. T. *Green Chem.* **2010**, *12*, 1253–1262.
- [40] Román-Leshkov, Y.; Barrett, C. J.; Liu, Z. Y.; Dumesic, J. A. *Nature* **2007**, *447*, 982–985.
- [41] Wu, X.; Li, Q.; Fu, J.; Tang, C.; Huang, Z.; Daniel, R.; Tian, G.; Xu, H. *Fuel* **2012**, *95*, 234 – 240.
- [42] Wu, X.; Daniel, R.; Tian, G.; Xu, H.; Huang, Z.; Richardson, D. *Appl. Energy* **2011**, *88*, 2305–2314.
- [43] Daniel, R.; Xu, H.; Wang, C.; Richardson, D.; Shuai, S. *Appl. Energy* **2012**.
- [44] Román-Leshkov, Y.; Chheda, J. N.; Dumesic, J. A. *Science* **2006**, *312*, 1933–1937.
- [45] Chheda, J. N.; Román-Leshkov, Y.; Dumesic, J. A. *Green Chem.* **2007**, *9*, 342–350.
- [46] Method for the synthesis of 5-alkoxymethylfurfural ethers and their use. September 19 **2007**.
- [47] *Pres-release: <http://www.pepsico.com/PressRelease/PepsiCo-Develops-Worlds-First-100-Percent-Plant-Based-Renewably-Sourced-PET-Bott03152011.html/> - March 15, 2011.*
- [48] Zhao, H.; Holladay, J. E.; Brown, H.; Zhang, Z. C. *Science* **2007**, *316*, 1597–1600.
- [49] Bali, S.; Tofanelli, M. A.; Ernst, R. D.; Eyring, E. M. *Biomass Bioenergy* **2012**.
- [50] Pidko, E. A.; Degirmenci, V.; van Santen, R. A.; Hensen, E. J. *Angew. Chem. Int. Ed.* **2010**, *49*, 2530–2534.
- [51] Pidko, E. A.; Degirmenci, V.; van Santen, R. A.; Hensen, E. J. *Inorg. Chem.* **2010**, *49*, 10081–10091.
- [52] Pidko, E. A.; Degirmenci, V.; Hensen, E. J. *ChemCatChem* **2012**, *4*, 1263–1271.
- [53] Zhang, Y.; Pidko, E. A.; Hensen, E. J. *Chem. Eur. J.* **2011**, *17*, 5281–5288.
- [54] Cao, Q.; Guo, X.; Yao, S.; Guan, J.; Wang, X.; Mu, X.; Zhang, D. *Carbohydr. Res.* **2011**, *346*, 956 – 959.

- [55] Hu, L.; Sun, Y.; Lin, L. *Ind. Eng. Chem. Res.* **2012**, *51*, 1099–1104.
- [56] Kiesel, A.; Semiganovski, N. *Trans. Chem. Pharmac. Inst. Moscow* **1927**, *18*, 82.
- [57] Waksman, S.; Stevens, K. R. *Ind. Eng. Chem.* **1930**, *2*, 167–173.
- [58] Saeman, J.; Bubl, J.; Harris, E. *Ind. Eng. Chem.* **1945**, *17*, 35–37.
- [59] Tian, J.; Wang, J.; Zhao, S.; Jiang, C.; Zhang, X.; Wang, X. *Cellulose* **2010**, *17*, 587–594.
- [60] Vanoye, L.; Fanselow, M.; Holbrey, J. D.; Atkins, M. P.; Seddon, K. R. *Green Chem.* **2009**, *11*, 390–396.
- [61] Choi, J.; Kim, S. *Korean J. of Chem. Eng.* **1994**, *11*, 178–184.
- [62] Bemiller, J. *Advan. Carbohydr. Chem.* **1967**, *22*, 25–108.
- [63] Overend, W. G.; Rees, C. W.; Sequeira, J. S. *J. Chem. Soc.* **1962**, *0*, 3429–3440.
- [64] Tao, F.; Song, H.; Chou, L. *ChemSusChem* **2010**, *3*, 1298–303.
- [65] Peng, L.; Zhang, J.; Zhuang, J.; Zhang, B.; Gong, Y. *Molecules* **2010**, *15*, 5258–5272.
- [66] Su, Y.; Brown, H. M.; Huang, X.; Dong Zhou, X.; Amonette, J. E.; Zhang, Z. C. *Appl. Catal. A* **2009**, *361*, 117–122.
- [67] Dutta, S.; De, S.; Alam, M. I.; Abu-Omar, M. M.; Saha, B. *J. Catal.* **2012**, *288*, 8–15.
- [68] Tao, F.; Song, H.; J. Yang, L. C. *Carbohydr. Polym.* **2011**, *85*, 363–368.
- [69] Rye, C. S.; Withers, S. G. *Curr. Opin. Chem. Biol.* **2000**, *4*, 573–580.
- [70] Saharay, M.; Guo, H.; Smith, J. C. *PLoS ONE* **2010**, *5*, 1–10.
- [71] Xiang, Q.; Lee, Y.; Petterson, P. O.; Torget, R. W. *Appl. Biochem. Biotechnol.* **2003**, *105*, 505–514.
- [72] X. Liang, A. M.; Haynes, B. S. *J. Phys. Chem. B* **2011**, *115*, 10682–10691.
- [73] Vernon, C. *Proc. R. Soc. London, Ser. B* **1967**, *167*, 389–401.
- [74] Nevell, T.; Upton, W. *Carbohydr. Res.* **1976**, *49*, 163–174.
- [75] Dee, S. J.; Bell, A. T. *ChemSusChem* **2011**, *1462*, 1166–1173.
- [76] Banks, B.; Meinwald, Y.; A.J. Rhind-Tutt, I. S.; Vernon, C. *J. Chem. Soc.* **1961**, *0*, 3240–3246.
- [77] Timell, T. *Can. J. Chem.* **1964**, *42*, 1456–1472.
- [78] Bower, S.; Wickramasinghe, R.; Nagle, N. J.; Schell, D. J. *Bioresour. Technol.* **2008**, *99*, 7354–7362.
- [79] Kresge, A.; Straub, T. *J. Am. Chem. Soc.* **1983**, *105*, 3957–3957.
- [80] Petersen, L.; Ardehvol, A.; Rovira, C.; Reilly, P. *J. Phys. Chem. B* **2009**, *113*, 7331–7339.
- [81] Liu, J.; Wang, X.; Xu, D. *J. Phys. Chem. B* **2009**, *114*, 1462–1470.
- [82] Lee, S.; Kim, I.; Ryu, D.; Taguchi, H. *Biotechnol. Bioeng.* **1983**, *25*, 33–51.
- [83] Garsoux, G.; Lamotte, J.; Gerday, C.; Feller, G. *Biochem. J* **2004**, *384*, 247.
- [84] Sonan, G.; Receveur-Brechot, V.; Duez, C.; Aghajari, N.; Czjzek, M.; Haser, R.; Gerday, C. *Biochem. J* **2007**, *407*, 293.
- [85] Li, L.; Flora, R.; King, K. *Arch. Biochem. Biophys.* **1965**, *111*, 439–447.
- [86] Ng, T.; Zeikus, J. *Appl. Environ. Microbiol.* **1981**, *42*, 231–240.
- [87] Bose, S.; Armstrong, D.; Petrich, J. *J. Phys. Chem. B* **2010**, *114*, 8221–8227.
- [88] Park, S.; Kazlauskas, R. *Curr. Opin. Biotechnol.* **2003**, *14*, 432–437.
- [89] Naushad, M.; AL-Othman, Z. A.; Khan, A. B.; Ali, M. *Int. J. Biol. Macromol.* **2012**.
- [90] Pottkämper, J.; Barthen, P.; Ilmberger, N.; Schwaneberg, U.; Schenk, A.; Schulte, M.; Ignatiev, N.; Streit, W. *Green Chem.* **2009**, *11*, 957–965.
- [91] Mosier, N.; Ladisch, C.; Ladisch, M. *Biotechnol. Bioeng.* **2002**, *79*, 610–618.
- [92] Mosier, N.; Sarikaya, A.; Ladisch, C.; Ladisch, M. *Biotechnol. Progr.* **2001**, *17*, 474–480.
- [93] vom Stein, T.; Grande, P.; Sibilla, F.; Commandeur, U.; Fischer, R.; Leitner, W.; de Marfa, P. *Green Chem.* **2010**, *12*, 1844–1849.
- [94] Charmot, A.; Katz, A. *J. Catal.* **2010**, *276*, 1–5.
- [95] Calvini, P.; Gorassini, A.; Merlani, A. L. *Cellulose* **2008**, *15*, 193–203.
- [96] Doner, L. W.; Irwin, P. L. *Anal. Biochem.* **1992**, *202*, 50–53.
- [97] Waffenschmidt, S.; Jaenicke, L. *Anal. Biochem.* **1987**, *165*, 337–340.
- [98] Zhang, Y.-H. P.; Lynd, L. R. *Biomacromolecules* **2005**, *6*, 1510–1515.
- [99] Miller, G. L. *Anal. Chem.* **1959**, *31*, 426–428.
- [100] Evans, R.; Wallis, A. F. *J. Appl. Polym. Sci.* **1989**, *37*, 2331–2340.
- [101] Evans, R.; Wearne, R. H.; Wallis, A. F. *J. Appl. Polym. Sci.* **1989**, *37*, 3291–3303.
- [102] Barthel, S.; Heinze, T. *Green Chem.* **2005**, *8*, 301–306.
- [103] Rinaldi, R.; Palkovits, R.; Schüth, F. *Angew. Chem. Int. Ed.* **2008**, *47*, 8047–8050.
- [104] Cruz, H.; Fanselow, M.; Holbrey, J. D.; Seddon, K. R. *Chem. Commun.* **2012**, *48*, 5620–5622.
- [105] Tan, S.; MacFarlane, D. *Top. Curr. Chem.* **2010**, pages 311–339.
- [106] Rinaldi, R.; Schüth, F. *ChemSusChem* **2009**, *2*, 1096–1107.
- [107] Dee, S. J.; Bell, A. T. *Green. Chem.* **2011**, *1462*, 1467–1475.
- [108] Pogliani, L. *React. Kinet. Catal. Lett.* **2008**, *93*, 261–191.
- [109] Suganuma, S.; Nakajima, K.; Kitano, M.; Yamaguchi, D.; Kato, H.; Hayashi, S. *J. Am. Chem. Soc.* **2008**, *130*, 12787–12793.
- [110] Phan, H. D.; Yokoyama, T.; Matsumoto, Y. *Org. Biomol. Chem.* **2012**, *190*, 7382–7391.
- [111] Pavia, D. L.; Lampman, G. M.; Kriz, G. S. *Introduction to spectroscopy*; Brooks/cole, 2001.
- [112] Engel, T. *Quantum Chemistry*; Pearson Education, first ed., 2006.
- [113] Nakamoto, K. *Infrared and Raman spectra of inorganic and coordination compounds 4th edition*; Wiley New York, 1986.
- [114] Gaussian 09 Revision A.1. Frisch, M. J.; Trucks, G. W.; Schlegel, H. B.; Scuseria, G. E.; Robb, M. A.; Cheeseman, J. R.; Scalmani, G.; Barone, V.; Mennucci, B.; Petersson, G. A.; Nakatsuji, H.; Caricato, M.; Li, X.; Hratchian, H. P.; Izmaylov, A. F.; Bloino, J.; Zheng, G.; Sonnenberg, J. L.; Hada, M.; Ehara, M.; Toyota, K.; Fukuda, R.; Hasegawa, J.; Ishida, M.; Nakajima, T.; Honda, Y.; Kitao, O.; Nakai, H.; Vreven, T.; Montgomery, Jr., J. A.; Peralta, J. E.; Ogliaro, F.; Bearpark,

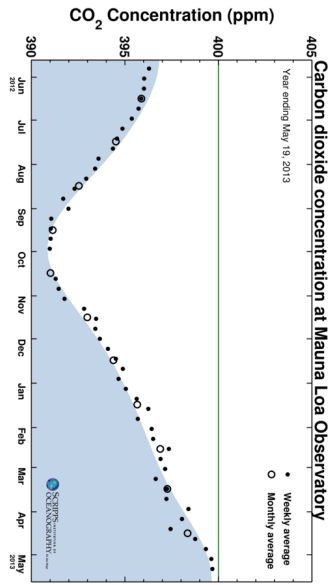
- M.; Heyd, J. J.; Brothers, E.; Kudin, K. N.; Staroverov, V. N.; Kobayashi, R.; Normand, J.; Raghavachari, K.; Rendell, A.; Burant, J. C.; Iyengar, S. S.; Tomasi, J.; Cossi, M.; Rega, N.; Millam, J. M.; Klene, M.; Knox, J. E.; Cross, J. B.; Bakken, V.; Adamo, C.; Jaramillo, J.; Gomperts, R.; Stratmann, R. E.; Yazyev, O.; Austin, A. J.; Cammi, R.; Pomelli, C.; Ochterski, J. W.; Martin, R. L.; Morokuma, K.; Zakrzewski, V. G.; Voth, G. A.; Salvador, P.; Dannenberg, J. J.; Dapprich, S.; Daniels, A. D.; Farkas, .; Foresman, J. B.; Ortiz, J. V.; Cioslowski, J.; Fox, D. J.
- [115] Bosma, W. B.; Schnupf, U.; Willett, J.; Momany, F. A. *J. Mol. Struct. THEOCHEM* **2009**, *905*, 59–69.
- [116] Ibrahim, M.; Alaam, M.; El-Haes, H.; Jalbout, A. F.; de Leon, A. *Eclética Quím.* **2006**, *31*.
- [117] Araujo-Andrade, C.; Ruiz, F.; Martínez-Mendoza, J.; Terrores, H. *J. Mol. Struct. THEOCHEM* **2005**, *714*, 143–146.
- [118] Kačuráková, M.; Mathlouthi, M. *Carbohydr. Res.* **1996**, *284*, 145–157.
- [119] Tul'chinsky, V. M.; Zurabyan, S. E.; Asankozhoev, K. A.; Kogan, G. A.; Khorlin, A. Y. *Carbohydr. Res.* **1976**, *51*, 1–8.
- [120] Sekkal, M.; Dincq, V.; Legrand, P.; Huvenne, J. J. *Mol. Struct.* **1995**, *349*, 349–352.
- [121] Marchessault, R.; Liang, C. *J. Polymer Sci.* **1959**, *37*, 385.
- [122] Marchessault, R.; Liang, C. *J. Polymer Sci.* **1959**, *39*, 269.
- [123] Marchessault, R.; Liang, C. *J. Polymer Sci.* **1962**, *59*, 357.
- [124] Pearson, F.; Marchessault, R.; Liang, C. *J. Polymer Sci.* **1960**, *43*, 357.
- [125] Blackwell, J.; Vasko, P.; Koenig, J. J. *Appl. Phys.* **1970**, *41*, 4375.
- [126] Gael, J.; Koenig, J.; Blackwell, J. *Carbohydr. Res.* **1973**, *29*, 123.
- [127] Buslov, D.; Nikonenko, N. *Appl. Spectrosc.* **1997**, *51*, 666.
- [128] Buslov, D.; Nikonenko, N. *Appl. Spectrosc.* **1998**, *52*, 613.
- [129] Nikonenko, N. A.; Buslov, D. K.; Sushko, N. I.; Zhbankov, R. G. *Biopolymers* **2000**, *57*, 257–262.
- [130] Nikonenko, N.; Buslov, D.; Sushko, N.; Zhbankov, R. J. *Mol. Struct.* **2005**, *752*, 20–24.
- [131] Kiefer, J.; Obert, K.; Fries, J.; Bösmann, A.; Wasserscheid, P.; Leipertz, A. *Appl. Spectrosc.* **2009**, *63*, 1041–1049.
- [132] Barsberg, S. *J. Phys. Chem. B* **2010**, *114*, 11703–11708.
- [133] Barsberg, S.; Sanadi, A. R.; Jørgensen, H. *Carbohydr. Polym.* **2011**, *85*, 457–464.
- [134] Kunov-Kruse, A.; Piltoft, J.; Petersen, C. *An add-on system for an ATR-IR cell, patent application no. EP12174780.2/US61667786* **2012**.
- [135] Kunov-Kruse, A.; Thomsen, J.; Piltoft, J.; Petersen, C. *An add-on system for photochemical ATR-IR spectroscopy studies, patent application no. EP12174782.8/US61667837* **2012**.
- [136] Kunov-Kruse, A.; Thomsen, J.; Piltoft, J.; Petersen, C. *An add-on cap for ATR-IR spectroscopy studies, patent application no. EP12174778.6/US61667923* **2012**.
- [137] Sinnott, M. *Chem. Rev.* **1990**, *90*, 1171–1202.
- [138] Foresmann, J.; Frisch, A. *Exploring Chemistry with Electronic Structure Method.*; Gaussian Inc., 1996.
- [139] Van Dam, H.; Kieboom, A.; Van Bekkum, H. *Starch-Stärke* **2006**, *38*, 95–101.
- [140] Horvath, I. T.; Akien, G. R.; Qi, L. *Chem. Commun.* **2012**.
- [141] Xiang, Q.; Lee, Y. Y.; Torget, R. W. *Appl. Biochem. Biotechnol.* **2004**, *115*, 1127–1138.
- [142] Girisuta, B.; Janssen, L.; Heeres, H. *Ind. Eng. Chem. Res.* **2007**, *46*, 1696–1708.
- [143] Marcotullio, G.; De Jong, W. *Green Chem.* **2010**, *12*, 1739–1746.
- [144] Binder, J.; Raines, R. T. *J. Am. Chem. Soc.* **2009**, *131*, 1979–1985.
- [145] Qi, X.; Watanabe, M.; Aida, T. M.; Smith Jr, R. L. *Ind. Eng. Chem. Prod. Res.* **2008**, *47*, 9234–9239.
- [146] Qi, X.; Watanabe, M.; Aida, T. M.; Smith Jr, R. L. *Green Chem.* **2008**, *10*, 799–805.
- [147] Saravanamurugan, S.; Prasetyanto, E. A.; Park, S.-E. *Microporous Mesoporous Mater.* **2008**, *112*, 97–107.
- [148] Melero, J. A.; Stucky, G. D.; van Grieken, R.; Morales, G. *J. Mater. Chem.* **2002**, *12*, 1664–1670.
- [149] Lai, D.-m.; Deng, L.; Li, J.; Liao, B.; Guo, Q.-x.; Fu, Y. *ChemSusChem* **2011**, *4*, 55–58.
- [150] Kunov-Kruse, A. J.; Kristensen, S. B.; Riisager, A.; Rasmussen, S. B.; Fehrmann, R. *J. Mater. Sci.* **2009**, *44*, 323–327.
- [151] Kristensen, S. B.; Kunov-Kruse, A. J.; Riisager, A.; Rasmussen, S. B.; Fehrmann, R. *J. Catal.* **2011**, *284*, 60–67.
- [152] Jørgensen, B.; Kristensen, S. B.; Kunov-Kruse, A. J.; Fehrmann, R.; Christensen, C. H.; Riisager, A. *Top. Catal.* **2009**, *52*, 253–257.
- [153] Li, C.; Zhang, Z.; Zhao, Z. K. *Tetrahedron Lett.* **2009**, *50*, 5403–5405.
- [154] Riisager, A.; Mossin, S.; Kunov-Kruse, A.; Fehrmann, R. *Absorption and oxidation of NO in ionic liquids, patent pending* **2011**.
- [155] Saravanamurugan, S.; Kunov-Kruse, A.; Riisager, A.; Fehrmann, R. *ChemSusChem, submitted* **2013**.
- [156] Shriver, D.; Atkins, P.; Overton, T.; Rourke, J.; Weller, M.; Armstrong, F. *Inorganic Chemistry*; Oxford, 2006.
- [157] Andersen, J. *In situ Spectroscopic Studies of Chromium Catalysts in Ionic Liquids, Master thesis DTU* **2012**.
- [158] Andersen, J.; Kunov-Kruse, A.; Malco, P.; Stahl, K.; Riisager, A. *Unpublished results* **2013**.
- [159] Lindqvist-Reis, P.; Munoz-Paez, A.; Diaz-Moreno, S.; Pattanaik, S.; Persson, I.; Sandstrom, M. *Inorg. Chem.* **1998**, *37*, 5281–5288.
- [160] Cotton, F.; Wilkinson, G. *Advanced Inorganic Chemistry*; Interscience Publishers, third ed., 1993.
- [161] Plumb, W.; Harris, G. *Inorg. Chem.* **1964**, *3*, 542–545.
- [162] Sutin, N. *Annu. Rev. Phys. Chem.* **1966**, *17*, 119–172.
- [163] Xu, F. C.; Krouse, H. R.; Swaddle, T. W. *Inorg. Chem.* **1985**, *24*, 267–270.
- [164] Banerjee, D.; Chatterjee, C. *J. Inorg. Nucl. Chem.* **1969**, *31*, 3845–3849.
- [165] Banerjee, D.; Mohan, M. *J. Inorg. Nucl. Chem.* **1964**, *26*, 613–617.
- [166] Banerjee, D.; Chaudhuri, S. *J. Inorg. Nucl. Chem.* **1968**, *30*, 871–880.
- [167] Narusawa, Y.; Kanazawa, M.; Takahashi, S.; Morinaga, K.; Nakano, K. *J. Inorg. Nucl. Chem.* **1967**, *29*, 123–132.
- [168] Abdullah, M.; Barrett, J.; O'Brien, P. *J. Chem. Soc., Dalton Trans.* **1984**, pages 1647–1650.

- [169] Khan, K.-u.-D. I. A. *Transition Met. Chem.* **1986**, *11*, 391–395.
- [170] Dei, J. K.; Pasupalak, N. N.; Mohanty, P. *Transition Met. Chem.* **1997**, *22*, 516–520.
- [171] Qi, X.; Watanabe, M.; Aida, T. M.; Smith, R. L. *ChemSusChem* **2010**, *3*, 1071–1077.
- [172] Zinato, E.; Ricciari, P.; Sheridan, P. S. *Inorg. Chem.* **1979**, *18*, 720–724.
- [173] Malcho, P.; Mossin, S. *Unpublished results* **2013**.
- [174] Anthony, J. L.; Anderson, J. L.; Maginn, E. J.; Brennecke, J. F. *J. Phys. Chem. B* **2005**, *109*, 6366–6374.
- [175] Eriksen, J.; Mønsted, L.; Mønsted, O. *Acta Chem. Scand.* **1995**, *49*, 713–721.
- [176] Bang, E.; Mønsted, J. E.; Mønsted, O. *Acta Chem. Scand.* **1994**, *48*, 12–19.
- [177] Rasrendra, C. B.; Soetedjo, J. N. M.; Makertihartha, I. G. B. N.; Heeres, H. J.; Adisasmito, S. *Top. Catal.* **2012**, *55*, 543–549.
- [178] Blackmond, D. G. *Angew. Chem. Int. Ed.* **2005**, *44*, 4302–4320.
- [179] Segel, L. A. *Bull. Math. Biol.* **1988**, *50*, 579–593.
- [180] Tzafriri, A.; Edelman, E. *J. Theor. Biol.* **2004**, *226*, 303–314.
- [181] Vasilyeva, E. A.; Minkov, I. B.; Fitin, A. F.; Vinogradov, A. D. *Biochem. J* **1982**, *202*, 9.
- [182] Luz, Z.; Meiboom, S. *J. Am. Chem. Soc.* **1964**, *86*, 4768–4769.
- [183] Li, Y.-N.; Wang, J.-Q.; He, L.-N.; Yang, Z.-Z.; Liu, A.-H.; Yu, B.; Luan, C.-R. *Green Chem.* **2012**, *14*, 2752–2758.
- [184] Amarasekara, A. S.; Williams, L. D.; Ebede, C. C. *Carbohydr. Res.* **2008**, *343*, 3021–3024.
- [185] Nunn, S.; Nishikida, K. *Application Note 01153: Advanced ATR Correction Algorithm, Thermo Electron Corporation, Madison, WI* **2003**.
- [186] Heller, W. *J. Phys. Chem.* **1965**, *69*, 1123–1129.
- [187] Sun, C. C. *J. Pharm. Sci.* **2005**, *94*, 2132–2134.
- [188] Nogi, M.; Handa, K.; Nakagaito, A. N.; Yano, H. *AAppl. Phys. Lett.* **2005**, *87*, 243110–243110.
- [189] Tariq, M.; Forte, P. A.; Gomes, M.; Lopes, J.; Rebelo, L. P. N. *J. Chem. Thermodyn.* **2009**, *41*, 790–798.
- [190] Huddleston, J. G.; Visser, A. E.; Reichert, W. M.; Willauer, H. D.; Broker, G. A.; Rogers, R. D. *Green Chem.* **2001**, *3*, 156–164.
- [191] Jeon, Y.; Sung, J.; Seo, C.; Lim, H.; Cheong, H.; Kang, M.; Moon, B.; Ouchi, Y.; Kim, D. *J. Phys. Chem. B* **2008**, *112*, 4735–4740.
- [192] Nishiyama, Y.; Langan, P.; Chanzy, H. *J. Am. Chem. Soc.* **2002**, *124*, 9074–9082.
- [193] Sundaraganesan, N.; Ilakiamani, S.; Saleem, H.; Wojciechowski, P. M.; Michalska, D. *Spectrochim. Acta, Part A* **2005**, *61*, 2995–3001.

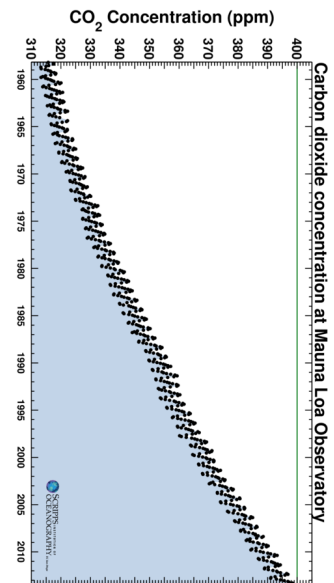
Appendix



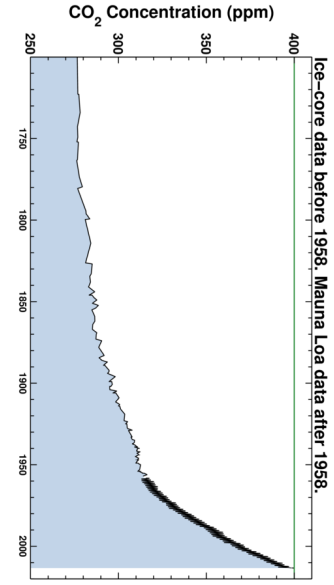
A. Supporting figures introduction



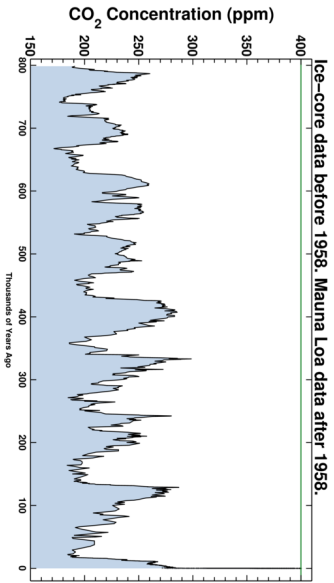
(c) 1 year



(b) Since 1958



(c) 300 years



(d) 0.8 million years

Figure A.1.: CO₂ levels in the atmosphere reported by the Scripps Institution of Oceanography 21th of may 2013. Data before 1958 is obtained from ice-core data [1].

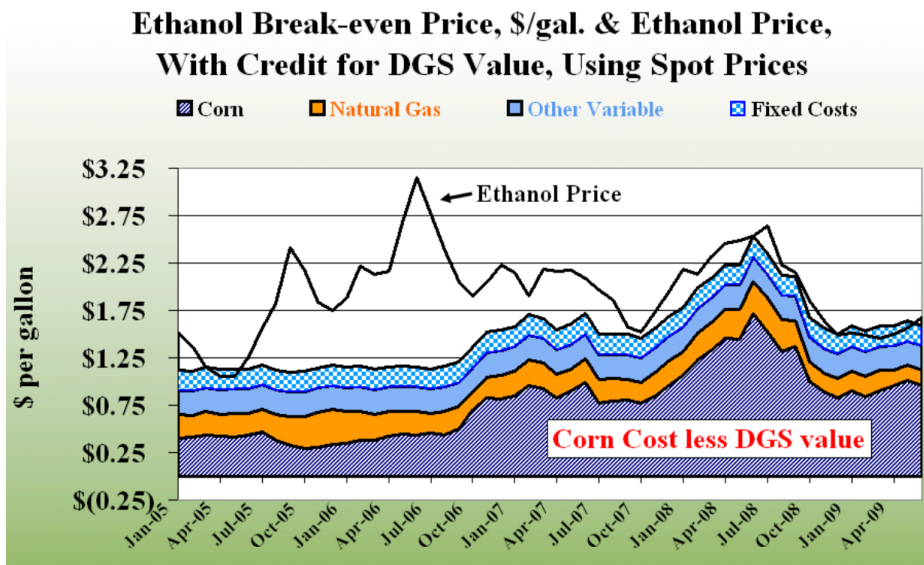
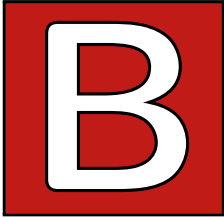


Figure A.2.: Prices of corn and ethanol 2005-2009^[16].

Appendix



Supporting spectral data cellulose hydrolysis

B.4. Calculated spectra of Cellulose related structures

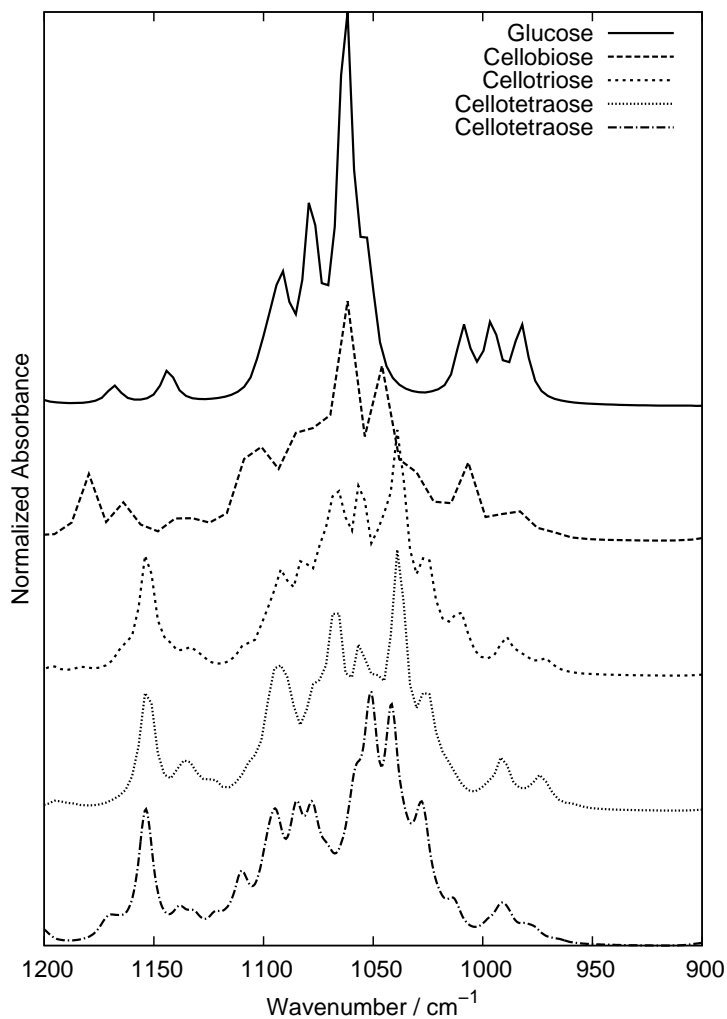


Figure B.1.: Calculated spectra of solid β -D-glucose and cellulose oligomers represented with narrow bandwidth ($\text{FWHM}=4\text{cm}^{-1}$). Intensities are normalized with respect to number of glucose units. Frequencies are scaled with a factor 0.983.

B.5. Experimental spectra of Cellulose related compounds

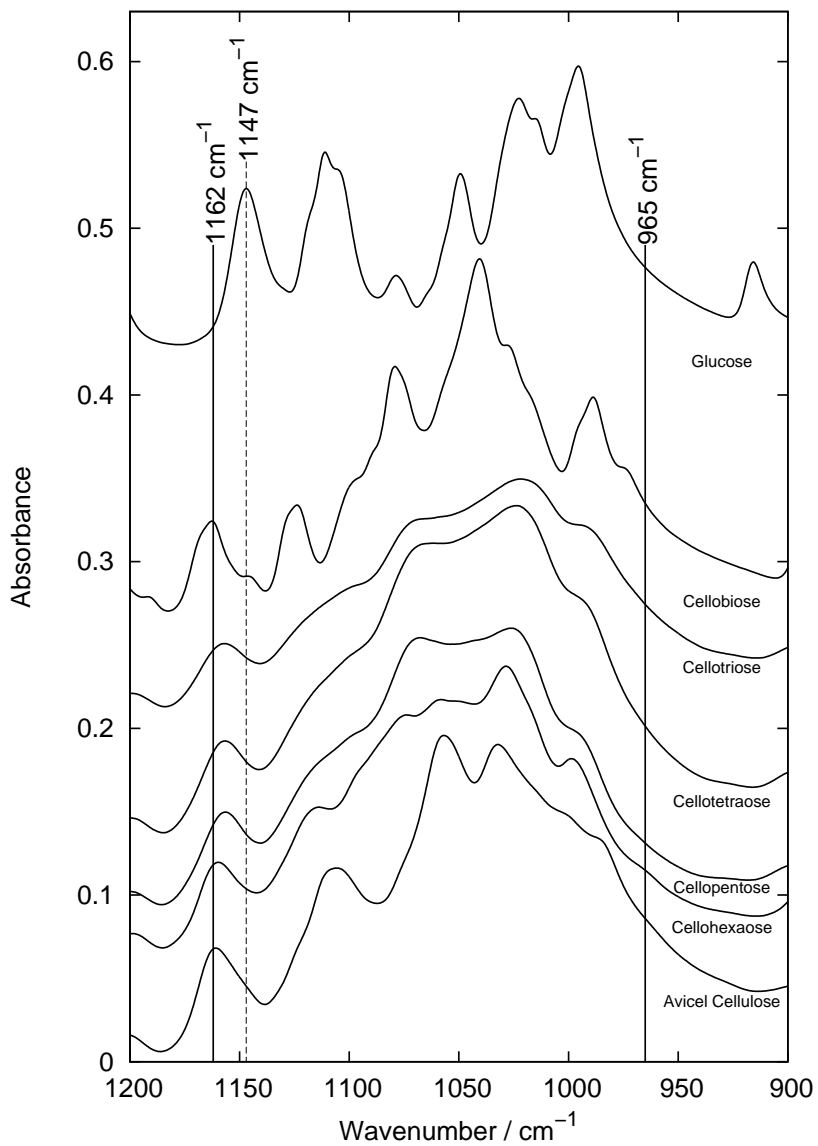


Figure B.2.: Experimental ATR-FTIR spectra of solid glucose, cellulose and cellulose oligomers at room temperature.

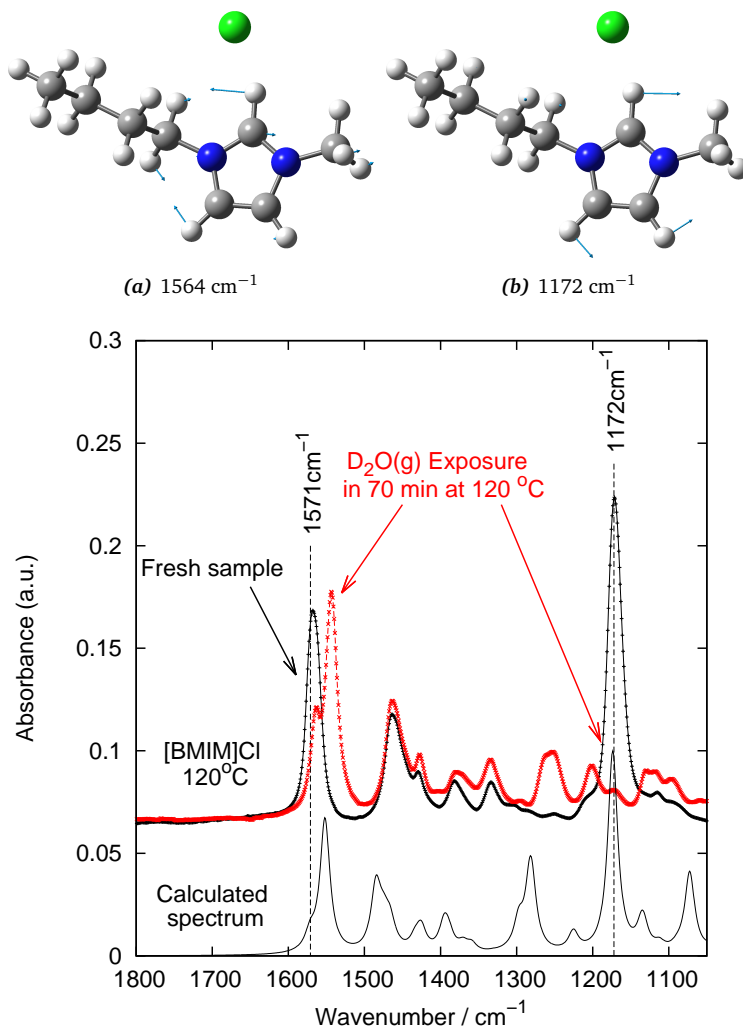
B.6. Elucidation of δ_{C2-H} modes in [BMIM]Cl

Figure B.3.: Calculated (gaussian09, B3LYP/6-311+(d,p), scaled with a factor of 0.983) and experimental ATR-FTIR spectra of [BMIM]Cl. The two vibrational C-H modes shown are equivalent to the two strong bands found in [BMIM]Cl. The black ATR-FTIR spectra in top shows a fresh [BMIM]Cl film in a flow of dry nitrogen at 120 °C. The red spectra shows the same [BMIM]Cl film at 120 °C after 70 minutes exposure to a flow of nitrogen saturated with D₂O. As its known that the C2 proton selectively can be exchanged with deuterium by exposure to D₂O in similar 1,3-alkylimidazolium ionic liquids^[191], the experiments very clearly confirms the result of the DFT calculations: that the bands of 1571 and 1172 cm⁻¹ are indeed caused by beding modes of the C2-H proton. Graphical representation showing the time resolved development can be found at figure B.4 on the next page.

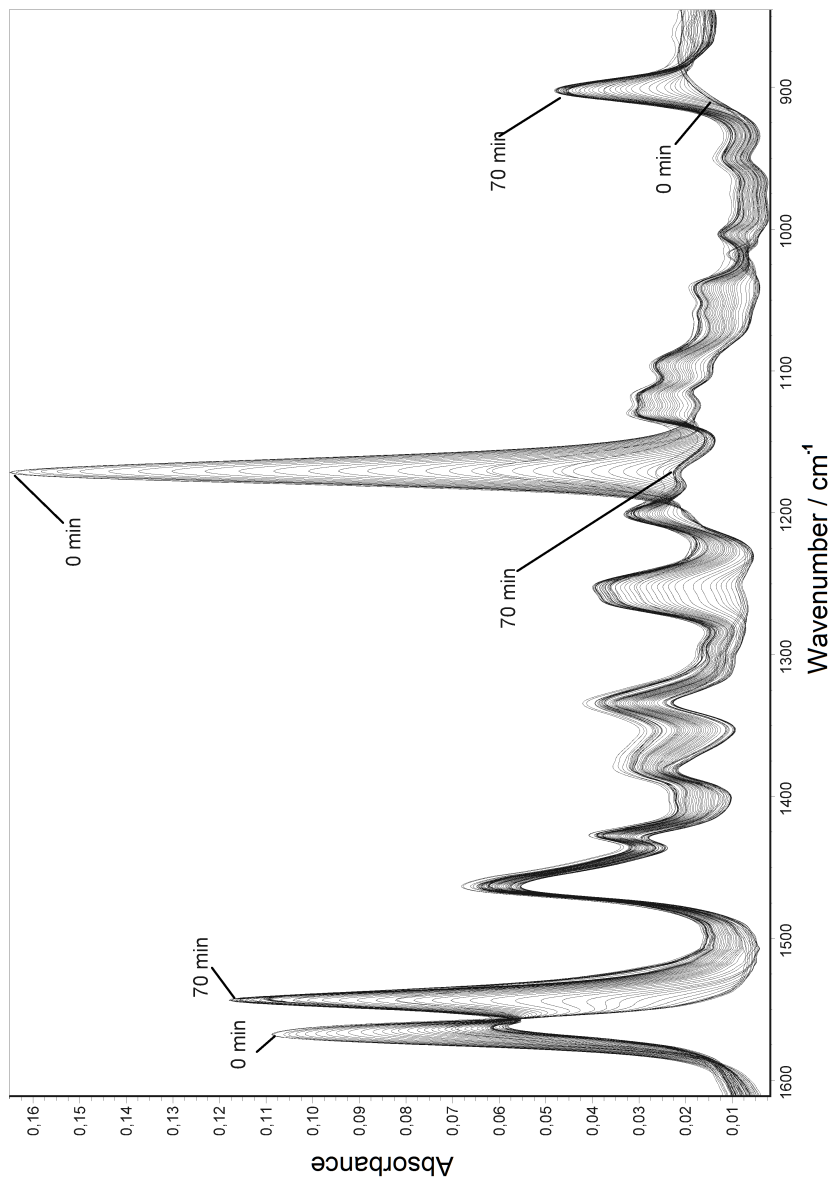


Figure B.4. Time resolved in-situ spectra recorded of a thin film of [BMM]Cl film at 120 °C during exposure to a flow of nitrogen saturated with D₂O. 64 scans were recorded for each spectra, yielding around 105 seconds between each spectra. For interpretation of experiment see figure B.3 on the preceding page.

B.7. Comparison of Experimental and Calculated spectra: Glucose and Cellobiose

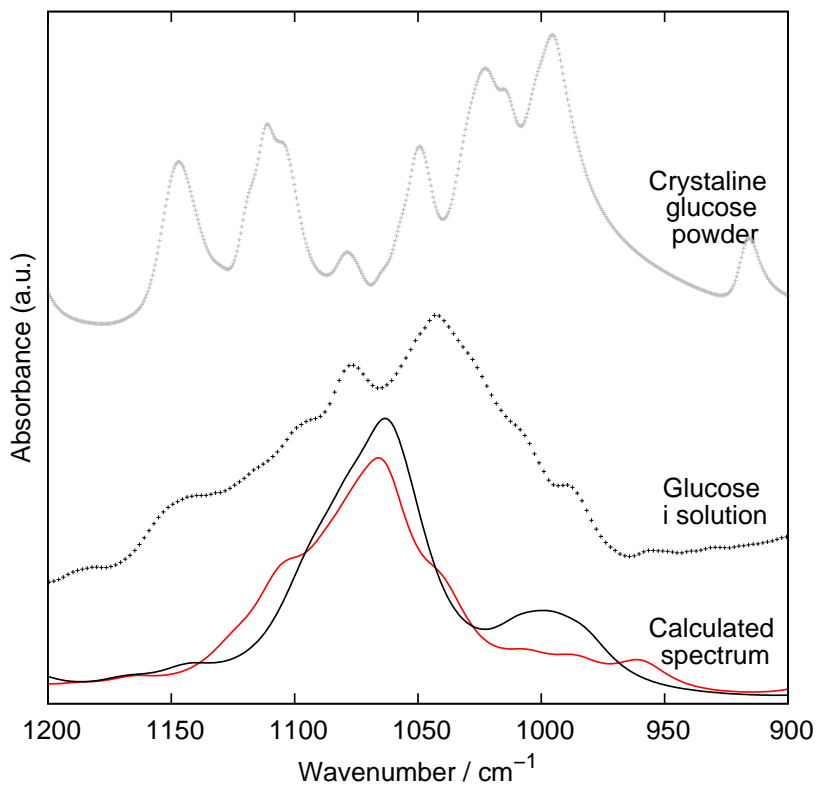


Figure B.5.: Comparison of experimental spectra compared to calculated spectra (red: α black: β forms of glucose). The top is solid glucose powder. In the middle a spectrum of 10 wt.% glucose in ionic liquid 1-butyl-2,3-dimethylimidazolium chloride at 120 °C, from which a spectrum of the pure ionic liquid was subtracted.

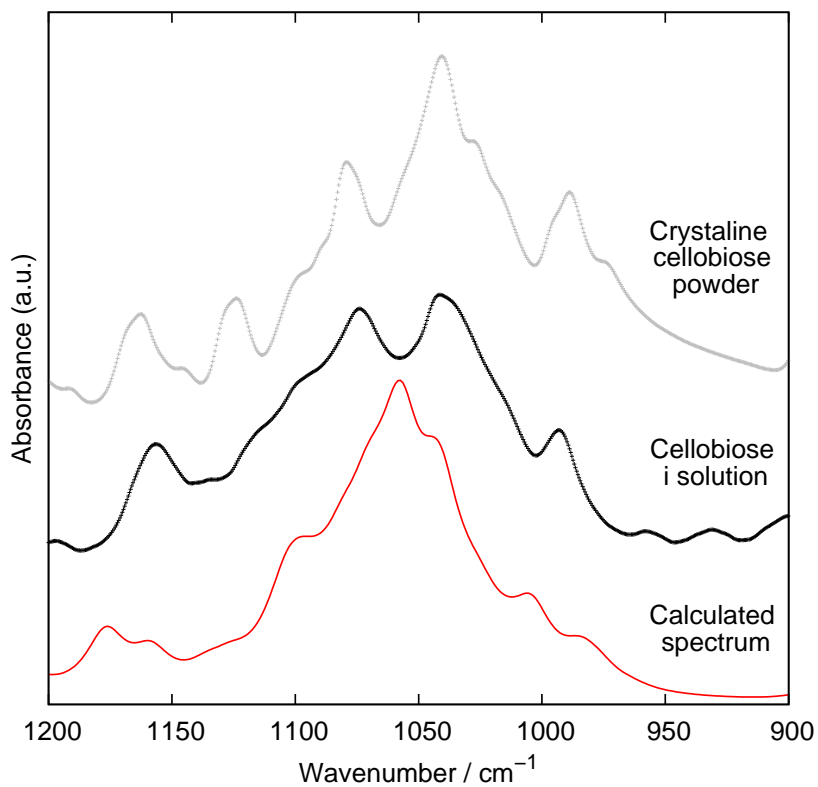


Figure B.6.: Comparison of experimental spectra compared to calculated spectrum. The top is solid cellobiose powder. In the middle a spectrum of 10.5 wt.% cellobiose in ionic liquid 1-butyl-2,3-dimethylimidazolium chloride at 120 °C, from which a spectrum of the pure ionic liquid was subtracted.

B.8. Detailed descriptions of selected vibrational modes

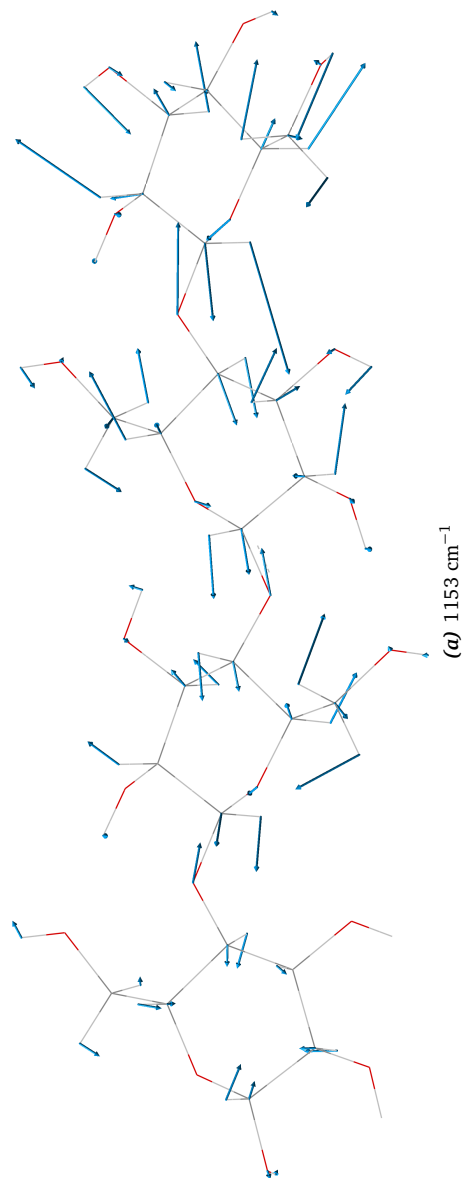


Figure B.7.: Showing graphical descriptions of $\nu_{\text{asym,C-O-C}}$ mode of cellulotetraose, calculated using gaussian09 B3LYP/6-311+G(d,p). Frequencies are scaled with $\alpha_{\text{factor}} 0.983$.

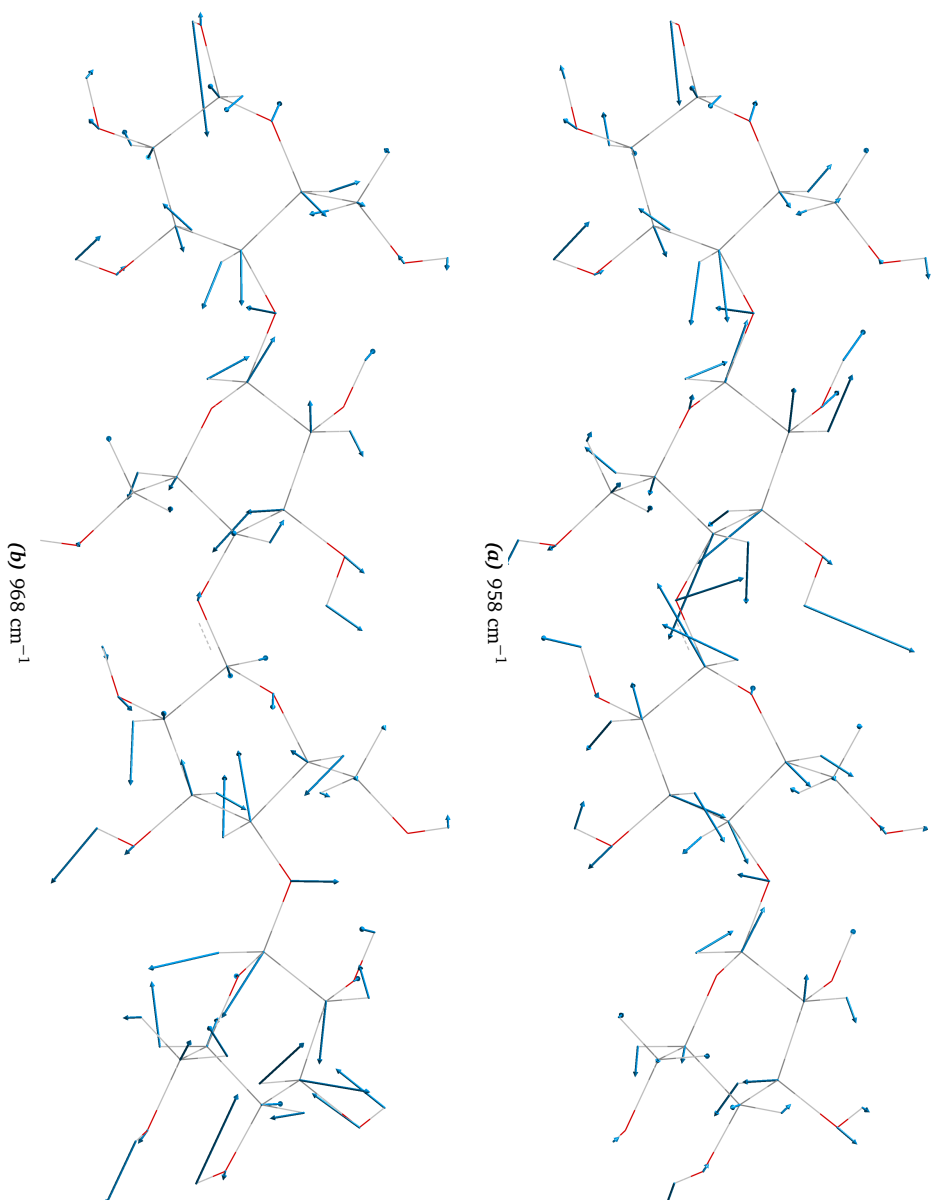
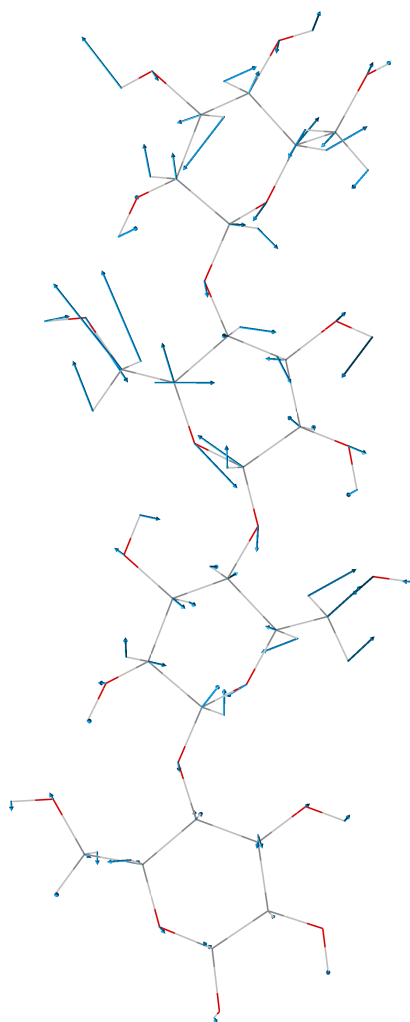


Figure B.8.: Showing graphical descriptions of $\nu_{\text{sym,C-O-C}}$ modes of cellulose, calculated using gaussian09 B3LYP/6-311+G(d,p). Frequencies are scaled with $a_{\text{factor}} 0.983$.



(a) 1039 cm⁻¹

Figure B.9.: Showing graphical descriptions of ν_{O-C-O} mode of the C1-O5 and C6-O6 bond, calculated using gaussian09 B3LYP/6-311+G(d,p). Frequencies are scaled with a factor 0.983.

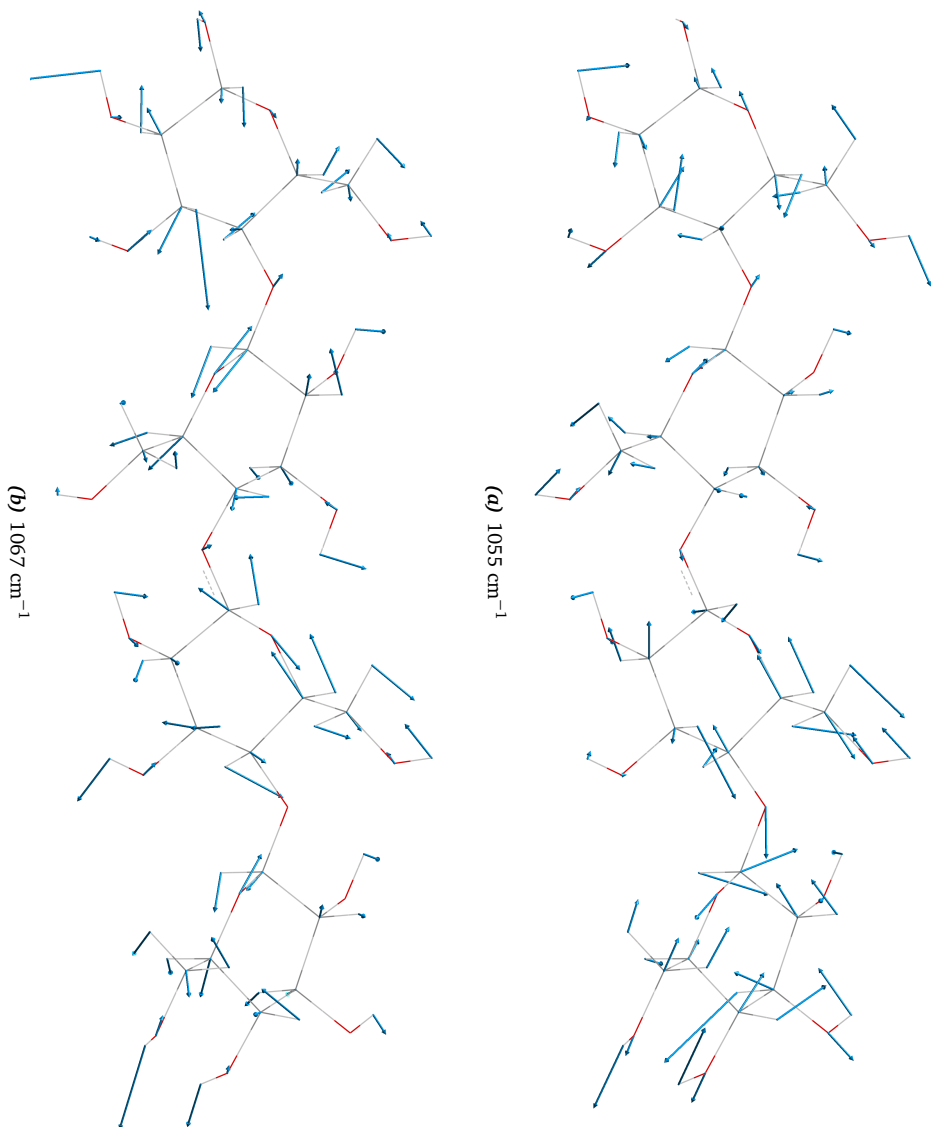


Figure B.10.: Showing graphical descriptions of $\nu_{\text{O}-\text{C}-\text{O}}$ acetal modes of cellulose, calculated using gaussian09 B3LYP/6-311+G(d,p). Frequencies are scaled with a factor 0.983.

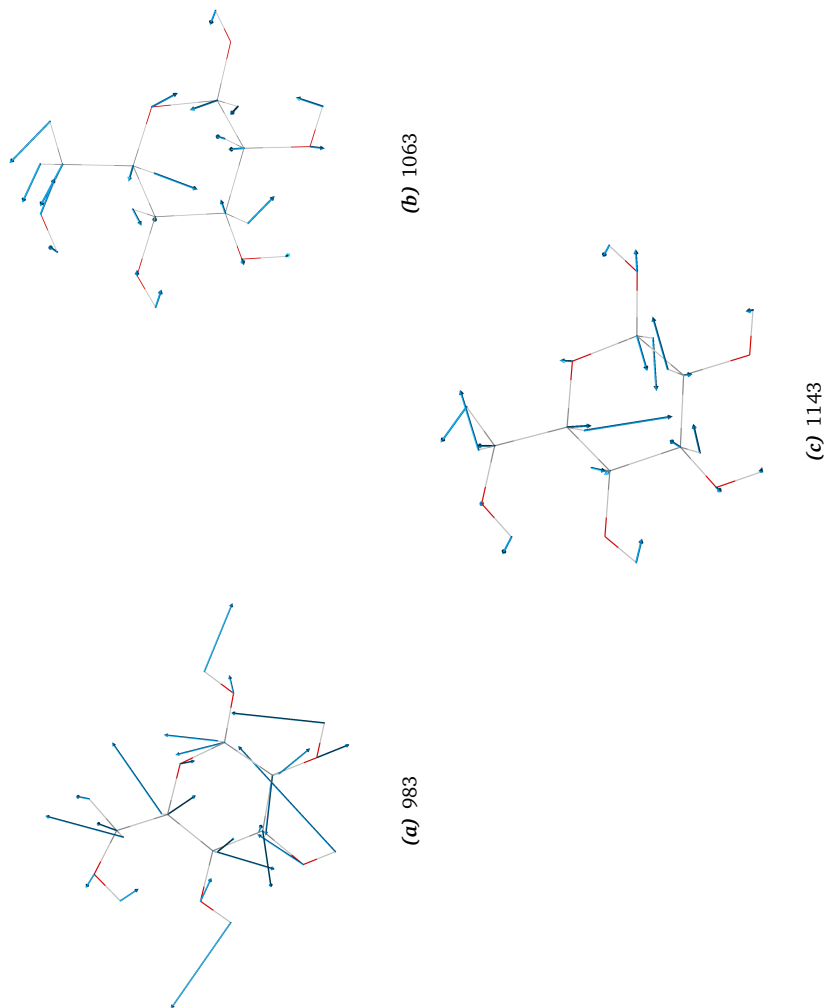


Figure B.11.: Showing graphical descriptions of selected modes of glucose calculated using gaussian09 B3LYP/6-311+G(d,p). (a) and (b) shows the ν_{C-O} mode of glucose and (c) the ν_{O1-H} mode which is closest to the 1152 cm^{-1} $\nu_{\text{asym},C-O-C}$ mode of the cellulose oligomers. Frequencies are scaled with a factor 0.983.

B.9. Spectra of HMF and Levulinic acid

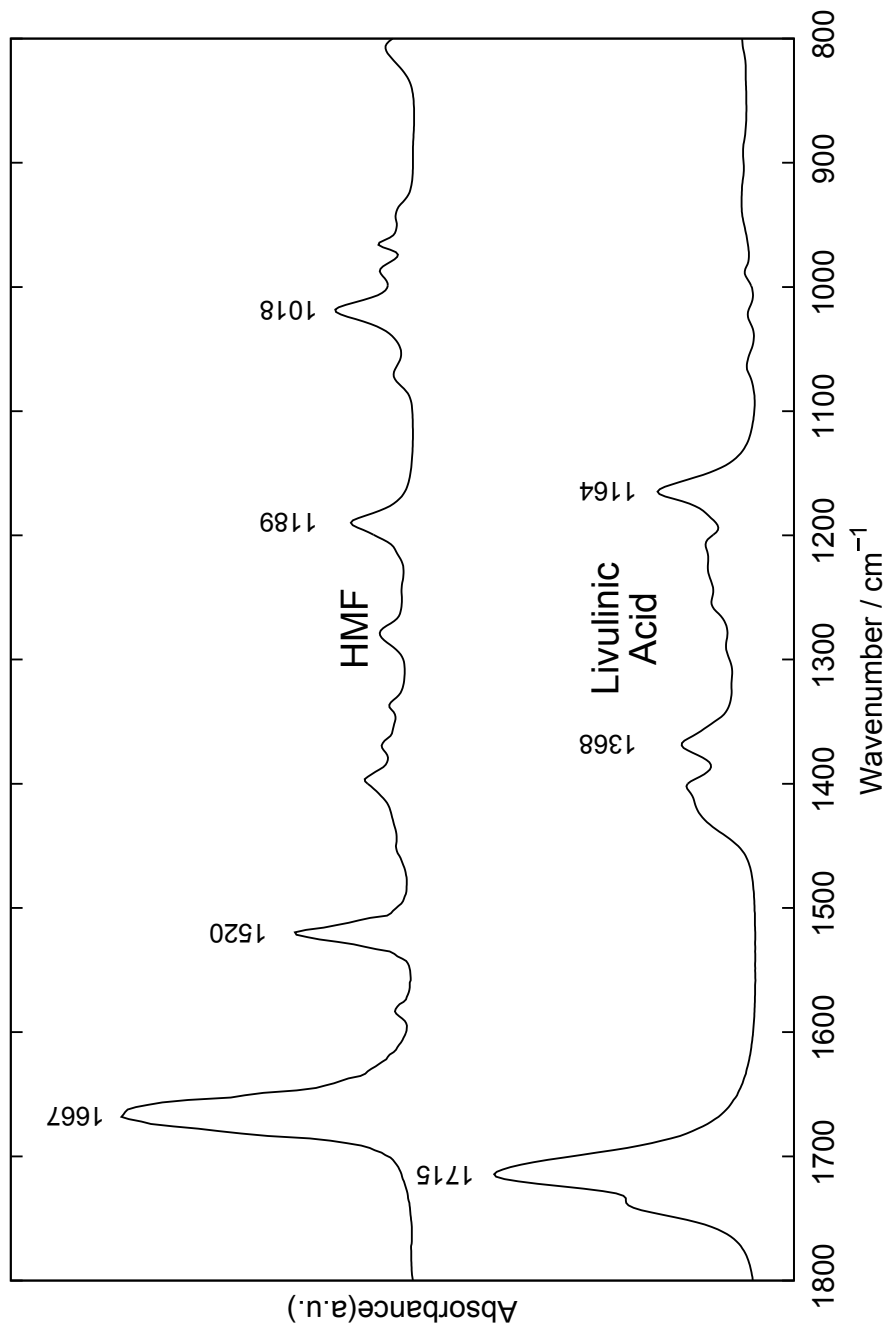


Figure B.12.: Corrected ATR-FTIR spectra of pure liquid 5-(Hydroxymethyl)-2-furfural and livulinic acid at 25 °C. Spectra were ATR corrected using refractive indices of 1.562 and 1.439 respectively.

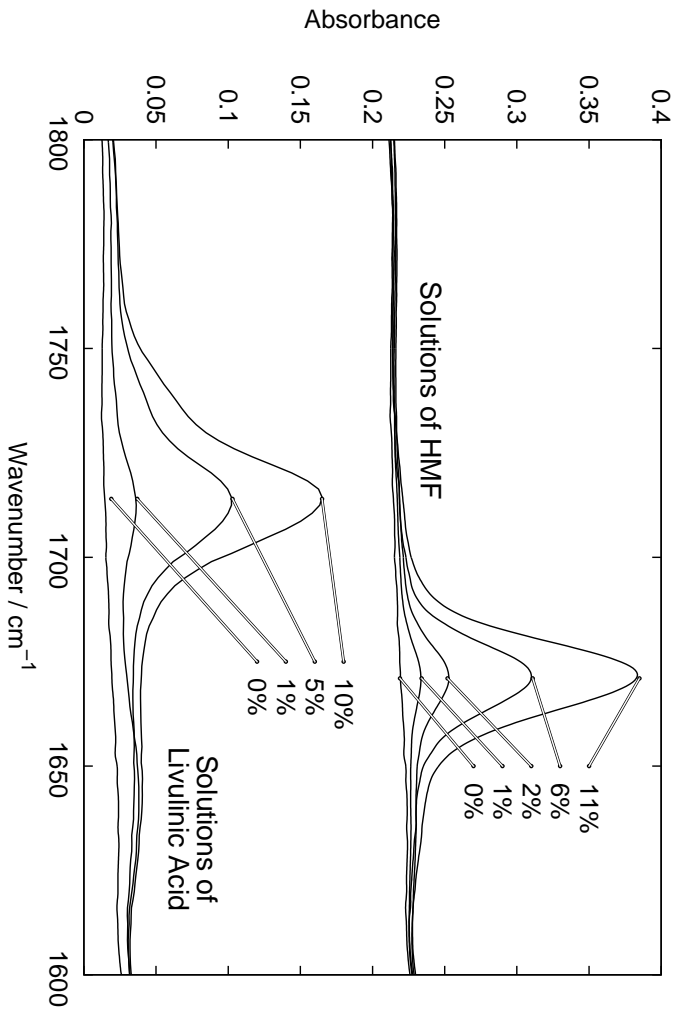


Figure B.13.: Corrected ATR-FTIR spectra showing $\nu_{C=O}$ region of solutions of liquid 5-(Hydroxymethyl)-2-furfural and Ivalinic acid in [BWM][Cl] at 25 °C. All spectra were ATR corrected using refractive index of 1.5.

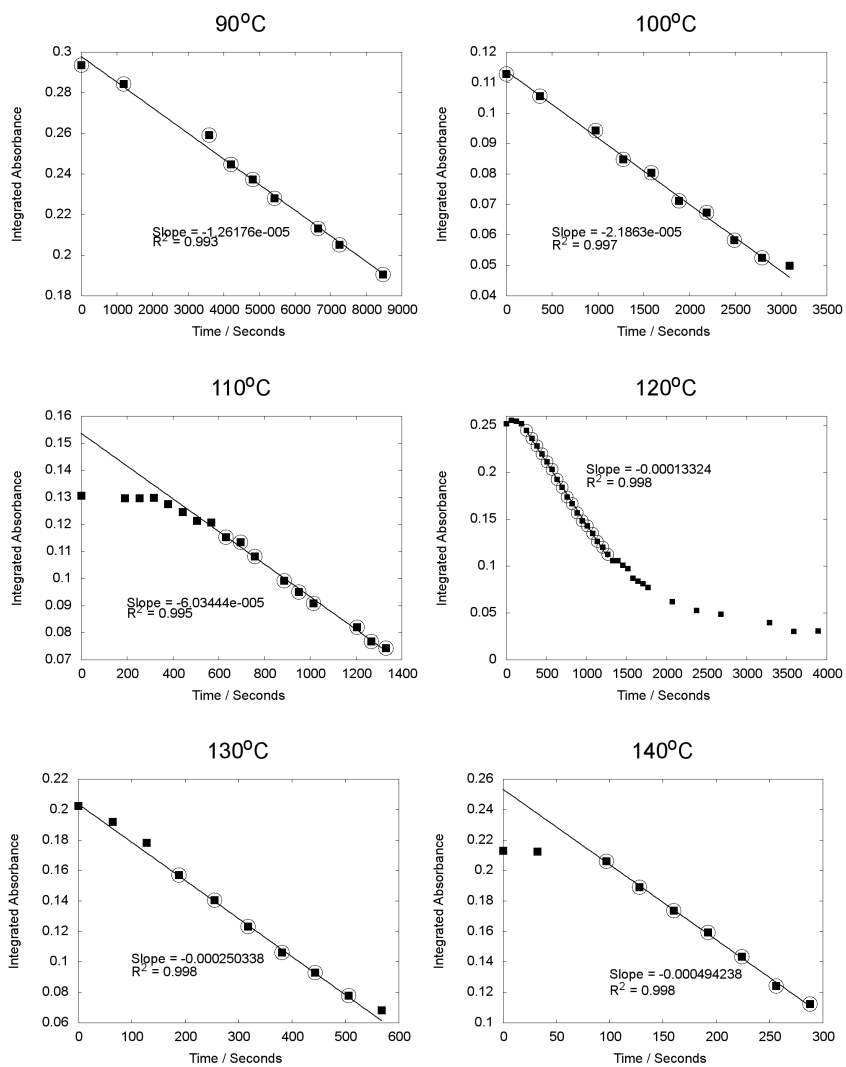
B.10. Rates of H_2SO_4 catalyzed cellulose hydrolysis

Figure B.14.: Rates of cellulose hydrolysis using 10 wt.% cellulose and 1.7 wt.% sulfuric acid in [BD-MIM]Cl.

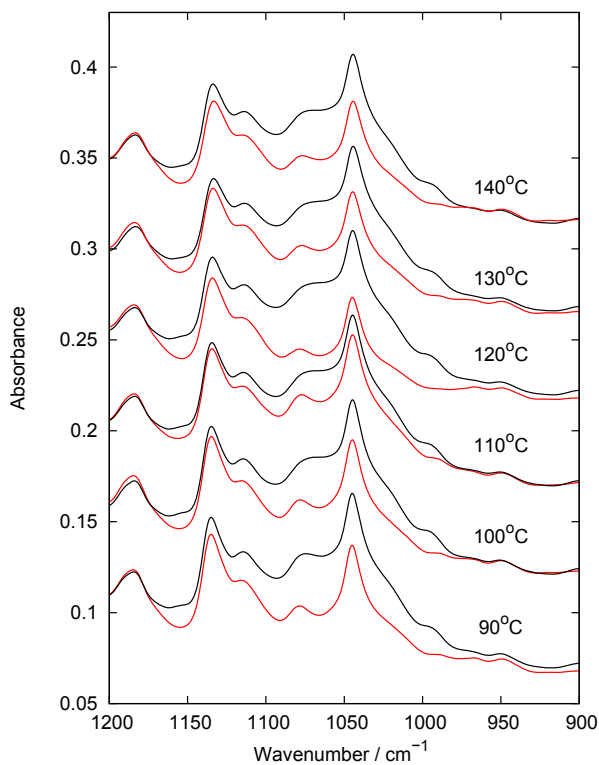


Figure B.15.: Spectra recorded during sulfuric acid catalyzed cellulose hydrolysis: Showing initial spectra compared to pseudo steady state spectra used to produce the difference spectra.

Table B.1.: Initial rates of the intensity decrease of the glucoside bond (1155cm^{-1}) during sulfuric acid catalyzed hydrolysis of cellulose.

Temperature	Rate (Absorbance s^{-1})	Standard deviation (Absorbance $^{-1}$)	Standard deviation (%)
90	-1.26E-05	4.00E-07	3.1
100	-2.18E-05	4.90E-07	2.2
110	-6.03E-05	1.70E-06	2.8
120	-1.37E-04	2.20E-06	1.6
130	-2.50E-04	4.80E-06	1.9
140	-4.94E-04	9.00E-06	1.8

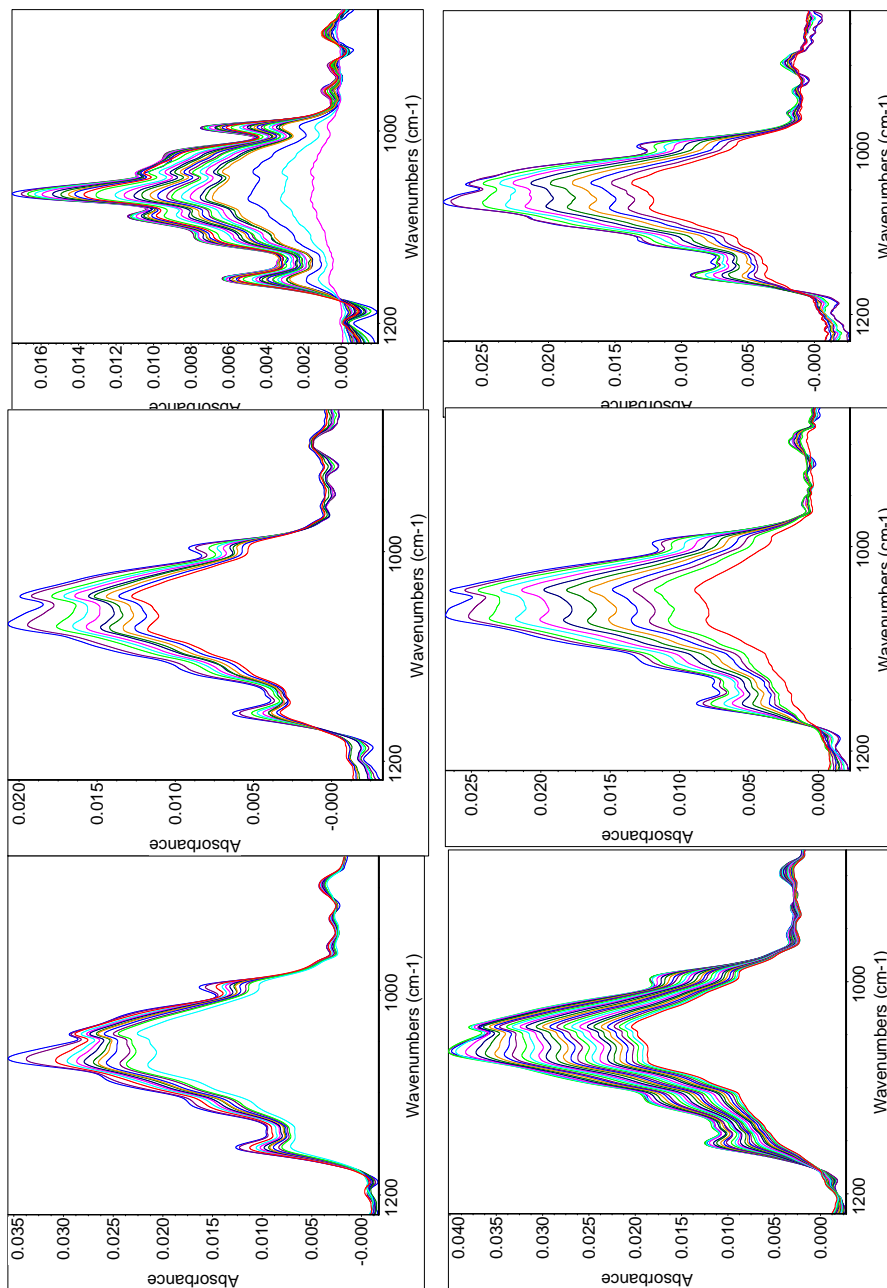


Figure B.16.: Selected difference spectra of cellulose hydrolysis using 10 wt.% sulfuric acid and 1.7 wt.% stifturic acid in [BDMM]Cl.

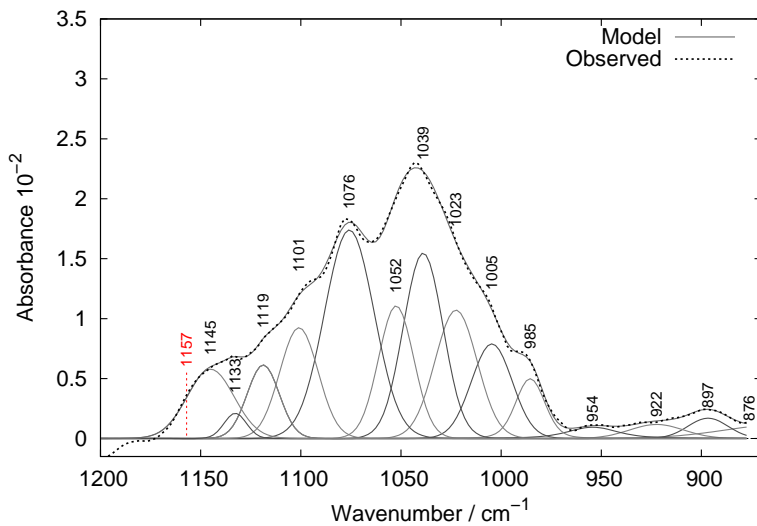


Figure B.17.: Corrected ATR-FTIR difference spectrum of 10 wt.% glucose corresponding to initial time minus spectrum after 45 minutes of reaction at 120 °C with sample containing 1.7 wt.% sulfuric acid. The spectrum were deconvoluted with voigt functions.

B.11. Rates of H₂SO₄ catalyzed cellobiose hydrolysis

Table B.2.: Initial rates of the intensity decrease of the glucoside bond(1155cm⁻¹) during sulfuric acid catalyzed hydrolysis of cellobiose.

Temperature	Rate (Absorbance s ⁻¹)	Standard deviation (Absorbance s ⁻¹)	Standard deviation (%)
90	-3.08E-05	6.43E-07	2.1
100	-6.76E-05	1.21E-06	1.8
110	-1.09E-04	4.87E-06	4.5
120	-1.87E-04	3.22E-06	1.7
130	-2.84E-04	9.71E-06	3.4
140	-4.94E-04	9.00E-06	1.8

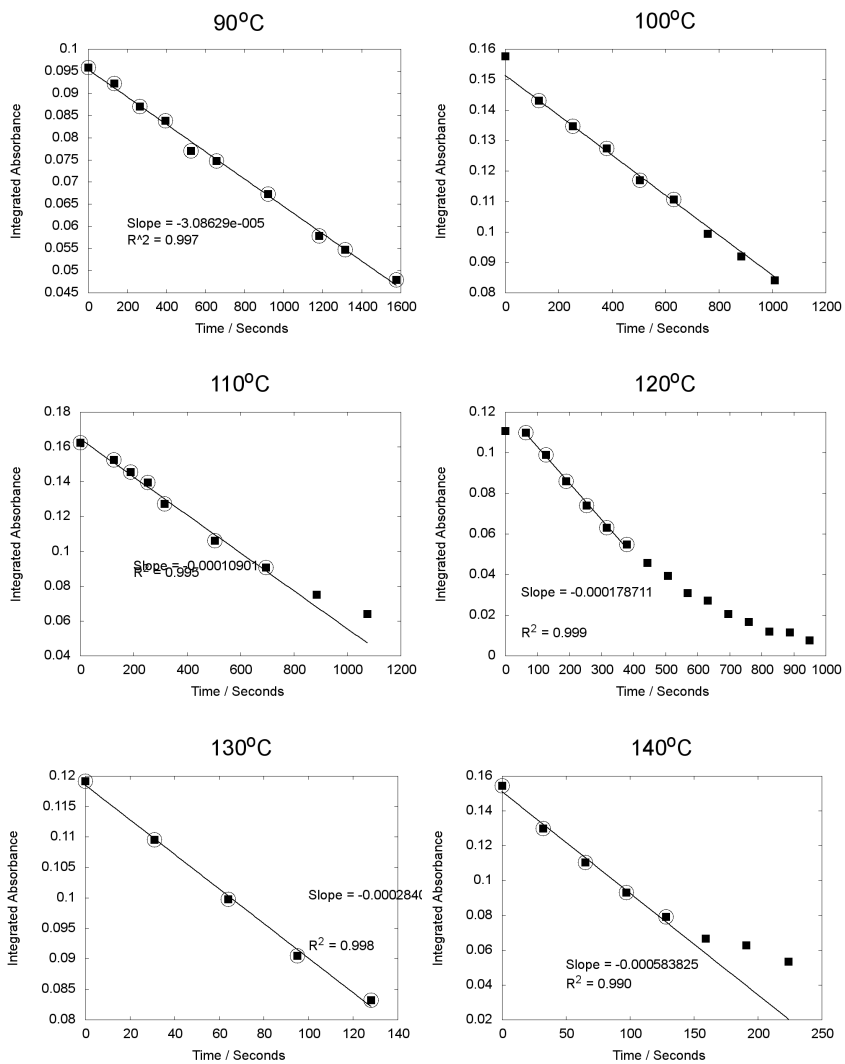


Figure B.18.: Rates of cellobiose hydrolysis using 10.5 wt.% cellobiose and 1.7 wt.% sulfuric acid in [BDMIM]Cl.

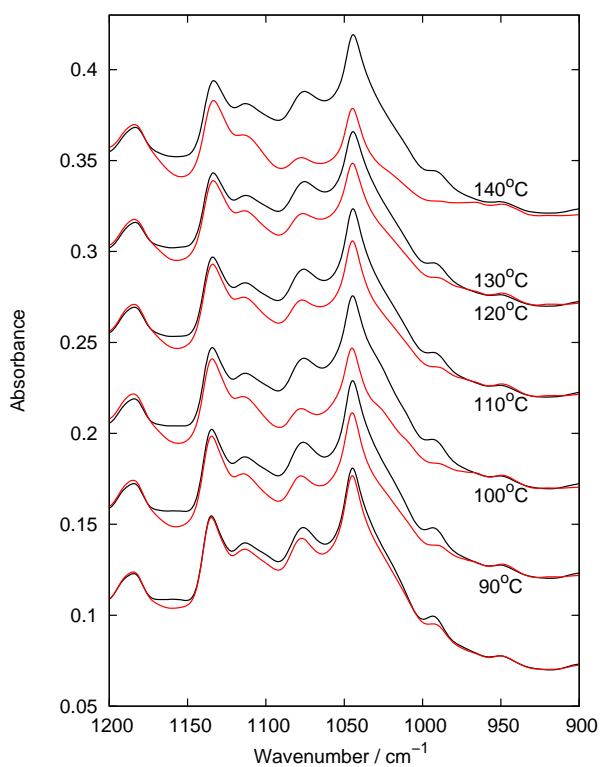


Figure B.19.: Spectra recorded during sulfuric acid catalyzed cellobiose hydrolysis: Showing initial spectra compared to pseudo steady state spectra used to produce the difference spectra.

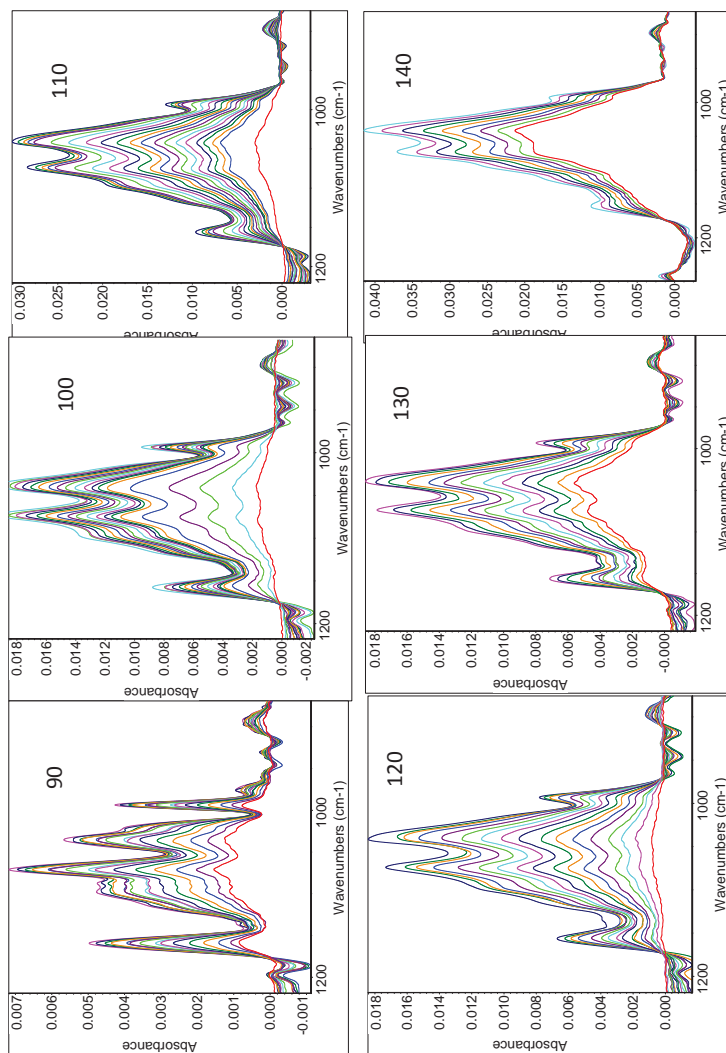


Figure B.20.: Selected difference spectra of cellobiose hydrolysis using 10.5 wt.% cellobiose and 1.7 wt.% sulfuric acid in [BDMM]Cl.

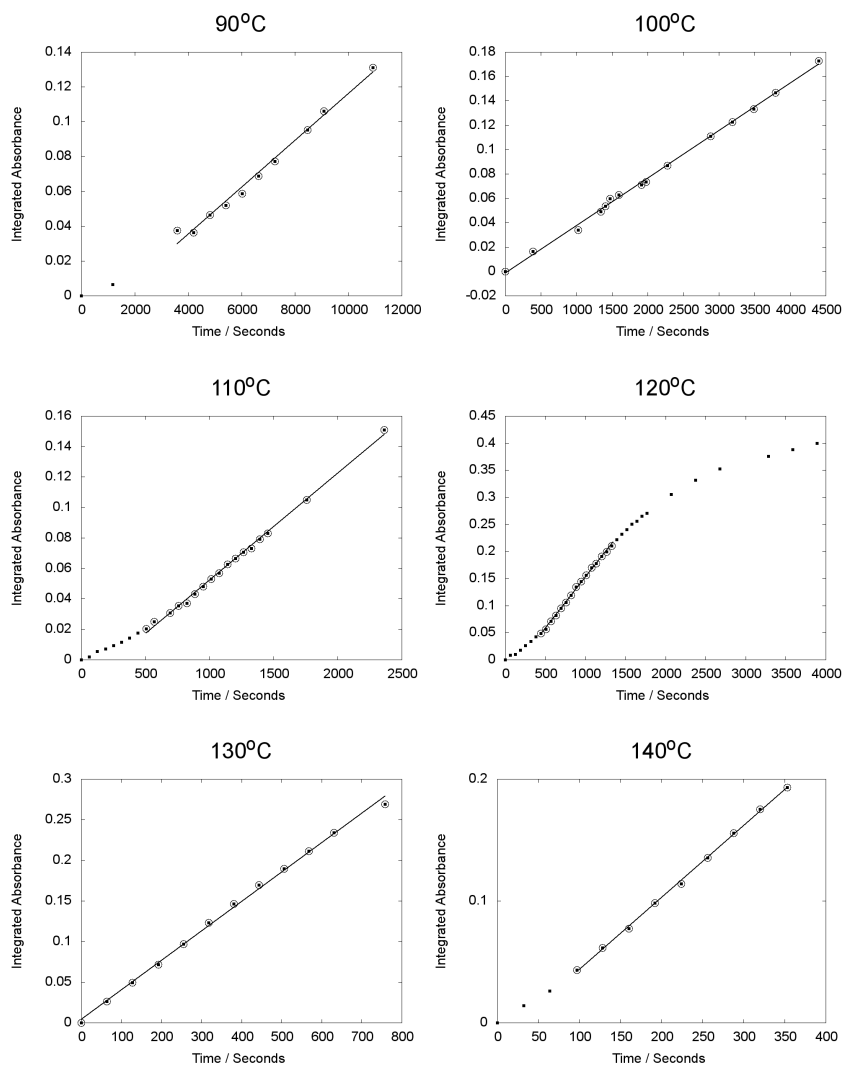
B.12. Rates of HMF formation during H_2SO_4 catalyzed cellulose hydrolysis

Figure B.21.: Rates of HMF formation during cellulose hydrolysis using 10 wt.% cellulose and 1.7 wt.% sulfuric acid in [BDMIM]Cl.

Table B.3.: Rates of HMF formation during sulfuric acid catalyzed hydrolysis of cellulose. Rates are given in integrated absorbance s^{-1} .

Temperature	rate	absolute std. error	rel. std. error
90°C	$3.84 \cdot 10^{-5}$	$\pm 1.44 \cdot 10^{-6}$	$\pm 3.76\%$
100°C	$9.01 \cdot 10^{-5}$	$\pm 3.24 \cdot 10^{-6}$	$\pm 3.61\%$
110°C	$1.73 \cdot 10^{-4}$	$\pm 4.89 \cdot 10^{-6}$	$\pm 2.82\%$
120°C	$3.53 \cdot 10^{-4}$	$\pm 5.18 \cdot 10^{-6}$	$\pm 1.47\%$
130°C	$6.29 \cdot 10^{-4}$	$\pm 8.17 \cdot 10^{-6}$	$\pm 1.30\%$
140°C	$1.23 \cdot 10^{-3}$	$\pm 4.02 \cdot 10^{-5}$	$\pm 3.27\%$

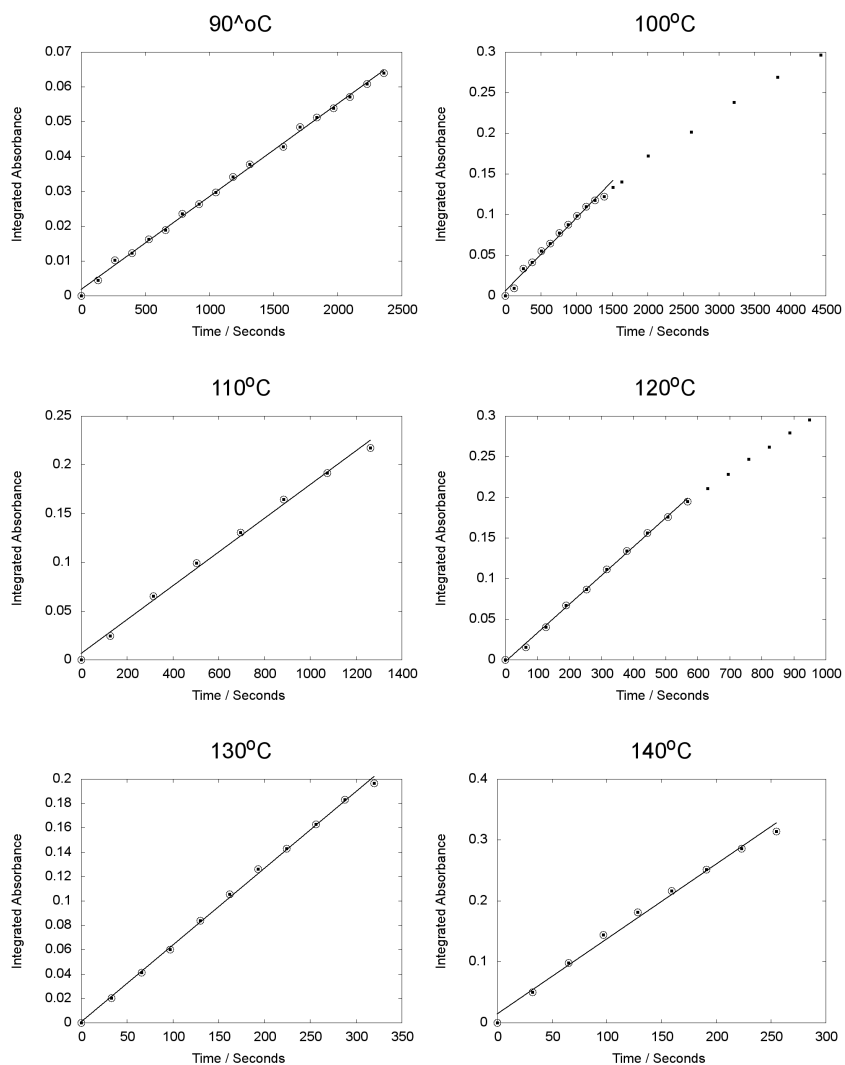
B.13. Rates of HMF formation during H_2SO_4 catalyzed cellobiose hydrolysis

Figure B.22.: Rates of HMF formation during cellobiose hydrolysis using 10.5 wt.% cellobiose and 1.7 wt.% sulfuric acid in [BDMIM]Cl.

Table B.4.: Rates of HMF formation during sulfuric acid catalyzed hydrolysis of cellobiose. Rates are given in integrated absorbance s^{-1} .

Temperature	rate	absolute std. error	rel. std. error
90°C	$1.35 \cdot 10^{-5}$	$\pm 5.13 \cdot 10^{-7}$	$\pm 3.80\%$
100°C	$3.90 \cdot 10^{-5}$	$\pm 4.99 \cdot 10^{-7}$	$\pm 1.28\%$
110°C	$7.02 \cdot 10^{-5}$	$\pm 9.04 \cdot 10^{-7}$	$\pm 1.29\%$
120°C	$1.80 \cdot 10^{-4}$	$\pm 3.03 \cdot 10^{-6}$	$\pm 1.69\%$
130°C	$3.62 \cdot 10^{-4}$	$\pm 5.40 \cdot 10^{-6}$	$\pm 1.49\%$
140°C	$5.91 \cdot 10^{-4}$	$\pm 6.76 \cdot 10^{-6}$	$\pm 1.14\%$

B.14. Theoretical structures during cellobiose hydrolysis

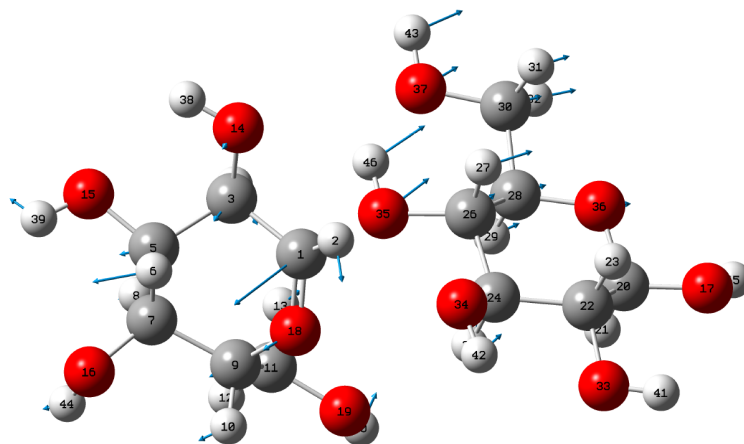


Figure B.23.: Showing the imaginary frequency of the critical transition state of cellulose hydrolysis,

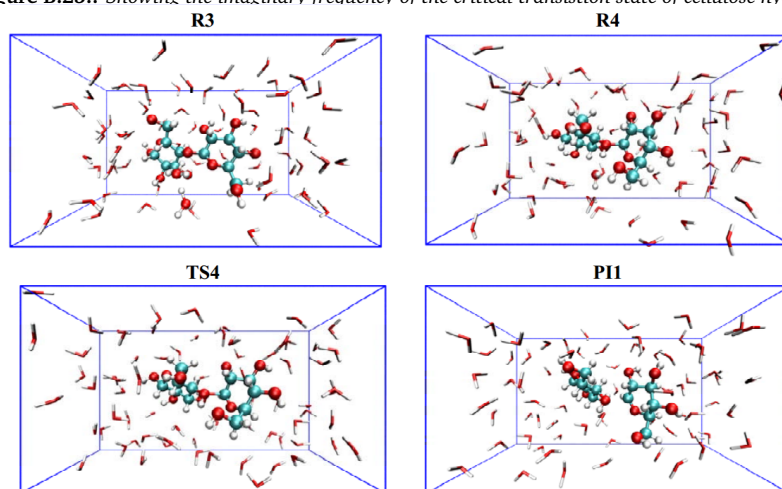


Figure B.24.: Showing some intermediates and the critical transition state during cellobiose hydrolysis in water of adapted from Liang et al. Notice the twisting of the pyranose rings from R3 to R4^[72].

B.15. Post reaction HPLC Analysis

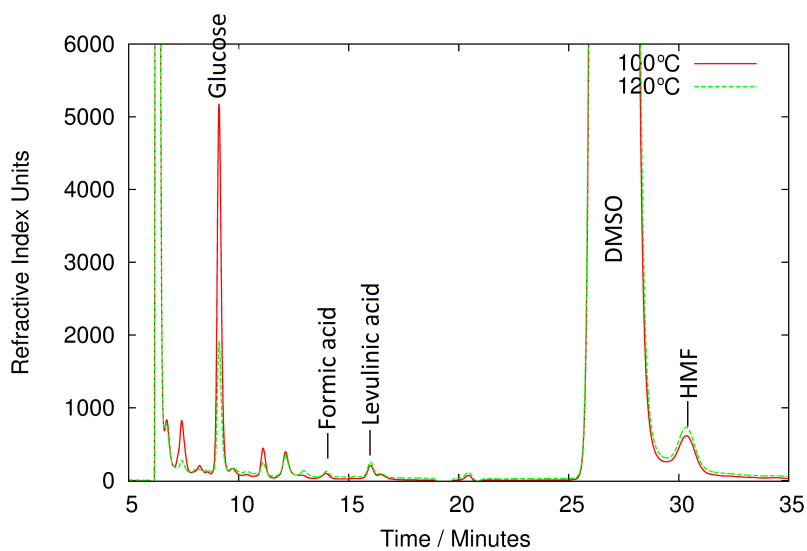


Figure B.25.: High-Performance Liquid Chromatography of samples after hydrolysis of cellulose in micro reactor at 100 and 120 °C, respectively. Sample composition: 10 wt.% cellulose, 1 equivalent of water and 1.7 wt.% H_2SO_4 in $[BDMIM]Cl$ in 0.7 mL d_6 -DMSO.

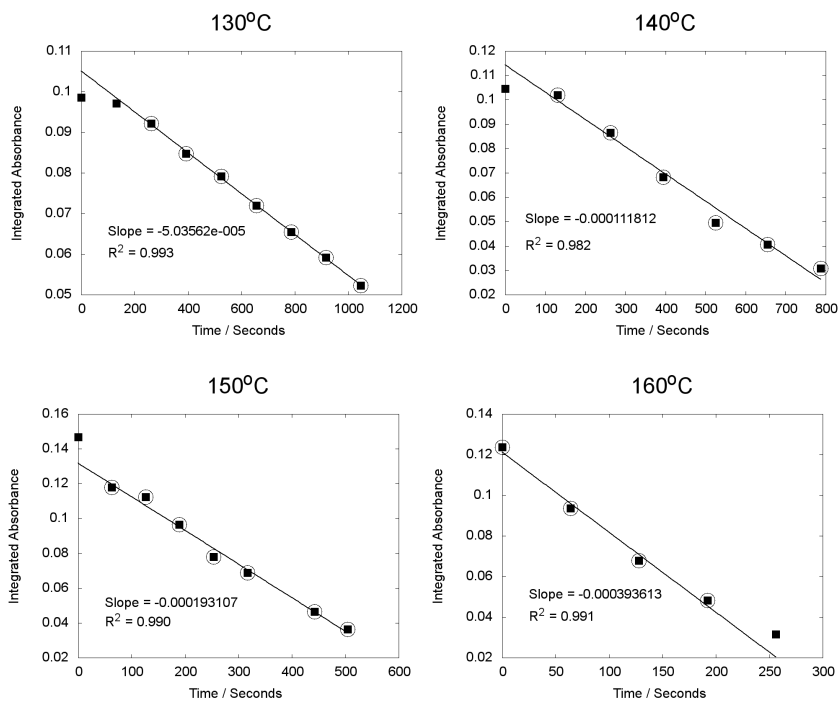
B.16. Rates of $\text{SO}_4^{2-}/\text{TiO}_2$ catalyzed cellulose hydrolysis

Figure B.26.: Rates of cellulose hydrolysis using 8wt.% cellulose and 20 wt.% sulfated anatase in $[\text{BDMIM}]\text{Cl}$.

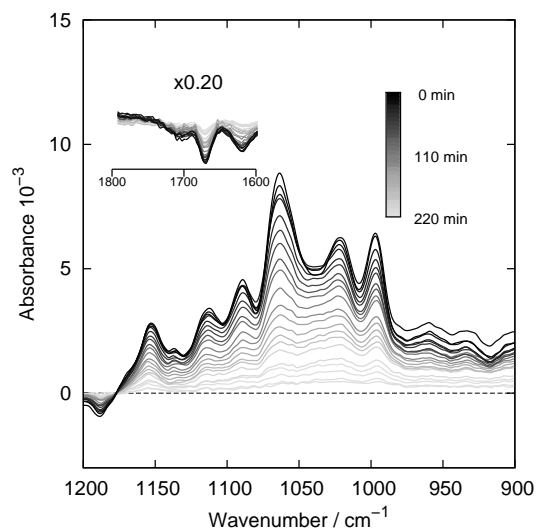
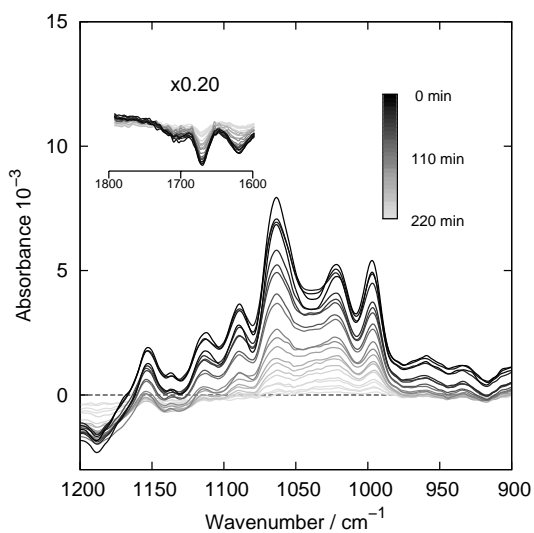
B.17. Correction of difference spectra from $\text{SO}_3\text{H-SBA15}$ catalyzed hydrolysis(a) Corrected via isospectic point at 1177cm^{-1} (b) Corrected via zero absorbance at 4000cm^{-1}

Figure B.27.: Hydrolysis of cellulose in $[\text{BDMIM}]\text{Cl}$ at 120°C using the $\text{SO}_3\text{H-SBA15}$ catalyst. Top shows correction via assuming an isospectic point at $(x,y)=(1177,0)$ and bottom the normal correction assuming zero absorbance at 4000cm^{-1} .

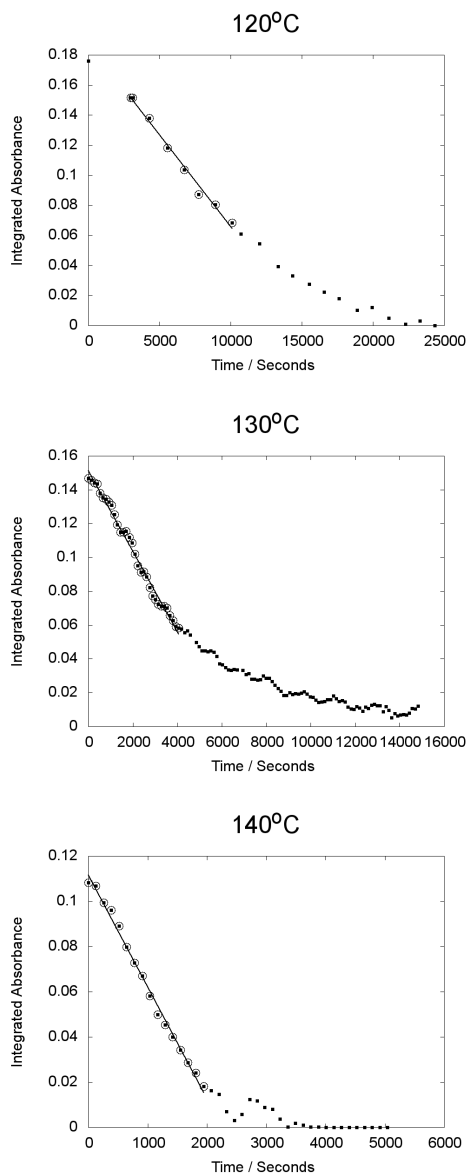
B.18. Rates of Cr^{3+} catalyzed cellulose hydrolysis

Figure B.28.: Rates of cellulose hydrolysis using 10 wt.% cellulose and $[\text{CrCl}_3]\cdot\text{H}_2\text{O}$

Table B.5.: Rates of CrCl_3 catalyzed hydrolysis of cellulose. Rates are given in Integrated Absorbance s^{-1} .

Temperature	rate	absolute std. error	rel. std. error
120°C	$-1.22271 \cdot 10^{-5}$	$\pm 4.7 \cdot 10^{-7}$	$\pm 3.90\%$
130°C	$-2.37545 \cdot 10^{-5}$	$\pm 4.4 \cdot 10^{-7}$	$\pm 1.90\%$
140°C	$-4.94608 \cdot 10^{-5}$	$\pm 9.7 \cdot 10^{-7}$	$\pm 2.00\%$

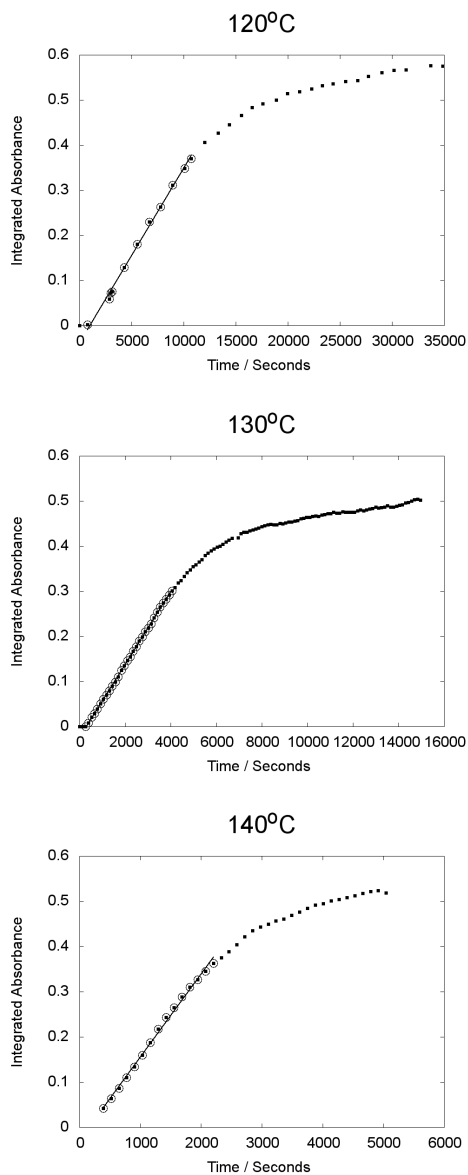
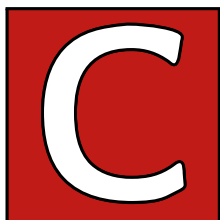
B.19. Rates of HMF formation during Cr^{3+} catalyzed cellulose hydrolysis

Figure B.29.: Rates of HMF formation during cellulose hydrolysis using 10 wt.% cellulose and $[\text{CrCl}_3]\cdot\text{H}_2\text{O}$.

Table B.6.: Rates of HMF formation during CrCl_3 catalyzed hydrolysis of cellulose. Rates are given in Integrated Absorbance s^{-1} .

Temperature	rate	absolute std. error	rel. std. error
120°C	$3.8750 \cdot 10^{-5}$	$\pm 0.76 \cdot 10^{-7}$	$\pm 1.70\%$
130°C	$8.0679 \cdot 10^{-5}$	$\pm 3.16 \cdot 10^{-7}$	$\pm 0.39\%$
140°C	$18.358 \cdot 10^{-5}$	$\pm 3.22 \cdot 10^{-7}$	$\pm 1.75\%$



Supporting data for chromium catalyzed conversions

C.20. HMF standard curve

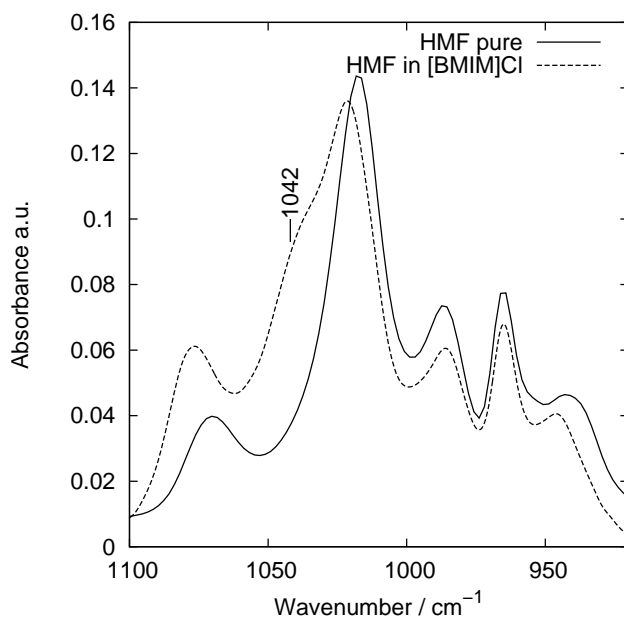


Figure C.1.: Spectra of pure HMF and difference spectra showing HMF in solution of [BMIM]Cl.

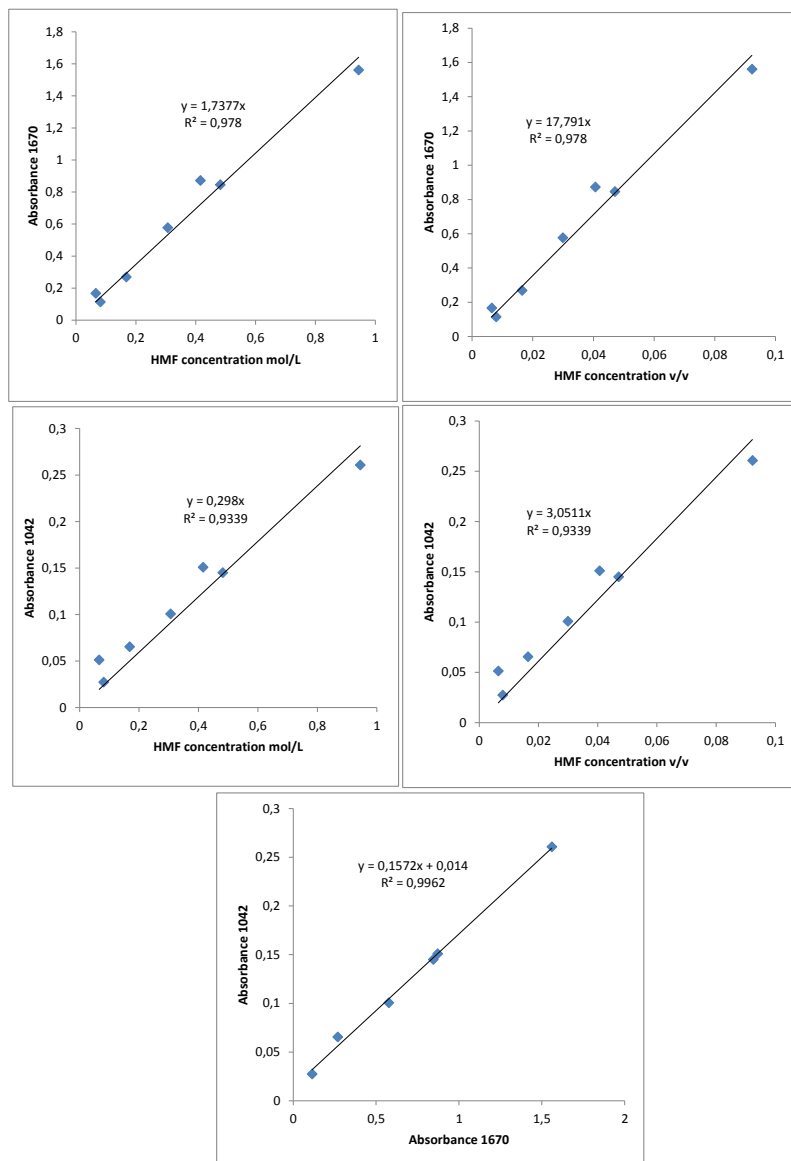


Figure C.2.: Standard curves for HMF in [BMIM]Cl. Showing relation between concentrations of HMF and integrated absorbance of 1670 and 1042 cm⁻¹ bands, and relation between the 1670 and 1042 cm⁻¹ bands.

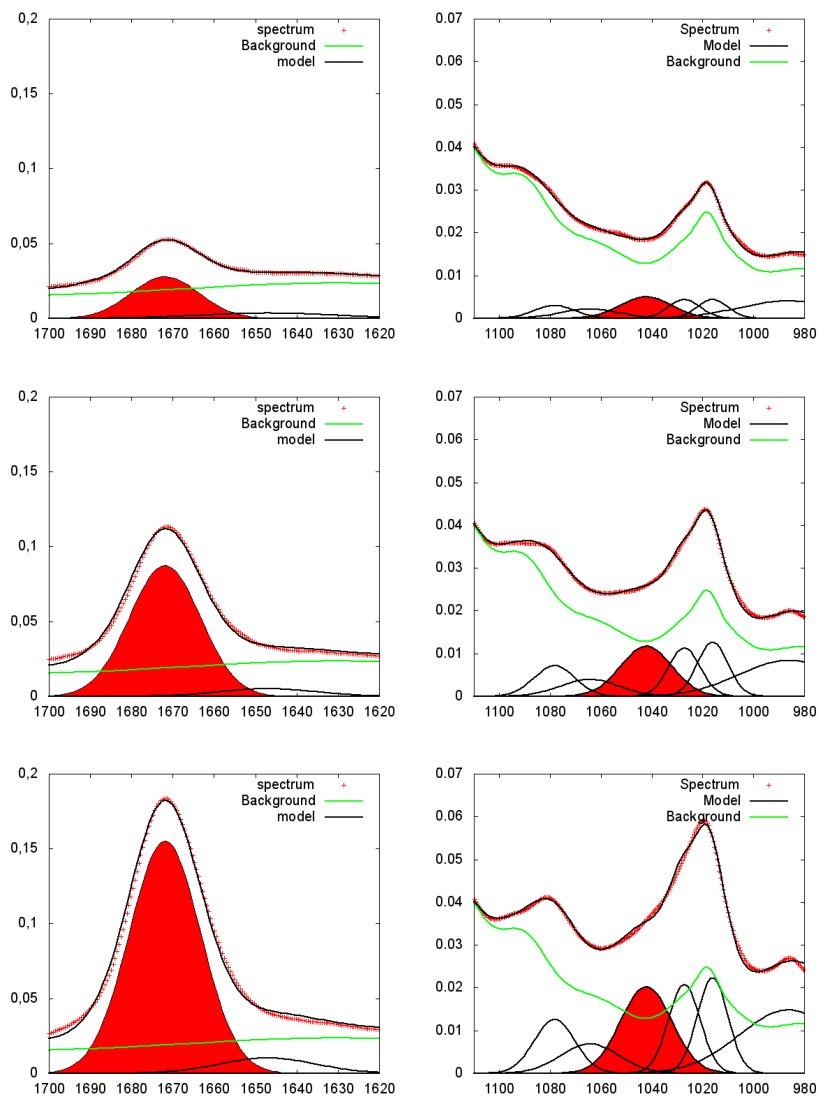


Figure C.3.: selected deconvolutions from standard curve: 11.1, 6.0 and 2.0 wt.% HMF in [BMIM]Cl.

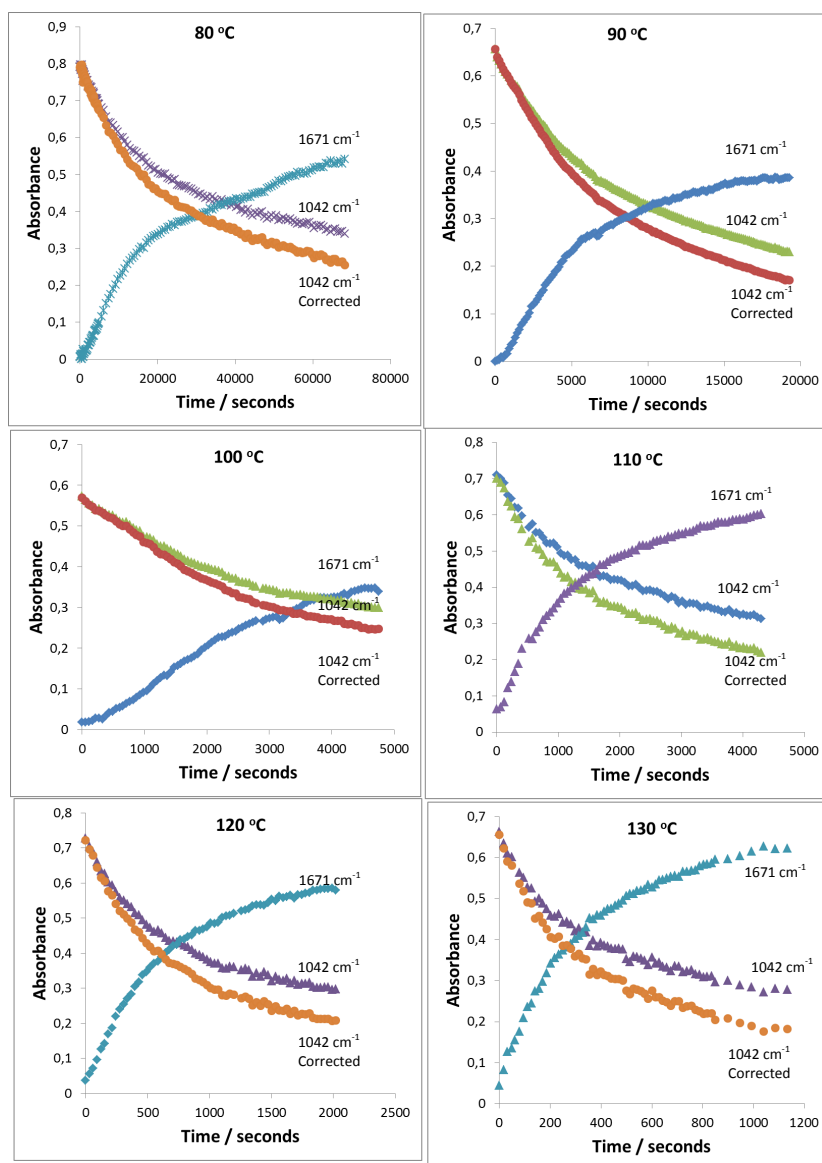
C.21. Glucose Conversion in Microreactor in Presence of $\text{CrCl}_3 \cdot 6\text{H}_2\text{O}$ 

Figure C.4.: Development of intensities of 1670 and 1042 cm^{-1} bands during conversion of glucose with $\text{CrCl}_3 \cdot 6\text{H}_2\text{O}$. The corrected absorbance of the 1042 cm^{-1} band is also shown where the contribution from HMF absorption at 1042 cm^{-1} is subtracted, according to relationship shown in figure C.2 on page 150.

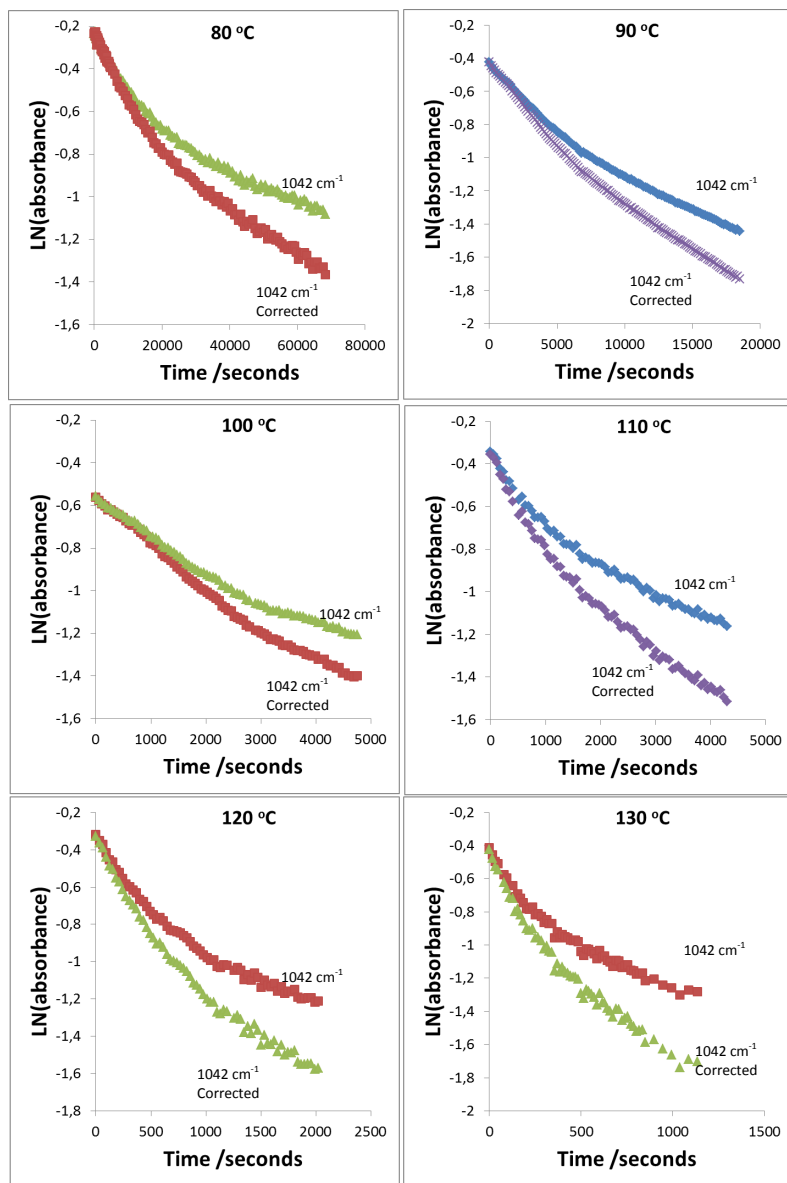


Figure C.5.: Logarithm to the area of the 1042 cm⁻¹ bands during conversion of glucose with CrCl₃·6H₂O. The corrected absorbance of the 1042 cm⁻¹ band is also shown where the contribution from HMF absorption at 1042 cm⁻¹ is subtracted, according to relationship shown in figure C.2 on page 150.

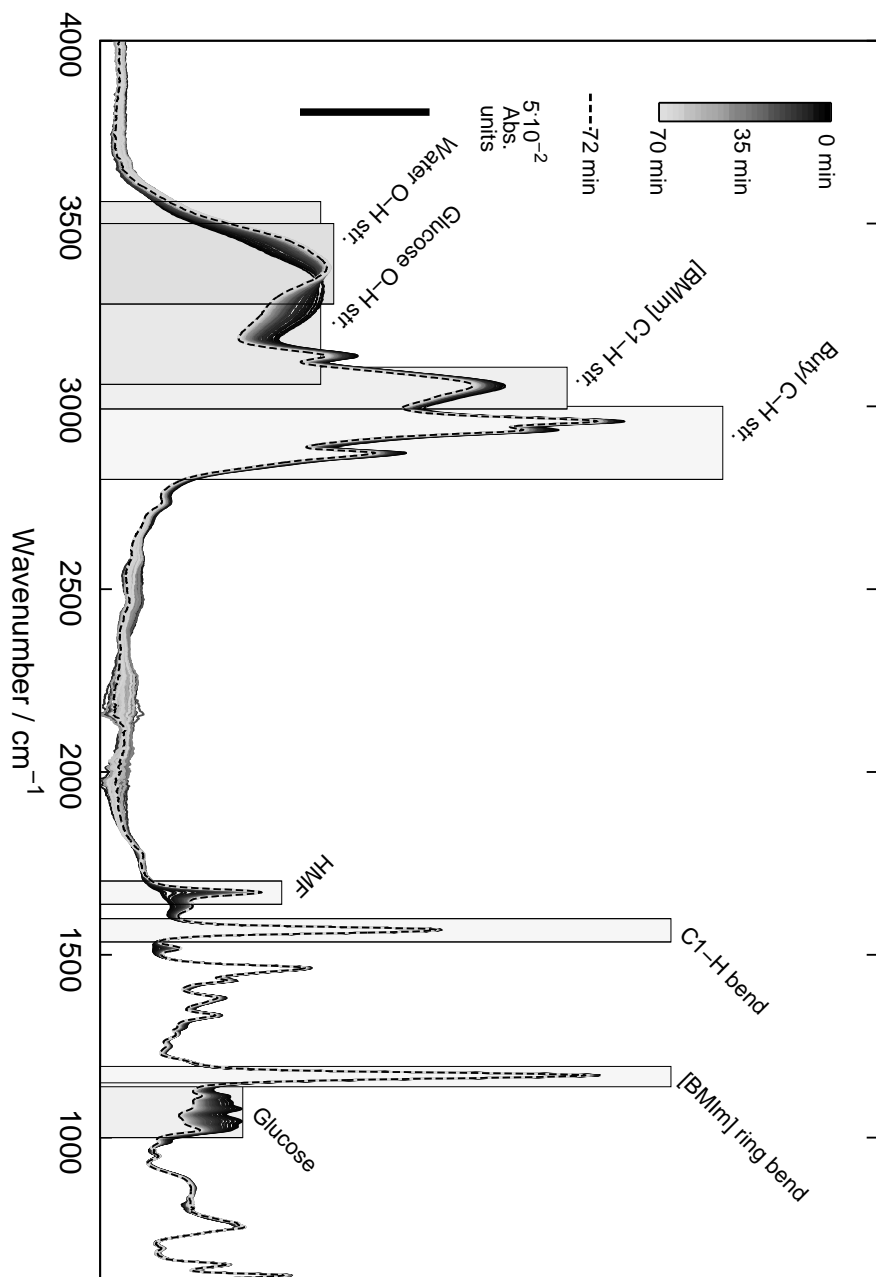


Figure C.6.: Full region in-situ spectra of conversion of glucose with $\text{CrCl}_3 \cdot 6\text{H}_2\text{O}$ in $[\text{BMim}]\text{Cl}$ in the sealed microreactor at 110°C .

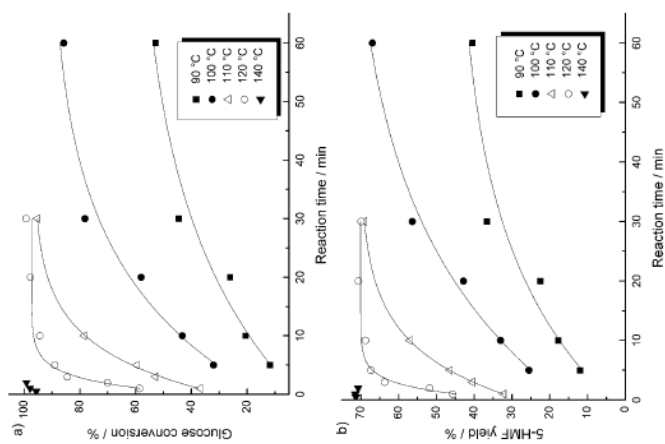


Figure 1. Effect of reaction temperature on a) glucose conversion and b) 5-HMF yield in a system using [BMIM][Cl] as solvent and CCl_4 as catalyst. Conditions: 0.05 g glucose and 0.015 g $\text{GrCl}_3 \cdot 6\text{H}_2\text{O}$ were dissolved in 1 g [BMIM][Cl] at 70°C for 10 min (water bath heating).

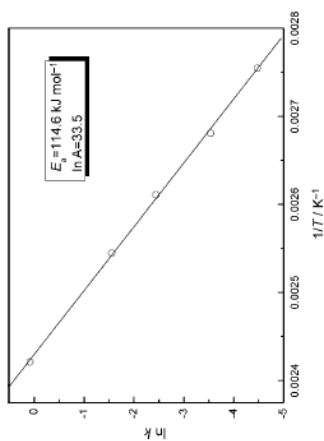


Figure 2. Arrhenius plot for glucose conversion into 5-HMF in ionic liquid [BMIM][Cl] solvent. First-order reaction kinetics constants at different temperatures were obtained for glucose conversion (X) at a certain reaction time (t) via $\ln(1-X)$ vs. t plots.

Figure C.7.: Kinetic data reproduced from Qi et al. [171].

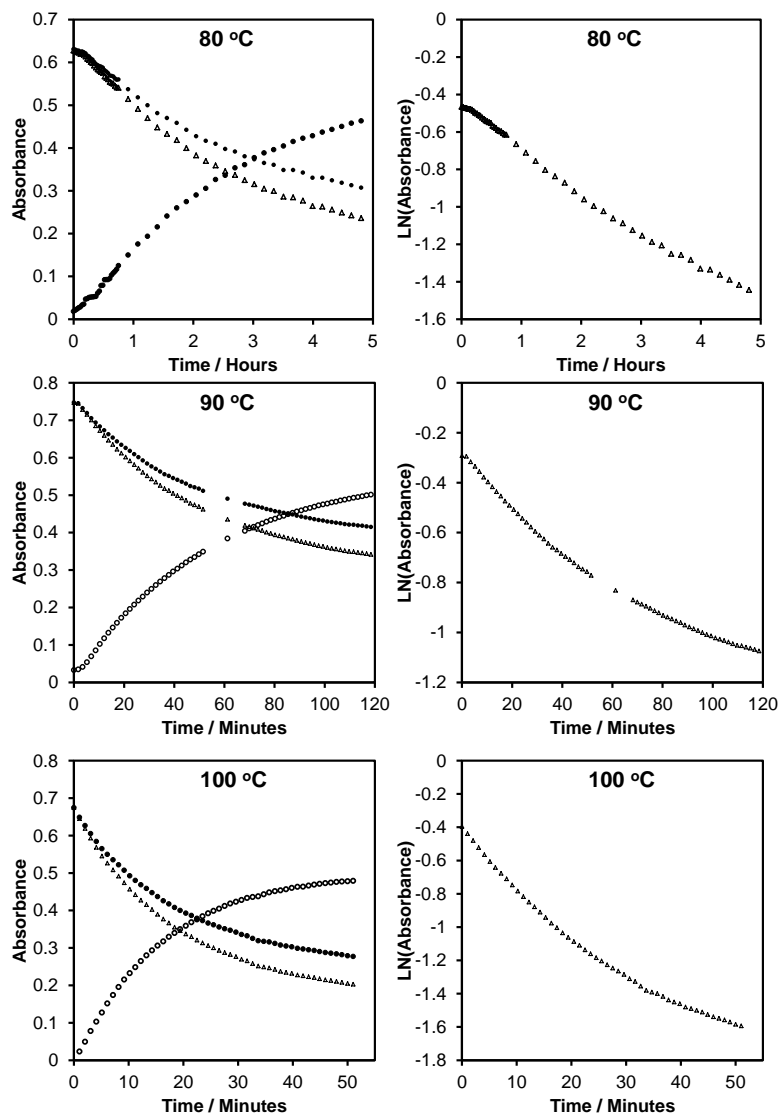
C.22. Glucose Conversion in Anhydrous Thin Films in Presence of $\text{CrCl}_3 \cdot 6\text{H}_2\text{O}$ 

Figure C.8.: Development of intensities of 1670 and 1042 cm^{-1} bands during anhydrous conversion of glucose with CrCl_3 . The corrected absorbance of the 1042 cm^{-1} band is also shown where the contribution from HMF absorption at 1042 cm^{-1} is subtracted, according to relationship shown in figure C.2 on page 150.

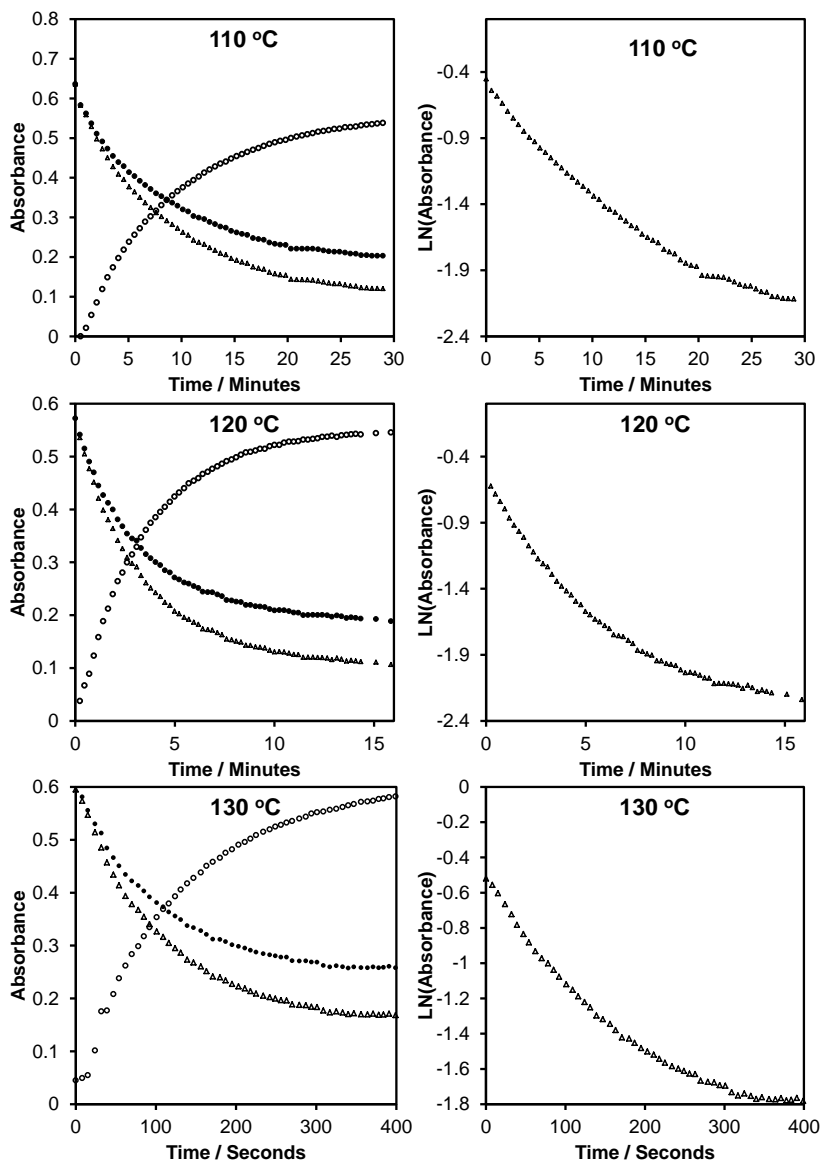


Figure C.9.: Development of intensities of 1670 and 1042 cm⁻¹ bands during anhydrous conversion of glucose with CrCl₃. The corrected absorbance of the 1042 cm⁻¹ band is also shown where the contribution from HMF absorption at 1042 cm⁻¹ is subtracted, according to relationship shown in figure C.2 on page 150.

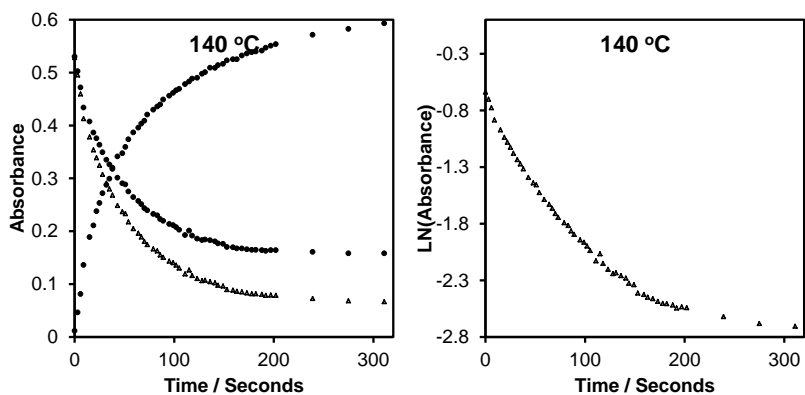


Figure C.10.: Development of intensities of 1670 and 1042 cm^{-1} bands during anhydrous conversion of glucose with CrCl_3 . The corrected absorbance of the 1042 cm^{-1} band is also shown where the contribution from HMF absorption at 1042 cm^{-1} is subtracted, according to relationship shown in figure C.2 on page 150.

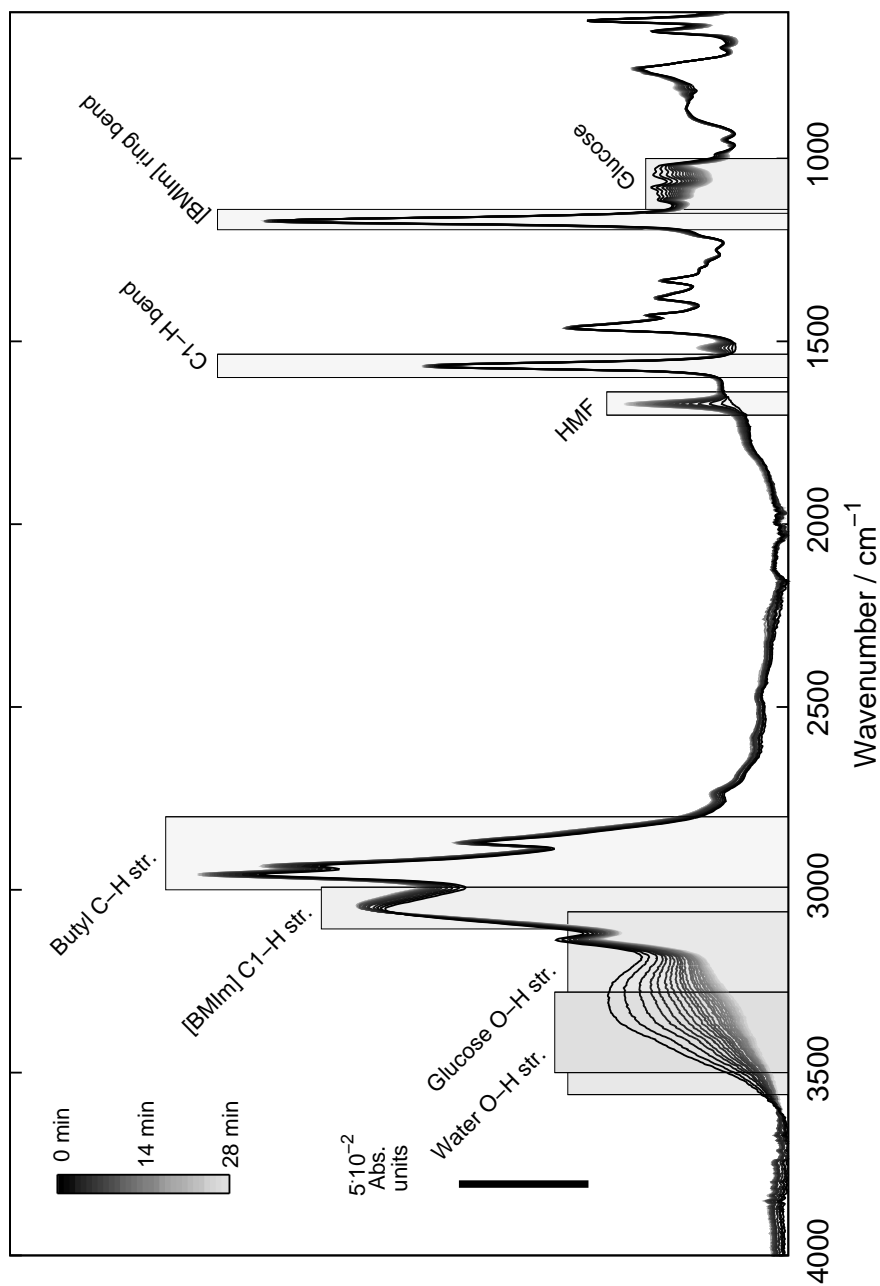


Figure C.11.: Full region in-situ spectra recorded during conversion of glucose with $\text{CrCl}_3 \cdot 6\text{H}_2\text{O}$ in [BMM]Cl in anhydrous thin film at 110 °C.

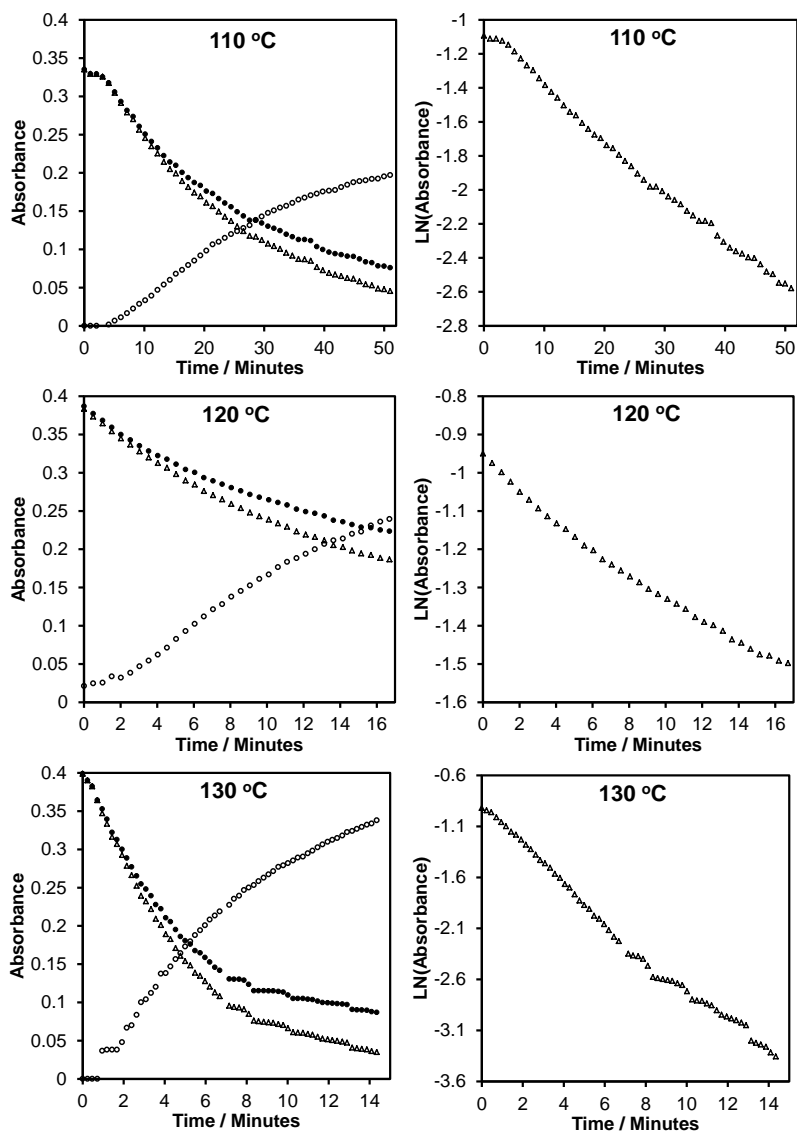
C.23. Glucose Conversion in Anhydrous Thin Films in Presence of CrCl_2 

Figure C.12.: Development of intensities of 1670 and 1042 cm^{-1} bands during anhydrous conversion of glucose with CrCl_2 . The corrected absorbance of the 1042 cm^{-1} band is also shown where the contribution from HMF absorption at 1042 cm^{-1} is subtracted, according to relationship shown in figure C.2 on page 150.

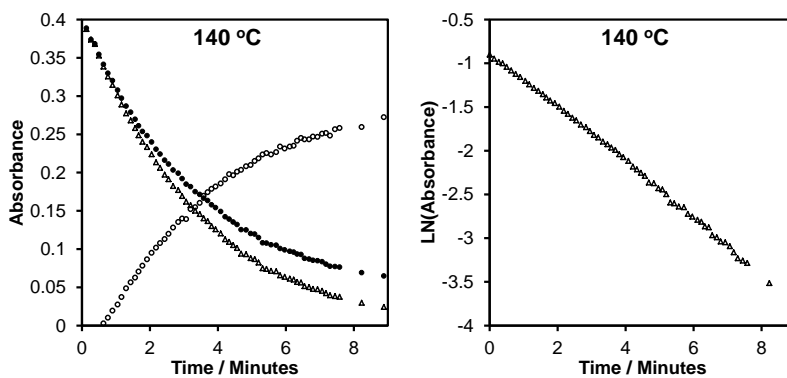


Figure C.13.: Development of intensities of 1670 and 1042 cm^{-1} bands during anhydrous conversion of glucose with CrCl_2 . The corrected absorbance of the 1042 cm^{-1} band is also shown where the contribution from HMF absorption at 1042 cm^{-1} is subtracted, according to relationship shown in figure C.2 on page 150.

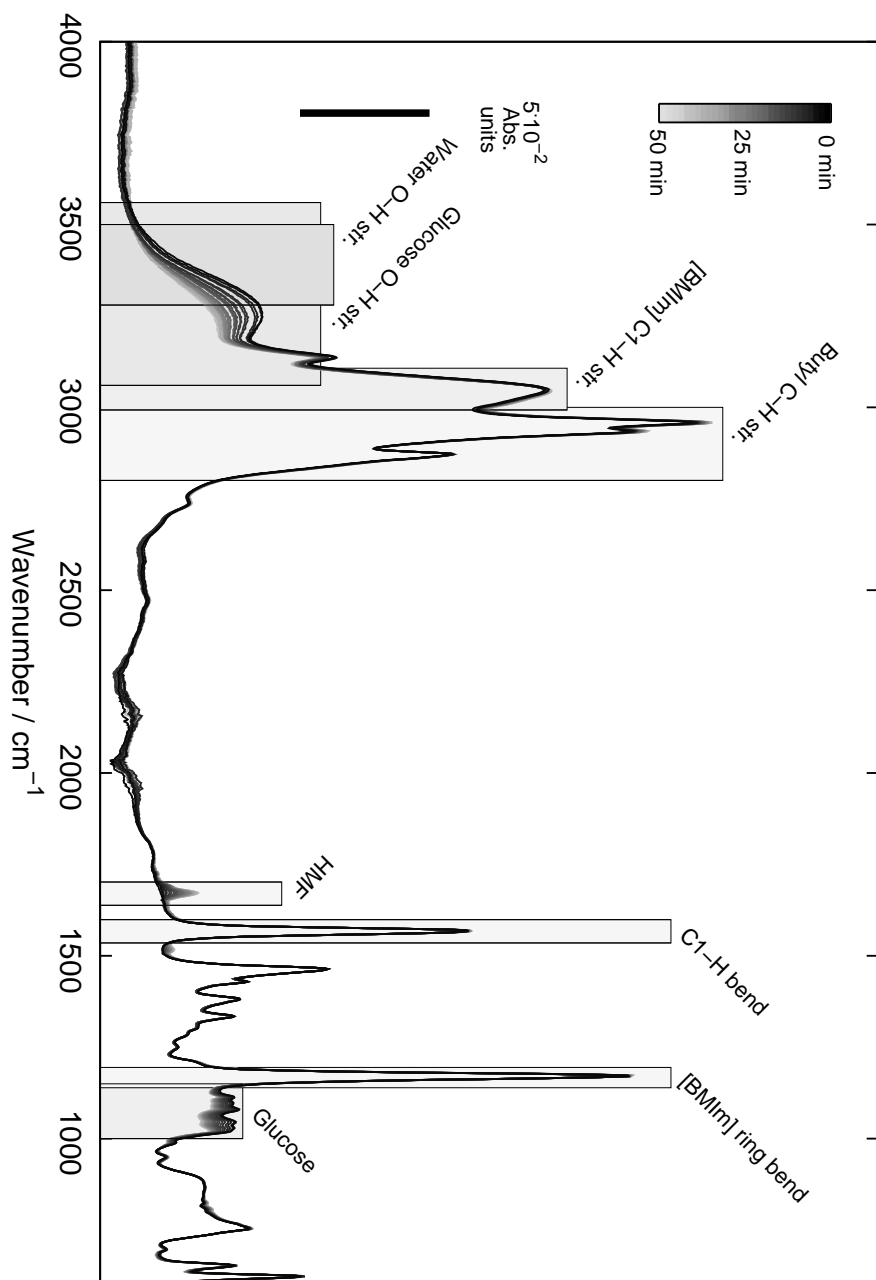


Figure C.14.: Full region in-situ spectra recorded during conversion of glucose with CrCl_2 in $[\text{BMIM}]\text{Cl}$ in anhydrous thin film at 110°C .

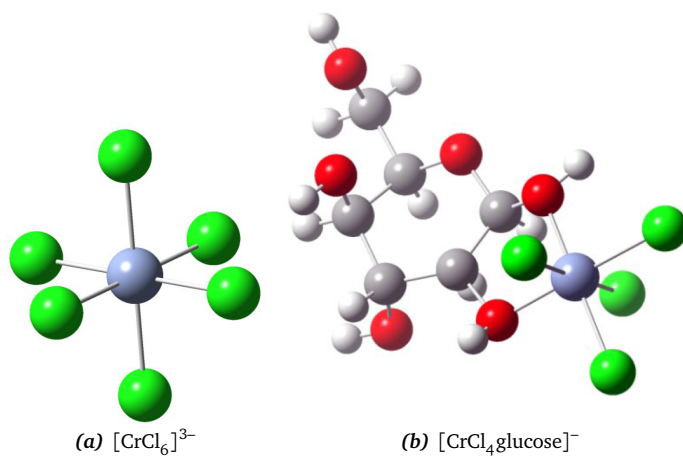


Figure C.15.: EXAFS structures by Andersen, showing Cr^{III} complexes found in solution of $[\text{BMIM}]\text{Cl}$ with and without glucose^[157,158].

C.24. Second order Plots

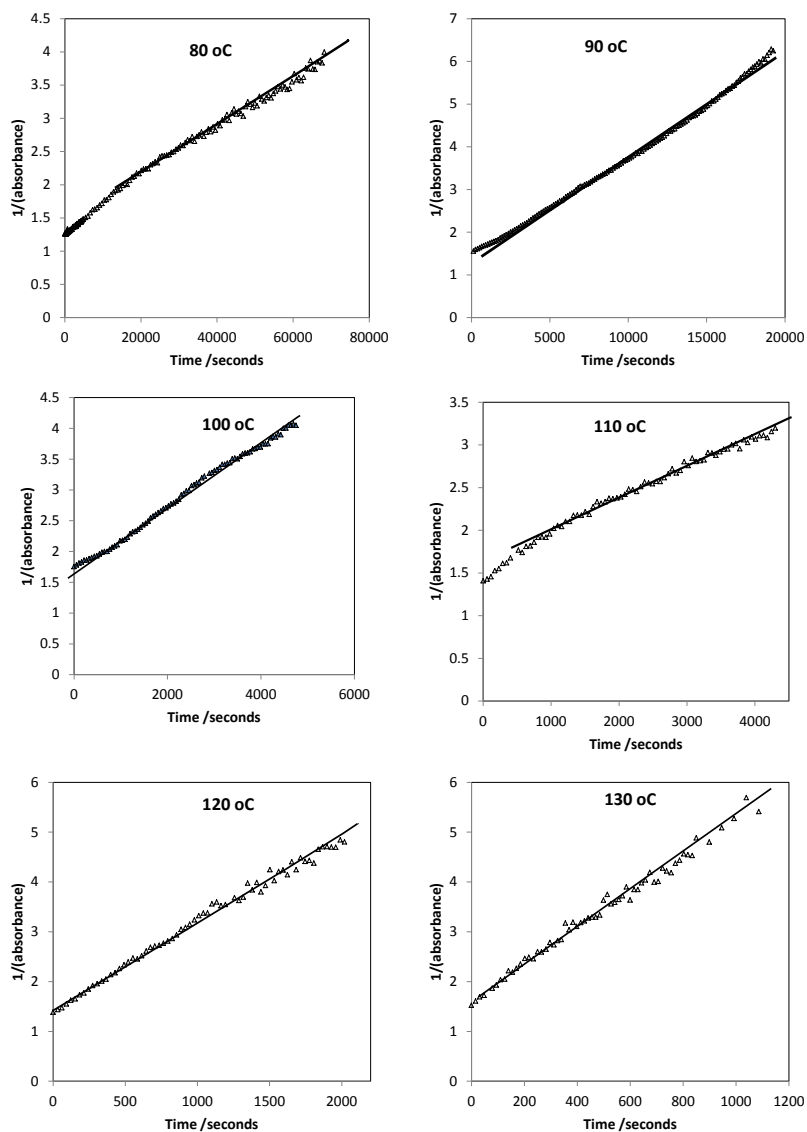


Figure C.16.: Apparent second order dependency of glucose during conversion in the presence of $\text{CrCl}_3 \cdot 6\text{H}_2\text{O}$ in $[\text{BMIM}]\text{Cl}$ in the microreactor. Indicatives lines are drawn to show second order domains.

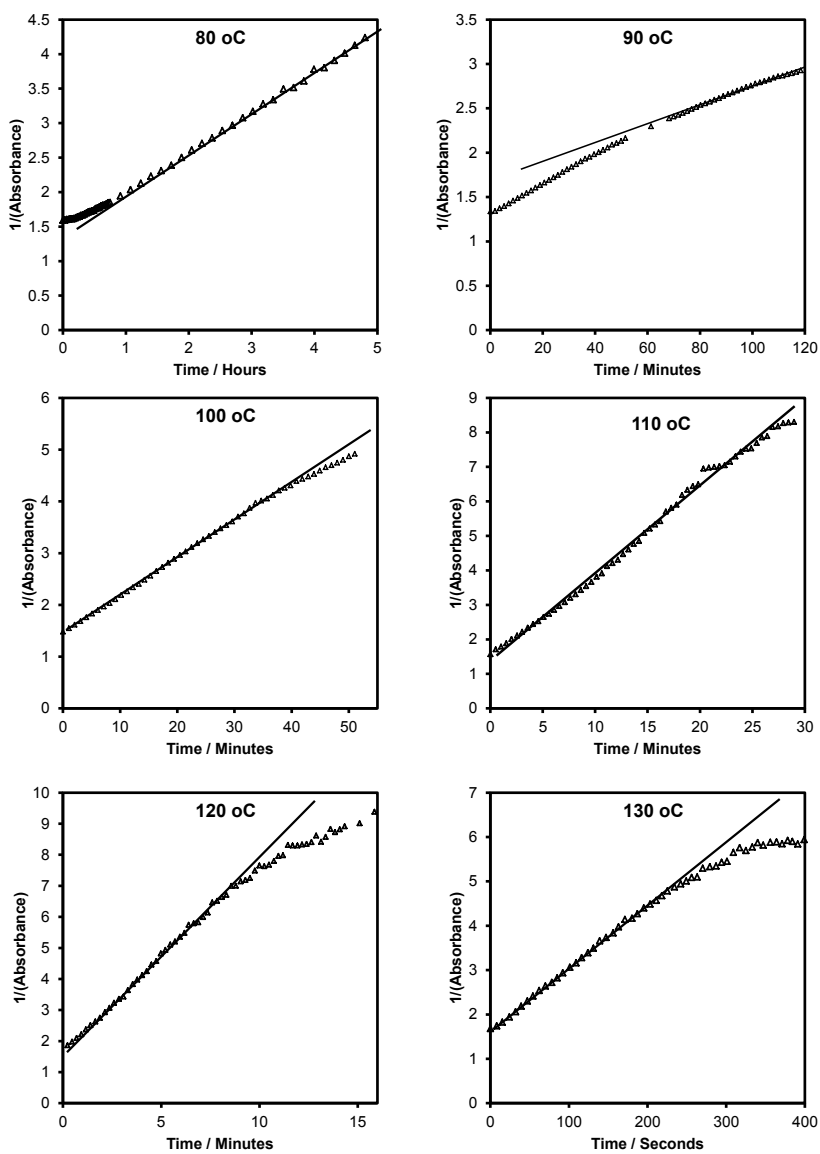


Figure C.17.: Apparent second order dependency of glucose during conversion in the presence of $\text{CrCl}_3 \cdot 6\text{H}_2\text{O}$ in the anhydrous $[\text{BMIM}]\text{Cl}$ thin films. Indicatives lines are drawn to show second order domains.

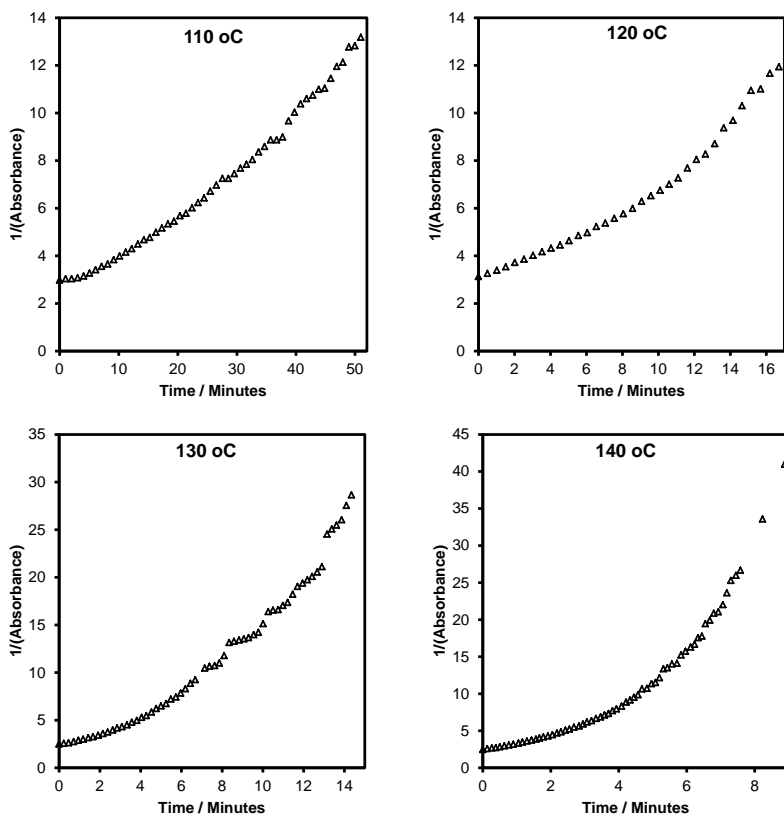


Figure C.18.: Apparent second order dependency of glucose during conversion in the presence of CrCl_2 in the anhydrous $[\text{BMIM}]\text{Cl}$ thin films.

C.25. Chloride Catalyzed Fructose Dehydration Thin Films

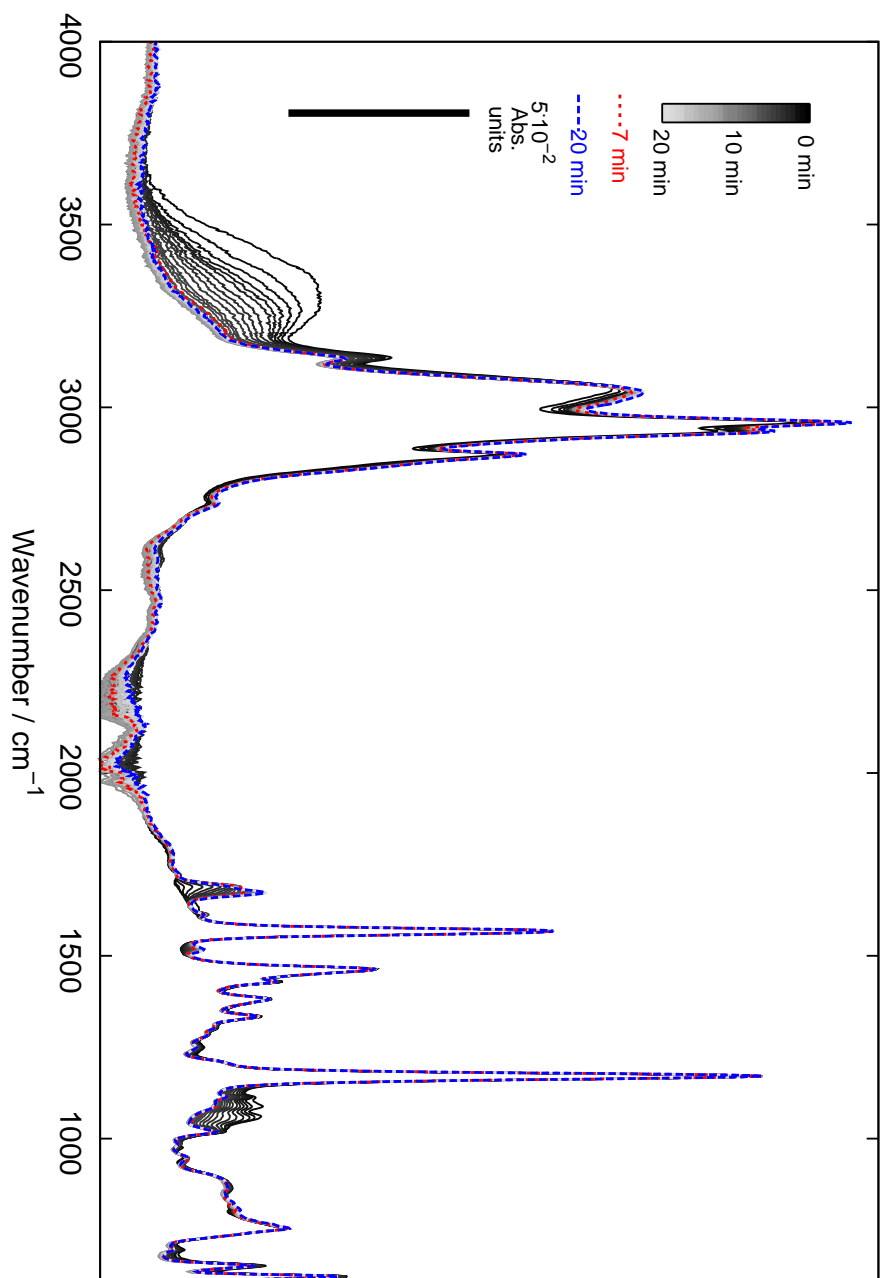


Figure C.19.: Full region in-situ spectra of fructose dehydration catalyzed by chloride in anhydrous film at 130 °C.

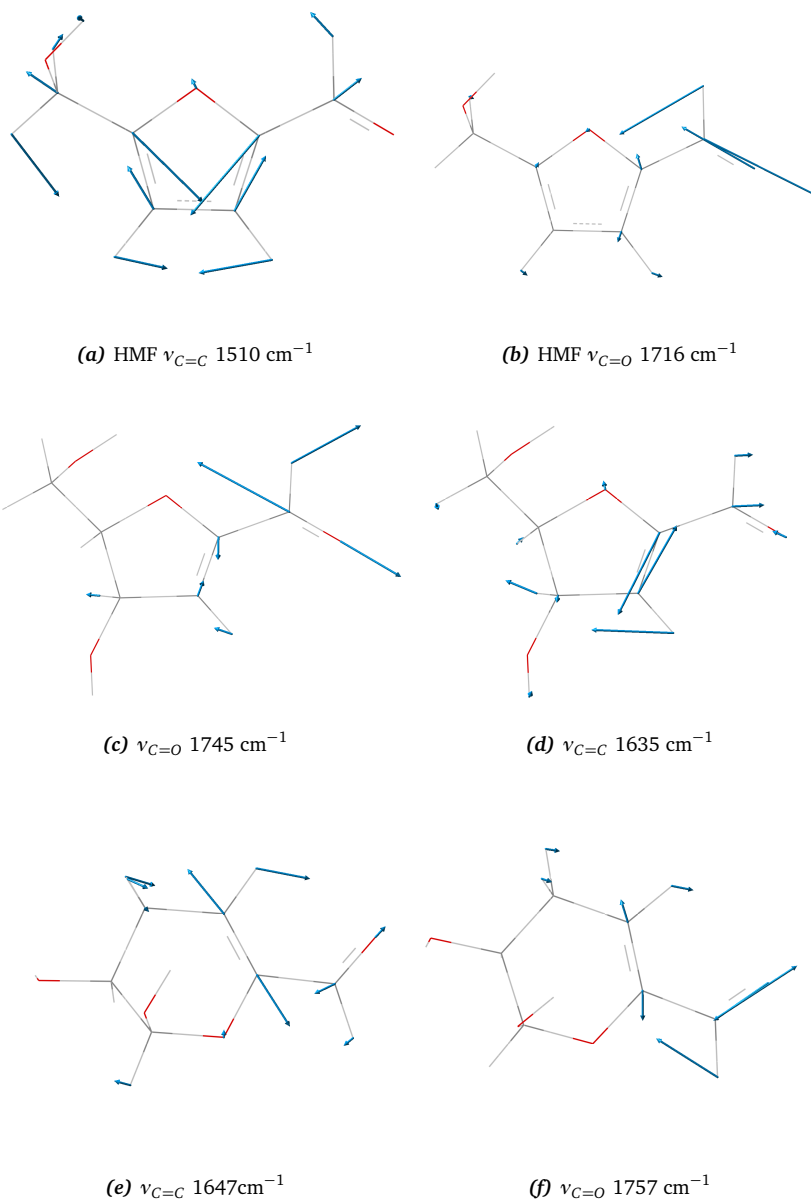


Figure C.20.: Calculated $\nu_{C=O}$ and $\nu_{C=C}$ modes of HMF and two possible intermediates/byproducts formed during dehydration of fructose. Structures and spectra are calculated using gaussian09 B3LYP/6-311+G(d,p) using a scaling factor of 0.983. As no solvent model are used, the position of the calculated $\nu_{C=O}$ should not be interpret absolute, but only relative to the bands of HMF

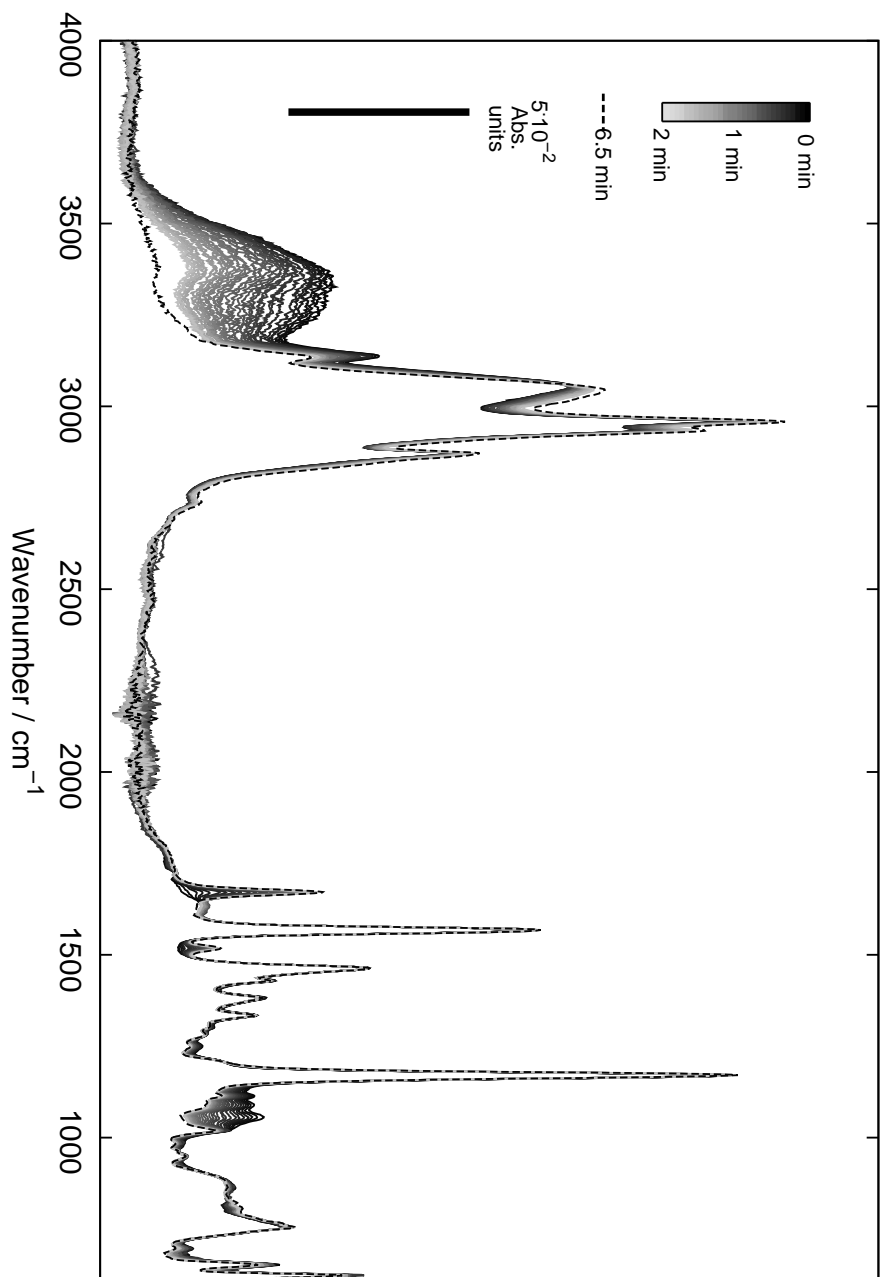


Figure C.21.: Full region in-situ spectra of fructose dehydration catalyzed by $\text{CrCl}_3 \cdot 6\text{H}_2\text{O}$ in thin film at 110 °C exposed to flow of dry nitrogen.

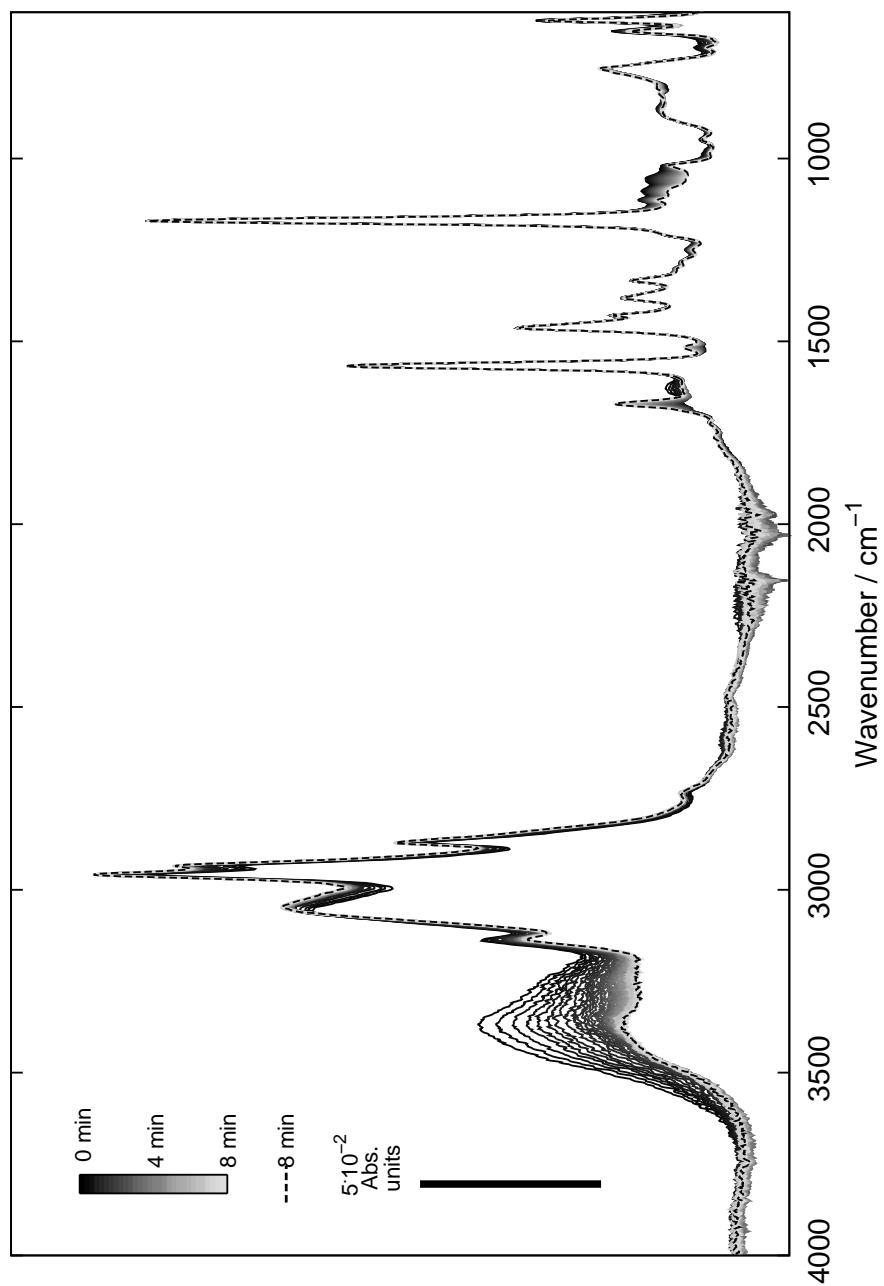


Figure C.22.: Full region in-situ spectra of fructose dehydration catalyzed by chloride in film at 130 °C humidified with nitrogen flow saturated with water at room temperature.

C.26. Chromium Catalyzed Fructose Dehydration Thin Films

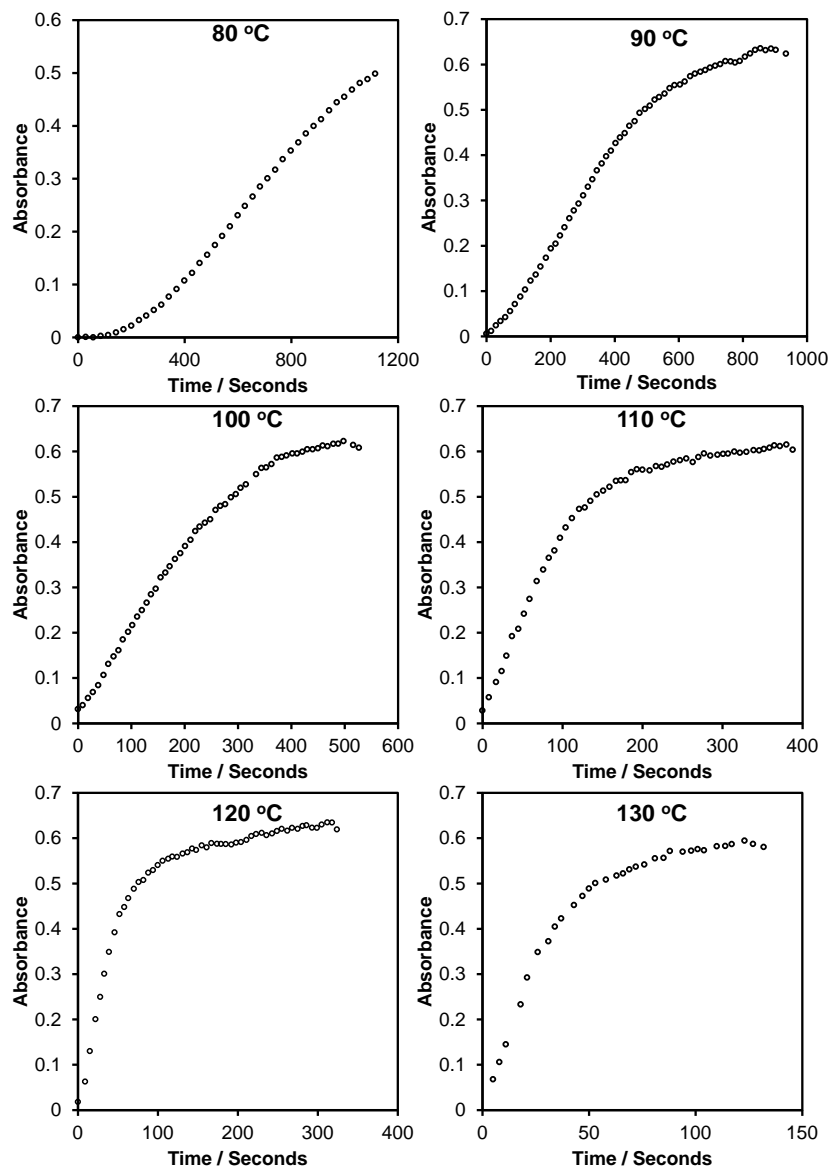


Figure C.23.: Development of intensities of the 1670 cm^{-1} band during anhydrous conversion of fructose in the presence of $\text{CrCl}_3 \cdot 6\text{H}_2\text{O}$.

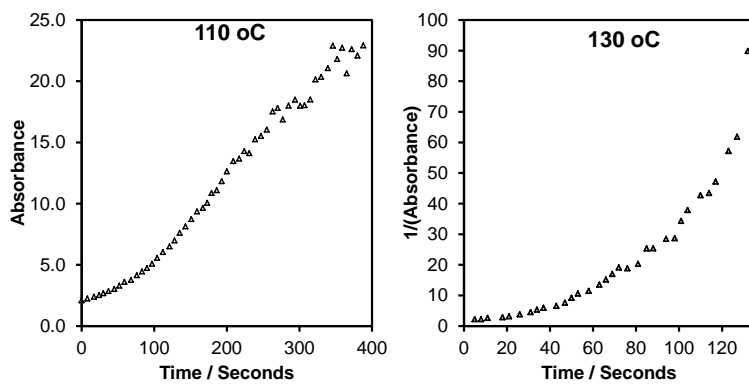


Figure C.24.: Fit for second order kinetics during $\text{CrCl}_3 \cdot 6\text{H}_2\text{O}$ catalyzed dehydration in $[\text{BMIM}]\text{Cl}$.

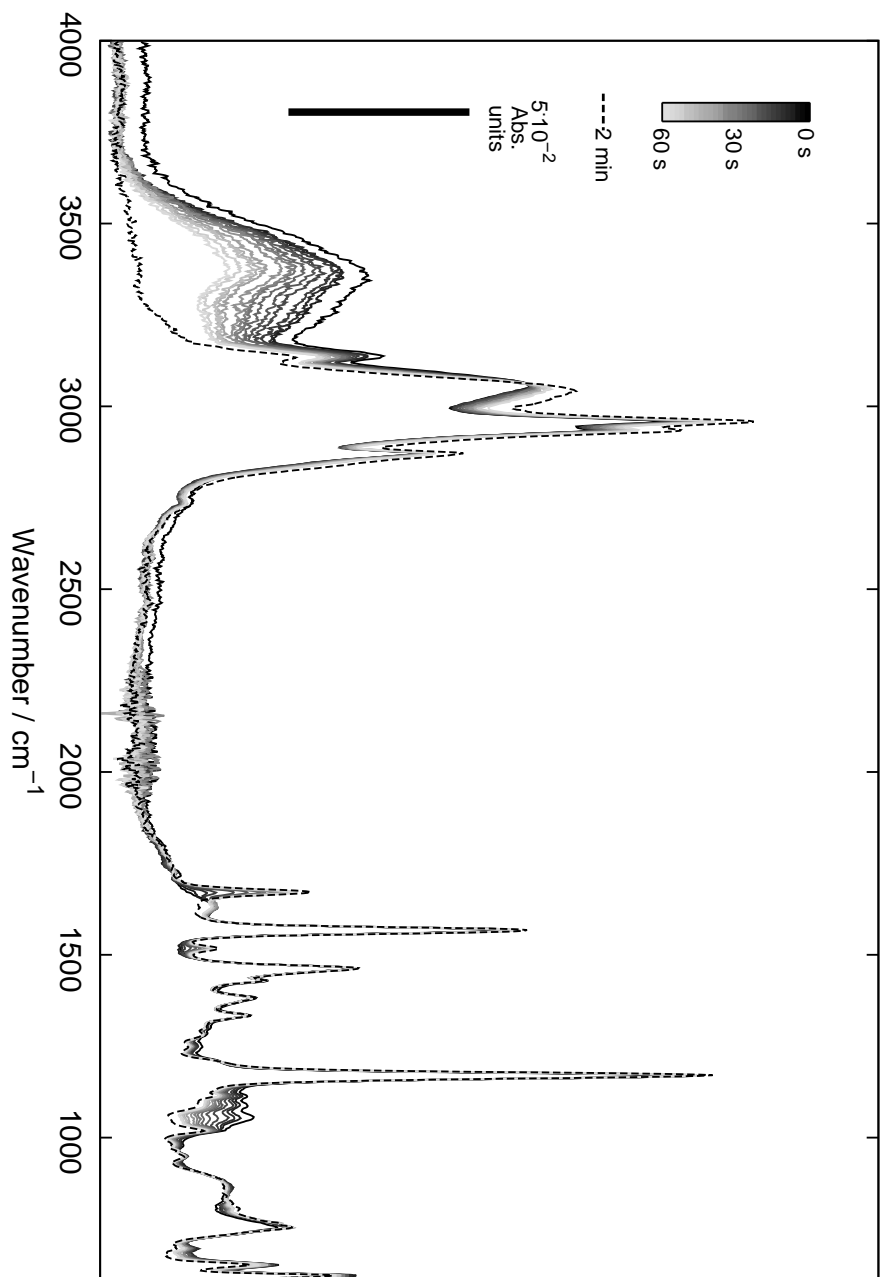


Figure C.25.: Full region in-situ spectra of fructose dehydration catalyzed by CrCl₃·6H₂O in thin film at 130 °C exposed to flow of dry nitrogen.

Appendix

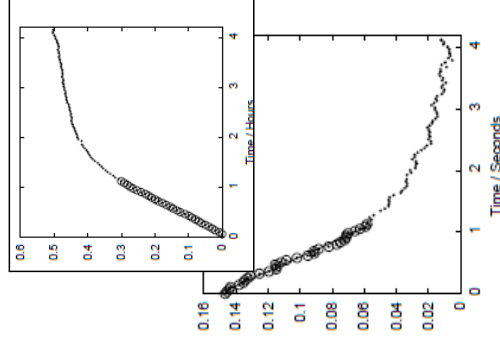
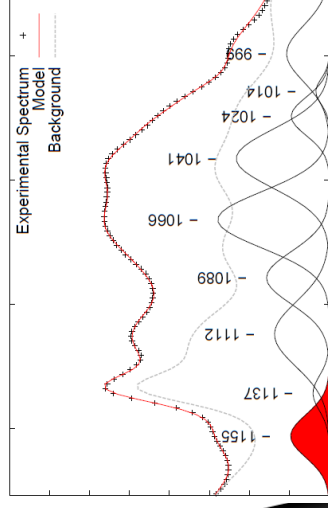
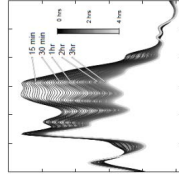


Automatic deconvolution package for gnuplot - Short documentation

Automatic Deconvolution Package for gnuplot

Short Documentation / Quick Guide

- All files Spectra and Scripts are Placed in the same folder
- Make list of files (content_formatted.txt)
- Point path in master_fitter.plt towards to correct folder
- Ensure functions, background, constrains and initial guess are reasonable for spectra – else use commercial software or the utilities described on the lase page to provide initial guess and background approximation
- Load master_fitter.plt to initiate deconvolution



Input of spectra: xy-format accompanied with list of filenames
(Use e.g. MS DOS command: *Dir *.csv > content_formatted.txt*)

Spectrum name1.CSV
...
Spectrum name1.CSV
All spectra to be fitted, should be placed in the same folder and defined in *content_formatted.txt*

Content_formatted.txt
List of filenames of each spectrum in saved in macro variables: *filenr1 ... filenri* (use "double string" syntax)

"Control panel" and the "backbone" that loads all important "slave scripts"

Global_parameters.plt

User defined:
Define decimal sign – european "." or US ""
Define datafile separator – e.g. ";" or tabular space
Use of analytical background? – *yes/no*
Request full optimization of initial spectra? – *yes/no*
Preferred output format? – *.Png/.eps/animated.gif*
Live graphical output in gnuplot during fit? – *yes/no*
Define which band area(s) should be extracted during deconvolution
Define x-range that should be used in plot
Define convergence criteria and maximum of iterations

Loading by default: *functions.plt, bg_functions.plt, content_formatted.txt, initial_guess.txt*

Master_fitter.plt

INITIATES THE DECONVOLUTIONS
Manage the overall fitting procedure by loading the important scripts:
Global_parameters.plt
fit_through_all.plt
print_table.plt

User defined: Path must be defined manually. If *fit_through_all_inverse.plt* are used, *filenri* must be defined manually

Important “slavescripts” that must be configured to fit the deconvolution type

Bg_functions.plt

Fundamental expressions for individual functions: *bg_gaus1(x)...**bg_gausi(x)*
background approximation:
*bgfunc(x)=SUM[bg_gaus1(x)...**bg_gausi(x)*]

Functions.plt

Fundamental expressions for individual functions
*gaus1(x)...**gausi(x)*
Sum function:
*gaus(x)=SUM[gaus1(x)...**gausi(x)]*

Parameters_to_fit.plt

Defines which parameters to optimize (must be consistent with *functions.plt*)

plotter.plt

Calls the *plot* command (must be consistent with *functions.plt*)

Initial_guess.txt

Values initial amplitudes, positions and widths

Bg_parameters.txt

Values initial amplitudes, positions and Widths

Fit_this_file.txt

Contains fitting profile, defines output terminal(s) and calls *plotter.plt* (custom profiles can easily be made)

Important “Flexible” slavescripts does not need configuration

Fit_through_all.plt

Fit_through_all_inverse.plt

LOOP (for *filenr1...filenr1*) [Requests a deconvolution of spectra; saves amplitude, position, width and areas of selected band(s) in program buffer]

If “inverse” version is loaded the loop starts backwards with *filenr1* and with *filenr1*

Print_table.plt

Prints table containing in terminal window containing spectrum name, width, position, amplitude and integrated area saved in program buffer
(is loaded by default when *fit_trough_all.plt* is finished – see *master_fitter.plt*)

Print_table.plt

Prints list of integrated band areas in terminal window.

Can be requested after deconvolutions

Usefull tools and accesories (are not loaded by default)

Print_parameters.plt

Loads the current parameters for amplitude, positions and widths for individual Gaussian functions.

Hint: Can be copy/pasted directly into initial guess

Single_fitter.plt

Deconvolutes single spectrum and loads *print_parameters.plt*

Which spectrum to fit is defined in file

Plotter_bg.plt

Plots the *bg_fit* during runs of *bg_fitter*. Must be configures to match *bgjfunctions.plt*

Print_bgparameters.plt

Like *print_parameters.plt* for background function variables

Hint: Can be copy/pasted directly into *bg_parameters.plt*

Bg_fitter.plt

Fits background parameters. Can in some version of the script package be loaded prior to each deconvolution series

Loads *print_bg_paramerts.plt*

Plotting Tools

Plot_ir_greyscale.plt

Uses *content_formated.plt* to initiate plot 2D representation in .eps format. Colors via files loaded. /plot_workfunctions folder must be present

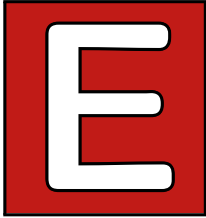
waterfall.plt

Uses *content_formated.plt* to initiate "waterfall/fence" plot of spectra in .eps format. /plot_workfunctions folder must be present

/plot_workfunctions

The working scripts for the greyscale and waterfall styles are placed here

Appendix



Article - Project related

Cite this: DOI: 10.1039/c0xx00000x

www.rsc.org/xxxxxx

ARTICLE TYPE

Revisiting the Brønsted acid catalysed hydrolysis kinetics of polymeric carbohydrates in ionic liquids by in-situ ATR-FTIR spectroscopy[†]

Andreas J. Kunov-Kruse,^{*a} Anders Riisager,^{*a} Shunmugavel Saravanamurugan,^a Rolf W. Berg,^b Steffen B. Kristensen,^a and Rasmus Fehrmann^a

Received (in XXX, XXX) Xth XXXXXXXXX 20XX, Accepted Xth XXXXXXXXX 20XX
DOI: 10.1039/b000000x

A new versatile method to measure rates and determine activation energies for the Brønsted acid catalysed hydrolysis of cellulose and cellobiose (and other polymeric carbohydrates) in ionic liquids is demonstrated by following the C-O stretching band of the glycoside bond with in-situ ATR-FTIR. An activation energy in excellent agreement with literature was determined for cellulose hydrolysis, whereas a distinctly lower activation energy was determined for cellobiose hydrolysis. The methodology also allowed independently to determine activation energies for the formation of 5-hydroxymethylfurfural in the systems.

Introduction

The demand for substituting petroleum products used today with biomass derived chemicals and fuels are continuously increasing.^{1,2} Extensive effort has in particular been put on developing systems based on the furanic platform, which are able to provide a diverse range of products.³⁻⁵ However, the initial production of 5-hydroxymethylfurfural (HMF) are in most cases focused on applying sugars such as fructose and glucose, which are derived from corn, starch sugar canes or other edible resources.⁶ These resources are far from unlimited and in a longer perspective such processes must apply lignocellulosic materials instead, which are available in surplus from various agricultural processes and waste streams. However, there still need to be a breakthrough in the conversion technologies of cellulose into sugars to make this approach competitive to food crops.

The acid catalysed hydrolysis of cellulose in ionic liquids has been subject to immense interest in the last decade since Rogers and co-workers⁷ discovered that some ionic liquids are able to dissolve cellulose. The dissolution of cellulose makes the glycoside bond more susceptible to attack by a catalyst than if the crystalline fibres are just suspended in a heterogeneous mixture. Most studies concerned with hydrolysis of cellulose in ionic liquids in the presence of homogeneous or heterogeneous acid catalysts have focused on the product distribution after hydrolysis⁸⁻¹⁰ and paid less attention to the hydrolysis kinetics. However, an interesting effect of dissolving cellulose in ionic liquids is, that the mechanism of hydrolysis seems to be altered as

studies of the hydrolysis kinetics in ionic liquids reports lower activation energies than normally observed in water.¹¹⁻¹³ Generally, the apparent activation energy observed for acid cellulose hydrolysis and its oligomers in water is relatively high around 120-130 kJ mol⁻¹.¹⁴ The high activation energy is induced by an unfavourable oxocarbenium ion which has considerably higher energy than observed for oxocarbenium ions in general, because the pyranose ring structure prevents the preferred planar geometry around the C=O⁺ group (activation energies of simple acetals are only in the order of 50-60 kJ mol⁻¹).^{15,16} In ionic liquids the strongly ionic environment may stabilise the positive charge of the oxocarbenium ion and thus lower its energy.¹³ This is supported by findings that the hydrolysis rate of the glucoside bond in water/1,4-dioxane mixtures is significantly enhanced in the presence of chloride and bromide ions.¹⁷

Cellulose and short chain cellulose oligomers are insoluble in conventional solvents. This makes it very challenging to estimate the initial reaction rate of hydrolysis by conventional analytical methods. Furthermore, analytical techniques dealing with analysis of all the hydrolysis products, including long chain oligomers, are very laborious.¹¹ Analysis is further complicated by formation of secondary products as acid catalysts are active for glucose dehydration to, e.g. HMF and levulinic acid.¹³ Such reactions occur simultaneously with hydrolysis and at considerable rates, making the produced glucose an unsuitable measure for the hydrolysis rate. Since the activation energies for cellulose hydrolysis and glucose dehydration by Brønsted acids are similar,^{18,19} methods solely taking the produced glucose into account, and not products produced hereof, are thus likely to underestimate the actual hydrolysis rate and thus overestimate the activation energy.

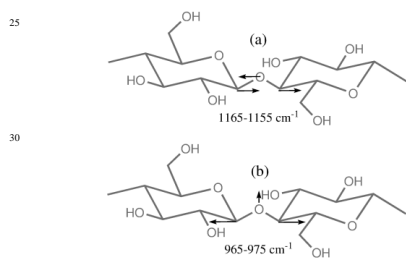
In this work we introduce a new approach to measure the hydrolysis kinetics of cellulose. Hence, instead of monitoring the formation of hydrolysis products, the disappearance of glycoside bonds are followed during hydrolysis by in-situ ATR-FTIR in a specially designed stirred micro reactor.²⁰

Results and Discussion

Initially, we performed a thorough investigation of vibrational modes in cellulose using DFT model calculations (B3LYP/6-

311+G(d,p) (ESI†, Fig. S10) to identify quantifiable bands. Among several new IR-active modes that are characteristic for the glucose moieties in cellulose, we were able to locate the position of the two group vibrations comprising C-O-C stretching vibrations at around 1165-1155 and 965 cm⁻¹ (anti-symmetric and symmetric modes, respectively; see ESI†, Table S2) in very good agreement with interpretations found in the literature.^{21–30} The modes are schematically shown in Scheme 1.

When using the popular ionic liquids 1-butyl-3-methylimidazolium chloride ([BMIm]Cl) and 1-ethyl-3-methylimidazolium chloride ([EMIm]Cl) as solvents for the hydrolysis, it was only possible to follow the time evolution of the very weak symmetric stretching mode at 965 cm⁻¹. Moreover, the 1160 cm⁻¹ band was here unsuited for accurate quantitative measurement due to overlap with a very strong mode comprising the bending of the C2-H proton on the [BMIM]⁺ cation. However, this C-H bending mode disappeared when the hydrogen in the C2 position was substituted with a methyl group, thus allowing quantitative analysis via the intense band due to anti-symmetric stretching of the glycoside bond (ESI†, Fig. S15). The ionic liquid 1-butyl-2,3-dimethylimidazolium chloride ([BDMIm]Cl) was accordingly chosen for the kinetic experiments.



Scheme 1 Schematic representation of the two characteristic anti-symmetric (a) and symmetric (b) vibrations of the glycoside bond.

Time-resolved difference spectra measured for the sulfuric acid catalysed hydrolysis of Avicel cellulose in [BDMIm]Cl are shown in Fig. 1. Notably, the spectra reflect the total change in the composition during hydrolysis and show thus a mixture of disappearing bands for both cellulose and glucose as the reaction proceeds. Therefore, care must be taken when a quantitative interpretation is done because the pyranose backbone of the cellulose chains show many similarities with glucose and several of the types of vibrational bands are found in the spectra of both structures (see ESI†, Table S2 and Fig. S19).

For the polymeric glucose species introduction of acetal groups with the glycoside bonding creates several modes involving deformation around the oxygen atom inside the pyranose. Consequently, new strong bands from C-O-C stretching in the pyranose ring and new C-C stretching and C-H bending modes were found in the cellulose spectrum around 1070-1060 cm⁻¹. The intensities of these bands decreased markedly during the hydrolysis of cellulose, and indeed these bands initially showed a linear decrease as a function of time that possibly could be used to determine the initial rates (ESI†, Fig.

S8). However, glucose also had intense bands in the same region. Therefore, these bands were unsuitable for quantitative analysis, as they expressed an unknown fraction of the hydrolysis rate of both cellulose and glucose (an elaborate discussion follows later). The anti-symmetric stretching of the glycoside bond has a relatively strong absorption band at around 1155-1160 cm⁻¹, which is found in cellulose and in cellulose oligomers including the dimer cellobiose (ESI†, Fig. S18). The spectra of glucose showed an intense band at around 1140 cm⁻¹ probably due to C1-O1 bond stretching and bending of C1-H and O1-H bonds, whereas cellulose and the cellulose oligomers only showed a weak absorption band. These bands can thus easily be distinguished and quantified by deconvolution of the ATR-corrected difference spectra. No general linear time dependency of the area of the 1140 cm⁻¹ band was observed during the experiments. The difference between these bands was further confirmed by experimental spectra of cellulose oligomers, which all showed that the C-O-C stretching band was only present in the polymeric species (ESI†, Fig. S18).

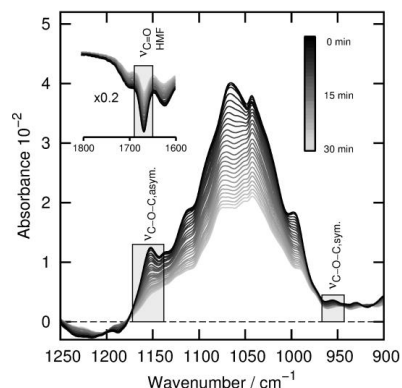


Fig. 1 Corrected ATR-FTIR difference spectra recorded during the first 30 min of sulfuric acid catalysed hydrolysis of Avicel cellulose in [BDMIm]Cl at 120 °C. The symmetric and anti-symmetric glycoside C-O-C stretching bands are highlighted with boxes. The insert shows the 1800-1600 cm⁻¹ range (full region spectra can be found in ESI†, Figs. S20-S22).

Knowledge about the kinetics of cellulose hydrolysis in ionic liquids is quite limited due to the earlier mentioned analytical difficulties, although some activation energies of cellulose hydrolysis in ionic liquids catalysed by strong mineral acids or similar systems have been reported.^{12,13} Here, we firstly investigated the hydrolysis using sulfuric acid as catalyst to allow direct comparison of the kinetics obtained by the in-situ FTIR method to kinetics derived from studies using more conventional analytical methods. The cellulose hydrolysis was investigated in-situ in [BDMIm]Cl from 90 to 140 °C in steps of 10 °C using 1.7 wt.% sulfuric acid catalyst. The small volume of the stirred detachable micro reactor ensured fast heating and equilibration of the cooled premixed reaction mixture.

In the IR spectra a slight increase of the intensity of the 1157

cm⁻¹ band was initially observed at the set temperatures, probably due to incomplete dissolution of the cellulose (see development in ESI†, Fig. S1). However, within a short time period a steady decrease of the band was measured for all the temperatures allowing first the initial rates to be determined by integration of the 1157 cm⁻¹ band of the deconvoluted spectra and, secondly, the initial rates (expressed as absorbance per second) to be established with high accuracy from the in-situ experiments (ESI†, Fig. S1 and Table S1). A plot of ln(abs) as a function of time confirmed that the reaction was first order in concentration of glucoside bonds, as expected (ESI†, Fig. S3). In Fig. 2 the experimentally determined rate constants for the hydrolysis are plotted in an Arrhenius plot as ln(-k) against 1/T. From the rate constants (first order with respect to catalyst concentration) the activation energy for the hydrolysis of cellulose with sulfuric acid was determined to be 96.4 ± 4.1 kJ mol⁻¹, which is in excellent agreement with recent values of 92-96 kJ mol⁻¹ reported for analogous cellulose hydrolysis in [EMIm]Cl.^{12,13}

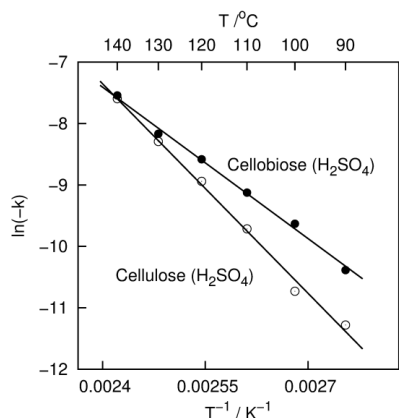


Fig. 2 Arrhenius plot showing the temperature dependency of the initial rates for cellulose and cellobiose hydrolysis with sulfuric acid catalyst.

Cellobiose is often used as a model for cellulose when modelling cellulose hydrolysis, due to simplicity and the comparative higher solubility of cellobiose in many solvents.¹² Accordingly, we also investigated cellobiose hydrolysis under the same conditions as described for cellulose above (Fig. 3 and ESI† Figs. S2 and S3). Notably, we found here the apparent activation energy for cellobiose hydrolysis to be 69.6 ± 3.0 kJ mol⁻¹, which is significantly lower than for cellulose. In the earlier work using [EMIm]Cl the activation energy for cellobiose hydrolysis was not reported, but it was observed that the hydrolysis rate of cellobiose was first order with respect to the concentration of glucoside bonds and indeed significantly faster than for cellulose.^{12,13} This directly supports our finding of a lower activation energy, even though the nature of the glucoside bonds of cellobiose and cellulose are rather similar, as also indicated by our DFT calculations.

A recent theoretical study on cellobiose hydrolysis suggests the high energy transition state to be associated with distortion of

the stable chair conformation, when the protonated glucoside bond is split into glucose and the oxocarbenium ion.³¹ In the transition state the two glucose units are orientated in a 90 degree angle, which is possible due to flexibility of both glucose units in the cellobiose dimer around the glycoside bond.³² This conformation allows the structure to rearrange so the reaction barrier for hydrolysis is lowered. In contrast, the polymeric cellulose chain will in general not bend 90 degrees around each glucoside bond, and thus behave more rigid with no possibility to undergo an analogous conformation change that can stabilise the transition state. The reason why the activation energies for hydrolysis of cellulose and cellobiose in water are still found to be similar seems to be an effect of poor stabilisation of the positive charge on the oxocarbenium ion. This effect can, however, be altered in strongly ionic environment to lower the reaction barrier significantly.^{11-13,17} Hence our results suggest that the difference in magnitude of the reaction barrier for hydrolysis of cellobiose and cellulose in ionic liquids is mainly caused by conformational effects.

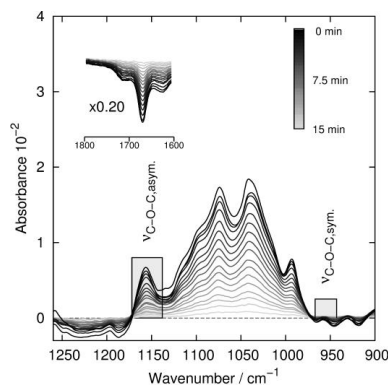


Fig. 3 Corrected ATR-FTIR difference spectra recorded during the first 15 min of sulfuric acid catalysed hydrolysis of cellobiose in [BDMIm]Cl at 120 °C. The symmetric and anti-symmetric glucoside C-O-C stretching bands are highlighted with boxes. The insert shows the 1800-1600 cm⁻¹ range (full region spectra can be found in ESI†, Figs. S23-S25).

A dehydration experiment with 10 wt.% glucose in [BDMIm]Cl and 1.7 wt.% sulfuric acid was performed to exclude that the observed decrease in intensity of the 1157 cm⁻¹ band from cellobiose was due to simultaneously conversion of the formed glucose into HMF. Such misinterpretation would namely increase the apparent rate and thus decrease the calculated activation energy. In addition, the experiment could corroborate that the observed intensity loss of the 1142 cm⁻¹ band of glucose was distinguishable from the glycoside 1157 cm⁻¹ band. From the results of the experiment it was clear that glucose was converted mainly into HMF and to a lower degree into carboxylic acids (increase of ν_{C=O} bands at 1669 and 1705 cm⁻¹, respectively; see discussion below), and that the 1157 and 1142 cm⁻¹ bands could easily be distinguished by deconvolution. Moreover, no absorption bands at 1157 cm⁻¹ was observed in the difference spectra as otherwise seen in the difference spectra of cellulose

and cellobiose (ESI†, Fig. S9). The experiment further showed that the strong vibration bands overlapping with the cellulose backbone at 1070-1060 cm^{-1} cannot be used for the kinetic analysis, since almost identical activation energies for the acid catalysed cellulose hydrolysis and the glucose dehydration to HMF^{18,19} results in an overall deceptive linear decrease. Examination of the spectra recorded during cellobiose hydrolysis at lower temperatures of 90 and 100 °C revealed, that the contribution from the simultaneously dehydration to the glucose backbone vibrations bands at 1140-970 cm^{-1} was significantly less pronounced. This strongly suggests that the cellobiose hydrolysis was faster than the subsequent glucose dehydration.

During the hydrolysis of cellulose an intense and sharp band at 1669 cm^{-1} appeared independently in the FT-IR spectra along with two broad bands at 1705 and 1623 cm^{-1} , respectively. As mentioned above, the former band can be assigned to C=O stretching from HMF being formed from the simultaneous glucose dehydration, while a related increase of the band at 1623 cm^{-1} corresponded to O-H bending from the water gradually being formed by the dehydration reaction. Similarly, the broad shoulder band at 1705 cm^{-1} was assigned to carboxylic C=O stretching from formic acid and levulinic acid formed by the rehydration of HMF. Post-reaction analysis by HPLC (high-performance liquid chromatography) confirmed that glucose, HMF and carboxylic acids were the main products of the reaction (ESI†, Fig. S11). The rate of the HMF formation was determined by quantification of the carbonyl C=O stretching band at 1669 cm^{-1} after deconvolution (ESI†, Fig. S12 and Table S3). Initially, a low rate was found until steady glucose concentration was established from the hydrolysis reaction. Here after the formation rate followed a pronounced first order kinetics (see ESI†, Fig. S14). When the rates were plotted in an Arrhenius plot (Fig. 4) the apparent activation energy for the HMF formation was determined to $94.7 \pm 3.7 \text{ kJ mol}^{-1}$, which is remarkably close to the activation energy of 96.4 kJ mol^{-1} determined for the cellulose hydrolysis. However, we interpret this result as an indirect reproduction of the cellulose hydrolysis kinetics, and not as the actual activation energy for the acid catalysed dehydration of the formed glucose.

The quantification method was also applied for the HMF C=O stretching band at 1669 cm^{-1} during cellobiose hydrolysis (Fig. 4). As expected, the initial rate indicated instantly release of glucose from the hydrolysis of the glucoside bond in cellobiose (ESI†, Fig. S13), and the activation energy was determined from the initial rates to be $85.0 \pm 1.8 \text{ kJ mol}^{-1}$. This value is higher than the activation energy of 69.6 kJ mol^{-1} determined for hydrolysis of the glucoside bond in cellobiose (*vide supra*), and resembles therefore more likely the actual activation energy for acid catalysed glucose dehydration in ionic liquids. This value is in perfect agreement with a recent value reported for glucose degradation in [EMIm]Cl of 84.7 kJ mol^{-1} . This is further supported by the finding, that the rate of HMF formation did not follow first order kinetics at longer reaction times. Instead the rate was here faster than predicted by a first order rate law (ESI†, Fig. S14), thus suggesting the glucose concentration to be regulated by a combination of fast first order kinetics of the hydrolysis of the glucoside bonds and slower first order kinetics of glucose isomerisation to form fructose, which generally is

believed to be an essential step for HMF formation.⁵ The activation energy for Brønsted acid catalysed fructose dehydration in an analogous system with [BMIm]Cl has been determined to be as low as 62.2 kJ mol^{-1} .³³ The large difference in activation for dehydration of fructose and glucose is expected to facilitate dehydration of fructose to HMF in mixed systems. Hence, the absence of fructose in reaction samples analysed from ionic liquid glucose dehydration systems¹³ is most likely related to kinetics and not necessarily indicative of an alternative mechanism.

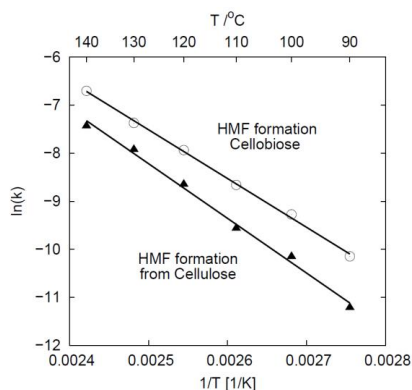


Fig. 4 Arrhenius plot showing the temperature dependency of the initial rates for HMF formation during hydrolysis of cellulose and cellobiose with the sulfuric acid catalyst.

Conclusions

Time-resolved in-situ ATR-FTIR spectroscopy has been introduced as a viable analytical tool to determine reaction rates and apparent activation energies for Brønsted acid catalysed hydrolysis of polymeric carbohydrates and simultaneous HMF formation from glucose in ionic liquids. The activation energy for hydrolysis of cellulose with sulfuric acid was experimentally found to be $96.4 \pm 4.1 \text{ kJ mol}^{-1}$, which is in excellent agreement with earlier reported activation energies. Notably, the activation energy determined for the analogous hydrolysis of cellobiose was significantly lower at $69.6 \pm 3.0 \text{ kJ mol}^{-1}$. In contrast, the apparent activation energy for HMF formation from glucose was determined to be 94.7 ± 3.7 and $85.0 \pm 1.8 \text{ kJ mol}^{-1}$ with cellulose and cellobiose, respectively. The study clearly emphasizes the limitations of using cellobiose as model substrate for cellulose in kinetic studies.

The work was performed within the framework of the Catalysis for Sustainable Energy initiative funded by the Danish Ministry of Science, Technology and Innovation.

Experimental and computational details

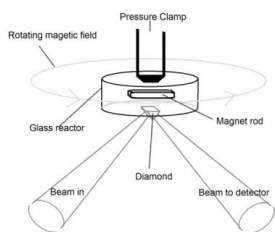
In-situ ATR-FTIR spectroscopy

Cellulose (Avicel, Sigma-Aldrich) or 1,4- β -cellobiose (99%, Sigma-Aldrich) were dissolved in 1-butyl-2,3-dimethylimidazolium (95%, Sigma-Aldrich) at 120 °C under

reduced pressure (10-15 mbar) by stirring for 2 h. One equivalent of water was then added and the solutions equilibrated for 2 h at 90 °C. About 2 g of the ionic liquids with water were subsequently added to the appropriate catalyst at 60 °C, rapidly mixed with a spatula for 1 min and then freeze quenched in acetone/dry ice. The resulting solutions of cellulose and cellobiose was 10.0 and 10.6 wt.%, respectively, thus containing almost identical concentrations of glucose monomers. Catalyst concentration was 1.7 wt.% (98%, Sigma-Aldrich) was used. The reaction mixtures were stored in a sealed glass container and cooled in dry ice prior to use.

For the FT-IR measurements approximately 15 mg of reaction mixture were loaded into a custom-made 25 µL glass reactor together with a small magnet rod. The reactor was applied on top of a preheated diamond ATR-plate and magnetically stirred by a commissioned device (Scheme 2). The spectra were recorded isothermally using a Nicolet iS5 Spectrometer equipped with a thermo regulated (up to 300 °C) GladiATR diamond cell (Pike Technologies). For each recording 16-80 scans with 4 cm⁻¹ resolution (approximately 15 s to 2 min recording time) were performed depending on the reaction rate. All spectra were background corrected by subtracting a constant under the assumption of zero absorbance at 4000 cm⁻¹. Then the spectra were ATR corrected with built-in algorithm in OMNIC 8.2 assuming a sample refractive index of 1.5. Difference spectra were produced by subtracting a spectrum corresponding to the pseudo steady-state from each spectrum before analysis (ESI†, Figs. S4-S7, S22 and S25), and deconvoluted with PeakFit using the built-in Voigt area approximation algorithm (ESI†, Fig. S17). The reaction rates of the hydrolysis reactions were determined on the basis of the area of the band at 1157 cm⁻¹ in the deconvoluted spectra (ESI†, Figs. S1 and S2 for hydrolysis and Figs. S12 and S13 for HMF formation).

Reference spectra of cellulose oligomers were recorded on powder samples with cellulotrose, cellotetraose and cellopentaose (Megazymes) (ESI†, Fig. 18).



Scheme 2 Schematic drawing of the stirred micro reactor used for the in-situ ATR-FTIR experiments.³⁰

HPLC analysis

After hydrolysis of the cellulose with sulfuric acid spot checks (100 and 120 °C) were performed on the reaction mixtures to confirm the presence of glucose and HMF. The reaction mixtures were analysed by HPLC with RI detection (Agilent 1200 series, 30 cm Aminex® HPX-87H column, 0.005M H₂SO₄ in MilliQ water as eluent at a flow rate of 0.6 mL min⁻¹). The formed products (glucose, HMF, levulinic acid and formic acid) were

identified by comparison with retention times of individual reference samples.

Calculation of theoretical IR spectra

DFT calculations were performed with Gaussian09³⁴ software using a starting structure adopted from an experimentally determined crystal structure.³⁵ Initially, the structure was optimized with Hartree-Fock and the 6-31G(d) basis set and then refined with DFT using the B3LYP functional and the 6-311+G(d,p) basis set (ESI†, structures are shown in Fig. S10 and the interpretation of the spectra in Table S2).

The theoretical spectra that are found in ESI†, Fig. S19 are normalized with respect to the number of glucose units in the structure.

Notes and references

- ^a Centre for Catalysis and Sustainable Chemistry, Department of Chemistry, Building 207, Technical University of Denmark, Denmark. Fax: +45 45883136; Tel: +45 45252390; Tel: +45 45252233; E-mail: ajoku@kemi.dtu.dk; E-mail: ar@kemi.dtu.dk
- ^b Department of Chemistry, Building 207, Technical University of Denmark, Denmark.
- [†] Electronic Supplementary Information (ESI) available: Experimental details, FT-IR spectra and interpretation of data, and HPLC analytic results. See DOI: 10.1039/b000000x/
- J. J. Bozell, *Science*, 2010, **329**, 522–523.
 - D. M. Alonso, J. Q. Bond, and J. A. Dumesic, *Green Chem.*, 2010, **12**, 1493–1513.
 - A. A. Rosatella, S. P. Simeonov, R. F. M. Fraude, and C. A. M. Afonso, *Green Chem.*, 2011, **13**, 754–793.
 - T. Ståhlberg, W. Fu, J. M. Woodley, and A. Riisager, *ChemSusChem*, 2011, **4**, 451–458.
 - A. Boisen, T. B. Christensen, W. Fu, Y. Y. Gorbanev, T. S. Hansen, J. S. Jensen, S. K. Klitgaard, S. Pedersen, A. Riisager, T. Ståhlberg, and J. M. Woodley, *Chem. Ing. Res. Des.*, 2009, **87**, 1318–1327.
 - P. Gallezot, *Chem. Soc. Rev.*, 2012, **41**, 1538–1558.
 - R. P. Swatloski, S. K. Spear, J. D. Holbrey, and R. D. Rogers, *J. Am. Chem. Soc.*, 2002, **124**, 4974–4975.
 - C. Li and Z. K. Zhao, *Green Chem.*, 2008, **10**, 177–182.
 - J. Guo, D. Zhang, C. Duan, and C. Liu, *Carbohydr. Res.*, 2010, **345**, 2201–2205.
 - F. Tao, H. Song, and L. Chou, *ChemSusChem*, 2010, **3**, 1298–1303.
 - R. Rinaldi, N. Meine, J. vom Stein, R. Palkovits, and F. Schüth, *ChemSusChem*, 2010, **3**, 266–276.
 - L. Vanoye, M. Fanselow, J. D. Holbrey, M. P. Atkins, and K. R. Seddon, *Green Chem.*, 2009, **11**, 390–396.
 - S. J. Dee and A. T. Bell, *ChemSusChem*, 2011, **4**, 1166–1173.
 - R. Rinaldi and F. Schüth, *ChemSusChem*, 2009, **12**, 1096–1107.
 - C. Vernon, *Proc. Roy. Soc. London B*, 1967, **167**, 389–401.
 - A. Kresge, T. J. Straub, *J. Am. Chem. Soc.*, 1983, **105**, 3957–3957.
 - H. D. Phan, T. Yokoyama, Y. Matsumoto, *Org. Biomol. Chem.*, 2012, **10**, 7382–7391.
 - K. Lourvanij and G. L. Rorrer, *Ind. Eng. Chem. Res.*, 1993, **32**, 11–19.
 - M. Bicker, J. Hirth, and H. Vogel, *Green Chem.*, 2003, **5**, 280–284.
 - A. J. Kunov-Kruse, *Patent pending*, 2012.
 - Buslov, D.; Nikonenko, N. *Appl. Spectrosc.* 1997, **51**(1), 666.,
 - Buslov, D.; Nikonenko, N. *Appl. Spectrosc.* 1998, **52**(1), 613.
 - N. A. Nikonenko, D. K. Buslov, N. I. Sushko, and R. G. Zhbakov, *Biopolymers*, 2000, **57**, 257–262.
 - N. A. Nikonenko, D. K. Buslov, N. I. Sushko, and R. G. Zhbakov, *J. Mol. Struct.*, 2005, **752**, 20–24.
 - S. Barsberg, *J. Phys. Chem. B*, 2010, **114**, 11703–11708.
 - S. Barsberg, A. R. Sanadi, H. Jørgensen, *Carbohydr. Polym.*, 2011, **85**, 457–464.
 - Marchessault, R.; Liang, C. J. *Polymer Sci.* 1959, **37**, 385.;
 - Marchessault, R.; Liang, C. J. *Polymer Sci.* 1959, **39**, 269.
 - Marchessault, R.; Liang, C. J. *Polymer Sci.* 1962, **59**, 357.,

..